UNIVERSITY OF SOUTHAMPTON

Faculty of Natural and Environmental Sciences

School of Ocean and Earth Sciences

National Oceanography Centre

EVOLUTION OF SUBMARINE SEDIMENT DENSITY FLOWS DEDUCED FROM LONG DISTANCE BED CORRELATIONS

by

Giuseppe Malgesini

Thesis for the degree of Doctor of Philosophy

July 2012

ABSTRACT

Submarine flows can transport huge volumes of sediment across the large submarine fans that dominate many parts of the deep ocean floor. Active flow events are notoriously difficult to monitor directly, and therefore our understanding of such flows still strongly relies on the analysis of the deposits they leave behind.

This thesis aims to investigate the transport and depositional processes, the stacking patterns and the time frequency distribution of turbidites and debrites deposited in the Miocene Marnoso Arenacea Formation (Italian Apennines). This location is unique because deposits from individual flow events (beds) can be traced for long distances, allowing the lateral and down flow evolution of single flow events to be analyzed in detail. Lateral changes in individual flow deposits are documented through extensive correlation of beds deposited in a stratigraphic interval below the most prominent Contessa Marker bed. The observed transitions in facies, and the external shape of different types of deposit, are used as an independent test of models that capture our understanding of submarine flow processes.

This work highlights how deposits of submarine density flows can be complex, even in relatively simple basin plain settings. A single event can comprise different flow types, and transformations can occur between these flow types. The initial volume, sediment concentration and grain size (including the proportion of fine cohesive mud) control the external shape of the deposits. Low density turbidity currents deposit clean sandstone beds with an exponentially tapering shape, while coarser grained high density turbidity currents produce massive or parallel laminated layers that maintain their thickness for longer (10's of kilometers) distances. Cohesive debris flows form distinctive ungraded mud-rich sandstone that can either pinch-out abruptly or gradually taper. Liquefied debris flows with elevated pore pressures can deposit clean (mud-poor) sand over large areas (up to 30 km) of the Marnoso Arenacea basin plain. This is suggested by the distinctive swirly, patchy fabric of a particular type of clean sandstone, that records pervasive liquefaction during the late stages of the flow, and confirmed by the rapid pinch-out geometry of flow deposits at their margins. Such debris flows most likely form through transformation from an initial high density turbidity current. A similar flow process may characterize the distal, rapid pinch out of sandstone lobes in Fan 4 of the Skoorsteenberg Formation (Karoo basin, South Africa).

The observed stacking pattern of turbidite beds in a 530 meters thick stratigraphic section indicates a long-term clustering. Debrite intervals however occur randomly, and bed correlation suggest that almost every large volume flow deposited clean or muddy debrite (or both) intervals in different positions of the basin.

Hemipelagic marl thickness is used as a proxy for time between flow events. The distribution of time between events is exponential, therefore related to a Poisson Process. This indicates that flow events (most likely triggered by submarine slope failures) occur independently one from the other through time.

Contents

Chapter 1: Introduction 1

1.1. SUBMARINE SEDIMENT DENSITY FLOWS. WHY ARE THEY IMPORTANT TO UNDERSTAND? 1

1.2. WHY MARNOSO FIELD DATA IS UNIQUE AND INFORMATIVE 2

1.3. THESIS LAYOUT 3

1.4. CONTRIBUTION TO PUBLISHED PAPERS 4

1.5. KEY QUESTIONS ADDRESSED BY THIS THESIS 4

1.6. TERMINOLOGY USED FOR FLOWS AND DEPOSITS 8

1.7. CONTRIBUTION BY AUTHORS TO CHAPTERS 10

Chapter 2: Geological settings of the Northern Apennines and the Marnoso Arenacea Formation 11

2.1 STRUCTURE AND EVOLUTION OF THE NORTHERN APENNINES 11

2.2. THE ROMAGNA APENNINES 13

2.3. THE MARNOSO ARENACEA FORMATION 15

Chapter 3: Can liquefied debris flow deposit clean sandstone over large areas of the sea floor? field evidence from the Marnoso Arenacea Formation, Italian Apennines 19

3.1. INTRODUCTION 19

3.2. AIMS 20

3.3. TERMINOLOGY 22

3.3.1. Turbidite and Debrite 22

3.3.2. Clean and muddy sandstone 23

3.4. METHODOLOGY 25

3.4.1. Sedimentary logs 25

3.4.2. Facies scheme 25

3.4.3. Textural data 29

3.5. RESULTS 29

3.5.1. Bed correlations 29

3.5.2. Palaeocurrent directions 30

3.5.3. Different types of sandstone 33

3.5.4. Bed architecture 37

3.5.5. Key beds in the above Contessa interval 43

3.6. DISCUSSION 45

3.6.1. Internal character and depositional processes for clean sandstone intervals 45
3.6.2 Bed shape as test for depositional processes 48
3.6.3. How could clean sandy debris flows originate and move on low gradients? 49
3.6.4. Significance of lateral transitions into clean sandstone deposited by turbidity current ...51
3.6.5. Comparison with previous studies 51
3.7. CONCLUSIONS 55

Chapter 4: External shape of turbidite beds in the Marnoso Arenacea Formation 57
4.1. INTRODUCTION 57
4.2. AIMS 59
4.3. METHODOLOGY 59
4.3.1. Bed correlations 59
4.3.2. Differential compaction 60
4.3.3. Foredeeep paleogeography 61
4.3.4. Bed volumes and cross sectional areas 63
4.3.5. Grain size 64
4.3.6. Facies scheme and depositional processes 64
4.3.7. Grouping of deposit types 69
4.3.8. Curve fitting 69
4.3.9. Numerical Modelling 69
4.4. RESULTS 70
4.4.1. Small volume beds 70
4.4.2. Intermediate volume beds 73
4.2.3. Large volume beds 74
4.4.4. Mudstone intervals 76
4.5. DISCUSSION 76
4.5.1. What is the external shape of turbidite beds? 76
4.5.2. What controls the external shape of turbidite beds? 90
4.6. CONCLUSIONS 96

Chapter 5: Thickness distribution, clustering and time frequency analysis of turbidites and debrites in the Marnoso Arenacea Inner Stage 99
4.1. INTRODUCTION AND AIMS 99
4.2. MATERIALS AND METHODS 100
4.2.1. Sedimentary logging 100
4.2.2 Hemipelagite or hemiturbidite? 101

4.2.3. Biostratigraphy 106
4.3.4 Thickness frequency distributions 106
4.2.5 Hurst statistic 107
4.3. RESULTS 109
4.3.1 Logged data 109
4.3.2 Biostratigraphy 109
4.3.3 Dated section 111
4.3.4. Paleocurrents 111
4.3.5. Bed thickness distributions 112
4.3.6 Hurst statistic 115
4.4. DISCUSSION 116
4.4. PART 1: THICKNESS DISTRIBUTION AND CLUSTERING OF GRAVITY FLOW DEPOSITS 116
4.4.1. What is the shape of the frequency distributions of deposit thicknesses? 116
4.4.2 Comparison of thickness distributions at Cabelli with those in correlated beds 121
4.4.3. Comparison to deposit thickness distributions in other locations, and Talling (2001) 123
4.4.4 What controls the frequency distribution of deposit thicknesses? 124
4.4.5 How strongly stratigraphically clustered are flow deposit thicknesses 127
4.4. PART 2: FREQUENCY OF FLOWS THROUGH TIME 129
4.4.6 Hemipelagic marl thickness as a proxy for time 129
4.4.7 What is the frequency distribution of recurrence times for flow events? 130
4.4.8. Implications of exponential distribution 134
4.4.9. Clustering of events in time, and temporal changes in mean flow frequency 136
4.4.10 Implications for processes triggering submarine flows 137
4.5. CONCLUSIONS 141

Chapter 6: Distal pinch-out of sandstone lobes: Karoo basin (South Africa) 145
6.1 INTRODUCTION AND AIMS 145
6.2 GEOLOGICAL SETTINGS 146
6.1.2 Fan 4 147
6.2 MATERIALS AND METHODS 149
6.2.1 Sedimentary logging 149
6.2.2 Bed correlations 150
6.2.3 Textural analysis 151
6.3 RESULTS 152
6.3.1 Lithofacies and textural analysis 152
6.3.2 Bed correlations 155

6.4 DISCUSSION....161
6.4.1 Origin of the abrupt pinch out of clean sandstone lobes....161
6.4.2 Controls on the finger-like geometry of lobes pinch-out....164
6.4.3 Authigenic origin of some heterolithic packages....166
6.5 CONCLUSIONS....167

Chapter 7: Summary and future work....169
7.1 SUMMARY....169
7.2. RESPONSES TO INITIAL QUESTIONS POSED IN THIS THESIS....170
7.3. FUTURE WORK....177

References....179

Appendices....CD-ROM

List of figures

Chapter 2

Figure 2.1. Simplified geological map of the northern Apennines (from Mutti et al., 2002).

Figure 2.2 Evolution of the Apennines area. Modified from Gasperi (1995).

Figure 2.3. Geological map of the Romagna Apennine. From Roveri et al. (2003).

Figure 2.4 . *Schematic stratigraphic log of the Cenozoic Umbro-Marchean succession and detail of the Miocene Marnoso Arenacea formation.*

Figure 2.5. Tectono-stratigraphic diagram showing the migration of the foredeep-thrust system of the northern Apennine (from Mutti and Di Base, 2002; modified after Ricci Lucchi, 1986).

Figure 2.6. General physical-stratigraphic framework of the Apennine foredeep basin (from Mutti and Di Base, 2002. Modified after Ricci Lucchi, 1986).

Figure 2.7. Summary of the stratigraphy of the Marnoso Arenacea foredeep basin (after Ricci Lucchi, 1986).

Figure 2.8. Detailed structural cross sections transverse to the basin axis in the vicinity of the Santerno (A) Bidente (B) and Savio Valleys (C). (From Roveri et al., 2002 and RER, 1994.)

Chapter 3

Figure 3.1. Location map showing the northern part of the outcrop of the Marnoso-Arenacea Formation.

Figure 3.2. A) Map showing the main sediment sources and dispersal patterns of the Marnoso-arenacea foredeep basin in its different evolutionary stages (after Mutti et al., 2002). B) Schematic paleogeographic reconstruction of the Marnoso-arenacea foredeep basin during the Serravallian (after Di Base & Mutti, 2002).

Figure 3.3. Cross-section along the Ridracoli element showing the correlation of the first 20 thick (>40 cm) beds below the Contessa marker bed.

Figure 3.4. Outcrop photograph illustrating the different types of sandstone deposits seen in the outcrops.

Figure 3.5. Map showing the direction of paleoflow measured for selected thick sandstone beds, based on measurements of flutes and grooves at the base of the beds.

Figure 3.6. Diagrams showing the textural characteristics of A) subfacies Cs5, B) subfacies Cs7, C) subfacies Cs6, D) Subfacies Ms1.

Figure 3.7. Cross-section along the Isola element showing the correlation of the first 20 thick (>40 cm) beds below the Contessa marker bed.

Figure 3.8. Cross-section along orientated orthogonal to the paleoflow direction across the Ridracoli, Isola and Pianetto structural elements.

Figure 3.9. Mean grain size plotted against A) mud matrix content and B) sorting (defined here as the standard deviation of grain size measurements).

Figure 3.10. Outcrop photographs illustrating the different types of massive sandstone deposits. See Table 1 for a full description of lithofacies Ms, subfacies Cs1 and Cs6.

Figure 3.11. Outcrop photograph illustrating the characteristic swirly fabric of subfacies Cs7 (Table 1).

Figure 3.12. Correlation panel illustrating the lateral changes of the four beds immediately below the Contessa marker bed in the most proximal outcrops.

Figure 3.13. Detailed bed diagrams showing the lateral variations of lithofacies and grain size along the Ridracoli thrust sheet for A) Bed -2, B) Bed -4, C) Bed -5, D) Bed -6, E) Bed -7, F) Bed -8, G) Bed -10, and H) Bed -11.

Figure 3.14. Generalized facies tracts observed for correlated beds within the Marnoso-arenacea Formation.

Figure 3.15. Down-flow transects through Beds 0, 2.5 and 5.1 above the Contessa Bed (modified from Talling et al., 2012b).

Figure 3.16. A to D) Lateral changes between turbidite clean sandstone (Cs1-to-6) and debrite clean sandstone (Cs7) in Bed 5 on the Isola thrust sheet.

Chapter 4

Figure 4.1. (A) Location map showing the northern part of the outcrop of the Marnoso-arenacea Formation (B) Palaeocurrent directions measured from flutes and grooves at the base of the beds in the below- Contessa interval.

Figure 4.2. Paleogeographic reconstruction of the Marnoso Arenacea Formation ‘‘inner’’ foredeep basin at the time of deposition for the above Contessa interval. From Talling et al. (2007a.)

Figure 4.3. Comparison between the sandstone volumes estimated by Talling et al. (2007b) using 109 locations on seven thrust sheets (figure 1), and the cross sectional areas calculated for each sandstone interval in the Ridracoli thrust sheet (figure 1).

Figure 4.4. Generalized graphic sedimentary logs that summarise the deposits produced by different types of submarine flow.

Figure 4.5. A) Down-flow transect through Bed -2 along the Ridracoli thrust sheet. B) Across flow transect through Bed -2 along the Ridracoli, Isola and Pianetto thrust sheets. C) Location map showing the position of the correlated sections.

Figure 4.6. Diagrams illustrating the lateral changes in thickness and internal facies architecture in the 32 turbidite beds from the above-Contessa and below-Contessa intervals, along the Ridracoli Element in a direction sub-parallel to palaeoflow.

Figure 4.7. Diagrams illustrating the lateral changes in thickness and internal facies architecture in the 32 turbidite beds from the above-Contessa and below-Contessa intervals, along the Ridracoli Element in a direction sub-parallel to palaeoflow (figure 1).

Figure 4.8. Variation of the maximum grain size measured using a grain size comparator card in the field, for A) small volume beds, B) intermediate volume beds, and C) large volume beds.

Figure 4.9. Rates of thinning within five specific beds that display different facies tracts (Talling et al., 2012).

Figure 4.10. Diagrams illustrating the lateral changes in thickness and internal facies architecture in the 32 turbidite beds from the above-Contessa and below-Contessa intervals, along the Ridracoli Element in a direction sub-parallel to palaeoflow. Beds are subdivided according to the downflow facies architecture (facies tracts).

Figure 4.11. Sandstone interval shape in small volume beds along the Ridracoli thrust sheet (figure 1).

Figure 4.12. Sandstone interval shape in intermediate and large volume beds (figure 4.6) along the Ridracoli thrust sheet (figure 4.1).

Figure 4.13. Explanation of the significance of a, b and c parameters in the two functions used to describe interval shape.

Figure 4.14. Regression curves showing the average thickness of beds with different facies tract shown in figure 4.10.

Figure 4.15. A) Regression line describing the lateral thickness variations in mudstone interval thickness.. B) and C) Comparison of a and b parameters of the regression line to the calculated mudstone cross sectional area for each bed.

Figure 4.16. A) Scheme summarizing the variations of bed shape and internal facies architecture for progressively larger sandstone volume beds. B) Scheme summarizing the variations of bed shape for progressively larger mudstone volume beds, and their relationship with the sea-floor topography

Figure 4.17. Turbidite deposit shapes obtained from depth-averaged numerical modeling by Goater (2011) for flows with different initial sediment concentration (ϕ0). Modified from Goater (2011).

Figure 4.18. Measured profiles for beds of glass beads from experiments of Middleton and Neale (1989). Modified from Middleton and Neale (1989).

Figure 4.19. A) Relative area proportion of the different lithofacies in each bed. B) Cross-sectional area percentage of mudstone (Te) plotted against the total bed area for beds with different facies tract.

Chapter 5

Figure 5.1. Location and geological map of the Cabelli section.

Figure 5.2. A) Outcrop photograph of the Cabelli section . B) Summary of the absolute age, stage boundaries, magnetic reversals and position of biohorizons in the dated interval. Modified from Raffi et al. (2006).

Figure 5.3. Summary log of the measured section.

Figure 5.4. A) Photograph illustrating the difference between turbidite mudstone and hemipelagic marl. Note the difference in color and texture. B) Correlation between the thickness of each event bed and the hemipelagic marl directly above.

Figure 5.5. Cumulative departure from the mean plot of single beds (sandstone and turbidite mudstone) thickness.

Figure 5.6. Plot of cumulative hemipelagite thickness as a time axis against turbidite bed thickness.

Figure 5.7. Paleocurrent direction diagrams.

Figure 5.8. Frequency histograms plots and logarithmic probability plots of A,B) whole beds, C,D) sandstone and E,F) mudstone intervals.

Figure 5.9. Clustering of turbidite beds.

Figure 5.10. Cumulative departure from the mean plot of hemipelagite intervals between all beds, thin (<40 cm sandstone) and thick (>40 cm sandstone) beds.

Figure 5.11. Log-probability plots for beds with different basal Bouma divisions and grain size classes.

Figure 5.12. Frequency histogram and log-probability plots for clean and muddy debrites.

Figure 5.13. Comparison between the thickness distribution of whole beds, clean and muddy debrites in a vertical section (Cabelli) and in randomly sampled beds in different positions along the basin (beds correlated in chapter 3 and by Amy and Talling., 2006).

Figure 5.14. Comparison between data from the proximal Coniale section (Talling, 2001) and the Cabelli section.

Figure 5.15. A) Comparison between the bed volumes estimated by Talling et al. (2007) and the thickness of the same beds at Cabelli. B) Relationships between bed thickness and basal grain size for each measured bed.

Figure 5.16. Relationships between bed thickness and the hemipelagite under each bed. Beds are classified according to the basal grain size class.

Figure 5.17. Cumulative distribution of hemipelagite.

Figure 5.18. A, B) Frequency histogram and Log-linear plot for the values of A,B) hemipelagite between thick (>40 cm sandstone) beds and C,D) beds containing clean or muddy debrite intervals.

Figure 5.19. Plot of the values of mean and standard deviation (in cm) for each consecutive 50 intervals of hemipelagite (1 to 50, 2 to 51…..646 to 696). In an exponential distribution the mean value corresponds to the standard deviation.

Chapter 6

Figure 6.1. (A) Satellite image of the field area showing the location of the Tanqua depocenter. (B) Generalized and simplified Permian palaeogeographic map of Gondwana (after Faure & Cole, 1999). From Prelàt et al. (2009).

Figure 6.2. Simplified representative stratigraphic column of the Karoo Supergroup. Modified from Prelàt et al. (2009).

Figure 6.3. Outcrop photographs of the Katjesberg outcrop.

Figure 6.4. Stratigraphy and paleogeography of fan 4. A) Diagram illustrating the window of observation afforded by the outcrop orientation, compared with the interpreted architecture of fan 4 at the time of deposition. Modified from Johnson et al. (2001). B) Oblique strike-oriented log correlation across the middle–outer fan of fan 4 (length 26.5 km). Modified from Van der Werff and Johnson (2003).

Figure 6.5. Map view of the northern face of the Katjesberg outcrop, with the position of logged sections.

Figure 6.6. Across stike cross section. The position of the logged stratigraphic sections is indicated

Figure 6.7. Parallel to Dip cross section. The position of the logged stratigraphic sections is indicated.

Figure 6.8. Lobe 5 in section 13. A) Outcrop photograph.B) Graphic log. The position of rock sample taken is indicated. C,D) S.E.M images in backscattered mode of massive sandstone deposits.

Figure 6.9. Outcrop photographs of the different lithofacies described.

Figure 6.10. Generalised summary of different process models for deposition of massive sandstone and resulting characteristic deposit shape.

Figure 6.11. Schematic view of possible mechanisms for the formation of finger-like protrusions. A) map view; B) and C) across strike section; C) and D) parallel to dip section.

Figure 6.12. Cartoon showing the difference between fine-grained units formed by allogenic and autigenic processes. From Prelàt et al. (2009).

Chapter 7

Figure 7.1. Pinch-out rates of the different facies tracts analyzed in this thesis

List of tables

Chapter 1

Table 1.1. Summary table of the facies scheme and terminology adopted.

Chapter 3

Table 3.1. Facies scheme adopted.

Chapter 4

Table 4.1. Cross sectional area in the Ridracoli thrust sheet of different lithofacies and sand/mud ratio for each bed.

Table 4.2. Regression curves for beds with different volume and facies tract. The regression parameters and the regression coefficient (R^2) are indicated.

Chapter 5

Table 5.1. Results of the Kolmogorov-Smirnov test for the different thickness populations considered.

Table 5.2. Hurst coefficients K and H and significance level for the populations analyzed with the Hurst test. See text for an explanation of the technique adopted

List of accompanying materials

Appendix 1. Cross section along the Ridracoli and Pietralunga thrust sheet showing the correlation of the first 20 thick (>40 cm) beds below the Contessa marker.

Appendix 2. Cross section along the Isola thrust sheet showing the correlation of beds comprised between the Contessa and Fiumicello (bed -37) marker.

Appendix 3. Cross section orientated orthogonal to the paleoflow direction across the Ridracoli, Isola and Pianetto structural element, for beds comprised between the Contessa and Fiumicello (bed -37) marker beds.

Appendix 4. Oblique-to-strike correlation panel of Fan 4 deposits in the Skoorsteenberg Formation (Karoo basin, South Africa).

Appendix 5. Oblique-to-dip correlation panel of Fan 4 deposits in the Skoorsteenberg Formation (Karoo basin, South Africa).

Appendix 6. Summary figure highlighting the external shape, facies architecture (facies tracts) and depositional processes studied in this thesis.

Appendix 7 (on CD-ROM). Excel spreadsheet containing the database obtained from the Cabelli section.

Appendix 8 (on CD-ROM). Results of the biostratigraphical analysis performed by Alessandra Negri (Univesità di Ancona) on hemipelagite samples of the Cabelli section.

Appendix 9 (on CD-ROM). Field guide for the 2011 BSRG postgraduate field trip in the Italian Apennines

DECLARATION OF AUTHORSHIP

I, Giuseppe Malgesini

declare that the thesis entitled

Evolution of submarine sediment density flows deduced from long distance bed correlation

and the work presented in the thesis are both my own, and have been generated by me as the result of my own original research. I confirm that:

- this work was done wholly or mainly while in candidature for a research degree at this University;
- where any part of this thesis has previously been submitted for a degree or any other qualification at this University or any other institution, this has been clearly stated;
- where I have consulted the published work of others, this is always clearly attributed;
- where I have quoted from the work of others, the source is always given. With the exception of such quotations, this thesis is entirely my own work;
- I have acknowledged all main sources of help;
- where the thesis is based on work done by myself jointly with others, I have made clear exactly what was done by others and what I have contributed myself;
- parts of this work have been published as:

  Talling, P.J**., Malgesini, G.** and Felletti, F. (2012) Can liquefied (debris) flows deposit clean sandstone over large areas of sea floor? Field evidence from the Marnoso-arenacea Formation, Italian Apennines. *Sedimentology, in press*.

  Talling, P.J., **Malgesini, G.**, Sumner, E.J. , Amy L.A. , Felletti, F. , Blackbourn, G., Nutt, C., Wilcox, C., Harding, I.C. and Akbari, S. (2012) Planform geometry, stacking pattern, and extra basinal origin of low-strength and higher-strength cohesive debris flow deposits in the Marnoso arenacea Formation. *Geosphere, in press.*

  Talling, P.J., Sumner, E.J., Masson, D.G and **Malgesini, G**. (2012) Submarine Sediment Density Flows: Depositional Processes and Deposit Types. *Sedimentology, in press.*

Signed: ……..

Date: 24/07/2012

Acknowledgements

Firstly I would like to thank Peter Talling, my main supervisor, for the great opportunity he gave me to study at NOCS. Pete has helped me in every aspect of my studies, from the development of scientific skills and writing style to the many lessons (and also a few beers) in the field. I would also really like to thank Fabrizio Felletti, my "unofficial supervisor" in Milan, for the useful discussions and great help in the field. I really appreciated the support I received from the Marine Geoscience Group, in particular Jessica Trofimovs, Doug Masson and Russell Wynn. Also thanks to Dave Hodgson, Steve Flint and the Strat. group in Liverpool for the support during fieldwork in South Africa.

Of course I can't forget my family, *mamma e papà* and my sisters Bea, Sara and Paola that supported me over this period abroad. I want to thank some special persons I met during these years. George, Lena, Konstantina, Carla and Hector: thanks for everything, you have been my family here in England. Of course I want to thank my officemates Chris and James; I was honored to be part of the 786/18 Turbidite Team, and I will remember both the days in the office and the fieldtrip adventures we had. P.s. Expanding Earth rules. Also thanks to the Postgraduate community at NOCS, especially Joe (or Giuseppe), Claudia, Claire, Ed, Mike, and everyone I forgot to mention (you know who you are). Finally I'd like to thank the University of Milano, ConocoPhillips and the UKTAPS consortium for the financial support during my PhD.

Chapter 1: INTRODUCTION

This introduction starts by outlining why submarine sediment density flows are important. This is followed by a brief introduction to the main study area, the Miocene Marnoso Arenacea Formation in the Italian Apennines, and why these rock outcrops are an outstanding natural laboratory for understanding density flow processes. A summary of the thesis structure is provided, together with a list of the key questions that the thesis addresses. There is then a brief note on the terminology used in the thesis to describe different types of submarine sediment density flow, followed by a summary of the contributions made to each chapter by colleagues.

1.1. SUBMARINE SEDIMENT DENSITY FLOWS. WHY ARE THEY IMPORTANT TO UNDERSTAND?

Submarine sediment density flows can transport huge volumes of sediment across the large fans that dominate many parts of the deep ocean floor, and they are arguably the volumetrically most important flow process for moving sediment across our planet (Allen, 2007; Talling et al., 2007a). A single submarine flow can transport over 100 km^3 of sediment (Piper et al., 1999), ten times the annual sediment flux from all of the World's rivers (Milliman & Syvitski, 1992). These flows can achieve run out distances in excess of 1,500 km, such as in the north western African margin (Wynn et al., 2012), and travel across remarkably low gradients of less than 0.01° (Talling et al., 2007c).

Understanding these submarine flows, and how they transport and deposit sediment, remains a grand challenge, as active flow events are notoriously difficult to monitor directly due to their inaccessible location, unpredictable occurrence and their ability to destroy monitoring equipment placed in their path. Velocities of long-run out submarine flows have been documented accurately by cable breaks or instruments at just five locations (Talling et al., 2012c), with the 1929 Grand Banks event (Piper et al., 1999) being the most well-known example.

Our understanding of these flows therefore relies strongly on the sedimentary deposits they leave behind, preserved in rock outcrops and on the modern sea floor, and on laboratory experiments (i.e. Middleton, 1970; Baas et al., 2011).

Ancient flows of this type have deposited thick rock sequences that now hold some of the World's largest oil and gas reserves (Weimer & Pettingill, 2007). Flow deposits also contain large volumes of terrestrial and marine organic carbon, and play a key role in the burial of organic carbon in the Deep Ocean, therefore influencing the pCO2 levels in the atmosphere (Galy et al., 2007).

It has been suggested that such deposits may be a valuable record of submarine landslide dynamics and associated tsunamis (Wynn & Masson, 2003; Hunt et al., 2011), major earthquakes (Goldfinger et al., 2007), river flooding (Mulder et al., 2003), and glacial outwash mega-floods (Piper & Normark, 2009).The flows themselves also pose a significant hazard to expensive infra-structure on the modern sea floor (Talling et al., 2007c; 2012a).

1.2. WHY MARNOSO FIELD DATA IS UNIQUE AND INFORMATIVE

This thesis mainly involves description and analysis of the Miocene Marnoso Arenacea Formation in the northern Italian Apennines. These outcrops are an outstanding natural 'laboratory' for understanding submarine flows. It is very unusual because deposits from individual flow events (beds) can be traced for long distances in this sequence (Ricci Lucchi and Valmori, 1980; Amy and Talling, 2006; Talling et al., 2007a, 2007b, 2012b, 2012c, Tinterri and Muzzi Magalhaes, 2010; Muzzi Magalhaes and Tinterri, 2010; Sumner et al., 2012). It is the only set of ancient rock outcrops where individual event beds can be correlated for over 100 km. This is important because it allows the lateral and down flow evolution of single flow events to be analyzed in detail. The observed down flow transitions in facies, and the external shape of different types of deposit, can be compared to the predictions of models that capture our understanding of submarine flow processes.

Mega-turbidites with a distinctive limestone-rich composition and provenance, carefully mapped by the Emilia Romagna, Tuscany and Umbrian geological surveys (Martelli et al., 1994), occur every 20–50 m in parts of the older (inner) basin sequence. These marker beds aid the correlation of intervening beds across an area of 120 × 30 km, between up to one-hundred and nine sections (Amy and Talling, 2006). Submarine channels are absent within the older part of the Marnoso Arenacea Formation, which was deposited in a relatively flat basin plain (Ricci Lucchi, 1986). Bed

amalgamation is rare, and these strata have a sheet-like bed geometry. Turbidite mudstone can be distinguished from background hemipelagite mudstone based on the color, texture and fossil content. Flows could traverse this basin plain in opposite directions (Gandolfi et al., 1983), and flow was consistently sub-parallel to the basin margins. The basin at this stage is wedge shaped, with a steep inner (southwestern) margin and a gentler northeastern thinning towards the flexural ramp. There is no evidence for strong flow reflection. This rather simple depositional setting, free from excessive topographic complexity, might be expected to produce beds with a simple geometry that conforms to classical models such as the Bouma sequence (Kneller and McCaffrey, 2003). This is not the case, especially for larger volume beds.

1.3. THESIS LAYOUT

This thesis work contains 7 chapter and 9 appendixes. **Chapter** 1 provides an introduction to the thesis, outline the content of each chapter and pose the key questions that will be discussed throughout the thesis. It also presents a general introduction on submarine sediment density flows. **Chapter 2** introduces the geological settings of the Northern Italian Apennines and the Marnoso Arenacea Formation. Chapter 3, 4 and 5 are based on field data from the Marnoso Arenacea Formation, whose geological settings are presented only in Chapter 2 to avoid repetition. Chapters 3, 4, 5 and 6 are presented as individual (unpublished) scientific papers. **Chapter 3** forms the basis of a scientific paper recently accepted by Sedimentology. It presents the correlation framework of the newly studied interval below the Contessa marker bed. Individual bed correlations provide an independent test for sandstone depositional processes inferred from field data and textural analysis, including deposition from clean sand liquefied debris flow. **Appendix 1, 2 and 3** present the full correlation panels of the below Contessa interval in a larger format. **Chapter 4** quantitatively analyses, and investigates the main controls on, the external shape of turbidite beds. **Chapter 5** investigates the frequency, long-term clustering, stacking patterns and vertical distribution of turbidite and debrite beds in the 600 m thick Cabelli section deposited in the Marnoso Arenacea inner (older) stage. **Appendix 7**(on CD-ROM) is a spreadsheet containing the database obtained from the Cabelli section. **Appendix 8** (on CD-ROM) contains the results of the biostratigraphical analysis performed by Alessandra Negri (Univesità di Ancona) on hemipelagite samples of the Cabelli section. **Chapter 6** analyzes the rapid distal pinch-out of submarine lobes in the Karoo basin (South Africa), applying the method developed in chapter 3 for the Marnoso Arenacea Formation beds. **Appendix 4 and 5** present the full correlation panels of

the below Contessa interval in a larger format. **Chapter 7** synthesizes the conclusions, answer the questions posed in Chapter 1 and outline possible further work and research directions. **Appendix 8** summarizes the down flow facies tracts, the external shape and the depositional processes of submarine sediment density flow deposits studied. **Appendix 9** (on CD-ROM) is the field guide prepared by the Author for the BSRG (British Sedimentological Research Group) post graduate field trip in the Northern Italian Apennines.

1.4 CONTRIBUTION TO PUBLISHED PAPERS

Chapter 3 formed the first draft of a paper recently accepted in *Sedimentology* (Talling et al. 2012a). Talling et al. (2012a) expanded the concept of clean debris flow suggested in this chapter to incorporate different types of debris flows, ranging from non-cohesive, to poorly cohesive and cohesive. The authors restructured the paper, and added a theoretical analysis of the time needed to dissipate excess poor pressures in flows containing different amounts of fine material (mud) not included in chapter 3. The concept of clean liquefied debris flow was also included in a paper accepted in *Sedimentology* (Talling et al, 2012b) that reviews submarine density flows classification and deposit types. Data on the character and frequency distribution of clean and muddy debrites in a 600 m thick stratigraphic section described in **chapter 5** are included in a paper recently accepted by *Geosphere* (Talling et al. 2012c).

1.5. KEY QUESTIONS ADDRESSED BY THIS THESIS

The thesis addresses the following major questions.

1) **What is the internal facies architecture of individual submarine density flow deposits obtained from bed-by-bed correlations? Can we use this information to test depositional models?**

Rationale: Submarine sediment density flows have proven to be notoriously difficult to study through direct monitoring . Our understanding of these flows is therefore based heavily on the deposits that they leave behind. Detailed correlations of single flow deposits (beds) in the Marnoso Arenacea Formation provide information usually unavailable in field studies, such as how various types of sand in a single bed are arranged in down-flow trending “facies tracts” (Mutti, 1992). This additional information provides an independent test of sand depositional models, such

as the widely used models of Bouma (1962), Lowe (1982), Pickering et al. (1986), Ghibaudo (1992), Mutti (1992) and Haughton et al. (2009).

2) Are liquefied debris flows able to deposit clean sandstone across large areas of the sea floor? How do such flows originate?

Clean sand debris flows: previous controversy

Thick divisions of clean (mud-poor) massive (unstratified) sand, generally lacking normal grading, are common building blocks of submarine fans (Shanmugam, 2000), and can form significant hydrocarbon reservoirs (Guy, 1992, Stow and Johansson, 2000). Post-depositional liquefaction or intense bioturbation may, in some cases, obliterate the original sedimentary structures, but in most examples the massive sand divisions appear to be the products of discrete depositional events from one or more gravity currents (Kneller and Branney, 1995).

The origin of the basal interval of thick-bedded deep-water sandstones has generated much controversy in recent years (Shanmugam and Moiola, 1995; 1997; D'Agostino and Jordan, 1997; Bouma et al., 1997; Coleman, 1997; Lowe, 1997; Slatt et al., 1997). Two contrasting depositional models have been proposed.

The traditional model for clean sand deposition across submarine fans is based on expanded turbulent flows with sediment concentrations low enough for individual particles to settle out from the flow, and progressively aggrade a bed (Kuenen and Migliorini, 1950; Lowe, 1982; Kneller and Branney, 1995; Stow and Johansson, 2000).

Shanmugam and Moiola (1995) proposed that clean (mud poor) sand was often deposited by much higher sediment concentration 'sandy debris flows'. They proposed that sandy debris flows deposit clean sandstones that pinch out abruptly at their margins, rather than the extensive tapering sheets produced by turbidity currents. This model was controversial because it dramatically changed predictive models for the extent and shape of oil of gas reservoirs hosted within clean deep-water sandstones. Shanmugam and Moiola's (1995) proposal was subsequently widely rejected, primarily in our view because of a failure to provide sufficiently convincing field data with which to validate the hypothesis. Recent

publications (Amy and Talling, 2006; Talling et al., 2007b) have demonstrated that thin but remarkably mobile debris flows can indeed deposit extensive sand layers far out in the deep ocean. However, those sandstone layers have high matrix mud content (20 to 49% mud; Talling et al., 2007b). These sandy debris flows were mud-rich and highly cohesive.

Field observations, laboratory experiments, and analytical and numerical models indicate that submarine debris flows and turbidity currents will produce deposits with markedly different shapes. Field studies (Johnson, 1970) and laboratory experiments (Marr et al., 2001; Mohrig et al., 1999) indicate that both subaerial and subaqueous debris flows produce deposits with well-defined steep edges and a lobate geometry. Both mud-rich (cohesive) and mud-poor sediment mixtures produce this type of abrupt termination (Major, 1997; Coussot, 1997). Subaqueous experiments involving dilute turbidity currents produce a different deposit shape that gradually tapers (Gladstone et al., 1998), and a similar gradual tapering of the deposit geometry is apparent in numerical simulations of dilute submarine sediment gravity flows (Harris et al., 2002).

Rationale: in chapter 3 we will test Shanmugam and Moiola (1995) original hypothesis; that submarine debris flows often deposit clean (i.e. mud-poor) sand with much lower (0 to ~7% by volume) mud content. In The Marnoso Arenacea basin plain some types of clean (mud-poor) sandstone with particular distinctive internal textures pinch out relatively abruptly, whilst other types of clean sandstone taper more gradually in a down flow direction. We use the long distance correlation framework and an extensive textural analysis of sandstone deposits to infer that a certain type of massive clean sandstone with a swirly or patchy texture was deposited by liquefied debris flow. We then discuss how such liquefied layers of sand could originate and potentially run out for long distances on a low gradient (< 0.1°) basin plain

3) What is the characteristic external shape of turbidites and debrites? What are the controls on this shape?

Rationale: Very few studies documented the external shape (down-flow and across-flow thickness variations) of turbidite beds through the correlation of individual flow deposits for long distances (Hirayama & Nakajima,1977; Ricci Lucchi and Valmori, 1980; Remacha & Fernandez, 2003; Amy and Talling, 2006). This is because turbidite deposits are commonly

eroded by subsequent flows, causing bed truncation and amalgamation (Enos, 1969). We quantitatively study the external shape of 33 turbidite beds, and the relative mudstone caps, along a 60 km down-flow transect, trough the analysis of the regression curves derived for beds of different volumes, internal architecture and grain size. The results obtained are used as a base to better constrain the dominant controls on the deposit external shape.

4) **What is the bed thickness frequency distribution of turbidites and debrites, and why does it occur? How strongly stratigraphically clustered are flow deposits in the Marnoso Arenacea Formation?**

Rationale: The frequency distribution of turbidite bed thicknesses contain information about the flow hydrodynamics, the processes by which flows are initiated and the migration of the source (Rothman and Grotzinger, 1996; Malinverno, 1997; Carlson & Grotzinger, 2001).We determine the thickness distribution of turbidites and debrites in the 600 meters thick Cabelli section, and we compare this vertical distribution to the interval of beds previously correlated laterally between many locations and studies from Talling (2001) and Sylvester (2007).

5) **What is the frequency of turbidity currents and debris flows in the Marnoso Arenacea basin plain? Can this frequency distribution provide information on tempo and triggers of processes that initiate possibly highly destructive flow events?**

Rationale: We dated a 600 meters thick stratigraphic section in the Marnoso Arenacea inner (older) basin using nannofossils biostratigraphy. In this stratigraphic section event beds are separated by intervals of hemipelagic marl, deposited by slow settling of mainly calcareous sediment from the water column. Assuming a constant background sedimentation rate these hemipelagic intervals can be used as a proxy for the time separating individual sediment density flow events. We use the time-framework obtained to determine the frequency and the long-term clustering of turbidites and debrites, providing insight into the triggering mechanisms for these large (often > $1km^3$ of sediment), and potentially destructive flow events.

6) **What is the origin of the abrupt pinch-out of submarine sandstone lobes in the Tanqua Karoo basin?**

Rationale: Fan 4 outcrops in the Tanqua Karoo basin (South Africa) provide an exceptionally good exposure of the distal pinch-out of sandstone lobes that allows a detailed study of the architecture and facies characteristics of the sandstone layers approaching their distal termination. We use a detailed analysis of the pinch out geometry, obtained through correlation of closely spaced (10's of meters) stratigraphic sections coupled with a facies and textural characterization of the deposits, to re-interpret the depositional mechanisms of the flows that deposited massive sandstone beds that pinch-out abruptly at the frontal termination of the submarine fan.

1.6. TERMINOLOGY USED FOR FLOWS AND DEPOSITS

The terms used in the thesis to describe different types of submarine sediment density flows are now briefly outlined (also see Talling et al., 2012a). A range of sediment density (or gravity) flows transport and deposit sediment into deep-water basins. Flows can have different rheologies (fluidal versus plastic) and may exhibit laminar, mixed or turbulent behavior giving rise to deposits with a characteristic geometry, texture and internal structure (Haughton et al., 2009).

Turbidity currents can be defined as turbulent sediment suspension from which larger grains tend to segregate and settle preferentially, depositing a turbidite (Talling et al, 2012b).

In *low density turbidity currents* sediment is supported by the upward component of fluid turbulence (Middleton and Hampton, 1973). Because turbulent, gravity driven currents can be maintained only for relatively low sediment concentrations, sedimentation is not hindered, and turbulence is not dampened significantly near the bed. This often allows the formation of bedforms such as ripples or dunes (Talling et al., 2012b).

In *high density turbidity currents* high suspended load fallout rates cause the sediment settling to be hindered, and a relatively high-concentration flow boundary may develop at the base of the current with reduced turbulence and enhanced grain interaction (Lowe, 1982; Kneller and Branney, 1995). Such currents can generate relatively thin layers of sheared and tractionally reworked sediment on the bed, termed traction carpets (Hiscott, 1994; Talling et al., 2012a). Deposition of massive and laminated sandstone occurs progressively in a layer-by-layer fashion (Lowe, 1982; Kneller and Branney, 1995).

A *(submarine) debris flow* is a laminar or very weakly turbulent flow in which sediment is supported mainly by processes other than fluid turbulence, which include excess pore fluid pressure, grain-to-grain interactions, or buoyancy due to a reduction in the relative densities of clasts and matrix (Talling et al., 2012b). On a strictly rheological base, a debris flow is defined as a flow with a finite cohesive strength, which provides a major support mechanism for the coarser grains (Middleton and Hampton, 1973). However recent studies by Iverson (1997), Major and Iverson (1999), Iverson and Vallance (2001), and Iverson et al. (2010) emphasized the importance of excess pore fluid pressure in determining debris flow behavior, and how the down slope component of sediment weight can sometimes be supported fully by the excess pore pressure (Iverson et al., 2010). A key feature of debris flows is that they are driven down-slope by their own weight and momentum. This distinguishes debris flows from 'traction carpets' (e.g. Hiscott, 1994) or 'sustained liquefied zones' (Kneller & Branney, 1995) that are driven primarily by overlying turbulent flow (Talling et al., 2012a). In debris flows, deposition often occurs en-masse, without segregation of coarser and finer particles, producing a debrite (Lowe, 1982; Talling et al., 2004). *Hybrid flows* can deposit both turbidite and debrite, at the same location, during a single flow event (Haughton et al., 2009).

Lithology	**Depositional interval**	**Subfacies (chapter 3)**	**Bouma's (1962) interval as modified by Talling et al. (2012b)**	**Inferred depositing flow type**	**Discussed in:**
Clean sandstone	Ripple cross laminated	Cs1	Tc	LDT	Table 3.1; 4.3.6
Clean sandstone	Dune cross laminated	Cs2	Tc	LDT	Table 3.1; 4.3.6
Clean sandstone	Parallel laminated	Cs3	Tb1, Tb2	LDT/HDT	Table 3.1; 4.3.6; 4.5.1
Clean sandstone	"stepped" laminated	Cs4	Tb3	HDT	Table 3.1; 4.3.6
Clean sandstone	Massive, normally graded	Cs5	Ta	HDT	Table 3.1; 3.6.1; 4.3.6
Clean sandstone	Massive, ungraded	Cs6	Ta, Dcs	HDT/LDF	Table 3.1; 3.6.1; 4.3.6
Clean sandstone	Swirly	Cs7	Dcs	LDF	Table 3.1; 3.6.1; 4.3.6
Muddy sandstone	Matrix supported with floating clasts	Ms1	Dm1	CDF	Table 3.1; 4.3.6

Muddy sandstone	Matrix supported without floating clasts	Ms2	Dm2	CDF	Table 3.1; 4.3.6
Siltstone	Laminated	Si1	Td	LDT	Table 3.1;
Siltstone	Unstructured normally graded	Si2	Td	LDT	Table 3.1;
Siltstone	Massive and ungraded	Si3	Td	LDT/CDF	Table 3.1;
Mudstone	Massive dark (turbidite)	M1	Te1, Te2, Te3	LDT/FML	Table 3.1; 4.3.6; 5.2.2
Mudstone	Massive calcareous (hemipelagite)	M2	Te (hemipelagite)	Settling from the water column	Table 3.1; 4.3.6; 5.2.2

Table 1.1. *Summary table comparing the facies scheme adopted in this thesis to the widely used Bouma's (1962) sequence as modified by Talling et al. (2012). LDT - low density turbidity current; HDT – high density turbidity current; LDF – liquefied debris flow; CDF – cohesive debris flow; FML – fluid mud layer. Each depositional interval (based on lithology and sedimentary structure observed) is discussed in the corresponding section of the thesis.*

1.7. CONTRIBUTION BY AUTHORS TO CHAPTERS

Chapter 3: Giuseppe Malgesini: principal investigator and main author. Peter J. Talling: fieldwork assistance, discussion, manuscript review. Fabrizio Felletti: fieldwork assistance, discussion.

Chapter 4: Giuseppe Malgesini: principal investigator and main author. Peter J. Talling: discussion, manuscript review.

Chapter 5: Giuseppe Malgesini: principal investigator and main author. Peter J. Talling: fieldwork assistance, discussion, manuscript review. Alessandra Negri: biostratigraphic analysis. Lawrence Amy: fieldwork assistance. Sam D. Murphy: fieldwork assistance.

Chapter 6: Giuseppe Malgesini: principal investigator and main author. D.M. Hodgson: logistic and fieldwork assistance, discussion. Emma Morris: fieldwork assistance, discussion. Peter J. Talling: manuscript review.

CHAPTER 2:
GEOLOGICAL SETTINGS OF THE NORTHERN APENNINES AND THE MARNOSO ARENACEA FORMATION

2.1 STRUCTURE AND EVOLUTION OF THE NORTHERN APENNINES

The Northern Apennines represent a part of a fold and thrust belt developed from the Upper Oligocene in relation to the geodynamic evolution of the Mediterranean area; its formation was controlled by the interaction between the European and African plate, and the micro-plates Iberia and Adria (Ricci Lucchi, 1986; Boccaletti et al., 1990; Argnani & Ricci Lucchi, 2001). The Northern Apennines are structurally divided into two sectors (figure 2.1): the western sector is formed by the igneous and metamorphic basement and by ocean-derived deposits (Ligurian Nappe).The Eastern sector includes Mesozoic and Cenozoic deposits previously deposited on the Thetis passive margin during the Jurassic and Cretaceous (Klingfield, 1979).

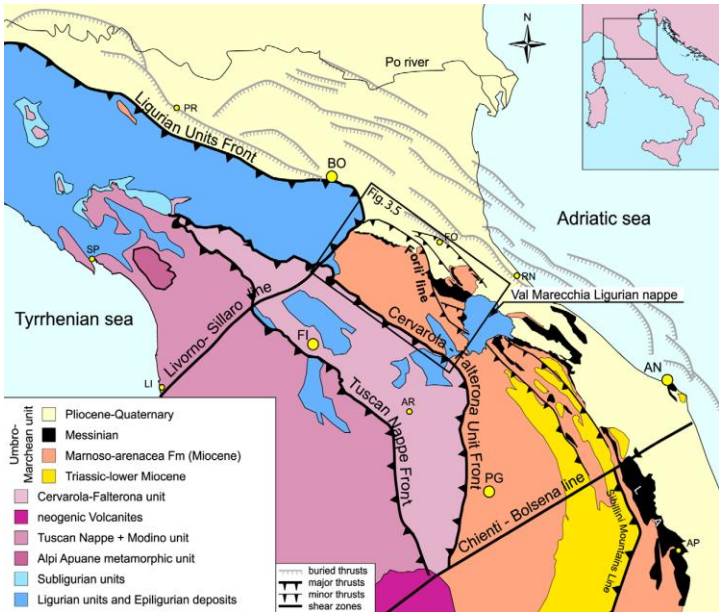

Figure 2.1. *Simplified geological map of the northern Apennines (from Mutti et al., 2002).*

During the Lower Cretaceous, the North Atlantic rifting caused the Adria and European plates to converge. The European plate began to subduct beneath the Adria plate along the northern (Alpine orogenesis) and eastern (Dinaric orogenesis) margin. At the same time the Adria and Iberia plates started to converge, producing the Apennine orogenesis (Roest and Srivastava, 1991).

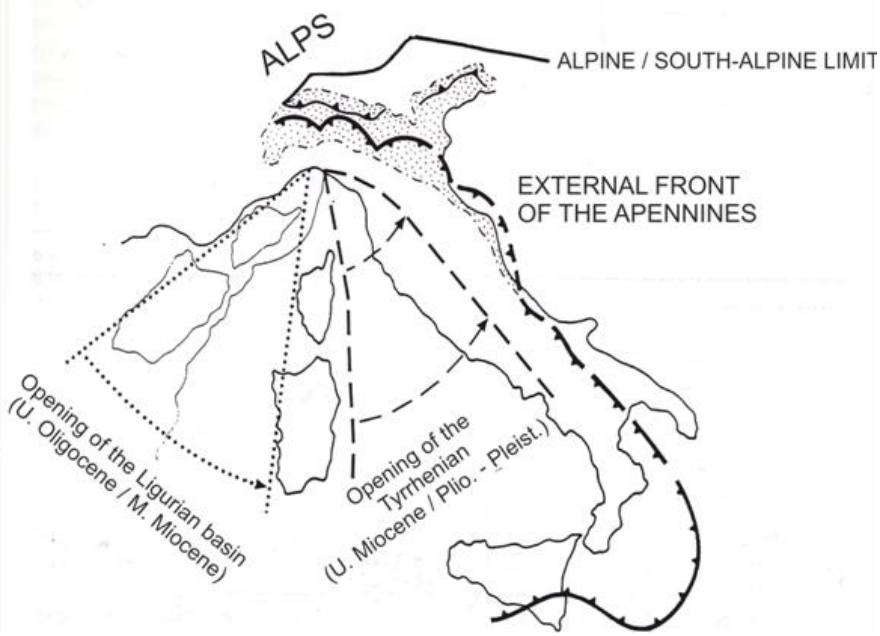

Figure 2.2 *Evolution of the Apennines area. The Apennine orogeny is strictly connected to the opening of the Ligurian basin (Upper Oligocene – Middle Miocene) and of the Tyrrhenian Sea (Upper Miocene – Plio-Pleistocene). Modified from Gasperi (1995).*

This convergence caused the formation of an orogenetic wedge, which includes inner units formed near the European margin and outer unite formed near the Apulo margin (Figure 2.1). Inner (Ligurian) units originated in an ocean, and possibly in the thinner part of the adjacent continental margins. These units were successively partially subducted and overthrusted from West to East, on the outer portion of the chain. Outer units represent the sedimentary cover of the Apulo margin (south-eastern), which was originated by the spreading of the Ligurian Ocean (Roest and Srivastava, 1991). The continental collision started in the Medium-Upper Eocene (meso-alpine phase). The oceanic lithosphere was entirely consumed under the European craton, and the ensuing Apenninic orogeny is thus called “post-collisional” and explained by ensialic or A-type subduction (Kligfield, 1979

2.2. THE ROMAGNA APENNINES

The Romagna Apennines extend from the Sillaro valley to the west up to the Marecchia Valley to the east (figure 2.3). They are characterized by siliciclastic deposits of early Miocene to Pleistocene age that overly Mesozoic to Cenozoic carbonates (Roveri et al., 2002). These carbonates have only been studied in hydrocarbon wells (Di Base & Mutti, 2002). This sedimentary succession represents the lowest structural unit of the Apennine orogenic wedge (Vai, 2001). West of the Sillaro Valley this tectono-stratigraphic unit is covered by the Ligurian Nappe, a chaotic complex composed of Jurassic to Eocene deep-marine sediments and mélange, or accretionary wedge, slabs of their oceanic crust basement (figure 2.3). This formed during the late Cretaceous eo-Alpine compressional phase and was subsequently thrust over the Adria plate during the Apennine orogeny in the Oligocene (Klingfield, 1979; Boccaletti et al., 1990; Pini, 1999). The Marnoso Arenacea Formation is detached from its lower Miocene carbonate basement along a basal flat thrust, and shows a deformational style dominated by fault propagation folds (Capozzi et al., 1991).

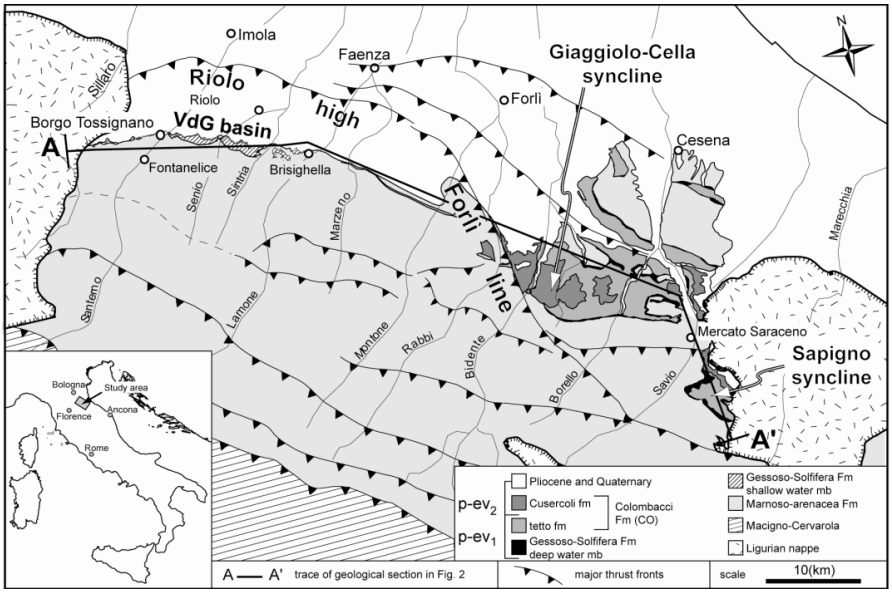

Figure 2.3. *Geological map of the Romagna Apennine. From Roveri et al. (2003).*

The inner, southern part of the Marnoso Arenacea Formation is overridden by a complex of older turbiditic units (Macigno and Cervarola formations) along a thrust front approximately

corresponding to the watershed of the Apennine chain. The axes of the thrust folds plunge toward the north-west and the south-east approaching the Sillaro and Marecchia valleys (figure 2.3). These two valleys represent tectonic depressions occupied since the early Pliocene by Ligurian units, whose emplacement mechanism (whether related to thrusting or gravity sliding) is still debated (De Jager, 1979; Ricci Lucchi and Ori, 1985). The outer, less deformed northern sector consist of a gentle north north-east dipping homocline of Messinian to Pleistocene deposits overlying the Marnoso Arenacea Formation. The Romagna Apennines can be split into two sectors (western and eastern) by the Forli' line (figure 2.3), a complex deformational belt characterized by reverse faults stretching normal to the Apenninic trend (NNE-SSW). This tectonic feature played a primary role in the geological evolution of the area, at least since the late Tortonian (Ricci Lucchi, 1986), but particularly during the Messinian (Roveri et al., 2002).

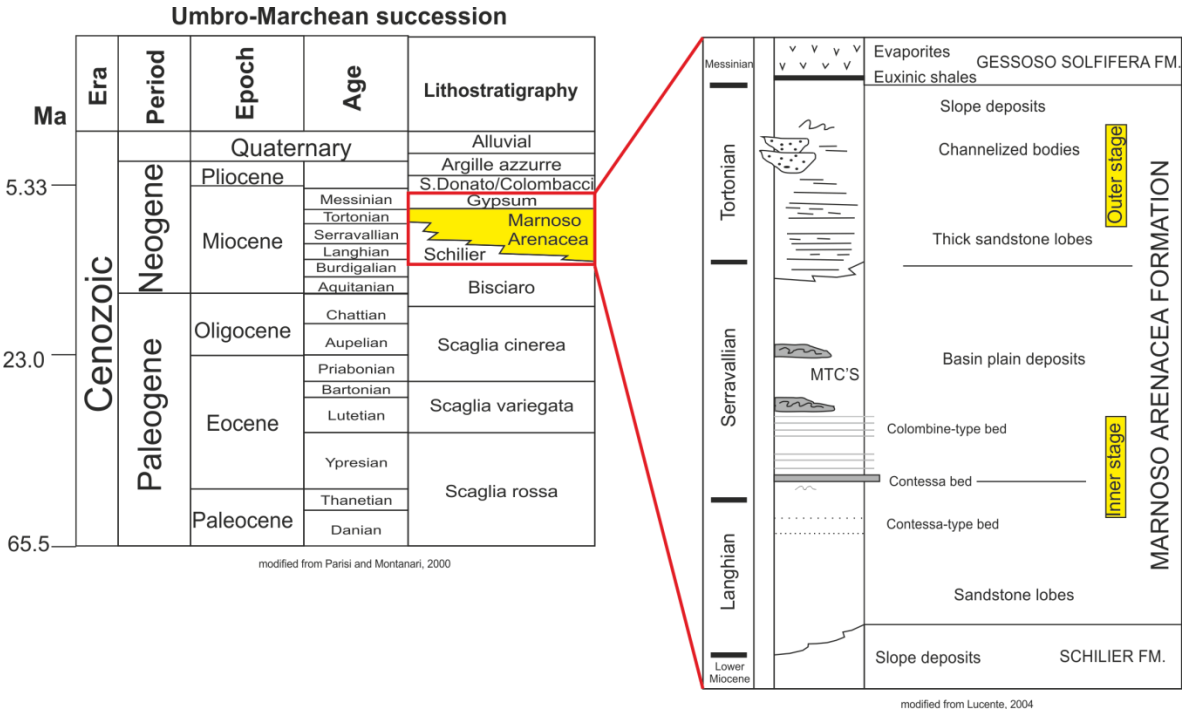

Figure 2.4 . *Schematic stratigraphic log of the Cenozoic Umbro-Marchean succession and detail of the Miocene Marnoso Arenacea formation. Modified from Parisi and Montanari (2000) and Lucente (2004).*

2.3. THE MARNOSO ARENACEA FORMATION

The Marnoso Arenacea Formation is late Burdegalian to Tortonian in age (*ca* 17-7 Ma) and crops out in the northern Italian Apennines (figure 2.1). It represents one of a series of foredeep basins that progressively migrated towards the north-east, in response to thrust front migration in the same direction (Ricci Lucchi & Valmori, 1980; Gandolfi et al, 1983; Ricci Lucchi, 1986; Van Warmenel & Zwart, 1990; Martelli et al., 1994; Roveri et al., 2002; Di Base & Mutti, 2002; Mutti et al., 2002; Lucente, 2004; Amy & Talling, 2006). The late Oligocene Macigno Formation and the early Miocene Cervarola Formation represent the fill of older foredeep basins located further to the south-west, and crop out in the innermost belt of the Apennine chain, while the younger Messinian to Pleistocene basin fills are buried below the Po Plain and the Adriatic Sea (Pieri and Groppi, 1986). Deposition within each foredeep was typically accompanied by shale-rich deposition within associated thrust-top basins (Fig. 2.4). Marls cap the sequence within each foredeep and drape the flexural margin. Eventually, these thrust-top and foredeep basins were overthrust by Ligurian and Subligurian units, with oceanic affinity, derived from significantly further to the west (figure 2.3; Ricci Lucchi, 1981, 1986; Martelli et al., 1994; Cerrina Feroni et al., 2001; Mutti et al., 2002; Zattin et al., 2002).

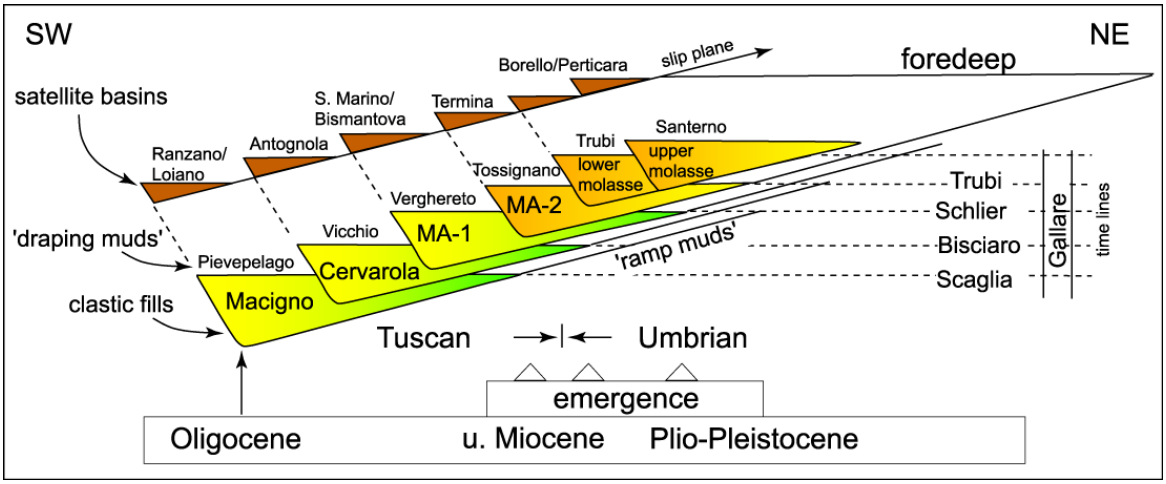

Figure 2.5. *Tectono-stratigraphic diagram showing the migration of the foredeep-thrust system of the northern Apennine (from Mutti and Di Base, 2002; modified after Ricci Lucchi, 1986).*

Deposition in the Marnoso Arenacea foredeep is subdivided into an 'inner stage' and an 'outer stage' (Ricci Lucchi, 1986). The strata analysed in this study were deposited during the inner stage. Inner-stage deposits are older (Late Burdegalian to Serravallian) and form the north-west (i.e. 'inner') part of the Marnoso Arenacea outcrop (figure 2.5).

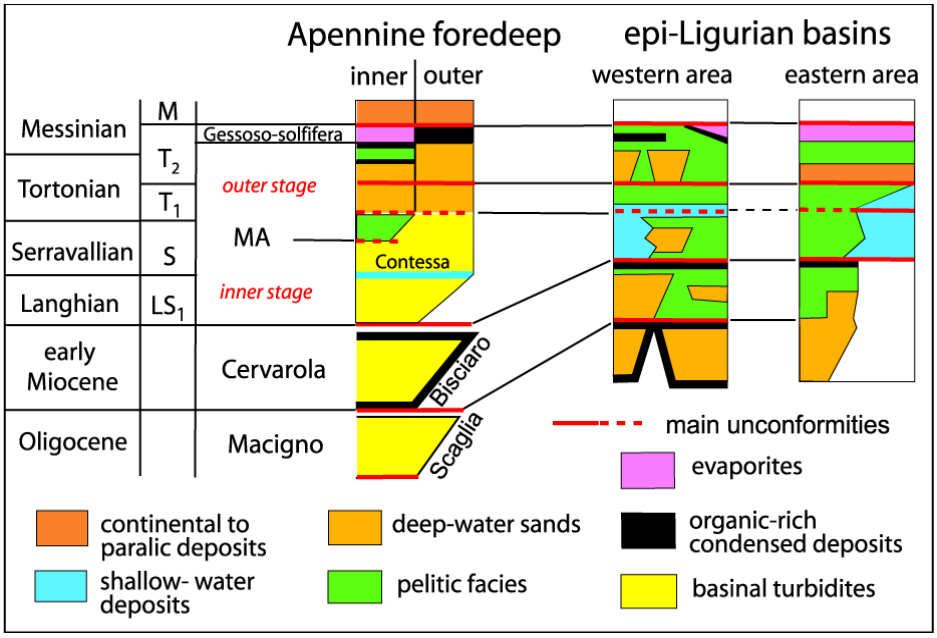

Figure 2.6. *General physical-stratigraphic framework of the Apennine foredeep basin showing the good correlability of the main sequence boundaries with epi-Ligurian basins successions (from Mutti and Di Base, 2002. Modified after Ricci Lucchi, 1986).*

The basin fill of the inner stage is wedge shaped; thinning to the north-east, in cross sections orientated normal to the thrust front (figure 2.6). Such thinning of the basin fill, towards the flexural ramp, is typical of foreland basins. Foreland basin deposits extend for more than 300 km along the basin axis, but the strata crop out only for ca 170 km to the south-east of the Santerno Valley. Further to the north-west, in the Emilia Apennines and Po Plain, bore holes and seismic profiles demonstrate that the strata are buried beneath Ligurian and Epiligurian units and alluvial sediments (see references in Cerrina Feroni et al., 2001 and Argnani & Ricci Lucchi, 2001). Inner-stage deposits also thin markedly to the south of the Perugia-Gubbio Line (Ricci Lucchi & Valmori, 1980). During this period, the foredeep was relatively wide (> 60 km) and unchannelized (Ricci Lucchi & Valmori, 1980).

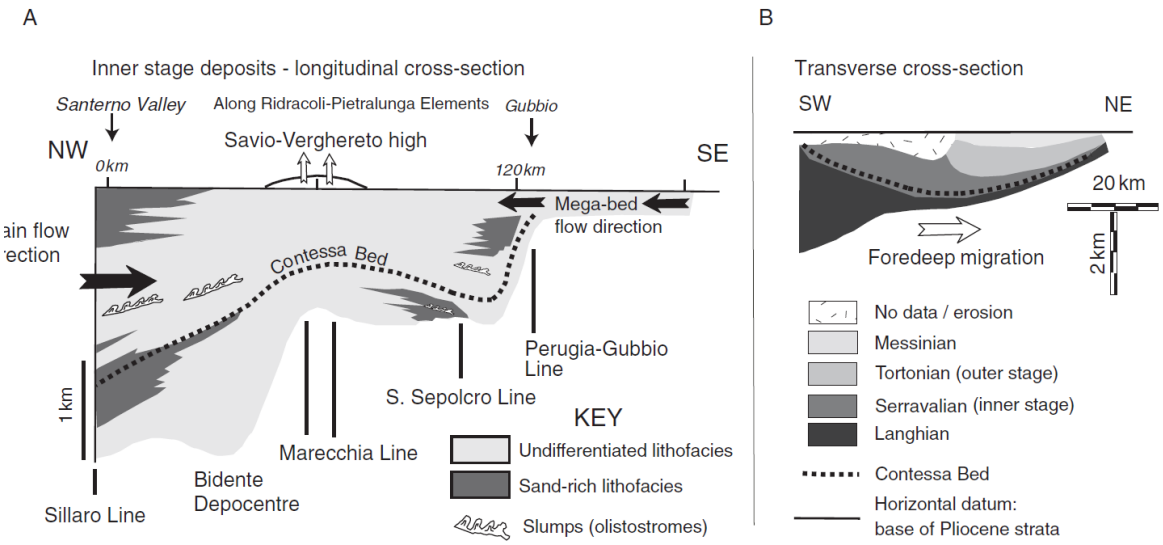

Figure 2.7. *Summary of the stratigraphy of the Marnoso Arenacea foredeep basin. (A) Cross section along the basin axis showing stratigraphic relationships within the inner-stage deposits (after Ricci Lucchi & Valmori, 1980). The line of section is approximately parallel to flow direction in most beds. (B) Transverse section normal to the basin axis, showing lateral migration of the infill of the Marnoso Arenacea foredeep during both 'outer' and 'inner' stages. Lateral migration of the foredeep reflects lateral migration of the coeval Apennine thrust front (after Ricci Lucchi, 1986).*

Disruption of the foredeep by thrust faults caused the transition to the outer stage, during which channelized deposition occurred locally within a narrower basin. Strata comprising the outer stage form the north-eastern (i.e. 'outer') part of the outcrop area. Deposition of the Verghereto Marls indicates closure of the Serravallian inner basin. During the Inner stage flows were able to transverse this basin plain in opposite directions. Most flows entered the basin from the north-west and originated from the Alpine and Apennine orogens (Gandolfi et al., 1983). A number of particularly large flows with a distinctive carbonate-rich composition occasionally entered the basin plain from the south-east, covering the entire outcrop area and producing laterally extensive "mega-turbidites" that are useful as stratigraphic marker horizons (Ricci Lucchi & Valmori, 1980; Martelli et al., 1994). The thickest mega-turbidite is called the Contessa Bed and it is formed of limestone fragments and Apennine-derived lithic fragments. It is an excellent marker horizon because of its unusual thickness, distinctive composition and palaeocurrent direction. The Contessa Bed was deposited between ca 14 and 14.5 Ma in the earliest Serravallian (Van Wamel & Zwart, 1990), and it is interpreted to have originated from the collapse of a limestone platform

that bounded the basin at its south-east margin (Gandolfi et al., 1983). This study analyses the stratigraphic interval immediately below the Contessa Bed. This interval was deposited in a relatively flat basin plan, as inferred from the ability of the flows to transverse the area in opposite directions, the absence of channelization and the continuous sheet-like general bed geometry (Ricci Lucchi & Valmori, 1980; Amy & Talling, 2006; Talling et al., 2007a). North-west to south-east orientated thrust structures subdivide the outcrop area into tectonic elements, with the major periods of deformation occurring after deposition of the stratigraphic interval studied here (figure 2.6; Martelli et al., 1994; Lucente, 2004; Talling et al., 2007).

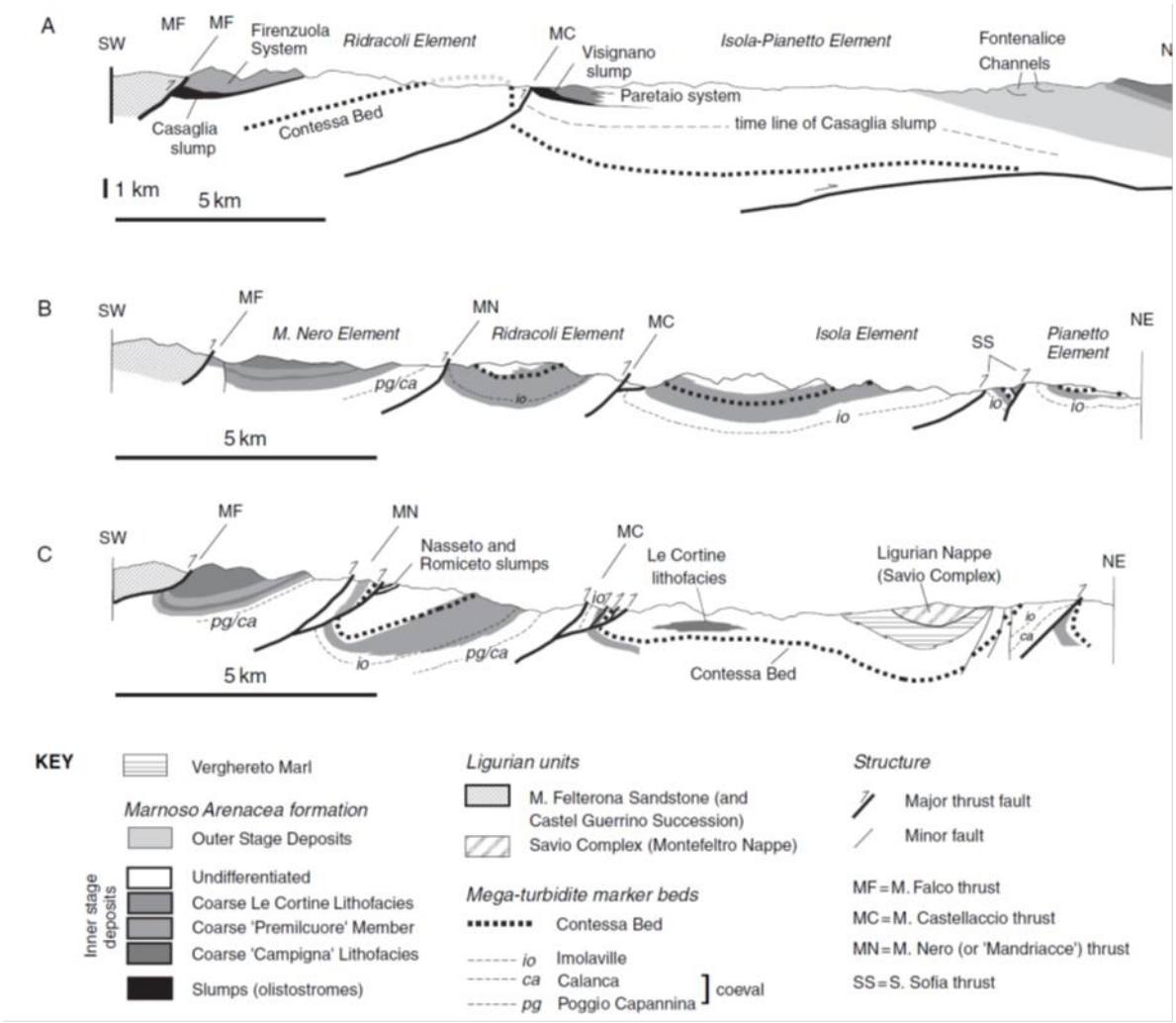

Figure 2.8. *Detailed structural cross sections transverse to the basin axis in the vicinity of the Santerno (A) Bidente (B) and Savio Valleys (C) showing the position of major thrust faults that subdivide the outcrop into structural elements. (From Roveri et al., 2002 and RER, 1994.)*

CHAPTER 3:
CAN LIQUEFIED DEBRIS FLOWS DEPOSIT CLEAN SANDSTONE OVER LARGE AREAS OF SEA FLOOR? FIELD EVIDENCE FROM THE MARNOSO ARENACEA FORMATION, ITALIAN APENNINES

3.1. INTRODUCTION

Submarine gravity flows dominate sediment transport into many parts of the deep ocean and produce submarine fans that are some of the largest sediment accumulations on Earth (Allen, 2007; Talling *et al.,* 2007a). Ancient flows of this type have deposited thick rock sequences that now hold some of the World's largest oil and gas reserves. These flows are capable of depositing relatively thick (0.5 to 3 m) layers of sand across large areas of the deep sea floor, and these layers are a major building block of submarine fans. These sand layers often contain thick intervals of relatively clean sandstone with low interstitial mud content that lack sedimentary structures such as planar or cross lamination; and these intervals are often referred to as the T_A division of Bouma's (1962) sequence.

The process involved in deposition of massive clean sand can be very difficult to determine unambiguously based on Information derived from a single outcrop. This ambiguity is one of the reasons for continued debate over the origin of massive clean sandstone. As noted by Stow and Johansson (2000), the only sediment-gravity processes able to transport relative coarse material over long (10's of kilometers) distances on low gradients and deposit massive sandstone layers are high-density turbidity currents and (sandy) debris flows. The ability of sandy debris flow to transport sand over long distances on low-gradient deep basin plains has been highly debated (Shanmugam and Moiola, 1995 and seven replies) and widely rejected, possibly because a lack of sufficiently convincing field data.

The Miocene Marnoso-arenacea Formation is very unusual in that individual flow deposits (beds) can be correlated over a large area (up to 120 x 30 km) between numerous (up to 109) individual outcrops (figure 3.1; Ricci-Lucchi & Valmori, 1980; Amy & Talling, 2006; Talling et al., 2007b). The correlated beds were deposited in a relatively flat basin plain without channels (figure 3.2). A series of distinctive marker beds that occur every 20 to 30 meters, and the almost complete lack of erosional bed amalgamation greatly simplify the correlation of intervening beds (Ricci-Lucchi & Valmori, 1980; Amy & Talling, 2006; Talling et al., 2007b). The

marker beds have been mapped out precisely by the Emilia-Romagna, Umbria and Marche geological surveys over many years (e.g. Martelli et al., 1994). Beds are consistently separated by intervals of hemipelagic mudstone (Talling et al., 2007b). The bed correlations in the Marnoso-arenacea are important because they provide the additional information needed to better constrain how massive clean sand is deposited by submarine density flows (Amy et al., 2005; Amy & Talling, 2006). This information comprises the external shape of clean sandstone intervals and the internal bed architecture, with the latter showing how various types of clean sand in a single bed are arranged in down-flow trending "facies tracts" (Mutti, 1992). This additional information provides an independent test of sand depositional models, which are based initially on features visible at the scale of a single outcrop.

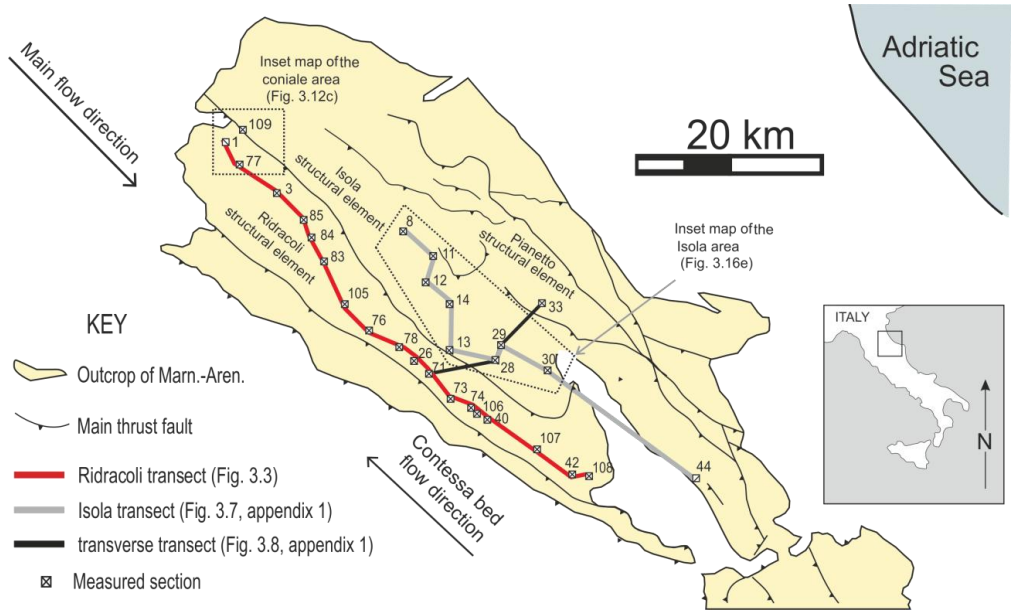

Figure 3.1. *Location map showing the northern part of the outcrop of the Marnoso-Arenacea Formation. The figure shows the position of measured sections and the transect panels presented in subsequent figures. The Ridracoli element Transect is shown in Fig.3.3. The Isola element transect is shown in Fig.3.7 and in appendix 2. The transverse cross section transect is shown in Fig. 3.8 and in appendix 3. Sections are numbered as follow: 109-Cabelli River, 1-Cabelli, 77-Mantigno, 3-Aquadalto, 85-Cavalmagra, 84-Marradi 2, 83-Marradi 1, 105-Il bagnato, 76-Gemelli, 78-Fiumicello Zohotecnica, 26-Lavacchio, 71-Corniolo, 73-Ridracoli2, 74-Ridracoli3, 106-Ridracoli4, 40-Pietrapazza, 107-Valanello, 42-Bagno di Romagna, 108-Poggio Pandella, 8-Poggio Dornata, 11-Montefreddo, 12-Bocconi, 14-Monte Roncole, 13-Premilcuore, 28-Badia, 29-Cabelli, 30-Isola, 44-Castel Priore, 33-Galeata.*

3.2. AIMS

Amy & Talling (2006) and Talling et al. (2007a; 2007b) correlated individual flow events between 109 locations for a ~30 m thick interval of strata immediately above the most prominent mega-turbidite marker bed, called the Contessa Bed.

The first aim of this chapter is to use the new bed correlations in a second interval of strata immediately below the Contessa Bed (figure 3.4a) to understand how submarine flows evolve in the deep ocean. Three main types of bed geometry occur in the new stratigraphic interval, and only two of these bed geometries were recognized in previous work. The second aim is to understand how relatively thick (>1m) clean sandstone layers that pinch out abruptly at their margins form within a basin plain. Our third aim is to understand how such liquefied clean sand debris flows could originate. Two sets of previous studies have inferred that clean sand can be deposited by dense liquefied flow (Mutti, 1992; Mutti et al., 2003 & 2009) or debris flow (Shanmugam & Moiola, 1995, Shanmugam, 1997, 2000, 2002) although they lacked detailed information on sandstone interval shape to test such models. Our fourth aim is to compare clean sandstone debrites in the correlated beds to the deposits that these authors described, and to determine whether similar or different criteria are used to infer deposition from liquefied debris flow.

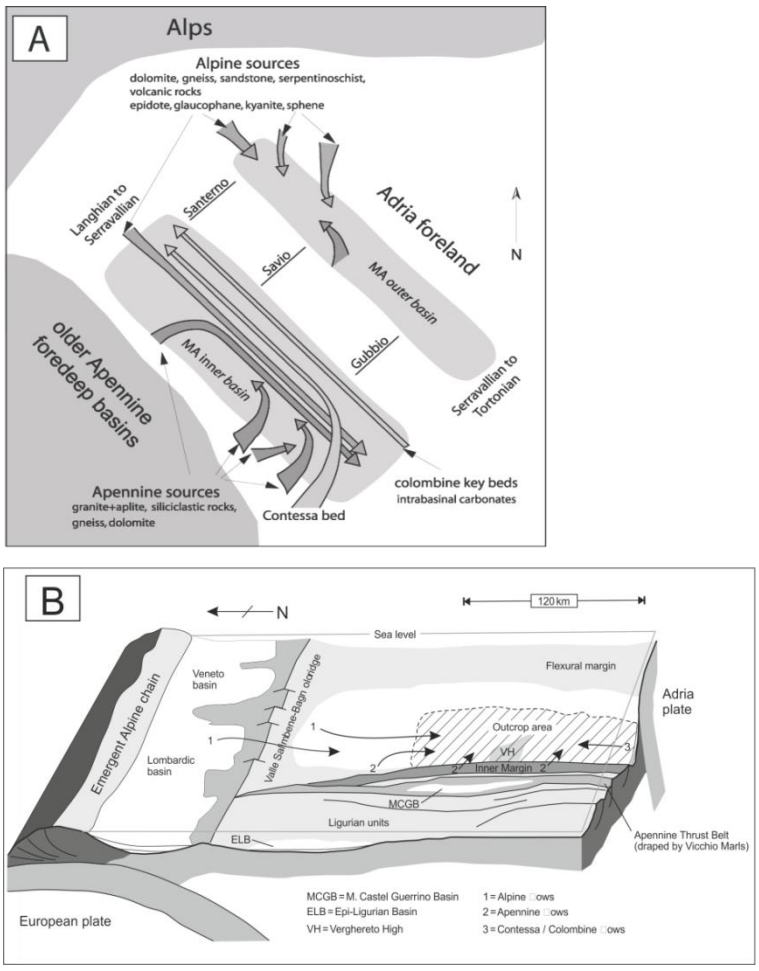

Figure 3.2. *A) Map showing the main sediment sources and dispersal patterns of the Marnoso-arenacea foredeep basin in its different evolutionary stages (after Mutti et al., 2002). B) Schematic paleogeographic reconstruction of the Marnoso-arenacea foredeep basin during the Serravallian (after Di Base & Mutti, 2002).*

3.3. TERMINOLOGY

3.3.1. Turbidite and Debrite

The term *turbidite* is here used to denote a deposit formed incrementally in a layer by layer fashion by a *turbidity current* from which larger grains preferentially settle (Amy and Talling, 2006; Talling et al., 2007a). A graded deposit (unless flow is perfectly steady), low interstitial mud content and outsize mud clasts occurring along discrete horizons (if they are present) are considered diagnostic features of such differential settling and incremental deposition. Turbidity currents deposits tend to have a gradually tapering shape in areas of subdued topography (Talling et al. 2007a; see also chapter 4).

The term *debrite* refers to a deposit formed en-masse by a *debris flow*. En-masse deposition occurs through rapid deceleration ('freezing') of the flow, and debrites tends to pinch out abruptly at their margins. Material at the sides or front of the flow can come to a halt first with the center of the flow remaining fluid for longer, such that en-masse 'freezing' of the flow is not instantaneous (Middleton and Hampton, 1973; Iverson et al, 1997). A debris flow does not segregate the majority of larger and smaller grains by differential settling during deposition (Talling et al., 2007a), although outsize clasts may settle and the uppermost part of the debris flow deposit may be reworked (Talling et al., 2012a). The four criteria used to infer en-masse settling are: a general lack of vertical grading (although outsize clasts and uppermost part of the debrite may sometimes be graded), relatively high interstitial mud content within sand, lack of sedimentary structures formed by bed load reworking, and a sharp grain size break at the top of the debrite interval. If mud clasts are present, they are distributed chaotically.

Turbidites (especially high-density turbidites deposited incrementally and rapidly) may show evidence of dewatering and liquefaction (Lowe, 1982), but this occurs in-situ after the deposit has come to a halt.

In a debris flow relatively small amounts of fine material can reduce permeability by several orders of magnitude (Coussot, 1997). These reductions in permeability will favor the retention of high excess pore pressures that can promote liquefaction (Iverson et al. 2010); therefore liquefaction and high pore pressures also occur as the sediment is being moved laterally down-slope. Cohesive mud also impart significant yield strength to the sediment-water mixture, preventing sand settling (Amy et al., 2006; Sumner et al., 2009). Cohesive mud content also

strongly influences whether the flow state is turbulent or laminar, whether bedforms develop, and whether transitions occur from turbulent to laminar flow as the flow decelerates and a network of cohesive bonds become better established (Talling et al., 2007a; Sumner et al., 2009)

Turbidite deposition occurs incrementally from a near-bed layer that is relatively thin, and this near bed layers is driven by the overlying flow. In contrast, a debris flow is driven down slope primarily by its own weight (and not an overlying flow), and its deposit thickness more closely resembles the thickness of the flow (Talling et al., 2012a)

3.3.2. Clean and muddy sandstone

The terms *clean* sand and *mud-rich* sand are used in this contribution to describe the relative amount of interstitial fine mud within sandstone intervals. The amount of fine mud within a sandstone interval is important for two reasons. First, it strongly influences the permeability and petroleum reservoir quality of the sandstone. Second, mud with cohesive properties strongly influences flow behavior. Cohesive (colloidal) bonds between mud particles become increasingly important as grain sizes decrease below ~40 to 10 μm (McAnally et al., 2007). However, the value of this threshold grain size also depends on mineralogy, as does the strength of the bonds (Shaw, 1992; Coussot, 1997; McAnally et al., 2007). Here we use a threshold grain size range of 20 μm for estimating the volume fraction of cohesive fine mud. We acknowledge that our measurements do not constrain the mineralogy of the fine mud fraction, and that some of the fine mud grains may be non-cohesive. The way in which grain size is measured can cause significant variations in estimated fine-mud content. For instance, it is difficult to compare measurements of grain diameters made from disaggregated samples or from images of thin sections (in which grains are sliced thereby reducing their measured diameter), or from images of thin sections with different resolutions made using optical or scanning electron microscopes. Our approach is to compare estimates of fine-mud content measured using the same technique for the same beds. *Clean sandstone* denotes relatively low volume fractions of fine-mud, such as those seen in sandstone intervals deposited by turbidity current. Clean-sand debrites would therefore contain a similar volume fraction of fine-mud as many turbidite sandstones. Conversely, *mud-rich sandstone* has a higher interstitial mud fraction than that commonly found in turbidite sandstone.

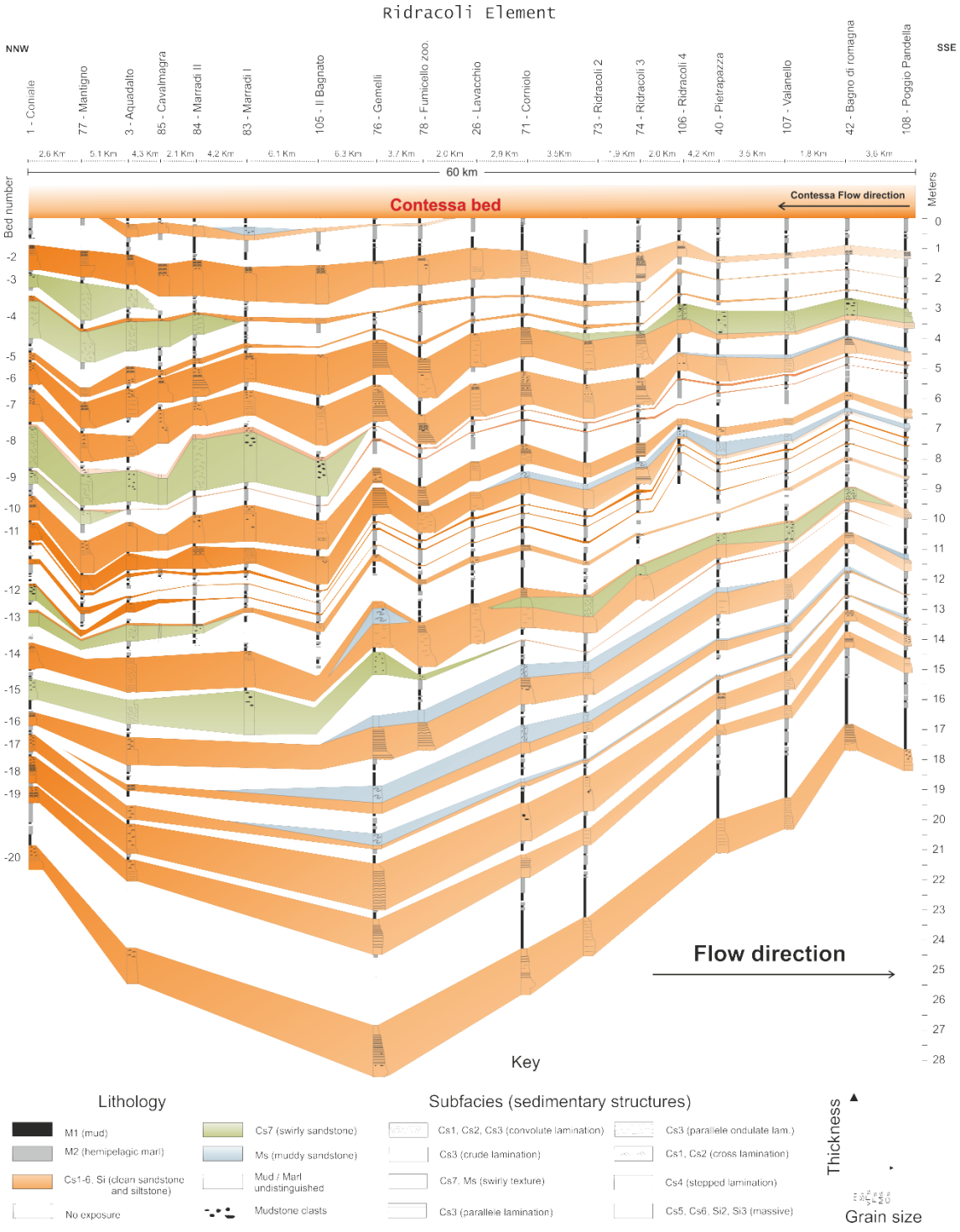

Figure 3.3. *Cross-section along the Ridracoli element showing the correlation of the first 20 thick (>40 cm) beds below the Contessa marker bed. Key is provided. Fig. 3.1 shows the location of the transect. The correlation panel is oriented approximately parallel to the paleoflow direction (Fig. 3.5). The paleoflow direction is north-west to south-east for all the correlated beds, but in the opposing direction for the Contessa marker bed.*

Sorting

Clean sandstone according to the definition adopted here can have large variations in sorting. Many of the clean sandstones described in this study have poor sorting, with standard deviations of 300 long axis measurements ranging up to 300 µm, for average grain long axes of up to 400 µm (see figure 3.9b). As these grain size measurements are for sliced grains (Johnson, 1994), and do not include the fine tail of grains < 20 µm, we do not use Folk and Ward's (1957) equation for sorting of disaggregated grains. Use of standard deviation of long axis measurements follows that of Sylvester and Lowe (2004).

3.4. METHODOLOGY

3.4.1. Sedimentary logs

Nineteen sections were logged in a down-flow transect along the Ridracoli structural element, and a further nine sections were logged within the Isola and Pianetto structural elements (figure 3.1).. Sections were logged at a scale of 1:10, and selected beds (bed 0, 5, 5.1) in the Above Contessa interval have been re-logged at a scale of 1:5. Grain size was estimated in the field using a grain-size comparator. Palaeocurrent directions (figure 3.5) were measured using flutes and grooves on the base of thick beds. Correlations are based on pattern matching of complex vertical bed sequences. Beds are constantly separated in each section by hemipelagic mudstone intervals, and bed amalgamation is extremely rare. Distinctive features occur consistently within the same bed in adjacent sections.

A bed-numbering scheme was adopted that is similar to the scheme used by Ricci-Lucchi and Valmori (1980) such that thick (> 40 cm) beds are numbered sequentially from -1 to -37. Sections on the Ridracoli structural element extended from the Contessa Bed to Bed -20 (Bed A-20 in the scheme of Ricci Lucchi & Valmori, 1980), whilst sections logged on the Isola and Pianetto elements extended down to the Fiumicello Bed (Bed -37).

3.4.2. Sedimentary facies scheme

The facies scheme adopted in this paper (table 3.1) is modified from the scheme proposed by Amy and Talling (2006). This scheme provides a simple tool to describe flow deposits in the correlated interval. It describes strata hierarchically as: (i) lithofacies based on

the dominant lithology and (ii) sub-facies based on sedimentary structures and grading patterns. A series of lithofacies and subfacies therefore define the internal architecture of an individual bed.

Lithofacies and *Subfacies*	*Grain size*: Mud / Silt / Vf. Sand / F. Sand / M. Sand / C. Sand; *Thickness*: Cm. / Cm. - m / > m.	*Description*	*Interpretation*
CS Litofacies: Clean Sandstone *Cs1: Ripple cross-laminated*		Thin laminae (< 3 mm.), commonly convolute or wawy Interval normally grade or ungraded.Common in thin (< 40 cm.) sandstones and in the upper part of m-thick sandstones.	Deposition from a traction-dominated flow-boundary zone. The current was sufficiently diluite to form ripples; relatively diluite and turbulent throughout. Equivalent to Bouma Tc division (Bouma, 1962).
Cs2: Dune cross laminated		Occour in thick sandstone beds typically near the top of bed, common below MS intervals. 1-2 mm. thick laminae. Bed forms have wawe-lenghts between 0,2-0,9 m. normally graded or ungraded clean sandstone interval. Isolated or climbing dune bedforms.	Deposition from a traction-dominated flow-boundary zone. The current was sufficiently diluite to form bedforms. Relatively diluite and turbulent throughout. (Dune scale cross-lamination of Ricci Lucchi and Valmori (1980); see theyr Fig. 4).
Cs3: parallel lamination - planar or gently undulating		Occour in thick sandstone beds typically above Cs5 and Cs6, and below Cs1 or Cs2. Typically 1 mm. or less thick (unlike Cs6). Normally graded clean sandstone intervals.	Deposition from a thin near bed zone with high sediment concentration dominated by grain to grain interactions. Lamination formed by repeated collapse of high concentration near bed layers or by traction within upper stage planar bed regime. Equivalent to Bouma Tb division (Bouma, 1962).
Cs4: parallel to sub-parallel "stepped grain size" statification		Cm thick stratification or >5 mm thick laminae displaying step-like normal or inverse grading patterns. Occasional low angle wawy surfaces or truncations. usually at the base of thick and coarse sandstone beds.	A) Deposition from an unsteady traction-dominated flow boundary beneath a relatively diluite and turbulent current. B)Deposition from a modified grainflow layer under unsteady flow conditions. Successive traction bed load grain layers (traction carpet sedimentation). SGF with a basal flow boundary dominated by grain interactions and/ or hindered settling. Equivalent to Lowe S2 division (Lowe, 1982).
Cs5: Unstructured normally graded		Grading pattern may be subtle (< 1 phi). Common in thick and thin sandstone beds. Usually located at the base of the bed, or separated from base of bed by CSX. Gradual grading at upper interval boundary.	Rapid suspension fall-out from a waning current with near bed zone dominated by grain to grain interactios. Overlying flow can be diluite and fully turbulent. Structurless deposits can form by repeated collapse of high concentration near bed layers . Equivalent to Bouma Ta (Bouma, 1962).
Cs6: Unstructured and ungraded (massive)		Devoid of structure or grading. Sharp grain size break at upper surface. Thin section analysis confirm similar mud content as other clean sandstone intervals.	A) "Suspension fall-out" from a steady current that is relatively diluite and turbulen throughout. B) Rapid deposition or "en-masse freezing" of a current with relatively high concentration where the basal flow boundary is dominated by grain interactions and/hor hindered settling.

Table 3.1. *Facies scheme adopted. Modified from Amy and Talling (2006).*

Lithofacies and *Subfacies*	*Grain size*								*Thickness*			*Description*	*Interpretation*
	Mud	Silt	Vf. Sand	F. Sand	M. Sand	C. Sand			Cm.	Cm. - m	> m.		
Cs7: swirly, predominantly ungraded												Swirly weathering and poorly sorted. Generally ungraded. Possibly weakly normally graded in the uppermost part. Sharp grain size break upper surface Can contain chaotically distributed mud clastsa, and large deformed clasts of sandstone. Patchy texture, with adjacent areas of coarser and finer grains. Thin section analysis confirm similar mud content to other clean sandstone lithofacies.	Rapid deposition or en-masse freezing of a current with relatively high sediment concentration throughout. Flow dominated by grain interactions and/or hindered settling.
MS Lithofacies: Muddy Sandstone													
Ms1: Matrix supported with floating clasts												Unclean grey hue and sticky when moist.Swirly fabric. Poorly sorted. Ungraded. Matrix supported. Usually <20% clasts. Millimetre to metre sized clasts of mudstone and marl, less commonly sandstone. Size and composition of clasts vary spatially. Often an abundance of micas and organic particles. Upper contact displays a sharp grain size discontinuity.	Cohesive flow with sufficiently high sediment concentrations to inhibit segregation of particles of different sizes; en-masse sedimentation.
Ms1: Matrix supported with floating clasts												Unclean grey hue and sticky texture. Poorly sorted, usually ungraded. Often with an abundance of micas and organic particles. Swirly, sheared-like fabric. Sharp, planar upper contact showing a break in grain size.	Cohesive flow with sufficiently high sediment concentrations to inhibit segregation of particles of different sizes; en-masse sedimentation.
Si Lithofacies: Siltstone													
Si1: Laminated												Planar or undular parallel laminated "fissile" silt. Often contains large amounts of organic fragments and mm-sized platelets of mica.	Deposition from a traction-dominated flow-boundary zone beneath a dilute and turbulent current. Equivalent to Bouma Td (Bouma, 1962).
Si2: unstructured normally graded												Graded interval often found between very-fine sand and mud at the top of sandstone beds. Often contains large amounts of organic fragments snd micas.Displays a gradual grading at its upper surface.	Suspension fall-out under waning flow conditions. A dilute flow that was fully turbulent throughout.
Si3: unstructured and ungraded (massive)												Featurless silt often found at the top of sandstone beds. Often contains large amounts of organic fragments and mm-sized platelets of micas. Similar to Ms2 but finer.	a) Suspension fall-out under waning flow conditions. A dilute flow that was fully turbulent throughout. b) A current with a basal flow boundary dominated by grain interactions and/or cohesion and/or hindered settling.
M Lithofacies: Mudstone													
M1: massive dark (turbidite/debrite) mud												Grey colour, darker than marl. Devoid of structures or grading	Suspension fall-out from a static or slow-moving mud cloud probably involving a fluid mud layer. Final deposition from a sediment gravity flow ewent. Equivalent to Bouma Te division (Bouma, 1962).
M2: massive calcareous (hemipelagite) mud												Light grey bluish, calcareous, speckled appearance containing white foraminifer tests. Massive.	Settling of individual hemipelagic particles from the overlying water column.

Table 3.1. *Facies scheme adopted (continued).*

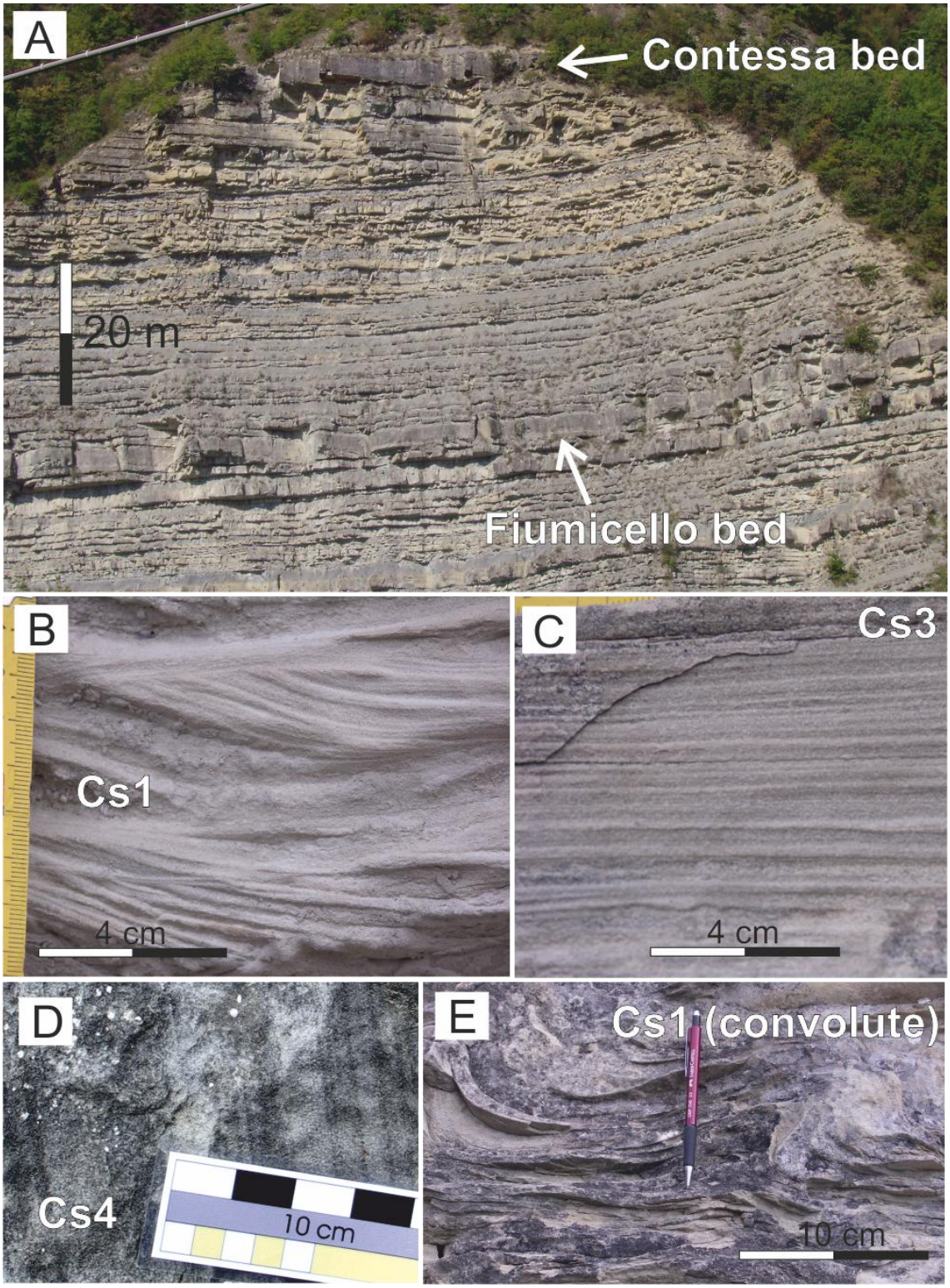

Figure 3.4. *Outcrop photograph illustrating the different types of sandstone deposits seen in the outcrops. See table 3.1 for description of subfacies Cs1, Cs3 and Cs4. A) Photo of the correlated interval near section 1 (Coniale) showing the position of the Contessa and Fiumicello marker bed. This section represents the most proximal outcrop for beds with provenance from the North-west. B) Detail of a ripple scale cross laminated sandstone interval (subfacies Cs1). Photograph from bed -7 in section 8 (Poggio Dornata). C) Detail of a parallel laminated sandstone interval (subfacies Cs3). Photograph from bed -7 in section 8 (Poggio Dornata,). D) Detail of a "stepped" laminated sandstone interval (subfacies Cs4). Photograph from bed -26 in section 44 (Castel Priore). E) Detail of a convolute ripple scale cross laminated sandstone interval (subfacies Cs1). Photograph from bed -20 in section 8 (Poggio Dornata).*

3.4.3. Textural data

Thin section analysis

Samples were taken to provide information about the textural characteristics of the deposits. A total of 70 samples were collected from beds -2 to -11 in the Mantigno section (section number 77 in figure 3.1). A further 82 samples were taken from Beds 2.5, 3 and 5.1 in the above Contessa interval. Vertical trends in grain size, sorting and matrix-mud content within these sandstone beds were quantified using images from a scanning electron microscope (SEM) in backscatter mode (figure 3.6). Three images with 150 times magnification were taken for each thin section. The longest axis of 100 grains coarser than 20 μm were measured each photo using image analysis software. Grain size data derived in this way from two dimensional slices through grains differ from the longest axis of grains (Johnson, 1994) but this technique provides a consistent method for documenting relative changes in grain size vertically through a bed (Talling et al., 2004). The mud-matrix content was measured for each image as the percentage area occupied by grains finer than 20 μm.

Large thin sections

Translucent slices of rock measuring 10 cm by 8 cm were made from samples of beds -2 to -11 in the Mantigno section. These "large thin sections" were viewed and photographed in transmitted light (figure 3.6). This technique facilitated the detailed study of sedimentary fabrics that are often difficult to discern in outcrops. See Garton & McIlroy (2006) for a full description of this technique. Large thin sections were especially useful to document the 'patchy' texture seen in Cs7 sandstones, which had previously been problematic to capture using optical or SEM images that produced highly irregular vertical grain size trends.

3.5. RESULTS

3.5.1. Bed correlations

Two dimensional bed geometry is shown by a series of vertical cross sections for the stratigraphic interval from the Contessa bed to either bed -20 or bed -37 (Fiumicello bed). Two sections (figures 3.3, 3.7 and appendix) are oriented approximately parallel to paleoflow along individual thrust elements. A single cross section is oriented across-flow along three different structural elements (figure 3.8 and appendix).

The bed numbering system continues from the numbering system adopted by Amy & Talling (2006) for the interval above the Contessa marker bed. Thick (locally >40 cm) beds are numbered. The first thick bed below the Contessa is numbered -1. The beds are numbered down to the stratigraphic lowest Fiumicello bed (Bed -37). Bed -20 is unusually thick and continuous over the entire study area. This bed is overlain by 40 to 70 cm of hemipelagic mud (figures 3.3, 3.7 and 3.8). For this reason it has been chosen as a marker bed for correlations along the Ridracoli structural element. Beds have been correlated between sections spaced typically every 2 to 5 km by empirical pattern matching of vertical bed sequences. Almost all (36 of 37) thick beds have been correlated over the entire study area.

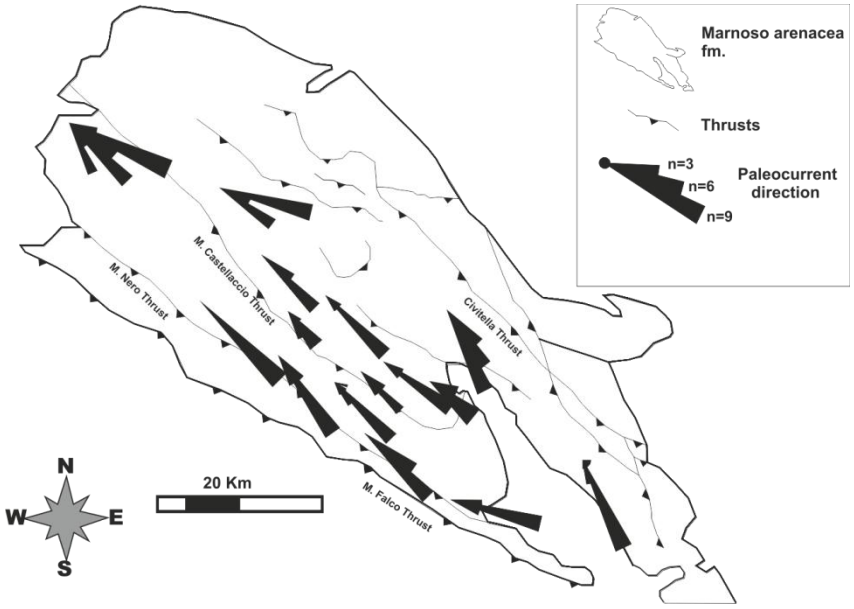

Figure 3.5. *Map showing the direction of paleoflow measured for selected thick sandstone beds, based on measurements of flutes and grooves at the base of the beds. The length of each arrow corresponds to the number of measurements with the same direction.*

3.5.2. Palaeocurrent directions

Palaeocurrent measurements at the base of thick sandstone beds indicate flow from the North-west for all beds in the interval (figure 3.5), except for the Contessa Bed that shows an opposing flow direction. Palaeocurrent indicators are remarkably consistent and indicate that flow occurred in a direction sub-parallel to the basin margins (figure 3.5), which is similar to the palaeocurrent directions measured for beds in the previously studied interval above the Contessa Bed (Amy & Talling, 2006). Talling et al. (2007c) provided a detailed analysis of palaeocurrent data and basin plain palaeogeography for the above Contessa interval (figure 3.2b).

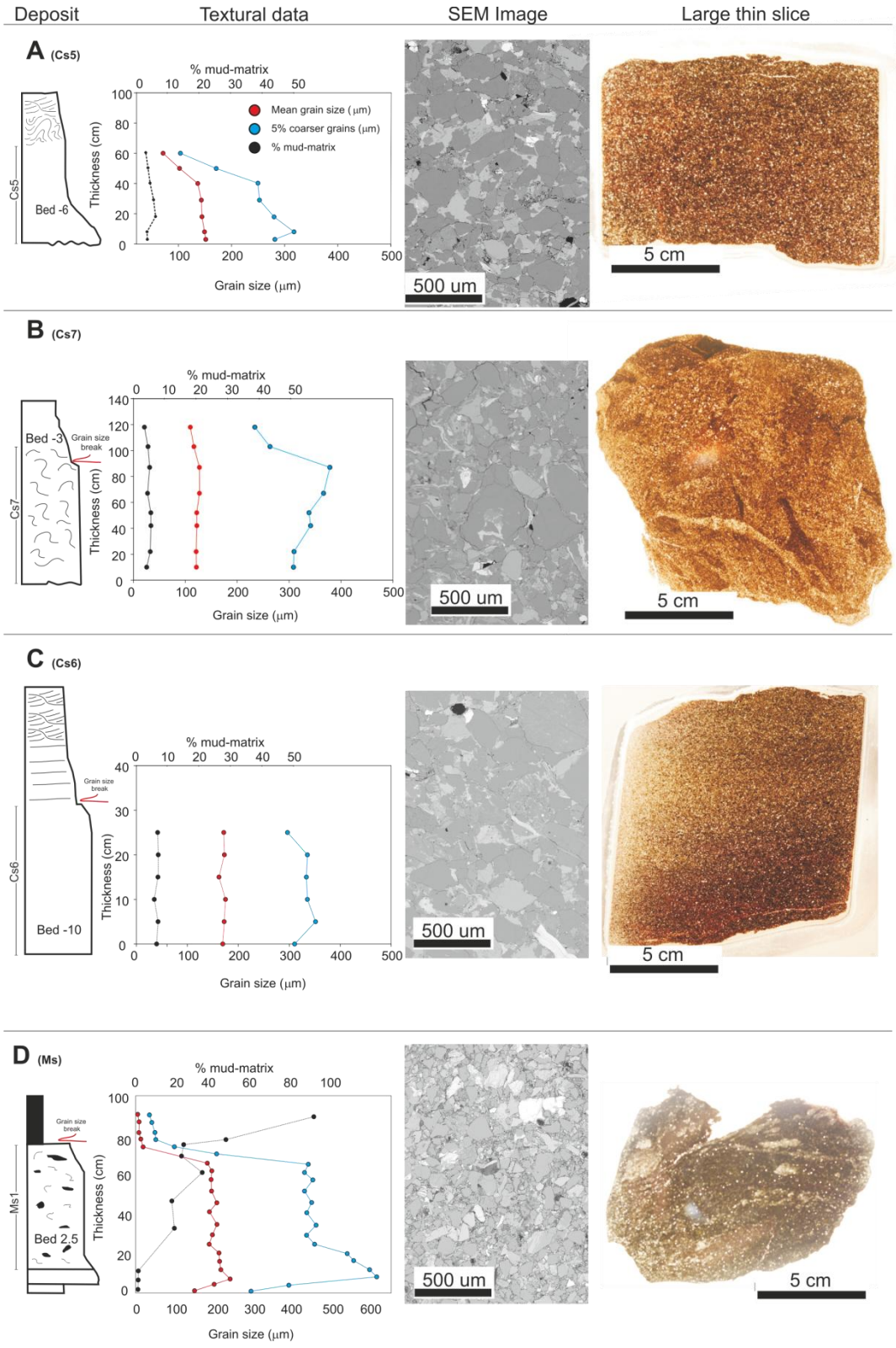

Figure 3.6. *Diagrams showing the textural characteristics of A) subfacies Cs5, B) subfacies Cs7, C) subfacies Cs6, D) Subfacies Ms1. For each subfacies are presented the mean and the 5% coarser grains vertical grading pattern and the percentage of interstitial mud; a representative SEM image; an image of a large thin slice photographed in trasmitted light, showing the sedimentary fabric. The four beds (Bed-6, Bed-3, Bed-10, Bed 2.5) are representative of the 4 different subfacies presented. The samples presented for subfacies Cs5, Cs6 and Cs7 were collected in section 77 (Mantigno). The sample presented for subfacies Ms1 was collected in section 14 (Monte Roncole).*

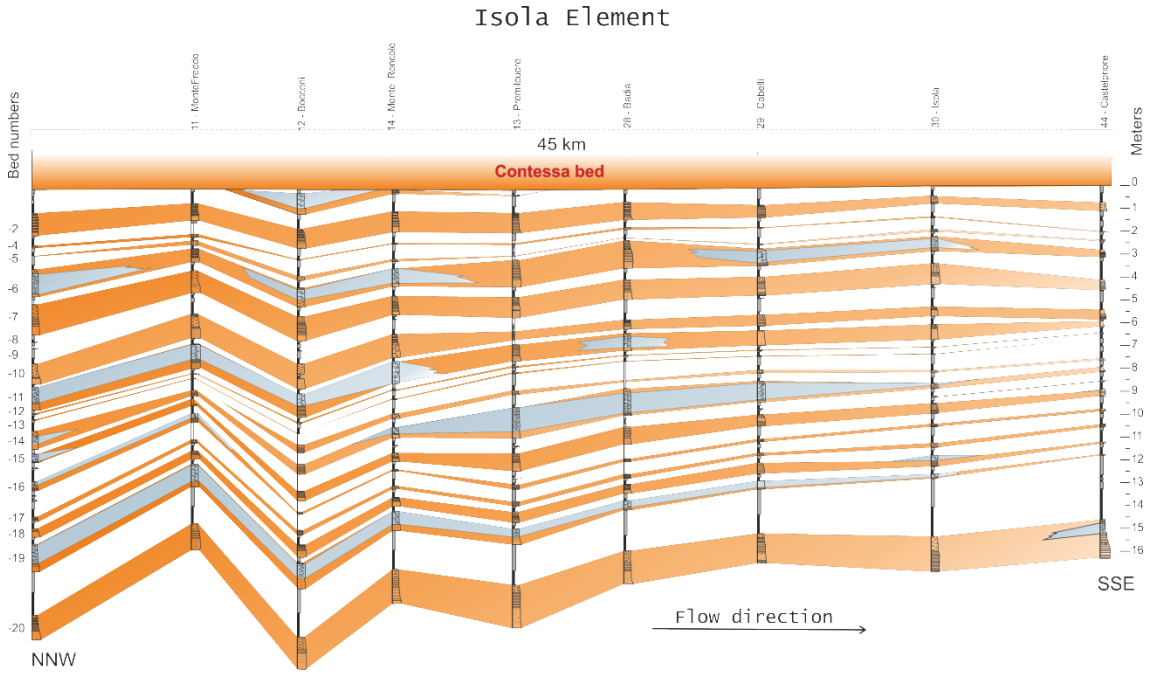

Figure 3.7. *Cross-section along the Isola element showing the correlation of the first 20 thick (>40 cm) beds below the Contessa marker bed. Key is provided in Fig. 3.3. Fig. 3.1 shows the location of the transect. The correlation panel is oriented approximately parallel to the paleoflow direction (Fig. 3.5); the direction is north-west to south-east for all the correlated beds but opposite for the Contessa marker bed. The complete correlation panel showing all the beds between the Fiumicello marker (-37) and the Contessa bed is provided in appendix 2.*

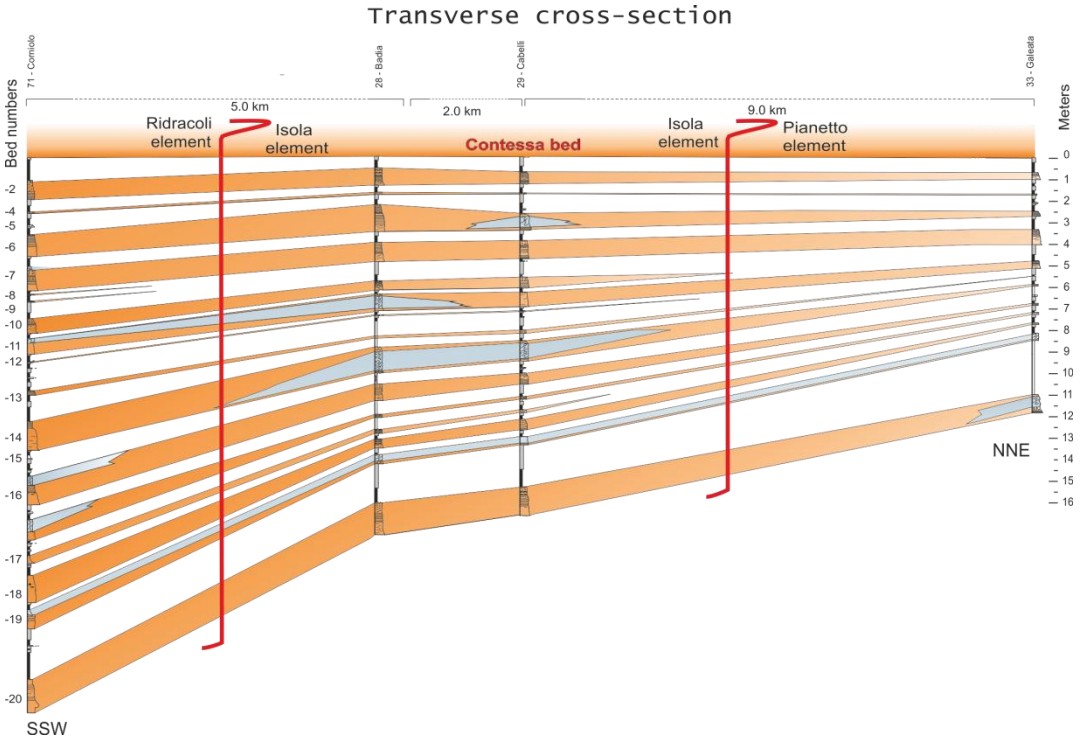

Figure 3.8. *Cross-section along orientated orthogonal to the paleoflow direction across the Ridracoli, Isola and Pianetto structural elements. Key is provided in Fig. 3.3. Fig. 3.1 shows the location of the transect. The complete correlation panel showing all the beds between the Fiumicello marker (-37) and the Contessa bed is provided in appendix 3.*

3.5.3. Different types of sandstone

Thin Beds

Deposits of thin (< 40 cm) sandstone beds are usually formed by clean normally graded sandstone with traction structures, and overlying turbidite mudstone. These traction structures are ripple-scale lamination (subfacies Cs1), dune-scale cross lamination (subfacies Cs2) and fine parallel lamination (subfacies Cs3).

Thick Beds

The upper part of thick (> 40 cm) beds comprises subfacies Cs1, Cs2 and Cs3 (figure 3.4b,d), whilst the lower part of thick beds comprises four additional types of sandstone which are normally graded, massive ungraded, clean swirly and muddy sandstone.

Normally graded sandstone (subfacies Cs3, Cs4, Cs5)

Normally graded, structureless (subfacies Cs5) or fine parallel-laminated (subfacies Cs3, fig. 3c) sandstone deposits commonly form the basal interval of thick sandstone beds (such as bed -20 in figure 3.3). A "stepped" parallel lamination (subfacies Cs4, fig. 3.4d), which is similar to the spaced lamination of Hiscott and Middleton (1979), is also sometimes present (Sumner et al., 2012). The mud matrix content is relatively low and comprises between 3% and 10% (Fig. 3.9a). The vertical normal grading of the coarser 5% of grains is recognizable using a grain size comparator and hand lens. Clasts occur along distinct horizons if they are present.

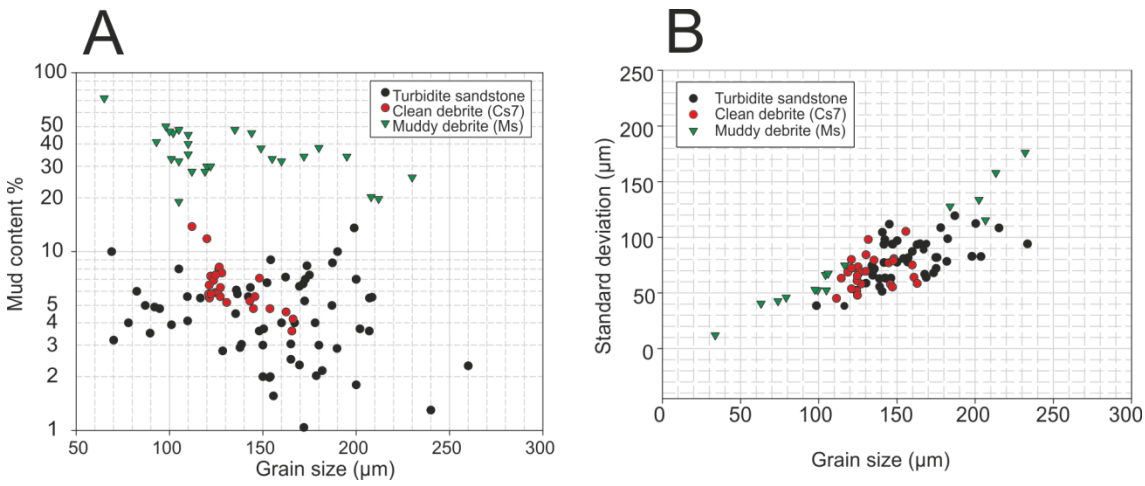

Figure 3.9. *Mean grain size plotted against A) mud matrix content and B) sorting (defined here as the standard deviation of grain size measurements). Grid counting was used to measure the longest axis of 300 grains in each sample. Data from scanning electron microscope (SEM) images of thin sections. The mud matrix content was estimated as the percentage area occupied by grains finer than 20 µm.*

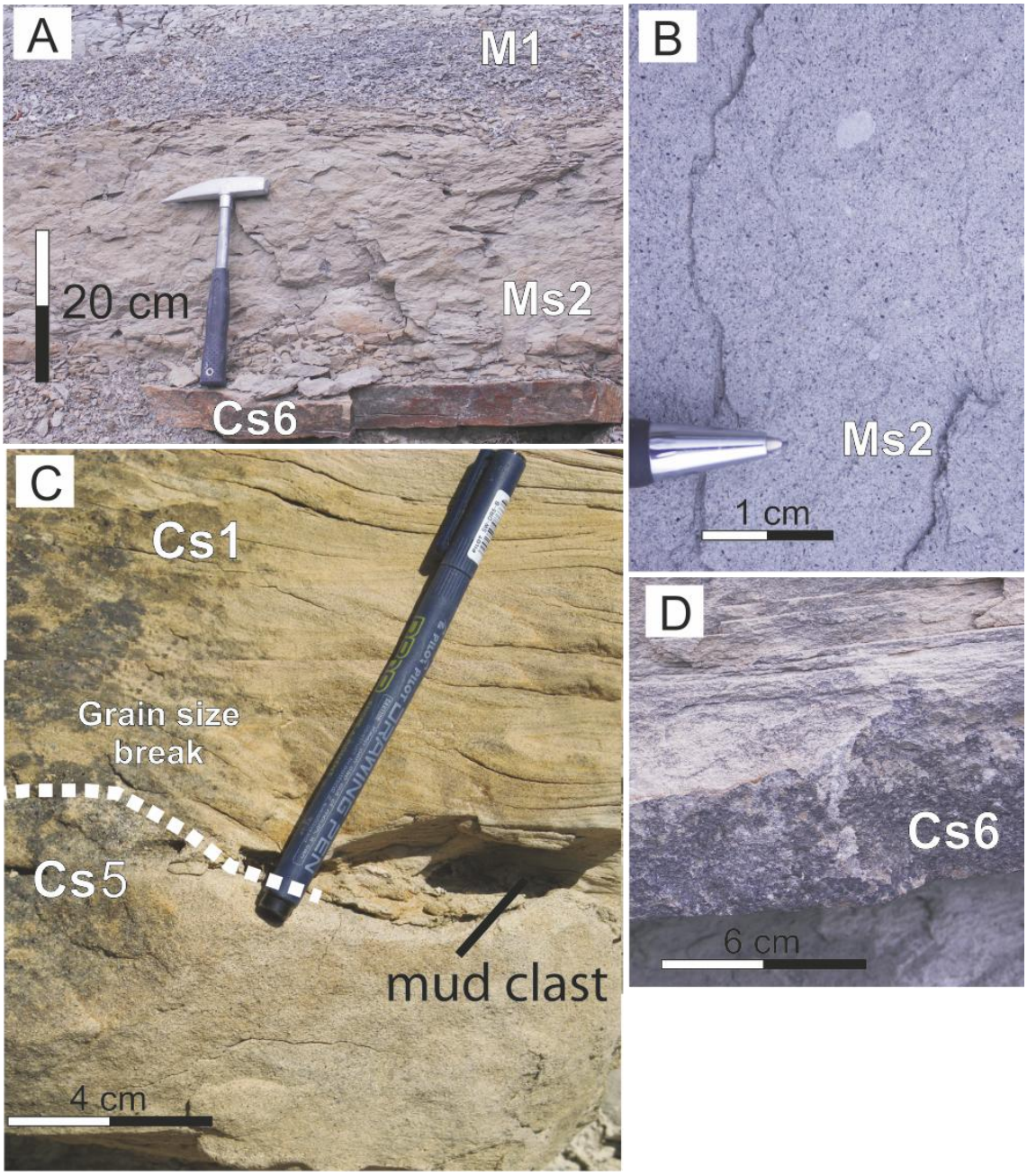

Figure 3.10. *Outcrop photographs illustrating the different types of massive sandstone deposits. See Table 1 for a full description of lithofacies Ms, subfacies Cs1 and Cs6. A) Bed -19 at section 30 (Isola) that comprises a thin basal clean sandstone interval (Cs6) overlain by a thick muddy sandstone interval (Ms1). B) Mud-rich sandstone with dispersed mud clasts (Ms1) in Bed -19 at section 8 (Poggio Dornata). C) Sharp grain size break between a massive graded sandstone interval (Cs5) and a cross laminated interval (Cs1) in Bed 7.9 at Coniale 1. D) Basal massive ungraded clean sandstone (Cs6) in Bed -32 at section 44 (Castel Priore).*

Massive ungraded sandstone (subfacies Cs6)

This subfacies (Cs6) is formed by visually unstructured and ungraded clean sandstone (such as in Bed -2 and Bed -10 in figure 3.3). The relatively low mud content is similar to that seen in other clean sandstone lithofacies (figure 3.6). Field observations and thin section

analysis show an absence of normal grading. Such normal grading is subtle but present in the otherwise similar subfacies Cs5. Subfacies Cs6 deposits are usually structureless, but in few cases a subtle, decimetric thick parallel lamination can occur (e.g bed -2 in section 26, Lavacchio). A sharp grain size break separates subfacies Cs6 from overlying laminated sandstone in thick sandstone beds (Fig. 3.10c). There are no mudstone or sandstone clasts present.

Clean swirly sandstone (subfacies Cs7)

A swirly weathering pattern distinguishes subfacies Cs7 in the field from other massive and normally graded clean sandstones (figure 3.11). This 'swirly' weathering pattern results from contorted areas of coarser grained and better sorted sandstone. This "patchy" or "swirly" texture can sometimes be subtle and it is not easily recognizable except in good exposure. However, large thin slices clearly show this patchy or swirly texture when viewed in transmitted light (figure 3.6). Cs7 sandstone intervals are either ungraded or have an irregular grading pattern due to the coarser grain size patches. The very uppermost part of the Cs7 intervals can be weakly normally graded.

The grey hue usually associated with mud-rich swirly sandstones (Ms lithofacies; figure 3.10a and 3.10b) is absent for the Cs7 subfacies both in weathered surfaces and fresh broken surfaces. Relatively low mud content is confirmed by thin section analyses, and this mud content is similar to that in other clean sandstone lithofacies (figure 3.9a). Small (<1 cm) mudstone clasts often occur chaotically dispersed within subfacies Cs7. Large (centimeters to meters) contorted sandstone clasts were seen in subfacies Cs7 at a single location (Cabelli River; figure 3.12). These clasts comprised unstructured or parallel laminated clean sandstone. The clasts formed most of the Cs7 interval, with the clast size increasing upwards (figure 3.12). Cs7 deposits comprise the basal interval of a number of thick sandstone beds, although in some cases they are underlain by normally graded sandstone that is up to 20 cm thick. A sharp grain size break separates subfacies Cs7 from overlying ripple cross-laminated sandstone intervals.

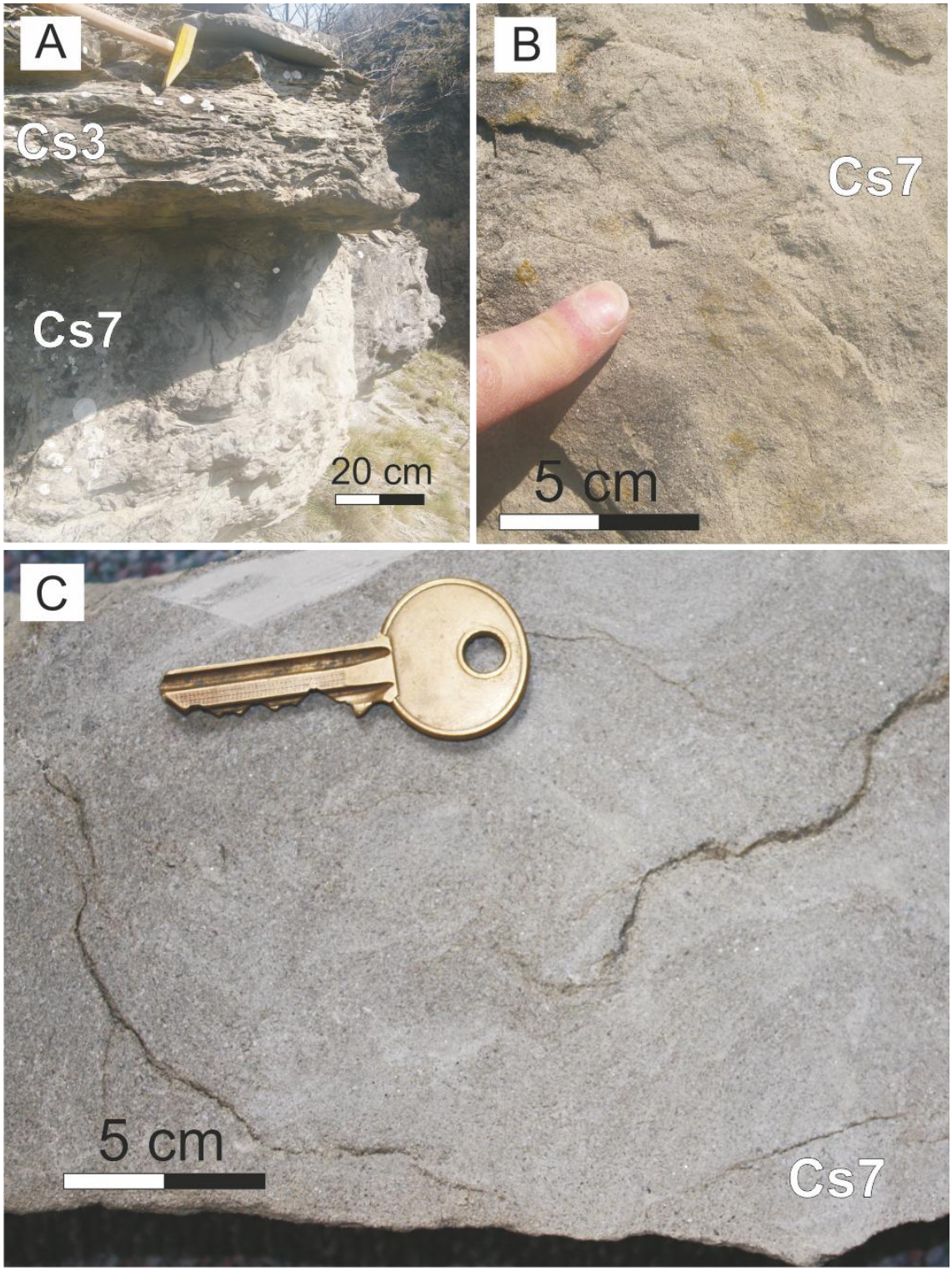

Figure 3.11. *Outcrop photograph illustrating the characteristic swirly fabric of subfacies Cs7 (Table 1). A) Bed 5.1 at section 13 (Premilcuore). The bed comprises swirly clean (Cs7) sandstone overlain by cross-laminated (Cs1) sandstone. B) Detailed photograph of a swirly clean (Cs7) sandstone in Bed 5.1 at section 13. C) Patchy areas of different grain size seen in a freshly cut surface of subfacies Cs7 from Bed 5.1 in section 13.*

Muddy sandstone (lithofacies Ms)

Swirly weathered, poorly sorted, ungraded mud-rich sandstone forms lithofacies Ms. The characteristic swirly fabric, coupled with a distinctive grey hue and the poor sorting ensure that these deposits are easily recognizable in the field (3.10a, 3.10b). Thin sections analysis reported by Talling et al. (2004) and Amy and Talling (2006) show a relatively high (20 to 50%) mud matrix content and the absence of vertical grading in this deposit type (figure 3.6d). Clast rich (subfacies Ms1) or clast deficient (subfacies Ms2) deposits are common in the interval studied here. Millimeter to meter-long turbidite mudstone and hemipelagic marl clasts are randomly scattered through intervals of subfacies Ms1. Abundant micas and organic particles are often present in the matrix. Muddy sandstone deposits are present in a number of thick beds, sandwiched between massive or laminated sandstone intervals and separated from the overlying laminated clean sandstone by a sharp grain size break.

3.5.4. Bed architecture

Single beds

Single bed diagrams illustrate the internal character of the first ten thick beds below the Contessa marker bed (figure 3.13). These diagrams illustrate the variation of thickness, facies characteristics and grain size distribution for each bed along the Ridracoli structural element. The diagrams show a down flow distance of 60 km. The beds show a rather complex internal architecture with a wide variety of facies that change both in down flow and across flow directions.

Down-flow facies tracts

The complex geometry is simplified and synthesized into down flow facies tracts (*sensu* Mutti, 1992; figure 3.14). Individual beds can show different facies tracts along adjacent down flow transects, as found by Amy and Talling (2006) for the interval above the Contessa marker bed.

Facies tract 1

Beds with facies tract 1 contain only clean sandstone and turbidite mudstone in downflow transects (figures 3.14a and 3.14b). Massive clean sandstone intervals are typically normally graded (Cs5) but can sometimes be visually ungraded (Cs6). Lateral transitions from massive to planar laminated intervals are common. These beds lack massive sandstone

intervals with a patchy or swirly texture (Cs7). The sandstone interval gradually thins in cross flow direction, whereas the mudstone caps tend to maintain its thickness (figure 3.8).

Facies tract 1a is characterized by a gradual transition from massive graded (CS5) clean sandstone into overlying laminated sandstone intervals. Facies tract 1b locally contains an internal grain size break that separates massive sandstone from overlying cross laminated sandstone. Massive sandstone below the grain size break is commonly ungraded (Cs6), but can be inversely graded (Cs5) in Bed -2.

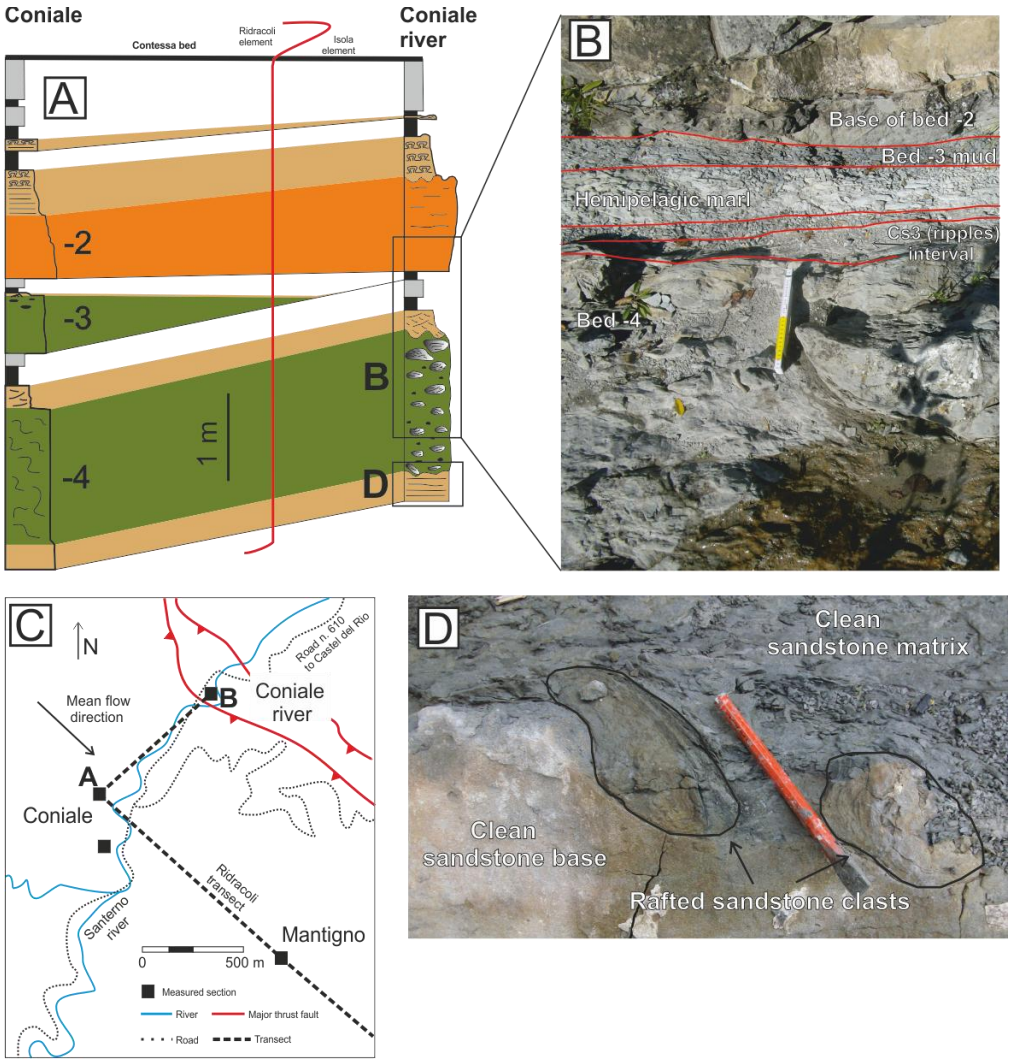

Figure 3.12. *Correlation panel illustrating the lateral changes of the four beds immediately below the Contessa marker bed in the most proximal outcrops. A) Correlation panel between the Coniale section and the Coniale river section. B) Photograph of the top of Bed -4, Bed -3 and the base of Bed -2 in the Coniale river section. C) Map of the Coniale area in the Santerno Valley. D) Photograph of the base of Bed -4 at the Coniale river section and line drawing of the rafted sandstone clasts.*

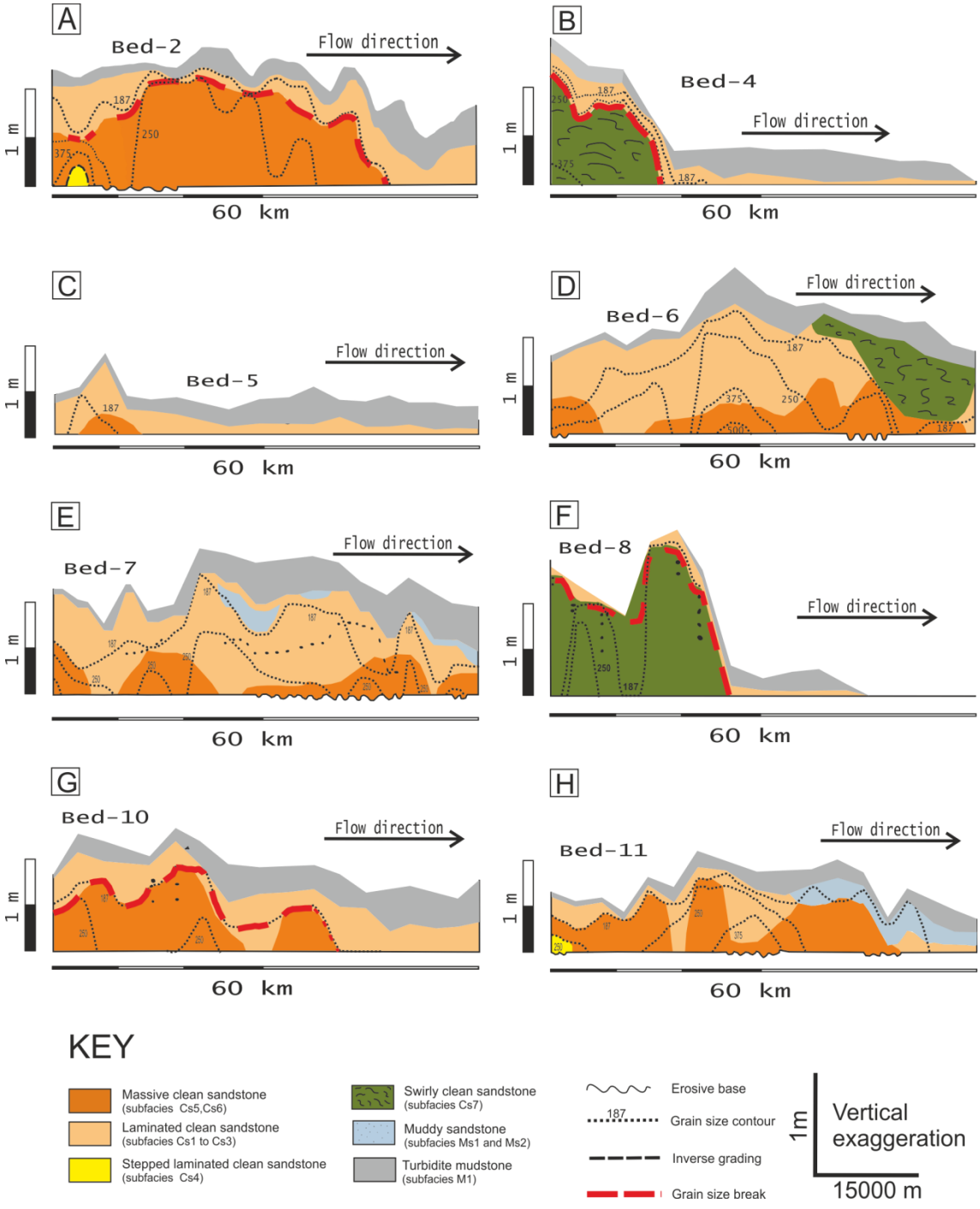

Figure 3.13. *Detailed bed diagrams showing the lateral variations of lithofacies and grain size along the Ridracoli thrust sheet for A) Bed -2, B) Bed -4, C) Bed -5, D) Bed -6, E) Bed -7, F) Bed -8, G) Bed -10, and H) Bed -11.*

Facies tract 2

Facies tract 2 comprises all of the beds containing intervals of swirly muddy sandstone (lithofacies Ms). Muddy sandstone intervals can be sandwiched between clean sandstone layers in facies tract 2b (figure 14d). The muddy sandstone can either abruptly pinch-out in a down flow direction (figure 14d) or gradually taper to become a thin layer of clean sandstone in the most distal sections (Fig. 14c). This particular facies tract has been described by Amy & Talling (2006) for the interval above the Contessa marker bed (it is equivalent to facies tracts 2a, 2b, 3a, 3b, and 3c of their figure 27).

Facies tract 3

Beds with facies tract 3 (figures 3.14e, 3.14f and 3.14g) comprise a basal interval of swirly weathered, visually clean, poorly sorted, generally ungraded sandstone with dispersed mudstone and sandstone clasts (subfacies Cs7) separated by the overlying cross laminated sandstone (subfacies Cs1) by a sharp grain size break (such as Bed -4 in figure 3,13b). The mudstone cap in facies tract 3 is relatively thin, and these beds have a relatively high sand to mud ratio. In facies tract 3a the swirly sandstone abruptly pinches out in a down flow direction over a relative short distance of less than 2 km. These beds comprise only a thin layer of laminated clean sandstone in distal sections beyond the pinch-out of the Cs7 interval. This rapid pinch out of the Cs7 interval is also evident in a cross-flow direction for Bed -3 (figure 3.12). Facies tract 3b is characterized by (sometime repeated) transitions from normally graded massive and laminated sandstone (Cs5 and Cs4) into swirly and patchy Cs7 sandstone, as shown by Beds 0 and 5.1 (figures 3.15b and 3.15c). In locations where swirly and patchy clean Cs7 sandstone is absent, the upper part of the bed can contain a mud-rich clast-poor sandstone interval, as seen for Bed 5.1 in the Isola transect (Fig. 3.15c). Cs7 sandstone intervals in facies tract 3b are underlain by a thin interval of structureless clean sandstone with coarse-tail normal grading, which appears to be associated with the overlying Cs7 sandstone because both pinch out in a similar location (Fig. 3.15a-c). Close to this pinch out, a thin interval of ripple cross laminated sandstone can appear at the base of the bed. Facies tract 3c displays down-flow transitions from massive and laminated clean sandstone into swirly or patchy clean Cs7 sandstone, as was the case for facies tract 3b. Beds -6 and -14 (facies tract 3c) lack clear evidence that Cs7 sandstone pinches out abruptly beyond its most down flow location (section 42; figure 3.3).

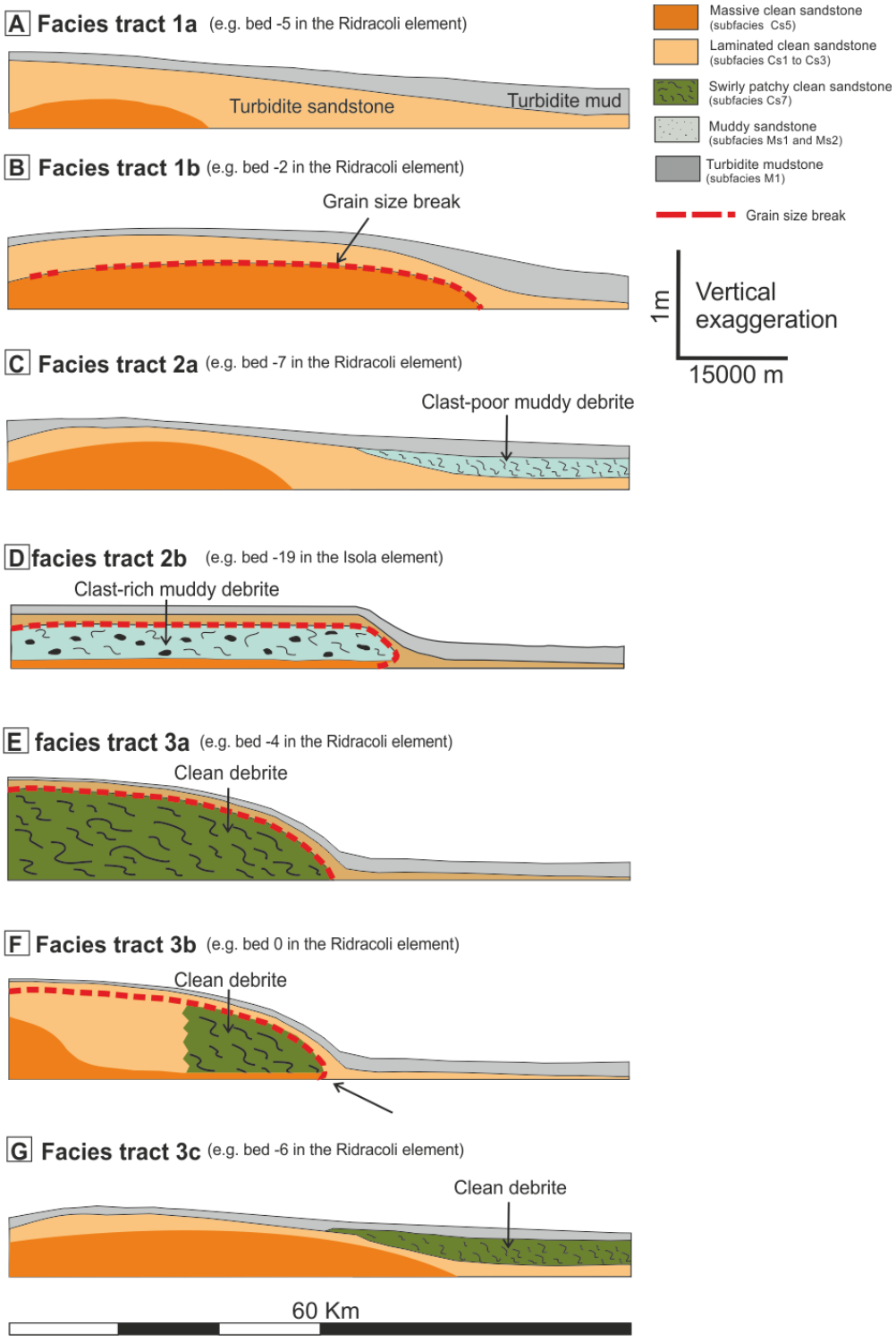

Figure 3.14.*Generalized facies tracts observed for correlated beds within the Marnoso-arenacea Formation.*

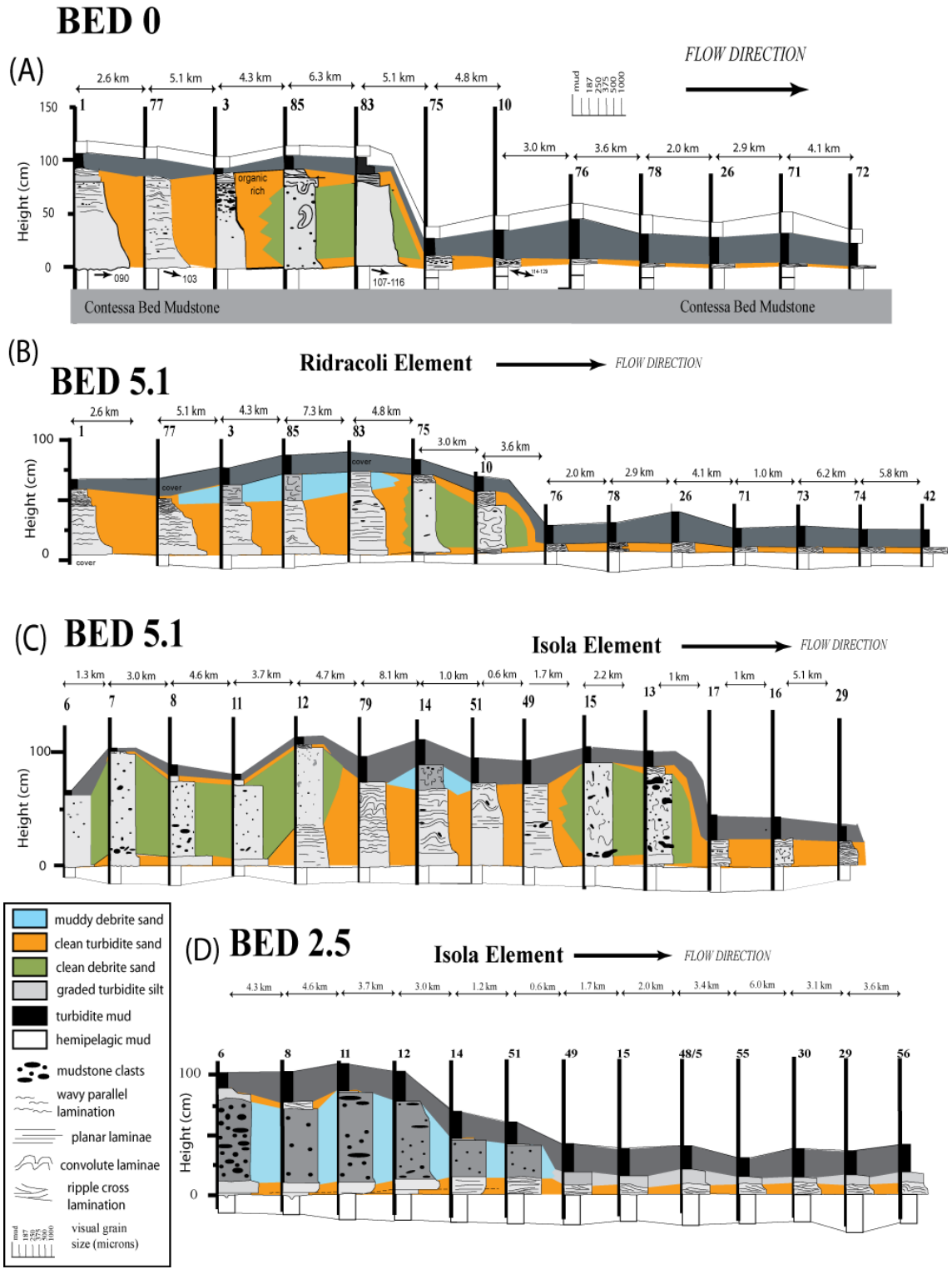

Figure 3.15. *Down-flow transects through Beds 0, 2.5 and 5.1 above the Contessa Bed (modified from Talling et al., 2012b). A) Bed 0 on the Ridracoli thrust sheet. B) Bed 5.1 on the Ridracoli thrust sheet. C) Bed 5.1 on the Isola thrust sheet. D) Bed 2.5 on the Isola thrust sheet.*

3.5.5. Key beds in the above Contessa interval

The stratigraphic interval directly above the Contessa marker bed, previously studied by Talling et al. (2004, 2007a,b) and Amy & Talling (2006), comprises three beds with characteristics comparable to the beds described here with facies tract 3. The lateral evolution of these beds is now briefly discussed.

Bed 0

Bed 0 is the first thick bed (>40 cm) above the Contessa mudstone (see Amy and Talling, 2006 for correlation panels). In the Ridracoli structural element bed 0 shows a down flow transition from normally graded clean sandstone (subfacies Cs5 and Cs1) to clean swirly sandstone (subfacies Cs7) between section 3 and section 85 (figure 3.15a). The Cs7 interval then pinches out abruptly over a few (less than 5.1) kilometers.

Bed 5.1

In the Ridracoli structural element, the top rippled interval (subfacies Cs3) of bed 5.1 shows a down flow transition to a clast-deficient muddy sandstone interval (subfacies Ms2) between section 77 and section 83 (figure 3.15b). In the Isola structural element the same transition is evident in section 14 (figure 3.15c). A transition from normally graded sandstone (subfacies Cs5 and Cs1) to swirly clean sandstone (subfacies Cs7) is evident between section 83 and section 75 in the Ridracoli element (figure 3.15b). The Cs7 interval then pinches out abruptly over less than 3.6 kilometers. In the Isola element a swirly clean sandstone interval (subfacies Cs7) changes into a normally graded sandstone interval between section 12 and section 79. This interval than changes back into swirly sandstone (subfacies Cs7) between section 49 and section 15, and then pinches out abruptly over less than 1 kilometer (figure 3.15c).

Bed 2.5

In the Isola structural element bed 2.5 comprises a basal interval of clast-rich muddy sandstone (subfacies Ms1). This interval pinches out relatively abruptly over a few kilometers between section 12 and section 49 (figure 3.15bd). The geometry of the pinch out resembles the one described in facies tract 3.

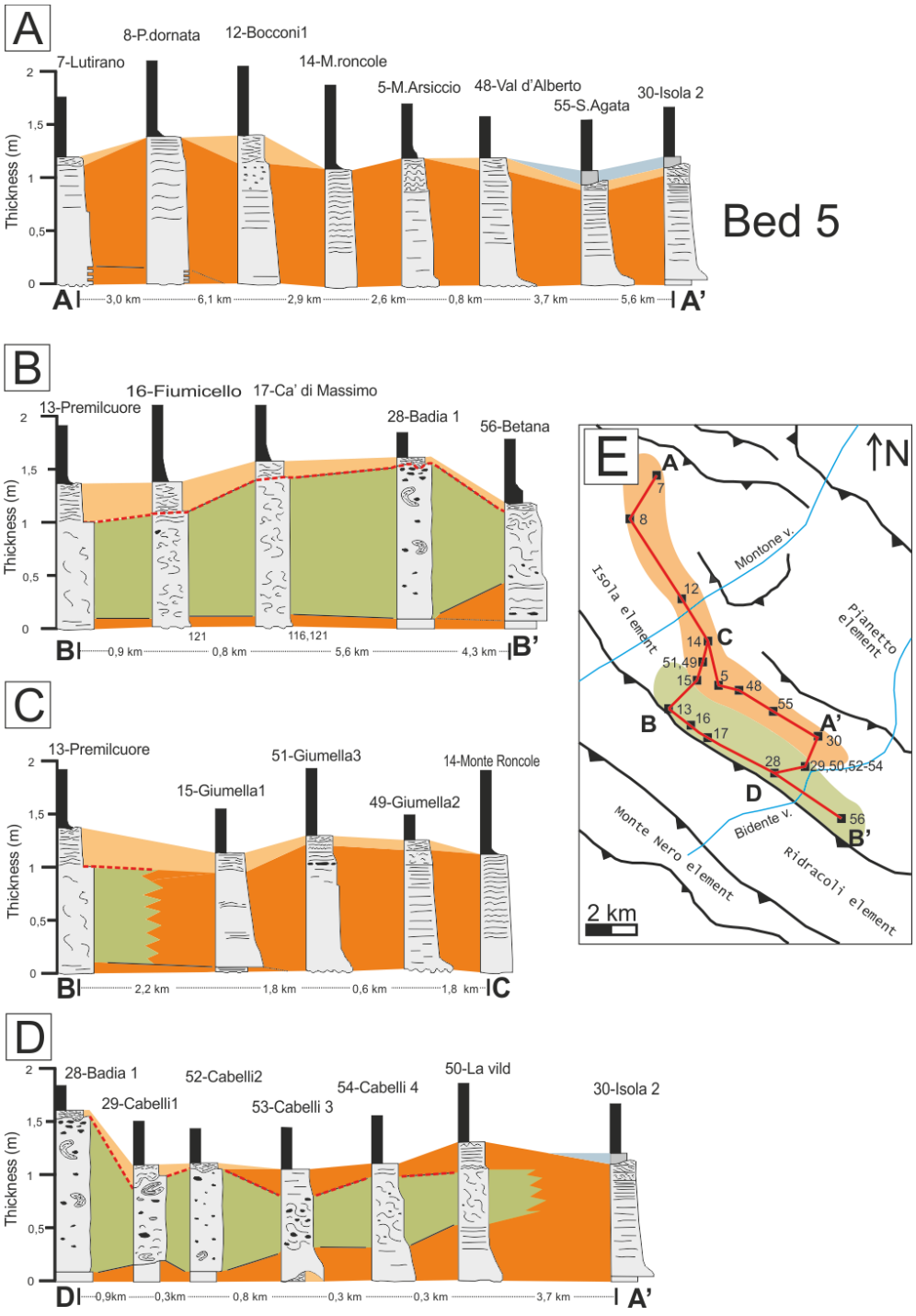

Figure 3.16. *A to D) Lateral changes between turbidite clean sandstone (Cs1-to-6) and debrite clean sandstone (Cs7) in Bed 5 on the Isola thrust sheet. Key is provided in figure 3.13.E) Location map of the logged sections in the Isola thrist sheet. The inferred lateral extension of turbidite sandstone (Cs1 to Cs6) and clean debrite (Cs7) is indicated.*

Bed 5

Bed 5 contains an interval of Cs7 sandstone in part of the Isola thrust sheet (figure 3.16), which is equivalent to laminated or massive turbidite sandstone in an across-flow direction. The Cs7 interval continues to the end of available outcrop on the Isola thrust sheet, such that it is not known whether it pinches out abruptly in a down flow direction. The Cs7 interval contains boulder-sized (up to 1.2 m) clasts that sometimes comprise three thin beds. This sequence of thin beds is not seen beneath bed 5 at any of the 109 logged sections (Talling et al., 2007c), and cannot have foundered from the ripple cross laminated sandstone interval that caps the bed at this location. It also differs from the single interval of ripple cross laminated sandstone that is occasionally seen at the very base of the beds. Some boulder-sized clasts therefore originated outside the study area, and travelled at least 7 km. The clasts in this Cs7 interval often comprise ripple cross laminated sandstone that is deformed and would be relatively easy to disaggregate. This suggests that sandstone clasts were not vigorously tumbled during transport. Bed 5 also contains mud-rich debrite sandstone with (Ms1) or without (Ms2) clasts in other parts of the outcrop area, as well as a range of turbidite sandstone facies (figure 3.16; Amy & Talling, 2006; Talling et al., 2012a).

3.6. DISCUSSION

The depositional processes inferred from outcrop observations and textural data will be now discussed. It's worth noticing that different depositional mechanisms can sometimes produce the same type of deposit, if observed in a single location. For this reason the depositional process of each single lithofacies cannot be unequivocally derived based on single outcrop, one dimensional data only. The external bed shape and the lateral facies variations will then be used to test the hypothesis inferred.

3.6.1. Internal character and depositional processes for clean sandstone intervals

The depositional processes for clean sandstone lithofacies are now discussed. Deposits of muddy sandstone (lithofacies Ms) have been described previously by Talling et al. (2004, 2007b) and Amy & Talling (2006) and are not discussed further in this contribution.

Normally graded sandstone (subfacies Cs1, Cs2, Cs3, Cs5)

This type of well-sorted normally-graded clean sandstone is either structureless (Cs5) or contains sedimentary structures (Cs1 to 3). Normal grading indicates differential settling of larger and smaller grains. It records layer-by-layer deposition from a turbidity current, as efficient differential sediment settling occurs at low to intermediate (< ~ 30 % volume) sediment concentrations (Druitt, 1995; Amy et al., 2006). If present, outsized mudstone clasts tend to settle in distinct horizons within the bed. Petrographical analyses show that these layers have a relatively low percentage of interstitial mud (figure 3.6a), again indicating effective segregation of larger and smaller particles from the flow. If present, cross-lamination records the reworking of settled particles in a near-bed tractional layer (Arnott & Hand, 1989). Planar lamination could have formed in either dilute or dense flow (Arnott & Hand, 1989, Sumner et al., 2008).

Massive ungraded clean sandstone (subfacies Cs6)

Vertical grading is a key feature for interpreting depositional process from deposits, and grading can sometimes be subtle in the field (Sylvester & Lowe, 2004). Petrographical analysis confirms that mud-poor, unstructured and ungraded clean sandstone layers (subfacies Cs6) are present in the studied beds (figure 3.6c). These sandstone intervals display no significant vertical grading of either the mean grain size or the coarsest 5% of grains. This type of ungraded clean sandstone can be deposited in a layer-by-layer fashion by a steady turbidity current (Kneller & Branney, 1995), but this would only occur if the flow was almost perfectly steady. The absence of traction structures indicates that settling grains were not reworked by near bed processes, possibly because of relatively high sediment fallout rates. A steady current however is unlikely to produce the upper grain size break separating these deposits from the finer grained sandstone interval constantly overlying these deposits. This sharp grain-size break can be interpreted as the result of sediment erosion or bypass due to a waxing turbidity current (Kneller & McCaffrey, 2003), or as a distinct interface between the basal, relatively high concentrated flow phase and the overlying (or following) more dilute phase (Amy & Talling, 2006). In this case, a waxing turbidity current is unlikely to form the grain size break, as the sediment overlying the discontinuity would be coarser than below. The thick, massive and ungraded sandstone intervals (subfacies Cs6) therefore most likely record rapid, possibly en-masse deposition.

Clean swirly sandstone (subfacies Cs7)

Deposits of swirly weathered, mud-poor, poorly sorted, generally ungraded sandstone (Subfacies CS7; figure 3.11) show characteristics of en-masse deposition from a mud-poor debris flow. The lack of vertical grading, coupled with the occasional presence of chaotically distributed mudstone clasts imply that the deposition occurred without effective segregation of larger and smaller particles. Ungraded clean sandstone can be deposited by sediment suspensions with very high sand concentrations, as shown by laboratory experiments (Druitt, 1995; Amy et al., 2006). The upper grain size break separating these deposits from the overlying finer- grained, ripple laminated sandstone interval (subfacies Cs1) is most likely a distinct interface between the basal, relatively high concentrated flow phase and the overlying (or following) more dilute phase (as described for bipartite flow in Mutti et al, 2003). Such a sharp interface was observed in the laboratory experiments by Marr et al. (2001). A perfectly steady turbidity current can also deposit ungraded clean sandstone (Kneller & Branney, 1995) but such a flow is unlikely to deposit chaotically distributed clasts. A steady turbidity current would be less likely to produce the upper grain size break. Areas of coarser grained and better sorted sandstone are common in subfacies Cs7 (figure 3.6b). This "patchy" texture is inferred to result from pervasive liquefaction. Slow convection and elutriation of fine material during this liquefaction process could cause the formation of patchy areas with different mean grain size (see figure 1 of Kuenen, 1965). Lithofacies Cs7 does not contain dewatering structures such as dish structures, pillars or dewatering pipes. The overlying ripple cross-laminated interval is typically undeformed, with a flat top and a foundered base. Fluid escape must therefore have ceased during deposition of this rippled interval. Evidence for soft sediment deformation occurs in a number of other beds (such as Bed -2, figure 3.4e), but this liquefaction never reached the base of the bed, and was insufficient to completely homogenize sediment and obliterate laminations in the basal interval. Sandstone clasts in Bed-4 at the Coniale river section (figure 3.12) most likely originated from basal sandstone previously deposited by the same event. Bed -4 shows how proximal deposits rich in sand-clasts transform laterally into clean sandstone with a patchy texture, and in these cases some of the patches may result from progressive disruption of weak sandstone clasts. The uppermost part of the Cs7 deposits can be weakly normally graded (Bed -3, figure 3.6b), and this may record the upper part of a highly-concentrated flow phase, where the sediment-water mixture is partially diluted by surrounding sea water. This partial dilution reduces the sediment concentration sufficiently to allow segregation of coarser and finer particles.

3.6.2 Bed shape as test for depositional processes

Tapering shape of turbidite sandstones

Sandstone intervals showing evidence of differential settling and layer-by-layer deposition (Cs1 to 5) have a gradually tapering shape. These turbidite sandstone intervals can comprise all of the sandstone-component in thin beds or facies tract 1a, or only the uppermost part of the sandstone interval as in facies tracts 2 and 3 (figure 3.14). This shape is consistent with the deposition from a turbidity current, as shown by experiments and numerical modeling (Gladstone et al., 1998; Harris et al., 2002).

What causes the abrupt pinch-out of Cs6 and Cs7 sandstone in facies tract 1b and 3?

Deposits of both subaerial and subaqueous debris flow often pinch-out abruptly at their margin (Aksu and Hiscott, 1989; Major, 1997; Mohrig et al, 1999; Marr et al, 2001). This abrupt pinch-out is a consequence of the rapid frictional interlocking of grains and the matrix yield strength of these high concentration flows. Previous contributions (Amy et al., 2005; Amy and Talling, 2006; Talling et al, 2007b) show that ungraded mud rich sandstone intervals pinch-out abruptly in the interval above the Contessa Bed. These intervals most likely represent cohesive (mud-rich) debris flow deposits. Similar muddy sandstone deposits are described in this contribution in facies tract 2. Facies tract 3 describes deposits of clean patchy sandstone (Cs7) that pinch-out abruptly over a few kilometers. Beds described by facies tract 1b show a lateral pinch-out of basal sandstone interval that is massive and ungraded (subfacies Cs6). This pinch out is somewhat less abrupt than that of the patchy clean sandstone (subfacies Cs7) in facies tract 3, and the pinch occurs further down the basin.

In both facies tract 3 and 1b a sharp grain size break separates the basal sandstone (subfacies Cs6 and Cs7) from overlying ripple cross-laminated sandstone (subfacies Cs3). This grain size break most likely records a sharp surface separating a dense lower part of the flow from a more dilute turbulent cloud. The lower denser part of the flow came to a relatively abrupt halt, suggesting that it was formed by a highly concentrated debris flow rather than steady turbidity current.

Local sea floor topography can produce abrupt thinning and fining of turbidite sandstone deposits. Such turbidite deposits could then undergo liquefaction. However, there is little evidence of such topography in the correlated interval near the pinch-out of the Cs6 and Cs7 deposits. Turbidite beds immediately underlying and overlying these deposits record no abrupt

changes in thickness or grain size (figure 3.3) and there is no evidence of flow reflection or deflection by local topography. Abrupt terminations of sandstone intervals have been attributed to lofting of submarine flows (Plink-Bjorklund and Steel, 2004). Lofting can occur when a sediment-water mixture is less dense than the surrounding sea water. However, lofting flows must have low (< 1 % volume) sediment concentrations at the point of lofting (Mulder et al., 2003). Cs6 and Cs7 deposits show characteristics related to the deposition from a high concentrated flow such as the chaotically distributed clasts and the lack of normal vertical grading. These deposits cannot be produced by a flow with such a low sediment concentration.

3.6.3. How could clean sandy debris flows originate and move on low gradients?

Two hypotheses can be proposed for the origin of the dense pervasively-liquefied debris flows of clean sand. The first hypothesis is that the clean sand debris flow originated outside the study area and then ran out for over 20 to 30 km. The second hypothesis is that the debris flows were generated locally by flow transformation from turbidity current, and the debris flows did not run out for long distances. This flow transformation boundary would have to migrate significant distances to explain the observation that debrite intervals are continuous for 20 to 30 km.

Long run out distances of liquefied debris flows

The presence of chaotically distributed sandstone and mudstone clasts in the proximal part of Bed -4 (figure 3.12) suggests that this flow entered the study area as a debris flow rather than as a turbidity current. Debris flows with significant amounts of cohesive mud can potentially run out for long distances due to their low yield strength (Talling et al., 2010). However, it is unclear how debris flow comprising mostly clean sand could travel for long distances across low gradients in a basin plain settings. It might be expected that the high excess pore fluid pressures needed to allow a clean sand mixture to flow would quickly dissipate through such a permeable sediment mixture. Lowe (1976) argued that thick layers of liquefied clean sand would tend to move for short distances of only a few kilometers before the excess pore pressure was dissipated and the flow stopped, and that these flows would only tend to be mobile on sea floor gradients in excess of ~3°-4°. Laboratory experiments by Ilstadt et al. (2004) and Breien et al. (2010) have shown the initially fluidized layers (in which sediment is predominantly supported by excess pore pressures) can move on relatively high gradients of ~6°. Their flows formed a turbulent frontal part, a fluidized central part supported by high

excess pore pressure, and a rear component in which sediment was matrix supported. These experiments produced massive poorly graded sand deposits, but the significance of the lack of grading is unclear because a very limited range of grain sizes was employed in the experiments. The deposit grain size was not sampled, and it is also unclear whether such flows could produce deposits with very low mud contents. The sediment contents in the flows were often relatively high (50 % vol). Modelling of the mobility of such liquefied layers suggests that in some situations (such as an initially 1m thick flow, with significant cohesive clay, on a 2° slope; Breien et al., 2010) the flows might run out for several tens of km.

It can be proposed that very small amounts of mud were indeed able to maintain high pore fluid pressures (Talling et al., 2012b). At high sediment concentrations, even a small (5%) amount of cohesive mud may also provide yield strength to the flow (Shanmugam, 1997).

It should be also noted that, due to the intense dewatering, a significant amount of fine particles could have been removed from the deposit through elutriation. Therefore the matrix mud content measured can be significantly lower than the original percentage at the moment of the deposition (Lowe and Guy, 2000).

Flow transformations

If a clean sand debris flow originated via transformation from an initial turbidity current then the debris flow would possibly not need to run out for long distances. Bed -2 comprises in the proximal sections inverse or normally graded massive sandstone deposited progressively by turbidity current (subfacies Cs4 and Cs5), that transforms laterally into massive ungraded sandstone (Cs6) before pinching out relatively abruptly. Beds 5.1 and bed 0 in the stratigraphic interval above the Contessa Bed show lateral and down flow transitions from clean turbidite sandstone (Cs5) to clean debrite sandstone (Cs7).

Erosion of basal sandstone intervals (such as in Beds -2 and -4) could inject sand into the base of the flow to aid flow transformation. However, the flow transformations would have to migrate for tens of kilometers to explain the origin of laterally extensive debrite within beds (such as Bed -4) in the newly studied interval. Laboratory experiments have shown how flow transformation from a fully turbulent turbidity current to laminar debris flow can produce mud-rich sandstones (Sumner et al., 2009). The beds containing clean debrite sandstone have relatively high sand to mud ratios, and this increased abundance might favor formation of clean sand (rather than muddy sand) debris flows. However, further experimental work is needed to demonstrate whether such flow transformations can indeed generate debris flows that deposit clean sandstone.

3.6.4. Significance of lateral transitions into clean sandstone deposited by turbidity current

Lateral transitions between liquefied debris flow (Cs7) and laminated (Cs3) or massive (Cs5) turbidite sandstone occur without major changes in the overall sandstone thickness (figure 3.15 and 3.16). This is significant because it suggests that the flow responsible for depositing the different types of sandstone was similar, at least in terms of the rate and duration of sand deposition. This may suggest that the planar laminated (Cs3) intervals were deposited from relatively high concentration turbidity current (Talling et al., 2012b), instead of dilute turbidity current as has sometimes been inferred (Lowe, 1982).

3.6.5. Comparison with previous studies

High density turbidity currents

Lowe (1982) proposed that massive clean sand intervals were formed incrementally from high concentration near-bed layers, when sediment fallout rates were sufficiently rapid to suppress tractional reworking of sediment along the bed. Lowe (1982) noted that this type of rapid sedimentation could lead to high excess pore pressures (liquefaction) in these near bed layers, and that the resulting massive deposits could be either vertically graded or ungraded and will often contain evidence of dewatering in the form of dish and pillar structures. These dish and pillar structures result from late-stage in-situ water escape rather than indicating that liquefaction was a primary process during preceding down-slope transport.

Kneller and Branney (1995) and Kneller (1995) outlined how thick intervals of massive sandstone could form incrementally by deposition from thin near-bed layers with high sediment concentration. These near bed layers are a small fraction of the total flow thickness, and they only record conditions near the bed. These authors described how temporal and spatial changes in flow speed could lead to a variety of grading patterns, including ungraded intervals if flow was temporally steady and spatially uniform.

Laboratory experiments have shown how massive clean sandstone layers can indeed form incrementally through deposition from thin near bed layers with high sediment concentration (that have been termed either ‘traction carpets’ or ‘’laminar shear layers’; Kuenen, 1966; Bannerjee, 1977; Arnott and Hand, 1989; Sumner et al., 2008 and 2012). Near bed layers in the

experiments tend to have a sharp top, and massive deposits occur when sediment deposition rates are sufficiently high (> ~ 0.4 mm/s) to suppress reworking along the bed.

The analysis of facies tracts 3 and 4 suggests that beds including Cs6 and Cs7 sandstone intervals are not deposited incrementally from a high density turbidity current, as in the models of Lowe (1982) and Kneller and Branney (1995). An almost perfectly steady turbidity current could have deposited massive ungraded (subfacies Cs6) or swirly patchy sandstone (subfacies Cs7). However, this type of steady current is unlikely to produce the sharp marginal pinch-out observed in facies tract 3 and 4. This pinch out is most likely expected from a rapidly depleting flow, such as a debris flow depositing en-masse.

Swirly (Cs7) sandstones never contain dish and pillars structures suggesting in-situ water escape. The patchy texture of Cs7 intervals suggests that liquefaction occurred when the sediment was still moving.

Hybrid beds

Haughton et al. (2009) classify hybrid event-beds, or turbidites with linked debrites, as the product of sediment-gravity flows able to deposit both a turbidite and a debrite phase. These beds are generally bipartite, with a lower clean sandstone layer overlaid by a mud-rich sandstone interval. In the Marnoso Arenacea Formation this structure is evident in beds containing Ms (muddy sandstone) lithofacies, described by facies tract 2a and 2b (figure 3.14c and 3.14d). Beds containing Cs6 and Cs7 sandstone (Facies tract 1b and 3, figure 3.14b,e,f,g) cannot be explained with this model, because they lack mud-rich sandstone. Following Haughton et al. (2009) classification, they could however be termed hybrid due to the contemporary presence of a basal debrite phase overlaid by a ripple laminated low-density turbidite interval.

Lowe and Guy (2000) and Lowe et al. (2003) describe sandstone layers deposited by slurry flows intermediate between turbidity currents and debris flows. Their M divisions are generally characterized by repetitively stacked darker (muddier) and lighter sand-prone bands. This banding is not observed in any of the beds described here. Their M_{2a} division (mixed slurried) can however lack bands, it is generally ungraded and it often contains irregular streaks and blobs interpreted as irregular water escape channels. Therefore it bears some resemblance with the Cs7 (swirly sandstone) subfacies described in this study. M_{2a} divisions contain an average mud percentage of 20.5% (Lowe and Guy, 2000). This mud matrix percentage cannot be directly compared with the ones obtained in this study, due to the different measurement techniques adopted. The flows depositing M_{2a} divisions are however described as “especially

mud-rich" (Lowe and Guy, 2000), and therefore may resemble the Ms lithofacies of this study, which contains an unusual (20% to 50%) percentage of mud matrix if compared to other sandstone intervals. Strikingly Cs7 intervals described here have a mud matrix content as low as the other lithofacies interpreted as turbidite sandstones. Another key difference is that Cs7 sandstones often contain patchy areas of different grain size (mean and 5% coarser), and not only areas of cleaner sandstone where the fine particles were removed by the escaping pore fluids. In Cs7 sandstones the mud content doesn't vary significantly within the bed (figure 3.6).

Bipartite flows

Facies tracts 3 and 4 are broadly consistent with the model proposed by Mutti (1992, 2010), Mutti et al. (2003) and Tinterri et al. (2003) of a bipartite flow with an upper turbulent suspension underlain by a much denser layer of fluidized sediment, with sediment supported primarily by excess pore pressures. These authors propose that the basal fluidized layer produces massive sand layers that can be graded or ungraded, and particularly poorly sorted. The term fluidized is more commonly used to denote an external source for the pore fluid, rather than upward flow generated by self-consolidation (Lowe, 1976). It might therefore be preferable to use the term liquefied rather than fluidized for this basal flow phase. Deposition from these fluidized (liquefied) layers occurred en-masse by rapid 'freezing'.

We concur with these authors in highlighting the primary role of excess pore pressure as a sediment support mechanism in dense flows depositing generally ungraded, poorly sorted massive sandstone intervals. We believe that this partial liquefaction is greatly enhanced by an even low (less than 10%) percentage of fine, possibly cohesive material. This cohesive mud is also likely to provide yield strength to the dense sediment water mixture, and we consider these two mechanisms as acting simultaneously to ensure long run-out distances to the flow even on low gradient basin plains such as the Marnoso Arenacea.

Mutti et al. (2003; their figure 17) proposed that down flow transitions may occur from massive sandstone formed by a fluidized (liquefied) dense flow (F5 facies) into laminated clean sand formed through traction carpets at the base of turbidity currents (F7 facies), or that if deceleration was rapid that the deposit of the fluidized (liquified) flow could be abruptly replaced by thinner turbidite sand (F9b facies). Facies tracts 3 and 4 illustrate how Cs6 and Cs7 intervals are constantly overlaid and pass downcurrent into a thin rippled laminated interval (Figure 6, 13b and 14c). This is consistent with Mutti's transition from F5 to F9b facies.

Mutti and coworkers infer that dense fluidized flows can also deposit graded sandstone (as part of the F5 facies). We do not think that continuous normally graded sandstone intervals

lacking traction structures are generally deposited by dense fluidized (debris) flows, although crude normal grading is possible in debris flow deposits (Shanmugam, 1995). We argue that normal grading is generally the result of hydraulic selection of grains, and therefore graded sandstone is less likely to be deposited en-masse. Beds containing a basal Cs5 interval don't have a clear grain size break underneath the top rippled interval (Cs1), so they show no evidence of a bipartite flow structure. Our facies tract 1 shows how normally graded sandstone intervals (Cs5) tend to form layers with a gradual tapering shape, with a progressive downcurrent transition to intervals with traction structures (Cs1, Cs2, Cs3). This is consistent with a gradual layer-by-layer deposition from a depleting turbidity current, rather than from a bipartite flow.

Sandy debris flows

The sandy debris flow model of Shanmugam and Moiola (1995) and Shanmugam (1997, 2000, 2002) can also be applied to beds described by facies tract 3 and 4. These authors proposed that massive layers of clean sand could be deposited en-masse by 'freezing' from sandy debris flows characterized by (i) significant yield strength (non-Newtonian rheology), (ii) laminar flow conditions, and (iii) sediment support through matrix strength, buoyancy, and grain-to-grain interactions. Unlike Mutti and coworkers the importance of excess pore fluid pressure was not specifically emphasized in their work. However, recent studies of subaerial debris flows have shown how debris flow behavior is strongly dependent on spatial and temporal variations in excess pore fluid pressures (Iverson, 1997; Iverson and Vallance, 2001; Iverson et al., 2010). The patchy texture of Cs7 sandstone layers records partial liquefaction of sandstone, and therefore supports this view.

Our criteria to identify debris flow deposits differ from those of Shanmugam and Moiola. The eight criteria listed by Shanmugam and Moiola (1995) and Shanmugam (1997) to identify debris flow deposits are (i) ungraded sand with evidence of basal shearing, (ii) concentration of mudstone clasts at the top of the sand interval, (iii) inverse grading of clasts, (iv) dispersed (floating) larger sand grains, (v) planar clast fabric, (vi) presence of shale clasts, (vii) irregular upper surface and lateral pinch-out geometries – suggesting en-masse freezing, (viii) relatively high detrital mud matrix sufficient to induce a plastic rheology with finite yield strength. The clean sand layers that we attribute to debris flow deposition have (i) a swirly fabric indicative of pervasive liquefaction or are ungraded and massive, (ii) a sharp grain size break at their upper boundary, (iii) abrupt lateral pinch outs, and (iv) they sometimes have chaotically distributed clasts. These different criteria result in disagreement over the types of clean sand

layers that were deposited by debris flow. Shanmugam and Moiola (1995) proposed that the Jackfork Group at the the DeGray Spillway in Arkansas, and Shanmugam (2002) proposed that the Annot Sandstone in the Piera Cave road section, also contains clean sand debris flow deposits. Based on our different criteria, we would not infer that either of these two sections contains clean sandstones deposited en-masse by debris flow, as discussed more fully by Talling et al. (2012a).

Our data show for the first time how dense debris flows can indeed sometimes deposit clean sand layers that pinch out abruptly. Therefore this work represents the first test of Shanmugam and Moiola (1995) hypothesis. Despite the different criteria adopted, and the different role attributed to excess pore pressure, we concur with these authors that dense sandy debris flows are indeed a viable mechanism for transporting and depositing sand, and that these flows can possibly travel for long distances on gentle (<1 degree) slopes.

Flow transformations

Submarine sediment gravity flows can transform from one type of flow condition to another down slope (e.g. Lowe, 1982; Kneller and Branney, 1995; Haughton, 2003; Talling et al, 2007a, 2012a). It has previously been proposed that an initial debris flow (Marr et al., 2001), liquefied flow (Lowe, 1976) or fluidized flow (Mutti et al., 2003) may evolve down slope into a more dilute turbidity current as it partially mixes with surrounding seawater. However, our field observations suggest that the reverse transformation occurs with an initial high density turbidity current evolving into a more-distal pervasively-liquefied debris flow (Fig. 3.15 and 3.16). A similar transformation was proposed by Lowe (1976) for a high density turbidity current eventually transforming into a partially liquefied flow due to decreasing slope and flow dispersion, but no field data were produced to support this view.

3.7. CONCLUSIONS

The Marnoso-arenacea Formation in the northern Italian Apennines is the only place worldwide where individual ancient flow deposits (beds) can be mapped out in such detail for up to 120 km. These unusually extensive bed correlations provide new insight into how submarine sediment flows evolved as they spread across a low gradient basin plain. The shape of sandstone intervals provides an independent test of depositional processes inferred initially from their internal characteristics at a single outcrop. Four deposit geometries (or facies tracts)

occur in down flow transects through beds in a newly studied stratigraphic interval below the Contessa marker bed. Individual beds can contain more than one of these facies tracts. Facies tracts 1 and 2 contains clean graded sandstone intervals that were deposited layer-by-layer by a turbidity current, and these clean sandstone intervals taper gradually down flow. Muddy sandstone deposited by debris flow occurs in facies tract 2. Facies tract 3 contains clean sandstone with a distinctive swirly fabric formed by patches of coarser and better sorted grains. This distinctive fabric most likely recorded pervasive liquefaction. This type of clean sandstone pinches out abruptly, and this pinch out geometry suggests it was most likely deposited by dense and pervasively-liquefied debris flow. Facies tract 1b contains massive ungraded sandstone intervals that pinch out abruptly, although less abruptly than the swirly clean sandstone in facies tract 3. This deposit shape most likely indicates deposition of massive ungraded sandstone by debris flow rather than by a steady turbidity current. We therefore present field data that suggest dense debris flows with elevated pore pressures can sometimes deposit clean sand over large expanses (up to 30 km) of sea floor. Down-flow transitions from turbidite sandstone to debrite sandstone suggest that clean sand debris flows sometimes formed through transformation from an initial turbidity current. However, in at least one case, a clean sand debris flow that contained chaotically distributed clasts may have run out for long distances on low gradients across this basin plain.

CHAPTER 4:
EXTERNAL SHAPE OF TURBIDITE BEDS IN THE MARNOSO ARENACEA FORMATION

4.1. INTRODUCTION

There are remarkably few direct measurements from active submarine density flows (e.g. Xu et al., 2011), even though they dominate sediment fluxes across large areas of the planet. This means that much of our understanding of such flows must be pieced together from studies of their deposits. These deposits must be mapped out in order to understand how flows evolve spatially, which is an important part of their character. Very few studies have documented the external shape of turbidite beds through the correlation of individual flow deposits for long distances. This is because turbidite deposits are commonly eroded by subsequent flows, causing bed truncation and amalgamation (Enos, 1969), and because suitable marker beds that allow correlation between individual outcrops are rare. Longer distance correlations have been made using sediment cores from beneath the modern sea floor (Talling et al., 2007; Frenz et al., 2008; Wynn et al., 2010) but such cores tend to be relatively short (< 10 m), which limits the number of beds that can be studied. Numerous much deeper and very expensive drill cores would be needed to study longer sequences of beds beneath the sea floor. The Miocene Marnoso Arenacea Formation, in the Northern Italian Apennines provides the most extensive correlation of individual flow deposits (beds) yet documented for any ancient turbidite sequence (Ricci Lucchi & Valmori, 1980; Amy & Talling, 2006; Talling et al., 2007a; Muzzi Magalles and Tinterri, 2010). It has an advantage over modern sea-floor cores in that many tens of beds can be studied allowing their full variability and characteristic shape of beds to be better constrained, although changes in sea floor gradient are more poorly constrained for such ancient outcrops.

The beds in the Marnoso Arencea sequence were deposited within a non-channelized basin plain, and are separated by intervening intervals of hemipelagic sedimentation. Megaturbidites act as marker beds, allowing intervening beds to be correlated between more than one hundred section across the whole basin. This topographically simple basin plain setting has produced a 'layer cake' stratigraphy with almost no bed amalgamation and little or no evidence of flow reflection (except in the megaturbidites; Talling et al., 2007b). It was thought that this basin plain setting would produce simple bed geometries that could be easily compared to modeling results. However,

despite the simple topographic setting, the beds are highly complex. They often record multiple very different flow types within a single overall event, with lateral or down flow transitions between these flow types within the basin plain (Amy and Talling, 2006; Talling et al., 2007a,b; Talling et al., 2012a,b; Sumner et al., 2012). Some of these flow transitions have now been recognized in hybrid beds from other locations worldwide (Haughton et al., 2003, 2009; Talling et al., 2004, 2010, 2012c).

Amy and Talling (2006), Talling et al. (2007a, b) and Sumner et al. (2012) documented the external shape and internal architecture of up to 56 beds correlated in a stratigraphic interval comprised between the Contessa megabed and the first overlying Colombine marker (the 'above-Contessa' interval). This study expands this database by mapping a further 13 beds deposited in the stratigraphic interval deposited below the Contessa megabed (the 'below-Contessa' interval) previously described in chapter 3. These below Contessa beds were mapped using detailed bed-by-bed correlations along a 60 km transect sub-parallel to the paleoflow direction, which represents a further 200 days of field work, in addition to the > 3 person years previously spent mapping the above Contessa interval beds (Amy et al., 2005; Amy and Talling, 2006; Talling et al., 2007a,b; Talling et al., 2012; Sumner et al., 2012). In this contribution, the shape of 32 individual beds from both above-Contessa and below-Contessa intervals are analyzed together, representing a stratigraphic interval that is ~60 m thick.

This study is novel because of the large number of beds described, which aids recognition of underlying trends in bed shape in this basin plain setting.. These beds include down-flow facies tracts not seen in the above-Contessa beds (Chapter 3). The previous analysis of bed shape by Talling et al. (2007a) and Sumner et al. (2012) was qualitative, rather than the quantitative analysis that is presented here for the much larger data set. This contribution also presents novel numerical modeling results that provide key insights into how deposit shape is related to sediment concentration within the flow. It is hoped that the results presented here will be compared in future studies to deposits produced by small-scale laboratory experiments and analytical or finite-element mathematical models, in order to assess the scaling issues and assumptions involved in such modeling.

4.2. AIMS

This study quantitatively describes the two-dimensional down flow shape of individual submarine density flow deposits in order to better understand the character and evolution of these flows. This includes analysis of the whole bed shape, the shape of individual lithofacies within the bed, and spatial changes in grain size. Field observations are used to infer which sandstone intervals were most likely deposited by low-density or high-density flow types, as a single bed can often contain both types of deposit (Talling et al., 2012a). In some cases it is equivocal whether an interval represents a low density or high density flow deposits (e.g. planar laminated intervals), and this issue is discussed. This subdivision then allows a separate analysis of sandstone deposit shape for low-density and by high-density flows, and their arrangement within a bed. The shape of turbidite mudstone intervals are then documented, and compared to the shape of sandstone intervals. The overall aims are to determine (i) whether beds or sub-intervals display consistent shapes, and what these shapes are, (ii) how bed or interval shape changes with increasing flow volume or grain size, and (iii) therefore how bed architecture most likely records flow processes.

4.3. METHODOLOGY

4.3.1. Bed correlations

This contribution is based on correlation of 32 individual beds along the Ridracoli structural element (figure 4.1). The cross section is sub-parallel to the basin's inner margin, and sub- parallel to the observed paleo-flow direction (figure 4.1). Each bed has been correlated between at least ten, and sometime up to nineteen sections in the below-Contessa interval. Beds correlated between nine or less sections have been discarded from this analysis to avoid inaccuracy in the bed shape modeling. The correlations extend for a total distance of approximately 60 km in a northwest to southeast direction (figure 4.1). Thickness, grain size and paleocurrent data for beds in the above Contessa interval were obtained from previous published work by Talling et al (2004, 2007a, 2007b) and Amy and Talling (2006). Correlation panels for the below-Contessa interval are presented in chapter 3. Thick (>40 cm) beds in the above Contessa interval were named bed 0 to bed 8. Beds located between key beds are numbered according to their position above each key bed. Beds in

the below Contessa interval are numbered sequentially from -1 to -20,with our Bed -20 also being bed A-20 in the scheme of Ricci Lucchi and Valmori (1980).

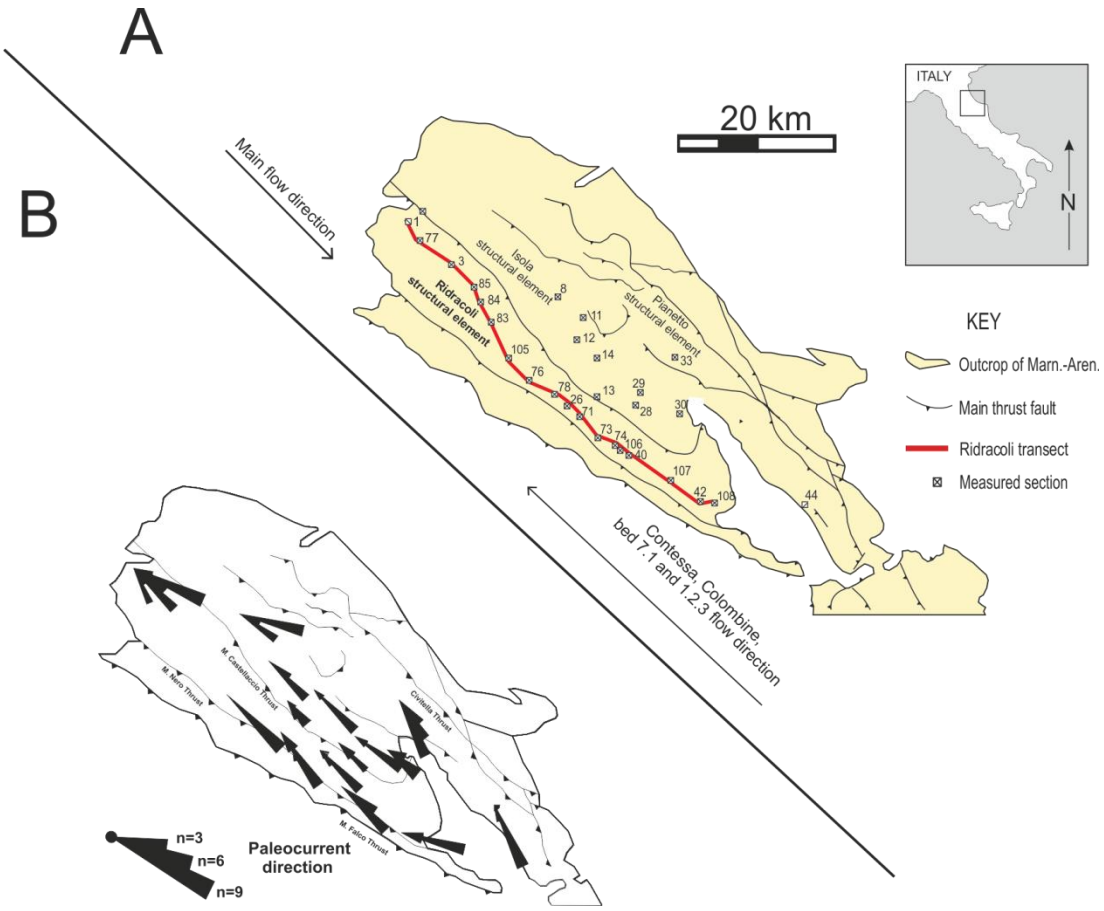

Figure 4.1. *Location map showing the northern part of the outcrop of the Marnoso-arenacea Formation. The figure shows the position of measured sections and the transect along the Ridracoli structural element (red line) along which bed in the below-Contessa interval have been correlated. Sections are numbered as for Amy & Talling, 2006 and chapter 3. (B) Palaeocurrent directions measured from flutes and grooves at the base of the beds in the below- Contessa interval.*

4.3.2. Differential compaction

It is assumed herein that uniform compaction affected sandstone intervals. The sandstone deposit is flattened but its shape is not otherwise distorted significantly. The maximum burial depth of Marnoso Arenacea outcrops varies from ~5 to ~2.5 km across the foredeep basin. This is likely to cause variations in the original sandstone thickness of approximately 16% (Amy & Talling, 2006). However, burial depths show less variation along transects used to define bed shape that

are orientated parallel to the basin axis (Zattin et al., 2002, their fig. 16). Mudstone intervals will have been compacted to a greater degree than sandstone intervals (Amy & Talling, 2006).

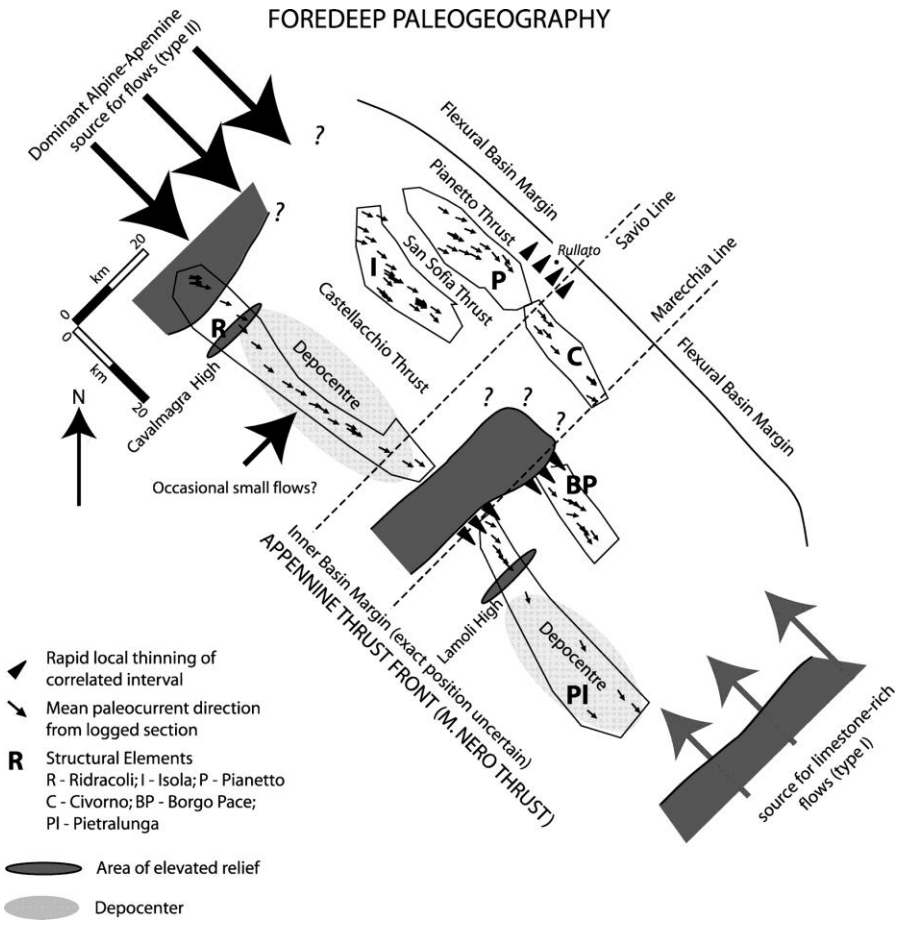

Figure 4.2. *Paleogeographic reconstruction of the Marnoso Arenacea Formation ''inner'' foredeep basin at the time of deposition for the above Contessa interval. Structural elements have been repositioned to reflect structural reconstructions that suggest that the basin was originally twice as wide (Ricci Lucchi and Valmori, 1980; Van Wamel and Zwart, 1990). It is inferred that most offset occurred on the Castelleccio Thrust. The mean paleocurrent direction for each logged section is shown. From Talling et al. (2007a.)*

4.3.3. Foredeeep paleogeography

Both stratigraphic intervals were deposited in a relatively flat basin plain as inferred from the ability of the flows to transverse the area in opposite directions, the absence of channelization and the continuous sheet-like general bed geometry (Ricci Lucchi & Valmori, 1980; Amy & Talling,

2006; Talling et al., 2007a). Modern basin plains have sea floor gradients that are often less than 0.05° (Talling et al., 2007a). At the time of deposition three subtle intrabasinal highs (Verghereto, Cavalmagra and Lamoli highs, figure 4.2) were present within the foredeep basin plain. They are inferred from the isopachs of the entire correlated interval for both the above-Contessa and below-Contessa intervals, and from the local termination of thin beds (Talling et al., 2007a; Chapter 3). The Verghereto high had a greater bathymetric relief than the Cavalmagra and Lamoli highs. The large majority of the flows where able to overtop the highs without significant deflection, and therefore the relief is inferred to be substantially less than the thickness of such flows (Talling et al., 2007a).

		Area (m^2)							
Bed	**Prov.**	**Total**	**Sand**	**Mud**	**Ta-b**	**Tc-d**	**Dcs**	**Dm**	**S/M**
Col.	SE	86569	12411	74158	0	12411	0	0	0,17
8.1.2	NW	8807	665	8142	0	665	0	0	0,08
8	NW	41029	20685	20344	16343	4341	0	0	1,02
7.9	NW	24122	11676	12446	1909	9767	0	0	0,94
7.1	SE	12862	471	12391	0	471	0	0	0,04
7	NW	59198	21188	38010	16000	1936	0	3251	0,56
6	NW	90795	51923	38872	30480	11995	0	9448	1,34
5.3	NW	16730	9399	7331	0	9399	0	0	1,28
5.1	NW	42840	28988	13852	12446	5425	11116	0	2,09
5	NW	76006	49987	26019	36284	5173	0	8529	1,92
4.1	NW	15929	6296	9633	0	6296	0	0	0,65
4	NW	94866	57319	37547	40800	16519	0	0	1,53
3	NW	73187	51569	21618	32888	5262	0	13418	2,39
2.5	NW	26633	12084	14549	7838	1382	0	2863	0,83
2	NW	66750	51944	14806	28220	23723	0	0	3,51
1.5	NW	10651	3018	7633	0	3018	0	0	0,39
1.2.3	SE	32135	6894	25241	0	6894	0	0	0,27
1	NW	40108	21359	18749	14056	2585	0	4717	1,14
0	NW	61173	49860	11313	23994	12874	12991	0	4,41
-2	NW	65892	49531	16361	35011	14519	0	0	3,01
-5	NW	16716	8081	8635	0	8081	0	0	0,94
-6	NW	67280	57621	9659	43820	5769	8031	0	5,97

Table 4.1. *Cross sectional area in the Ridracoli thrust sheet of different lithofacies and sand/mud ratio for each bed.For each bed the provenance (North-West or South-East), the cross sectional area and the area of sandstone, mudstone, Ta-b, Tc-d, clean and muddy debrite is provided.*

4.3.4. Bed volumes and cross sectional areas

Talling et al. (2007a) estimated the volume of sandstone and mudstone intervals for each bed in the above-Contessa interval based on 109 stratigraphic sections spread across the whole Marnoso Arenacea outcrop area. Volumes were estimated independently for each thrust sheet (which have been called structural elements in previous work) using an 'inverse distance to a power' algorithm. In structural elements where sections are located primarily along down-basin transects, such as the Ridracoli Element, Talling et al. (2007a) considered the thickness of each bed nearly constant across the basin. These are most likely minimum estimates of volume because they do not consider sediment deposited outside the outcrop area.

This contribution analyses 32 beds from both the above-Contessa and newly studied below-Contessa intervals along a single transect along the Ridracoli structural element (figure 4.1). The cross sectional area of sandstone and mudstone intervals in the correlation panel was estimated for each bed, instead of the bed volume. This avoids uncertainties in volume estimates due to the basin width. The area of each bed, and of each lithofacies is presented in table 4.1.

Across-basin correlation between the Ridracoli, Isola and Pianetto thrust sheets, for both the above and below Contessa intervals, indicate a gradual thinning of the beds towards the flexural basin margin located in the East of the study area (chapter 3; Amy and Talling, 2006). It is reasonable to assume that beds with larger cross-sectional area in the Ridracoli Element would correspond generally to larger volume beds in the wider basin (figure 4.2) and the paleocurrent direction consistently sub-parallel to the basin margins (chapter 3, figure 1b). This correspondence is confirmed by a comparison between the cross sectional area calculated in this study and the total sandstone volume obtained by Talling et al., 2007b (figure 4.3).

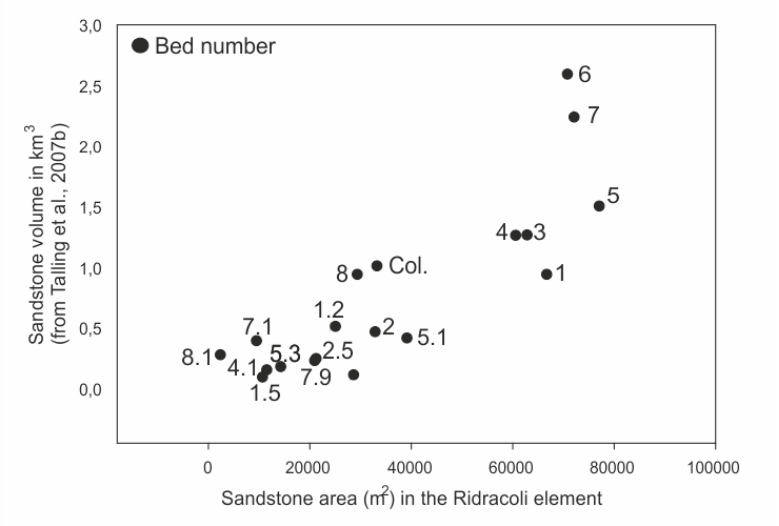

Figure 4.3. *Comparison between the sandstone volumes estimated by Talling et al. (2007b) using 109 locations on seven thrust sheets (figure 4.1), and the cross sectional areas calculated for each sandstone interval in the Ridracoli thrust sheet (figure 4.1). Data are from beds in the above-Contessa stratigraphic interval.*

4.3.5. Grain size

Grain size was measured in the field using hand lens and a grain size comparator.

4.3.6. Facies scheme and depositional processes

The deposits that form the basis of this study are fully described in chapter 3, and summarized in table 3.1. In this chapter the widely used Bouma (1962) facies scheme will be adopted, as modified by Talling et al. (2012b). Talling et al., (2012b) provides a full summary of definitions, including those for turbidity current and debris flow.

The near-bed sedimentation processes for each division (Ta to Te, plus clean and muddy debrite) will now briefly be described, in order to distinguish between intervals deposited by low density and high density flow types. This then allows the shape of high-density and low-density turbidity current, and mud-rich or mud-poor debrites, to be analyzed separately. A summary of the different bed types, and the most likely depositional mechanism is presented in figure 4.4.

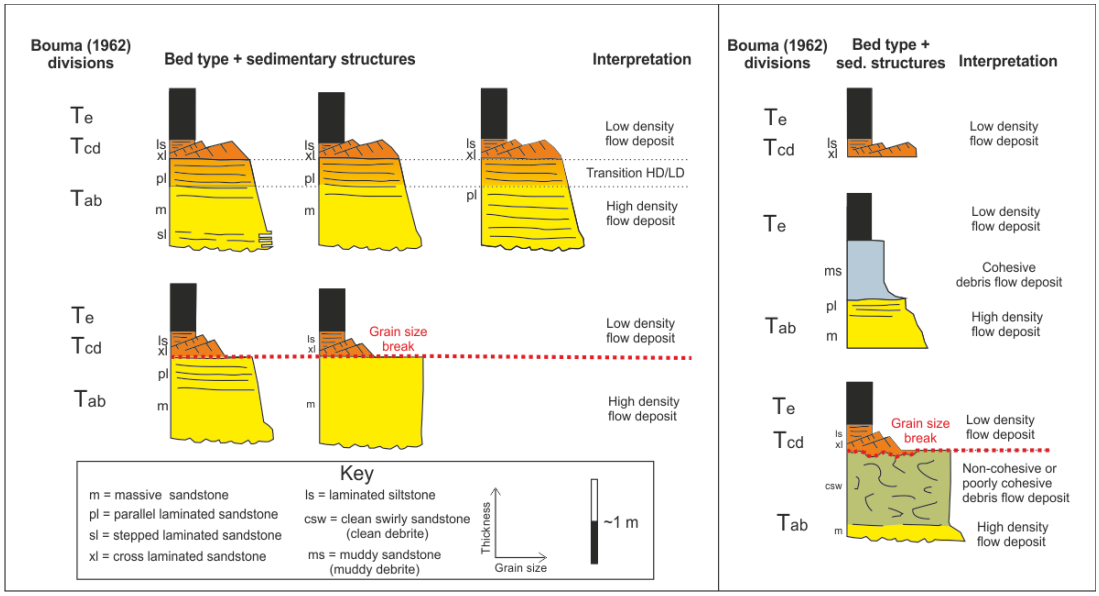

Figure 4.4. *Generalized graphic sedimentary logs that summarise the deposits produced by different types of submarine flow. Depositional intervals and the corresponding Bouma (1962) division are shown. The most likely depositional process is indicated for each type of interval.*

Massive sandstone (Ta) lacking a swirly texture

As discussed in chapter 3 clean (mud-poor) massive sandstone (subfacies Cs5 and Cs6) can be deposited in two distinct ways; incrementally in a layer-by-layer fashion by high-density turbidity currents or in an en-masse fashion by (liquefied) debris flow. Experiments (Leclair & Arnott, 2005; Sumner et al., 2008) demonstrate that structureless sand forms when deposition rates are sufficient to suppress bedform formation. Structureless sand can form either from direct sedimentation with little movement of particles along the bed before burial in the deposit, or via the rapid collapse of shearing high-concentration near-bed layers, termed laminar sheared layers (Sumner et al., 2008). In the Marnoso Arenacea Formation, clean structureless sandstone deposits are poorly sorted, suggesting that the basal region of the flow was sufficiently concentrated to inhibit segregation of particles of different sizes (Amy et al., 2006; Dorrell et al., 2010).

Clean debrite intervals (D_{CS})

Mud poor, swirly sandstone intervals with common chaotic and swirly areas of coarser grained and better sorted grains (subfacies Cs7) are inferred to result from deposition by a relatively dense liquefied debris flow (chapter 3), as confirmed by the characteristic abrupt lateral pinch-out of the deposits. The “patchy” texture most likely results from slow convection and

elutriation of fine material during the liquefaction process. Cs7 intervals may extent to the most proximal available outcrops, or have lateral and up-flow transitions from into clean massive (Cs5, Cs6) or parallel laminated (Cs3, Cs4) intervals. These D_{CLS} intervals can be distinguished from massive TA clean sandstone intervals as set out by Chapter 3.

Muddy debrite intervals (D_M)

Mud-rich (25% to 50% of particles <30 μm, Talling et al., 20012c) and ungraded sandstone lithofacies record evidence of en-masse settling in which size-segregation was suppressed (Amy et al., 2006), and are inferred to be the deposits of cohesive debris flows. Mud-rich sandstone intervals observed in the Ridracoli element contain either no mud clasts or very small (< 5 mm) mud clasts. Clast-rich muddy sandstone intervals are common in other structural elements (Isola and Pianetto). The absence or small size of mud clasts suggests relatively low strength, as does the passive infilling of dune crests (Talling et al., 2012c). The muddy ungraded debrite sandstone grades laterally down-flow into even finer-grained graded muddy-silt. This lateral grading may result from progressive dilution of the low strength debris flow as it mixes relatively easily with surrounding seawater (Talling et al., 2007a). The most likely origin of these low-strength cohesive debris flows is that a flow transformation did occur within the basin from fully-turbulent turbidity current to (laminar) debris flow (Talling et al., 2012c). The flow transformation occurred as the flow slowed down, such that cohesive bonds developed between the existing cohesive fine-mud particles within the flow, as suggested by laboratory experiments of Baas et al. (2009, 2011) and Sumner et al. (2009).

Tb intervals

Laminated sandstone intervals (T_B) are difficult to classify because they have the potential to be formed by both low-density and high-density turbidity currents. Fine scale planar lamination can be formed in two ways: (i) incrementally by migration of low amplitude bed waves beneath dilute flows (Best & Bridge, 1994), or (ii) by repeated collapse of traction carpets beneath high-density turbidity currents (Kuenen, 1966; Leclair & Arnott, 2005; Sumner et al., 2008). The boundary between high density and low density turbidite deposition therefore lies most likely within the Tb interval, and planar laminations produced by dilute flows and high-density flows may be very difficult to distinguish unambiguously (figure 4.4).

This boundary can be recognized more confidently when Tb intervals are overlaid by a clear grain size break to finer graded intervals. This grain-size brake has ben inferred previously to represent a distinct interface between the high and low density part of the flow (chapter 3; Talling et al. 2012a; Sumner et al. 2012).

In this study Tb divisions are considered as a part of the high density flow deposits because a lateral transition between massive (Ta) and parallel laminated (Tb) sandstone intervals is commonly observed between adjacent sections, without significant changes in thickness or grain size (i.e. bed -2, figure 4.5). A similar transition is observed between clean debris flow (Cs7) and laminated (Tb) or massive (Ta) turbidite sandstone. This is significant because it suggests that the flow responsible for depositing the different types of sandstone was similar, at least in terms of the rate and duration of sand deposition. This may suggest that the planar laminated (Tb or Cs3) intervals were deposited from relatively high concentration turbidity current (Talling et al., 2012b), instead of dilute turbidity current as has sometimes been inferred (Lowe, 1982).

Stepped planar laminations (subfacies Cs4) are most likely produced incrementally by traction carpets formed in coarser grain sizes beneath high density turbidity currents (Hiscott & Middleton, 1979 & 1980; Lowe,1982), although in the Marnoso Arenacea Formation they lack inverse grading (Sumner et al., 2012).

Tc-d intervals

Ripple-scale and dune-scale cross-lamination (Bouma Tc intervals, subfacies Cs1) provides unambiguous evidence for deposition from low density turbidity current (Simons et al., 1965; ; Allen, 1982; Baas, 1994; Talling et al., 2012b).

Parallel laminated siltstone, or interlaminated siltstone and mudstone (Bouma Td, subfacies Si1 and Si2) most likely results from the deposition from a traction-dominated flow boundary zone beneath a dilute and turbulent current (Amy and Talling, 2006), although its origin is uncertain, and is yet to be reproduced satisfactorily in flume experiments (Talling et al., 2012a). Td divisions are rarely seen in these Marnoso arenacea beds.

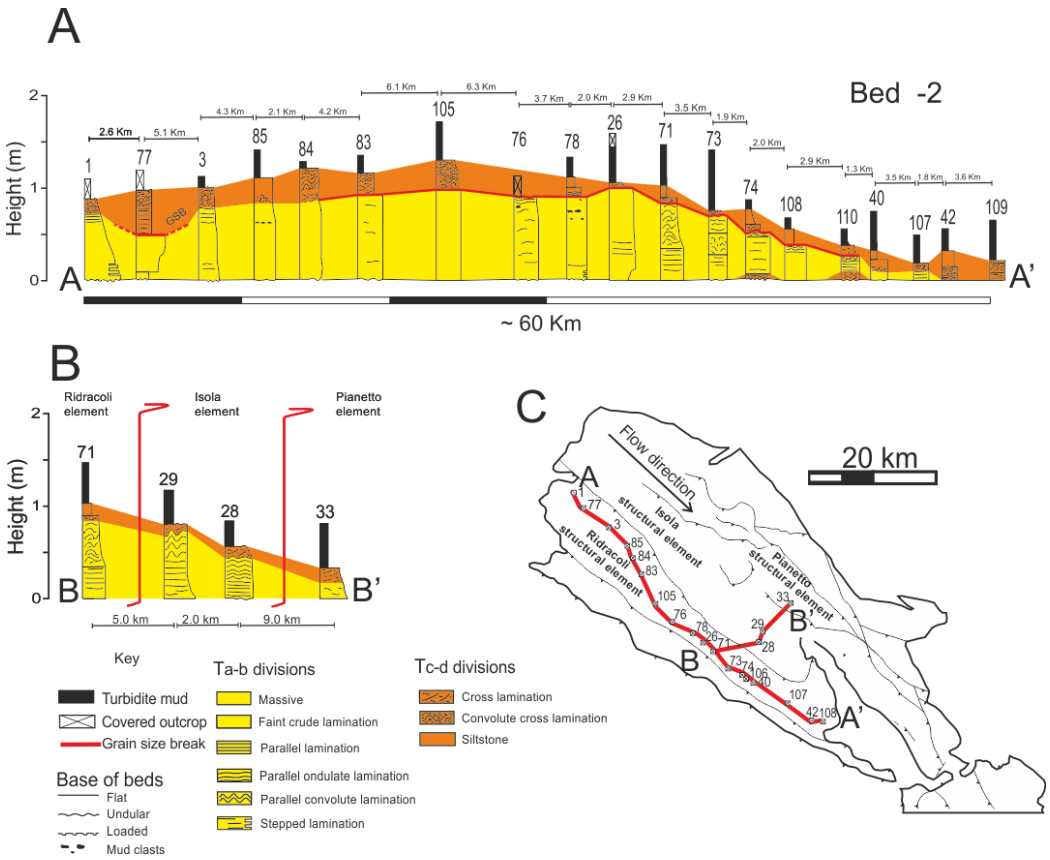

Figure 4.5. A) *Down-flow transect through Bed -2 along the Ridracoli thrust sheet. B) Across flow transect through Bed -2 along the Ridracoli, Isola and Pianetto thrust sheets. C) Location map showing the position of the correlated sections.*

Te intervals

The uppermost mudstone dominated (TE) division of Bouma's (1962) sequence is clearly differentiated in the Marnoso Arenacea deposits from overlying hemipelagic mudstone that settled out from the water column, based on the texture, color and fossil content of the deposits. Turbidite mudstone intervals have been divided into laminated and graded (Te-1), massive and graded (Te-2) and massive and ungraded (Te-3) by Piper (1978). Laminated mudstone (Te-1) is differentiated from very fine sandstone and coarse siltstone laminated intervals of the Bouma's Td division on the basis of the modal grain size. Te intervals have been deposited from a mud density flow which can be initially fully turbulent and dilute, but may also form a denser fluid mud layer that consolidates en masse. See Talling et al. (2012a) for a full discussion on this subject.

4.3.7. Grouping of deposit types

Flow deposits were grouped into the following four classes (i) mudstone, (ii) sandstone deposited by high denity turbidity current (T_{AB}), (ii) sandstone deposited by low density turbidity current (T_{CD}), (iii) cohesive (mud-rich) debite sandstone (D_M), and (iv) clean sandstone debrite (D_{CS}).

4.3.8. Curve fitting

A curve-fitting procedure was adopted in order to quantitatively describe the characteristic shape of turbidite beds or the four deposit types within those beds. The analysis further subdivide beds into those with small, or intermediate to large, cross sectional areas on the Ridracoli thrust sheet. Regression curves were fitted using the *SigmaPlot12* software package regression tool. Each curve was chosen based on the least-square regression coefficient (R^2) and the capacity to match the main geometric characteristics observed in each set of beds, such as the type of distal pinch-out shape (exponential or linear thickness decrease), the presence of a proximal thickening and the variations in the position of the thickness maximum. For each curve, the characteristic constrain parameters (i.e. a and b in a linear equation $y=a+bx$) were then compared to known physical parameters, such as the cross-sectional area, the position of the maximum sandstone thickness *etc.*, in order to better understand the controls on the characteristic bed shape.

4.3.9. Numerical Modelling

A variety of approaches are employed in mathematical modeling of turbidity currents and their deposits. The simplest is a box model, where the height and the length of the current are averaged and the model does not resolve the internal structure of flow (i.e. Dade and Huppert, 1994). Depth averaged models (i.e. Zeng and Lowe, 1997) use the shallow water equations, in which the height of the current is averaged, without trying to resolve vertical velocities within the flow. More computationally demanding models calculate vertical gradients of velocity, turbulence intensity and sediment concentration within the turbidity current (i.e. Felix, 2001; Blanchette e al., 2005).

Depth-averaged numerical modeling of turbidity currents has been performed by Goater (2011) to investigate the effects of hindered settling and particle concentration. In this model it is assumed

that the flow is uniform in the cross slope direction, reducing the model to two dimensions. It's also assumed that the distance travelled by the flow far exceeds the height of the flow and hence the model is depth averaged, ignoring accelerations perpendicular to the lower boundary. The authors consider the effect of hindered settling within the current as opposed to a conventional Stokesian settling law. The Stokesian settling law is generally employed for dilute suspensions. For suspensions of higher concentrations however the settling velocity will be reduced by the effect of an increased viscosity due to the presence of nearby particles and by the motion of interstitial fluid opposing the gravitational settling of the particle due to the motion of surrounding particles (Richardson and Zaki, 1954). Thus a range of models for `hindered settling' have been proposed to model this modification to the Stokesian settling velocity. The authors consider the effect of hindered settling within a turbidity current for a flow over a horizontal surface without entrainment and basal drag to analyze only how this enhanced viscosity will affect the shape of the deposits.

4.4. RESULTS

Bed thickness was normalized by the thickness in the most northwesterly section, in order to show the characteristic shape of beds with increasing volume. The base of each bed is shown as a horizontal datum, in order to illustrate lateral changes in deposit thickness. The external shape (downflow thickness variations) and internal facies architecture (i) turbidite mudstone intervals, (ii) small volume sandstone beds comprising low density flow deposits only (Tc-d), (iii) intermediate and large volume beds comprising both high and low density flow deposits, and the variation of maximum grain sizes deposited for increasing volume beds are shown in figure 4.6, 4.7 and 4.8;. Beds are further subdivided in figure 4.10 into those from different facies tracts, as described in chapter 3.

4.4.1. Small volume beds

Nine small volume (cross sectional sandstone area <10000 m2) beds are described in this study. Seven beds (bed 8.1.2, -9, 1.5, -12, 4.1, 5.3 and -5) with a paleocurrent direction from the Northwest show a consistent shape in normalized graphs (figure 4.6). The turbidite sandstone interval thickness declines abruptly over a distance of ~20-30 km in an approximately exponential fashion, and sandstone thickness is relatively constant in the distal part of the Ridracoli Element. Paleocurrent indicators of two beds (bed 7.1 and 1.2.3) show that these flows originated from the southeast and their sandstone interval have an almost tabular shape in the Ridracoli thrust sheet.

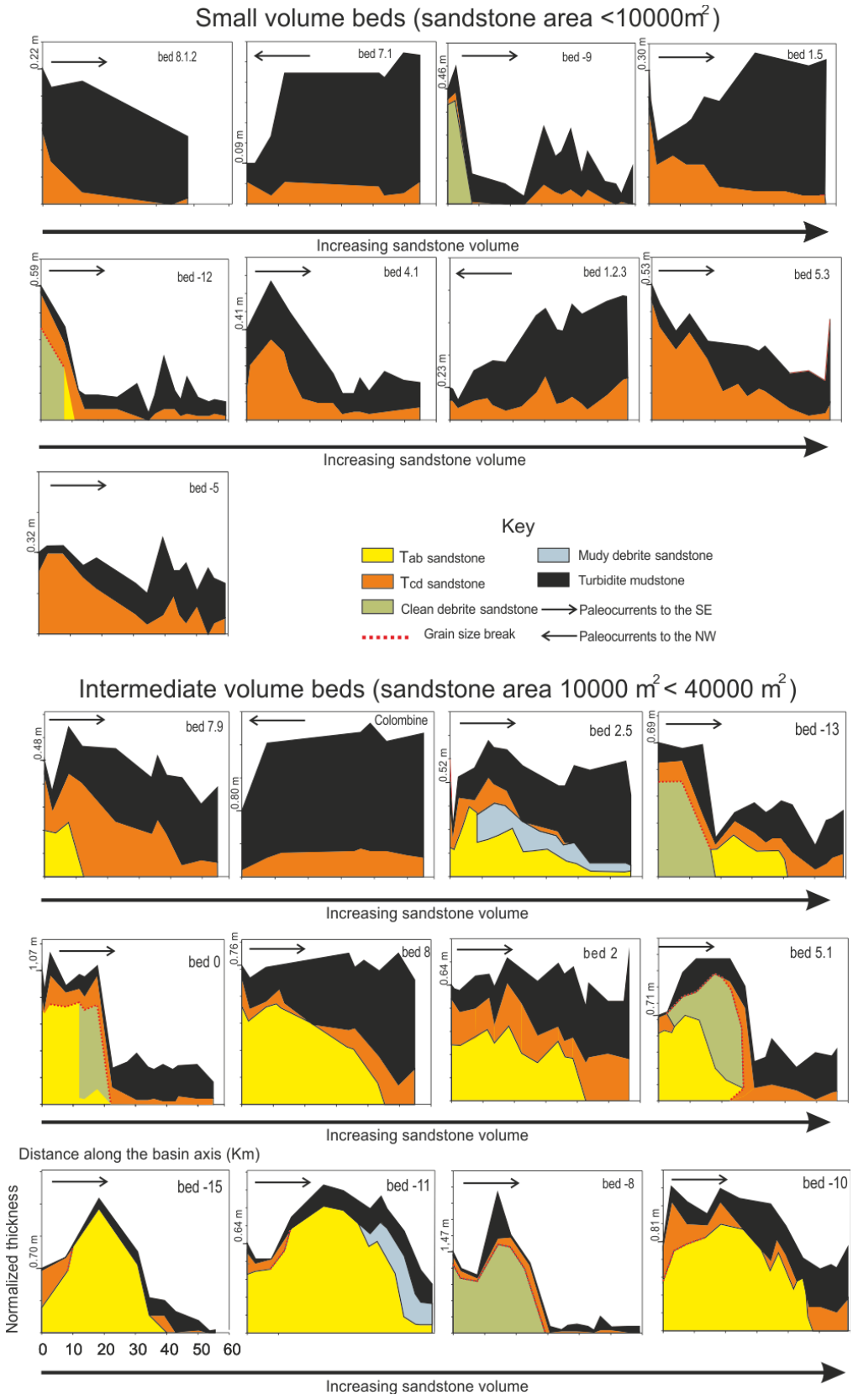

Figure 4.6. (continued)

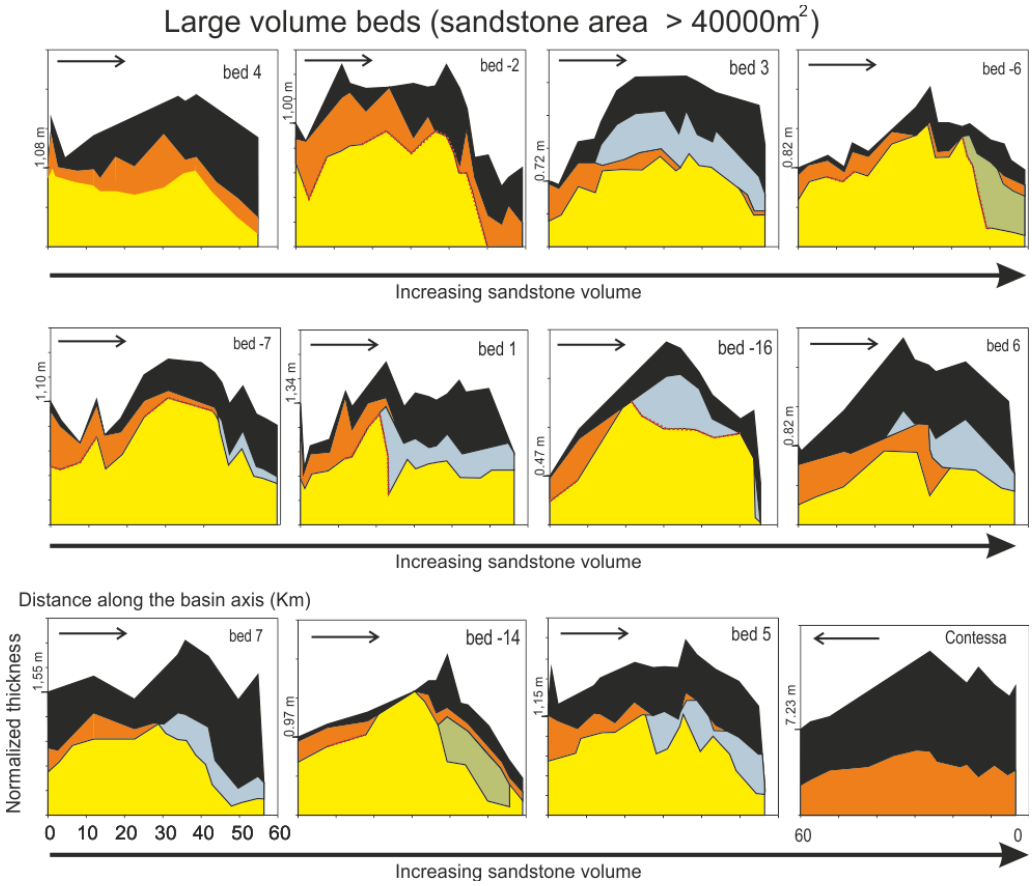

Figure 4.6. *Diagrams illustrating the lateral changes in thickness and internal facies architecture in the 32 turbidite beds from the above-Contessa and below-Contessa intervals, along the Ridracoli Element in a direction sub-parallel to palaeoflow. Beds are ordered with increasing sandstone cross sectional area. As shown by arrows, flows traversed this basin floor in one of two opposing directions. Bed thickness has been normalized. This was done by dividing each thickness by the thickness of each bed at the most proximal section at Km 0 (Coniale 1 section, see figure 4.1a). The total bed thickness at km 0 (coniale) is indicated for each bed. Note that the vertical exaggeration is very large, typically about 1: 30,000. The key shows the facies types used to subdivide each bed, whose rationale is discussed in the text.*

Talling et al (2007a) observed a consistent shape for small volume beds entering the Marnoso Arenacea Foredeep basin from opposite direction, considering also the Pietralunga element.

Sandstone intervals in small volume beds described by facies tract 1 (figure 4.10a) comprise only Tcd and Te divisions, indicating deposition from dilute turbidity currents. Bed -9 and -12 contain a proximal clean sandstone debrite interval (Dcs) that pinches out abruptly, and are described by facies tract 3a (figure 4.10b). The coarser grain size deposited is constantly <187 µm, with a limited fining trend in a basinward direction for beds with provenance from the northwest (figure 4.8a).

4.4.2. Intermediate volume beds

Twelve beds (bed 7.9, Colombine 1, 2.5, .13, 0, 8, 2, 5.1, -15, -11, -8 and -10) have an intermediate sandstone volume (cross sectional area comprised between 10000 and 40000 m^2). All beds have a provenance from the northeast, with the exception of Colombine-1 bed, that shows an opposite paleoflow direction. The sandstone interval of the Colombine-1 bed has a tabular shape, similar to the one observed in other smaller volume beds (7.1 and 1.2.3) with a similar southeasterly provenance.

In proximal and intermediate locations, the sandstone interval of intermediate volume beds characterized by facies tract 1 (beds 7.9, 8, 2,-15, -10) comprises a basal Tab interval constantly overlain by a Tcd interval.

Clean debrite intervals can extend to the most proximal section (facies tract 3a) or have an up-flow transition into Tab sandstone (facies tract 3b) in bed -13, 0, 5.1 and -8.

The point of maximum sandstone thickness is progressively moved basinward with increasing bed volume, and a basinward thickening of the sandstone interval in the most proximal sections is observed.

After the sandstone thickness maximum the basal Tab or clean debrite division pinches-out, with clean debrite divisions pinching out more abruptly than Tab divisions (figure 4.9 and figure 4.10).In beds with facies tract 1, 3a and 3b the distal sandstone component resembles the shape seen in small volume beds, with a gradual thinning of the Tcd interval.

In two beds (bed 2.5 and -11) the top Tcd sandstone interval is not present in the mid-distal sections, replaced by a clast-poor muddy debrite interval (facies tract 2a, figure 4.10).

Flows deposited the coarser grain-size population in the proximal sections, with the exception of beds containing clean sand debrite (Facies tract 3a and 3b, beds 0, 5.1 and -8) that show irregular downflow variations between 0 and ~17 km. A rapid fining is observed in all beds in correspondence to the downflow pinch-out of the basal Tab or clean debrite sandstone interval (figure 4.8b).

4.2.3. Large volume beds

The sandstone thickness of large (cross sectional area >40000 m2) volume beds (bed 4, -2, 3, -6, -7, 1, -16, 6, 7, -14 and 5) is relatively uniform for considerable distances (figure 4.6). A sandstone thickening is observed in the proximal sections, approximately for 20 km, followed by a broad thickness maximum that extends ~30 to 45 km across the central part of the Ridracoli element.

Large volume sandstone beds characterized by facies tract 1 (beds 4 and -2) are constituted by a thick basal interval of Tab sandstone of lenticular shape, overlaid by a thinner interval of Tcd ripple and planar laminated sandstone.

The majority of large volume beds (beds 3, -7, 1, -16, 6, 7 and 5) comprise a lens shaped interval of clast-poor muddy debrite in the central and distal locations (facies tract 2a). Where the muddy debrite interval is present a Tcd clean sandstone interval is not recognized, with the exception of bed 3 and bed 6.

In two beds (bed -6 and -14, facies tract 3c) the Tab interval shows a lateral downflow transition into clean debrite sandstone at approximately 40 km.

A sharp grain size break commonly separates the basal Tab and clean debrite divisions from the top Tcd and muddy debrite intervals , although this break becomes less well developed in distal sections (i.e. bed -2, figure 4.5). An abrupt thinning (pinch-out) of the basal Tab and clean debrite divisions occurs in the distal sections, between 40 and 60 km. The complete pinch-out of Tab and clean debrite divisions is not observed in the Ridracoli element.

Flows depositing large volume beds carry considerably coarse grain size populations (>375μm) for long distances across the basin (figure 4.6c). The maximum grain size profile for each large volume bed across the Ridracoli element show two distinct trends: in a first set of beds (beds 4, -2, 3, -7, 1, 6, 7,-14, 5) the coarser grain size population is deposited in the proximal sections (0 to 15 km), and a relatively coarse (>375μm) maximum grain size is maintained until the mid-distal sections (~45 km) in correspondence to the pinch-out of Tab and clean debrite divisions. A second set of flows (beds -6,-7 -14 and -16) carries its maximum grain size population to the central part of the basin (~30 to 35 km) in correspondence to the sandstone thickness maximum, followed by an abrupt fining.

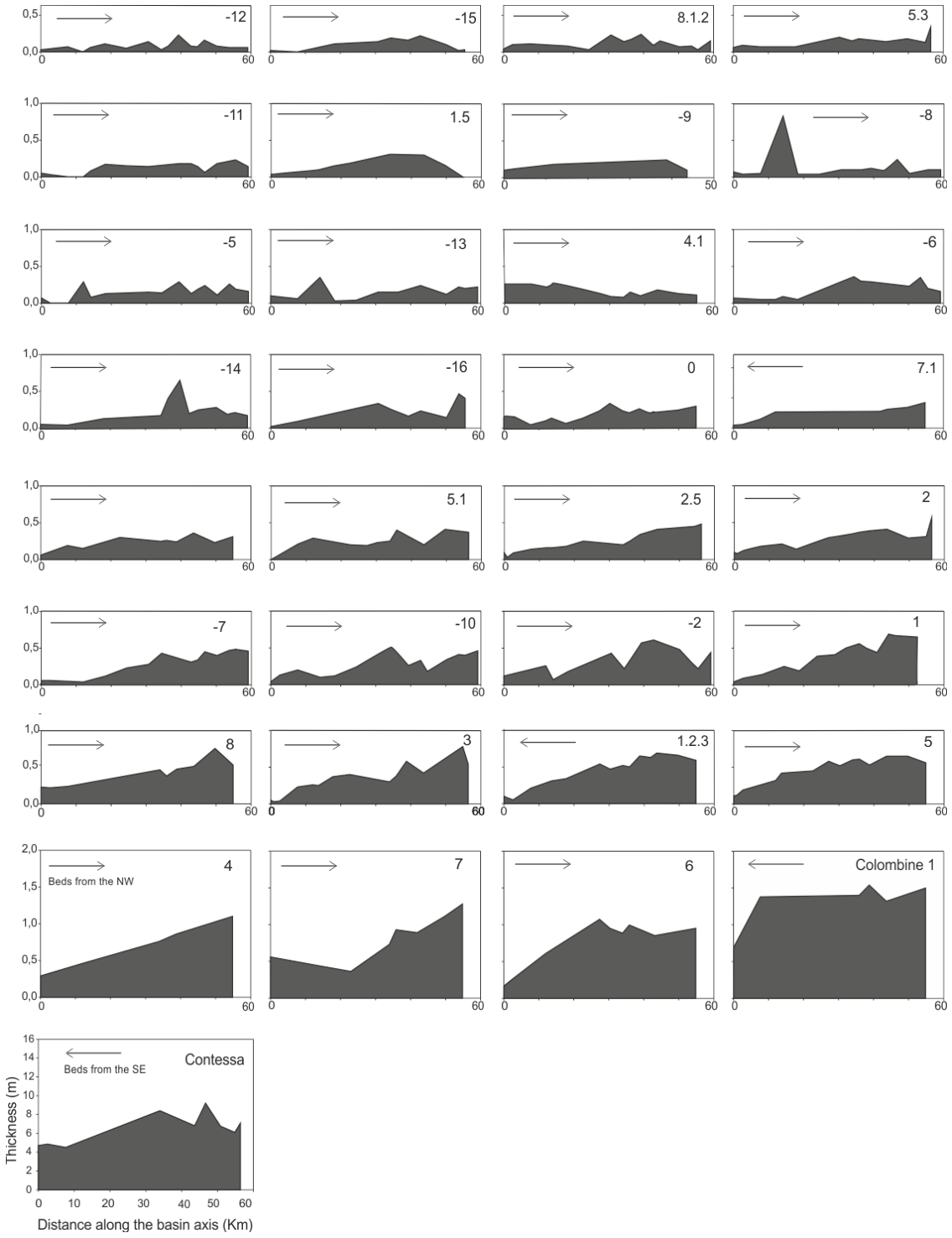

Figure 4.7. *Diagrams illustrating the lateral changes in thickness in the 32 turbidite beds from the above-Contessa and below-Contessa intervals, along the Ridrcoli Element in a direction sub-parallel to palaeoflow (figure 4.1). Diagrams are ordered according to increasing mudstone cross sectional area (a proxy for mud volume). Note that the vertical exaggeration is very large, typically about 1: 30,000.*

4.4.4. Mudstone intervals

The shape of Te intervals for progressively larger mudstone volume beds is presented in figure 4.7. Mudstone thickness was not normalized by its thickness at Coniale, because the total mudstone volume of each bed is not correlated to the total volume of the bed. The volume fraction of mud is higher in small volume beds, and can represent >70% of the total volume (Talling et al., 2007a).The mudstone interval of all the 32 studied beds show a consistent shape, with an increase in thickness from northeast to southwest for beds derived from both the northeast and the southwest. Local thickness variations are not due to erosion by successive flows, because each mudstone interval measured in this study is capped by a hemipelagic marl interval. The two largest volume mudstone beds (bed 6 and Colombine) have a broad thickness maximum in the central and distal part of the Ridracoli element.

4.5. DISCUSSION

4.5.1. What is the external shape of turbidite beds?

Sandstone shape of small volume beds

The turbidite sandstone interval thickness of small volume (<10,000 m^2) beds with provenance from the North-West (beds 8.1.2, -9, 1.5, -12, 4.1, 5.5 and -5) declines abruptly over a distance of 20-30 km in an approximately exponential fashion. Sandstone thickness is then relatively constant in the distal part of the Ridracoli Element. Talling et al (2007a) noted that small volume beds entering the Marnoso Arenacea foredeep basin from opposite direction are characterized by this similar geometry.

This shape is well approximated by an exponentially decreasing function $y=ae^{-bx}$ (figure 4.11a, 4.14a, 4.14b). The parameter *a* is the intercept with the y axis, correspondent to the bed thickness at the section located at 0 km (Coniale section). This value is directly correlated to the total sandstone volume of the bed (figure 4.10b). The parameter *b* corresponds to the curvature of the function. It is more easily defined by its inverse *1/b* that is the distance on the x axis at which y declines to 1/e (~38% of the initial thickness). This parameter (the *e-fold length*) increases with increasing sandstone volumes (figure 4.10c). It is interesting to note that both *a* and *1/b* are

directly correlated to the total sandstone volume. The rate at which sandstone intervals thin appears to decrease as

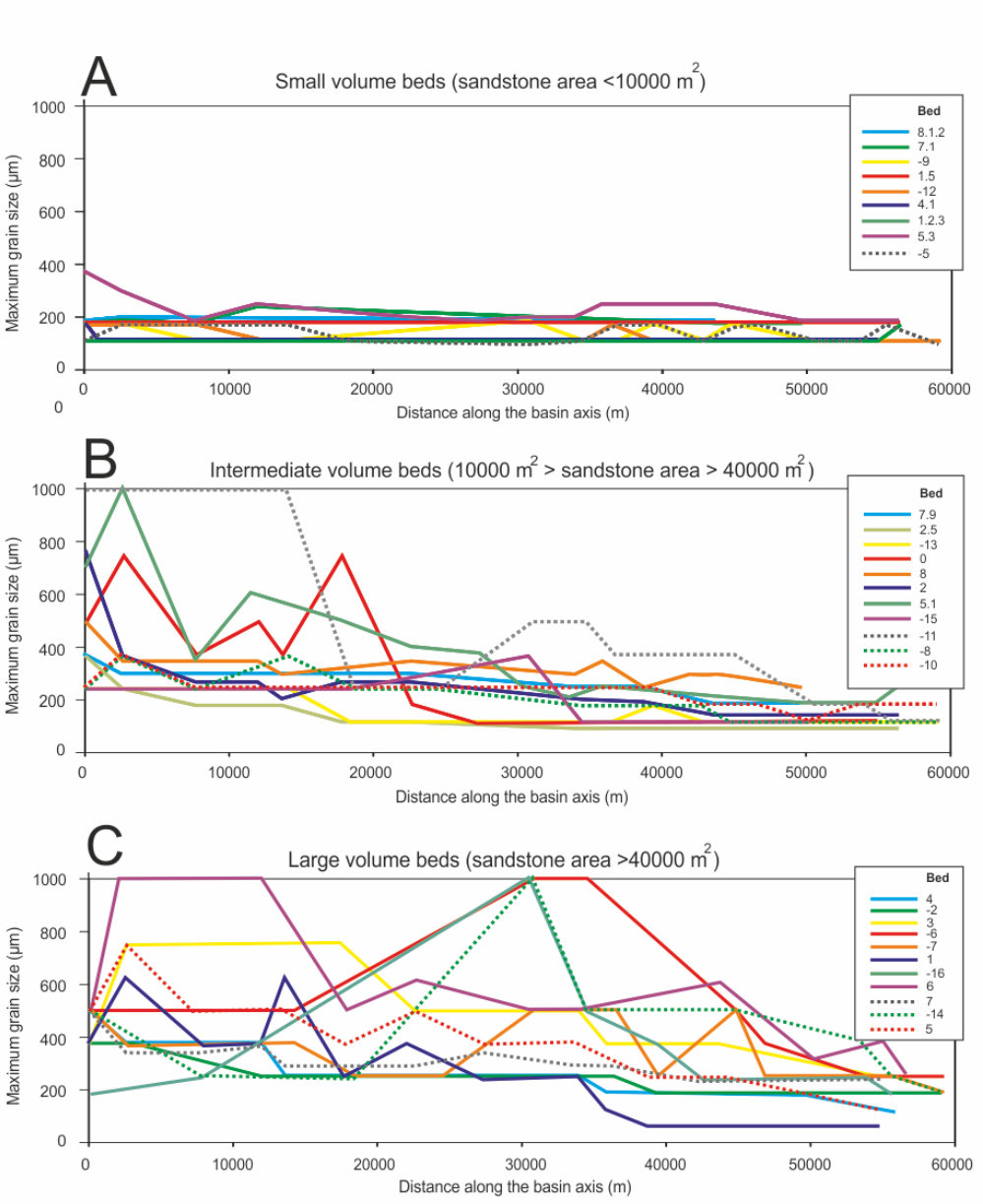

Figure 4.8. *Variation of the maximum grain size measured using a grain size comparator card in the field, for A) small volume beds, B) intermediate volume beds, and C) large volume beds. Note that these values typically correspond to approximately the coarsest 95% percentile of grain size distributions measured from long-axes of grains in thin sections (Talling et al., 2004).*

sandstone volume increases (figure 4.10d). Larger volume beds might be expected to have coarser sand grains with faster settling velocity, which would favor more rapid bed thinning. Therefore, a

more likely explanation for this association could be that larger volume flows are thicker and carry more of their sandy load high above the bed. The bypass of a greater fraction of the sand in this way might lead to a reduced rate of deposit thinning.

Small volume beds with facies tract 3a (beds -9 and -12), that contain a proximal interval of clean debrite, have a higher *a* parameter and lower *b* parameter than beds with facies tract 1 (beds 8.1.2, 1.5, 4.1, 5.5 and -5), resulting in a more rapid downflow thinning (figure 4.14a,1b, table 4.2) and therefore a slightly different shape.

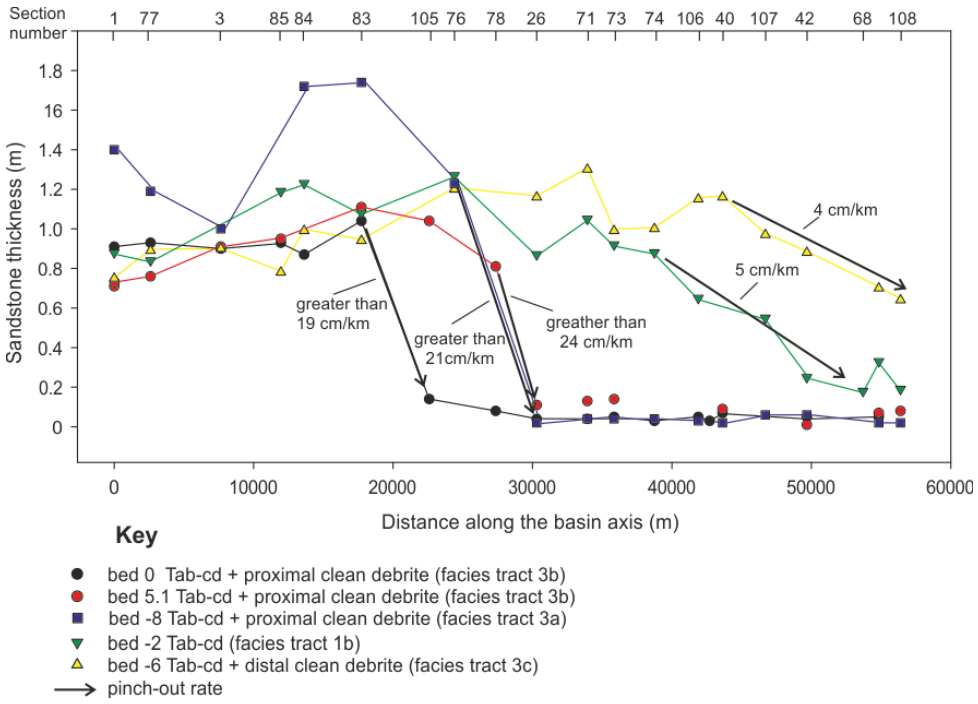

Figure 4.9. *Rates of thinning within five specific beds that display different facies tracts (Talling et al., 2012). See chapter 3 for a full description of the different facies tracts. Rates of thinning in beds 0, 5.1 and -8 are minimum values because pinch out could occur within covered areas lacking rock outcrop, between adjacent logged sections whose position is shown by coloured symbols. Note that there is a ~15,000 fold vertical exaggeration.*

Comparison to small volume beds in levee sequences

Intervals of thin-bedded turbidites are most commonly observed in levee facies adjacent to submarine channels. Submarine levee packages, comprising numerous thin-bedded turbidites, tend to thin away from levee crests in an exponential (i.e. Skene et al. 2002), or power-law fashion (Kane et al., 2007; Dykstra et al., 2011).

Skene et al. (2002) studied the geometry of six submarine channel-levee systems of different size using seismic profiles, and quantitatively described the external shape of levee packages as exponentially thinning both in down-channel and across-channel direction in all the studied systems. The levee packages *e-folding length* (down-channel) and *e-folding width* (across-channel) was found to directly correlate to the channel dimensions (channel width and relief; their figure 9 and 10); the product of the two was found to correlate to the through-channel fluid volume discharge.

In this contribution the *e-folding length* of exponentially thinning small volume basin plain turbidites increases with the total sediment volume of each bed (figure 4.10c). This is most likely because thicker and larger volume flows carry more of their load high above the bed, leading to the bypass of a greater fraction of the sand and therefore a reduced rate of deposit thinning.

In the Marnoso Arenacea turbidites the across-flow *e-folding width* may be much less important, because paleocurrents indicate that flows were forced in a consistent down-basin direction, and were not able to spread radially such as in channel-levee systems.

Nakajima and Kneller (2011) observed that the variation in levee thickness away from the channel shows a pattern of power-law decay on steeper levee-flank slopes (generally >0.7°) and either exponential or logarithmic decay on gentler slopes.

A theoretical analysis of Birman et al. (2009) indicate that this difference in thickness decay style may be related to an higher fluid entrainment rate of levee-depositing turbulent flows on steeper slopes, compared to low gradient basin floor slopes.

Kane et al. (2010), based on laboratory experiments, explain this difference indicating that levee-depositing flows in a basin floor environment are typically fine-grained, and slope angles are very low; here sedimentation is dominated by suspended load deposition, which leads to an exponential decay in levee thickness away from the channel. In slope environments, where flows carry a wider sediment grain-size range and are strongly overspilling, the capacity of flows to maintain their suspended load is overcome at the point of loss of confinement; deposition by fallout becomes dominant, leading to power-law thinning trends.

Tc-d small volume turbidites in this study (facies tract 1) thins in an exponential fashion, and this is in agreement with deposition from a fine grained, low-density flow where the large majority of

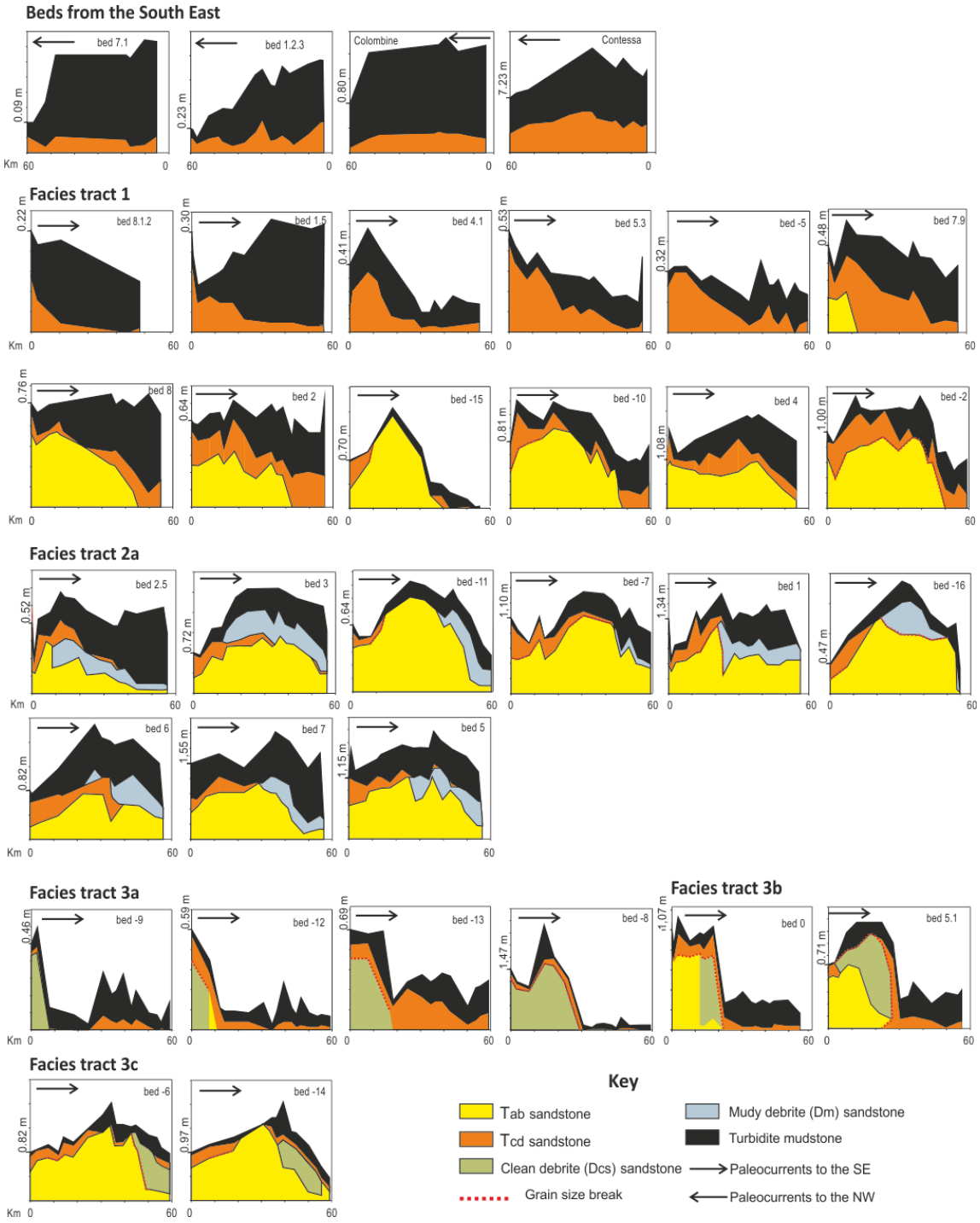

Figure 4.10. *Diagrams illustrating the lateral changes in thickness and internal facies architecture in the 32 turbidite beds from the above-Contessa and below-Contessa intervals, along the Ridracoli Element in a direction sub-parallel to palaeoflow. Beds are subdivided according to the downflow facies architecture (facies tracts).. As shown by arrows, flows traversed this basin floor in one of two opposing directions. Bed thickness has been normalized. This was done by dividing each thickness by the thickness of each bed at the most proximal section at Km 0 (Coniale 1 section, see figure 4.1a). The total bed thickness at km 0 (Coniale) is indicated for each bed. Note that the vertical exaggeration is very large, typically about 1: 30,000. The key shows the facies types used to subdivide each bed, whose rationale is discussed in the text.*

sandstone grains are carried in suspension high above the bed. Flow depositing small volume beds containing clean debrite (facies tract 3a, beds -9 and -12) carried an overall coarser and less well sorted grain size range, and have a more rapid down-flow thinning in respect to Tc-d beds of similar volume (figure 4.10d). This is in agreement with the observation of Kane et al. (2010), although here Dcs sandstone was most likely deposited by liquefied debris flow (as explained in chapter 3) and Tcd and Dcs beds experienced a similar slope gradient.

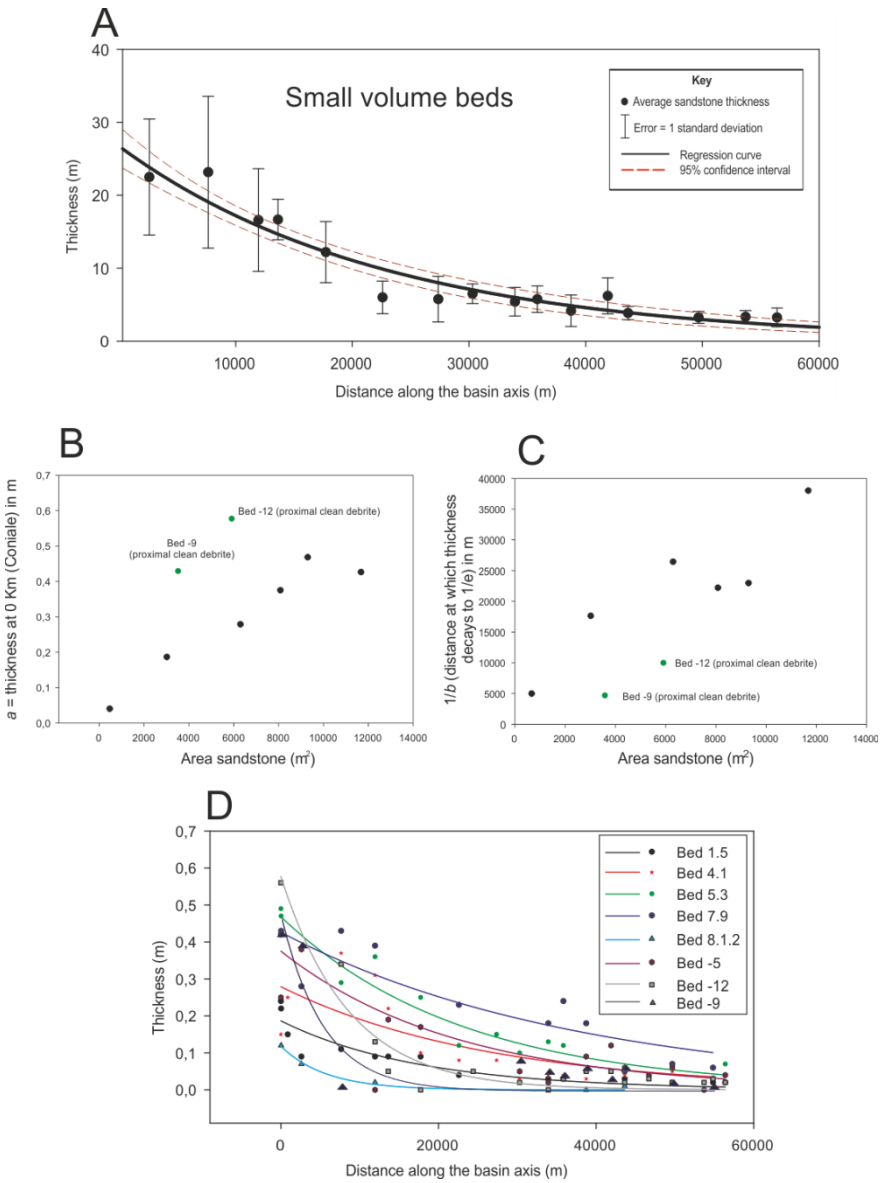

Figure 4.11. *Sandstone interval shape in small volume beds along the Ridracoli thrust sheet (figure 1). A) Regression curve describing the lateral thickness variations in the average thickness of sandstone intervals in small volume beds, which are shown on figure 4.6. The 95% confidence limit and the standard deviation of sandstone thickness in each section are shown. The regression .coefficients are shown in table 2. B) Sandstone thickness in each of the nine beds at the Coniale*

section (corresponding to the 'a' parameter in the regression curve) plotted against the calculated sandstone cross sectional area. Maximum sandstone thickness plotted against the calculated sandstone cross sectional area. C) Distance over which thickness decays to 1/e (37%) of its original value, which is equivalent to 1/b in the best fit line. This distance is also named the e-fold length, and here it is plotted against the cross sectional sandstone area of small volume beds. D) Regression curve describing the exponential thinning of sandstone intervals in small volume beds with provenance from the North West.

Sandstone shape of intermediate and large volume beds

The characteristic sandstone shape of intermediate and large volume beds differs from the one of small volume beds formed by Tcd sandstone only (figure 4.6 and 4.12). At progressively larger sandstone volumes a thickness maximum moves basinward, defining a broad maximum in the central part of the Ridracoli thrust sheet in large volume beds. The thickness of the sandstone maximum is directly correlated to the total sandstone volume in small and intermediate beds, but become less dependent from the sandstone volume in beds with large cross sectional area >40,000 m^2 (figure 4.12b). It is evident that this change in the characteristic bed shape is not only due to the increased bed volume, but is also dependent on the presence of a basal Tab (or clean debrite) sandstone division. Intermediate and large volume beds contain an increasing cross sectional area fraction of Tab sandstone (figure 4.12e). This basal division controls the position and the downflow extent of the sandstone thickness maximum observed.

The characteristic shape of the basal Tab (plus clean debrite) division can be approximated by a third order polynomial function $y=a+bx+c^3$ (figure 4.12a, table 4.2). The significance of a, b, and c parameters is shown in figure 4.13. The parameter *a* is directly correlated to the bed thickness at the section located at 0 km (Coniale section). It can vary between approximately 40 and 140 cm, and it is not correlated to the total sandstone area of each bed (figure 4.12d). The parameter *b* controls the proximal slope of the function. The parameter *c* controls the curvature of the function; *b* and *c* interact to control the value and the position of the sandstone thickness maximum. These values are directly correlated to the total sandstone area of the bed (figure 4.12b and 12c). The rate of pinch-out of Ta and clean debrite divisions (figure 4.9) is also controlled in this model by *b* and *c*, and cannot vary as an independent parameter. This approximation is necessary in order not to use a regression curve that becomes too complex, with coefficients that are difficult to then relate to any geological parameter.

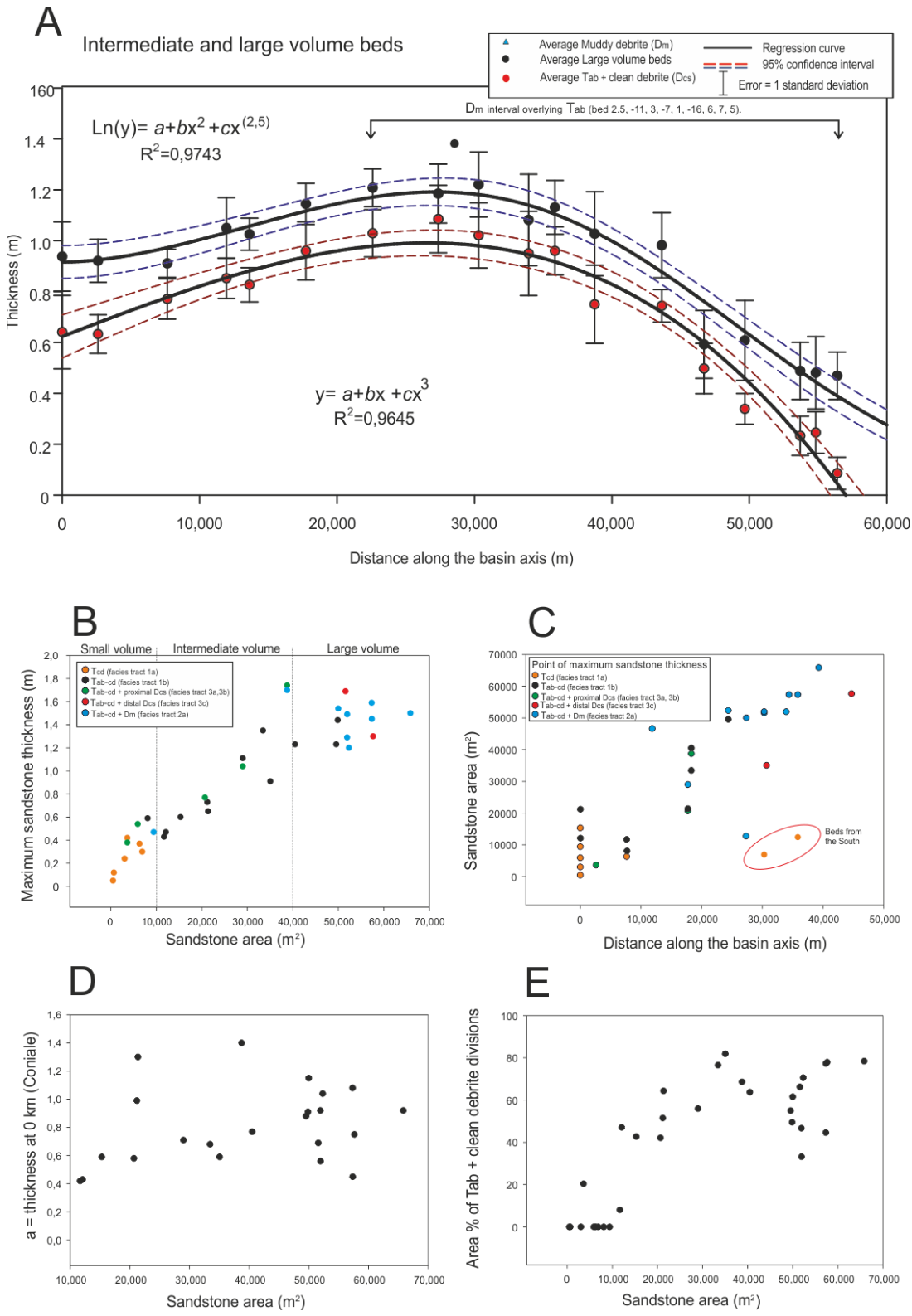

Figure 4.12. *Sandstone interval shape in intermediate and large volume beds (figure 4.6) along the Ridracoli thrust sheet (figure 4.1). A) Regression curve showing the average thickness of intermediate and large volume beds shown in figure 4.6. The average thicknesses of different groups of lithofacies are shown for (i)*

Bouma divisions T_{AB} and clean sandy debrite (D_{CS}), and (ii)Bouma divisions T_{CD}. The 95% confidence limit and the standard deviation of sandstone thickness in each section are shown. The regression coefficients are shown in table 2. B) Maximum sandstone thickness plotted against the sandstone cross sectional area on the Ridracoli thrust sheet. C) Position of the sandstone thickness maximum along the basin axis, plotted against the sandstone cross sectional area. D) Sandstone thickness at the most northwesterly Coniale section (corresponding to the 'a' parameter in the two equations) plotted against the calculated sandstone cross sectional area. E) Area percentage of high-density basal T_{AB} and/or clean debrite divisions (D_{CS}) in beds with increasing sandstone area.

The shape of intermediate and large volume sandstone beds is inherently more complex. The regression curve used to describe the characteristic sandstone shape is similar to the one used for the Tab division in the proximal and intermediate sections, but needs to also describe the approximately exponential thinning of the upper Tcd interval in the distal sections of the Ridracoli element, and the very gradual thinning for at least a further 60 km along the Pietralunga element (Talling et al., 2007b).

The simpler function that describes these characteristics is a third order rational $Ln(y)=a+bx^2+c^{(2.5)}$ (figure 4.12). As for the function describing the Tab interval shape, the parameter *a* is correlated to the bed thickness at the section located at 0 km (Coniale section, figure 4.12d); *b* and *c* however are more complex, and cannot be directly related to physical parameters (figure 4.13).

Sandstone shape of beds with different facies tracts

Intermediate and large volume beds characterized by facies tract 1, 2a, 3a, 3b and 3c can be described by the same characteristic function $Ln(y)=a+bx^2+c^{(2.5)}$. The rate of proximal thickening, the position of the thickness maximum and the type of pinch out however differs for each facies tract (figure 4.14). For instance, beds with facies tract 1a and 1 b maintain an approximately constant thickness for 20 km, followed by a gradual thinning (figure 4.14c). On average the thickness declines from 1 to 0.30 m in approximately 40 km. This gradual thinning corresponds to the progressive transition from deposits dominated by Tab divisions to deposits comprising only Tcd sandstone (figure 4.10), indicating a more dilute and turbulent flow.

Beds containing a clast-poor muddy debrite interval (facies tract 2a) are characterized by an initial sandstone interval thickening to the maximum between 0 and 30 km, followed by a gradual thinning (from 1.2 m to 0.4 m).

The thinning of beds with facies tract 3a and 3b is much more rapid (from 1m to 5 cm in 10 km on average, figure 4.10) and is due to the complete pinch out of clean debrite intervals (Dcs), most likely because of the frictional freezing of a debris flow (see chapter 3). The complete pinch out of Dcs intervals in beds with facies tract 3c is not observed (figure 4.10). It can be however noticed that, on average, these beds have a more rapid distal thinning rate (from 1.2 to 0.5 m in approximately 10 km) if compared to beds of similar volume with facies tract 1 and 2a (figure 4.14).

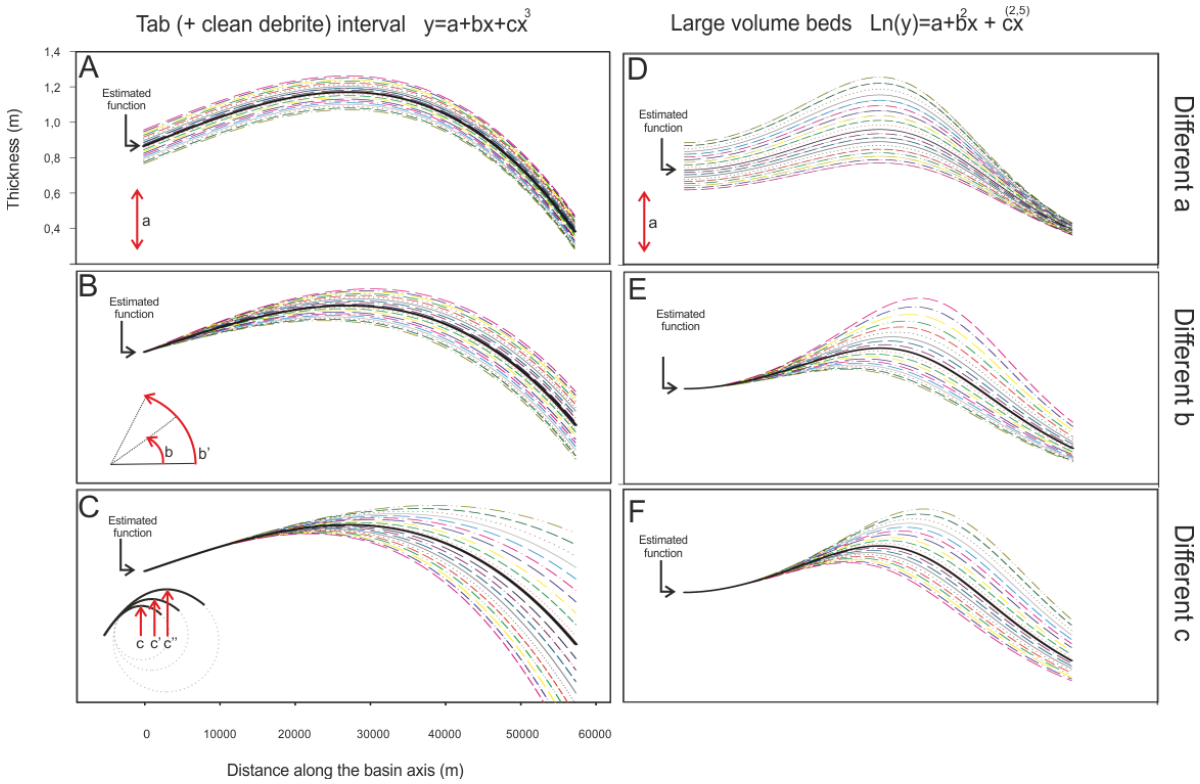

Figure 4.13. *Explanation of the significance of a, b and c parameters in the two functions used to describe interval shape. The first function is (A-to-C) is* $y = bx + cx^3$*, where y is the thickness and x is the distance down the basin described Tab and/or clean debrite sandstone intervals. The second function (D-to-F) is* $Ln(y) = a+bx^2+cx^{2.5}$ *describes the whole sandstone shape of intermediate and large volume beds.*

Core and drape geometry of turbidite sandstone

Each intermediate and large volume bed can be divided into a basal, lenticular shaped Tab or clean debrite "core" that defines the rate of proximal thickening, the position and broadness of the thickness maximum and the rate of distal thinning. Tcd and muddy debrite divisions form a "drape" that extends further down the basin. The thickness of this "drape" can be very variable, although a general observation is that Tcd divisions tend to thicken near the pinch-out of the basal Tab division, and then gradually thin in a fashion similar to the small volume beds. Clast-poor muddy debrite intervals are generally lens-shaped, and replace Tcd intervals in the central and distal portion of the Ridracoli element in some beds.

The thick 'core' that comprises the base of the bed, formed by Ta, Tb and clean debrite divisions, is most likely deposited by high density flows. Tc and Td intervals form a more extensive "drape", sometimes replaced by a clast-deficient muddy debrite interval. Tc and Td intervals were deposited by low-density turbidity currents. Although muddy debrite intervals were deposited by a low-strength cohesive debris flow, this most likely resulted from the transformation of a fully turbulent flow (Talling et al., 2007c). A grain-size break (that records sediment bypass) sometimes occurs at the boundary between low-density and high-density turbidite components; where this break is not present the boundary most likely lies within the Tb interval (figure 4.4).

This bipartite relationship between high-density and low-density turbidite components has been observed in other turbidite systems where bed have been mapped over long distances, such as the Bosu peninsula in Japan (Hirayama and Nakajima, 1977) and the Moroccan Turbidite system (Talling et al., 2007c). It has also been noted by Mutti (1992 and Mutti et al.2003), that described highly efficient basin plain turbidites as deposited by bipartite flows, with a basal, inertia driven highly concentrated flow overlaid by a more dilute and fully turbulent flow phase.

Mudstone shape

The thicker mudstone interval in each of the 32 studied beds, derived from both the northwest and southeast, occur in the southeastern part of the Ridracoli element, just before the Verghereto High (figure 4.7). This consistent geometry, observed in beds with opposite paleocurrent directions, suggests that muddy fluid was able to drain back towards the lowest point of the foredeep, as also observed by Ricci Lucchi and Valmori (1980), Amy and Talling (2006) and Talling et al. (2007a,b).

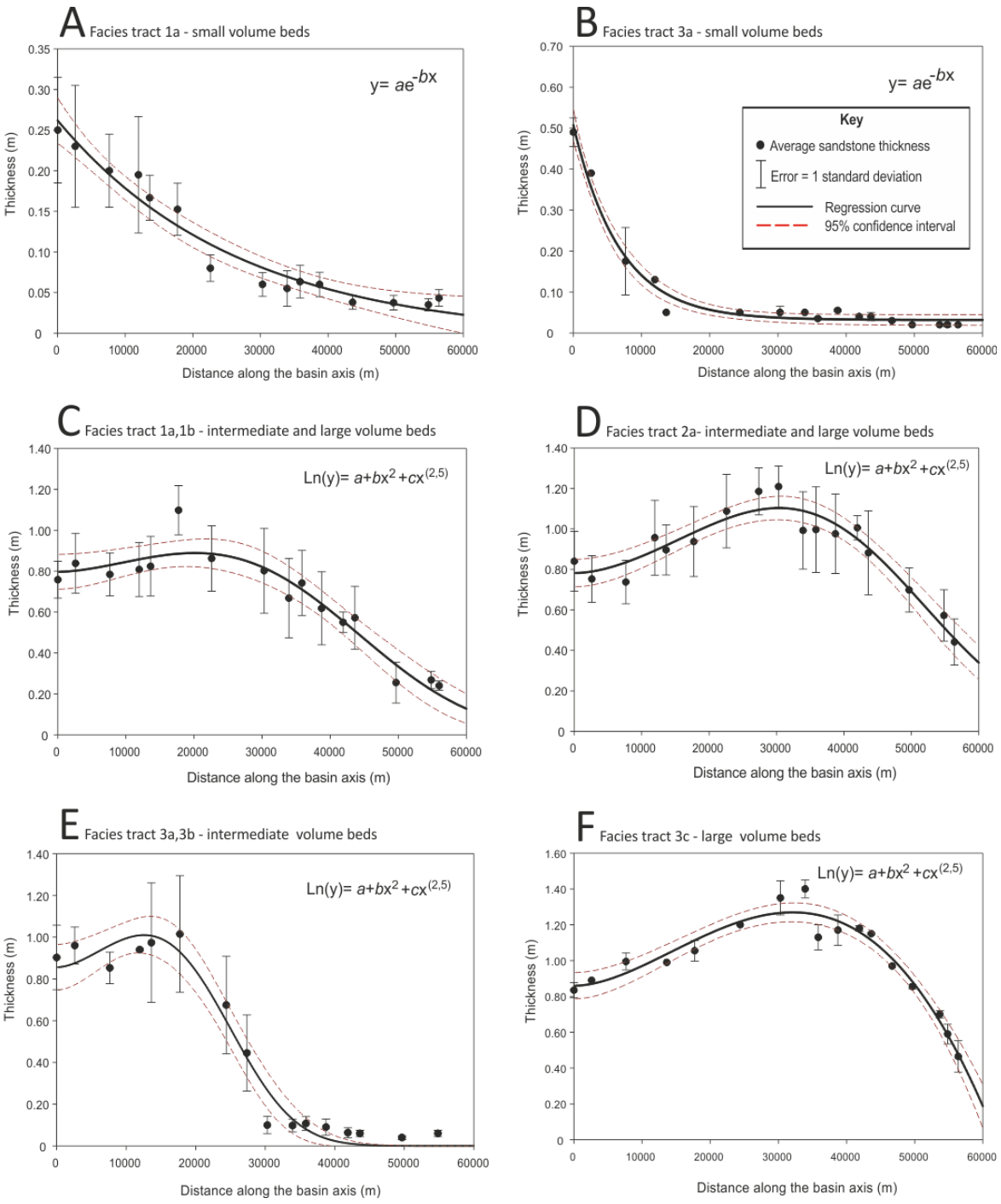

Figure 4.14. *Regression curves showing the average thickness of beds with different facies tract shown in figure 4.10. Also shown are 95% confidence limits for the regression line of average thickness with distance The average thicknesses of different groups of lithofacies are shown for a) small volume beds with facies tract 1; small volume beds with facies tract 3a; c) intermediate and large volume beds with facies tract 1a and 1b; d) intermediate and large volume beds with facies tract 2a; e) large volume beds with facies tract 3c. The 95% confidence limit and the standard deviation of sandstone thickness in each section are shown. The regression coefficients are shown in table 2.*

Despite local variations, especially in lower mudstone volume intervals, the characteristic mudstone shape can be described by a linear function y=*a*+*b*x (figure 4.15a). The parameter *a* represents the intercept with the y axis, and correspond to the mudstone thickness in the section located at 0 km (Coniale section, figure 4.15b). This thickness at Coniale is not strongly correlated with the total mudstone volume. The parameter *b* corresponds to the gradient of the regression line, and increases linearly with increasing mudstone volume (figure 4.15c).

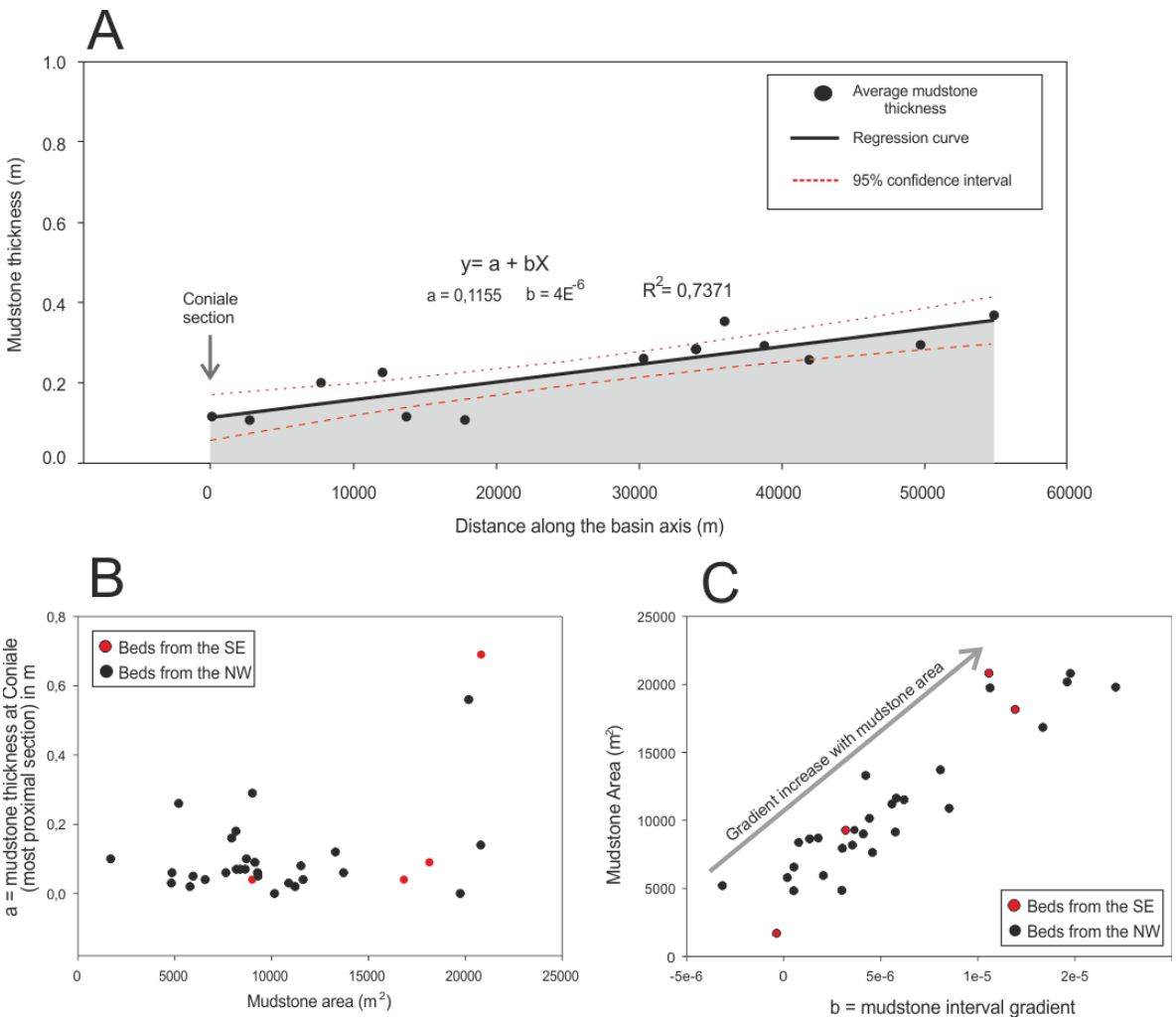

Figure 4.15. *A) Regression line describing the lateral thickness variations in turbidite mudstone interval thickness. The prediction interval calculated at a 95% confidence limit is also plotted. B) and C) Comparison of a and b parameters of the regression line to the calculated mudstone cross sectional area for each bed.*

Assuming that flows experienced approximately the same basin floor profile, the analysis of the regression coefficients indicate that the almost linear thickening of mudstone towards the distal

sections of the Ridracoli element is most likely due to a partial ponding of the muddy flow against the Verghereto High (figure 4.2, 4.16). The *a* coefficient is independent from mudstone volume and paleocurrent direction, because the muddy fluid drained toward the southeast, ponding against the Verghereto High. The *b* coefficient increases with mudstone volume, and records the progressive filling of the bathymetric low created on the Northwestern side of the Verghereto High. Large volume mudstone intervals have a broader thickness maximum located on the Northwestern side of the Verghereto High (figure 4.7, 4.15b). This broad maximum represents another evidence of the strong control of relatively subtle sea-floor topography on flows depositing mudstone intervals.

Talling et al. (2007a,b) analyzed the shape of the mudstone interval of beds in the above Contessa interval across a 120km transect in the Ridracoli and Pietralunga structural elements, and observed an additional mudstone thickness maximum, located on the downflow side of the Verghereto High in the Pietralunga element, presumably the lowest point of the basin (Talling et al. 2007a; their figure 11, 12, 14).

Beds -8, -5 and -13 have a local mudstone thickness maximum at about 10 km (figure 4.7). This location corresponds to the downflow side of the Cavalmagra high, recognized by Talling et al. (2007a) based on the local termination of some small volume beds in the above Contessa interval. This local thickening of the mudstone interval can be used as evidence that this subtle intrabasinal high was present also at the time of deposition of the newly studied below Contessa interval. Other local thickness variations in small mudstone volume intervals (figure 4.7) are also most likely due to ponding against extremely subtle sea-floor topography, probably too subtle to directly influence sandstone deposition.

A local thickening of the mudstone interval is also observed directly downflow from the pinch-out of clean debrite intervals in bed 0, 5.1 and -8 (figure 4.7). This rapid (figure 4.9) sandstone interval thinning is not due to pre-existent sea-floor topography because other sandstone beds maintain an approximately constant thickness in the same position (chapter 3). It may be hypothesized that mudstone thickening resulted from ponding of the muddy fluid against the subtle topography created by the pinch-out of the clean debrite interval deposited by the same flow-event.

Studies on modern turbidite systems where sea-floor gradient is known, such as the Moroccan turbidite system, confirm how subtle variation in sea floor topography greatly influence the shape

of mudstone intervals, with the deposition of thicker mudstone deposits related to a subtle decrease in sea-floor gradient (Wynn et al., 2002, 2012; Talling et al., 2007c).

				Parameters			
Figure	**Volume**	**Facies tract**	**Regression curve**	***a***	***b***	***c***	**R^2**
11a	Small	1a,3a	$y=ae^{-bx}$	0,2413	3,25E-05		0,8947
14a	Small	1a	$y=ae^{-bx}$	0,2631	3,92E-05		0,9589
14b	Small	3a	$y=ae^{-bx}$	0,4935	0,0001		0,9476
12a	Intermediate and large	1b,2a,3a,3b,3c	$Ln(y)=a+bx^2+cx^{(2.5)}$	-0,0876	1,77E-09	-8,60E-12	0,9484
14c	Intermediate and large	1a,1b	$Ln(y)=a+bx^2+cx^{(2.5)}$	-0,2268	1,34E-09	-7,55E-12	0,9096
14d	Intermediate and large	2a	$Ln(y)=a+bx^2+cx^{(2.5)}$	-0,2462	1,86E-09	-8,56E-12	0,8999
14e	Intermediate and large	3a,3b	$Ln(y)=a+bx^2+cx^{(2.5)}$	-0,1557	5,23E-09	-3,73E-11	0,9681
14f	Large volume	3c	$Ln(y)=a+bx^2+cx^{(2.5)}$	-0,2032	2,22E-09	-9,91E-12	0,9046
12a	Tab int. and large	1b,2a,3a,3b,3c	$Y=a+bx+cx^3$	0,7067	1,68E-09	-7,98E-12	0,9398

Table 4.2. *Regression curves for beds with different volume and facies tract. The regression parameters and the regression coefficient (R^2) are indicated*

4.5.2. What controls the external shape of turbidite beds?

The data obtained from the analysis of the shape and facies variations of progressively larger volume sandstone and mudstone beds will now be used to better constrain the dominant controls that act to modify the characteristic shape of turbidite beds.

Sea floor topography

The characteristic shape of sandstone beds may be related to variation in the slope gradient and possibly to the ponding of sandstone and mudstone intervals upslope from bathymetric highs. Talling et al. (2007a) observed that the sandstone interval of thin beds sourced from both the Northwest and the Southeast had a “mirror” shape, characterized by an exponential proximal thinning (Talling et al., 2007a; their figure 11-14). It is unlikely that the flows encountered the same changes in sea-floor gradient. This suggests that variation in the slope gradient was not the dominant control on sandstone deposit shape.

The shape of large and intermediate sandstone volume beds previously described, with a maximum sandstone thickness that broadens and moves basinward for progressively larger volume beds (figure 16a), is not related to ponding of sandstone controlled by the position of the

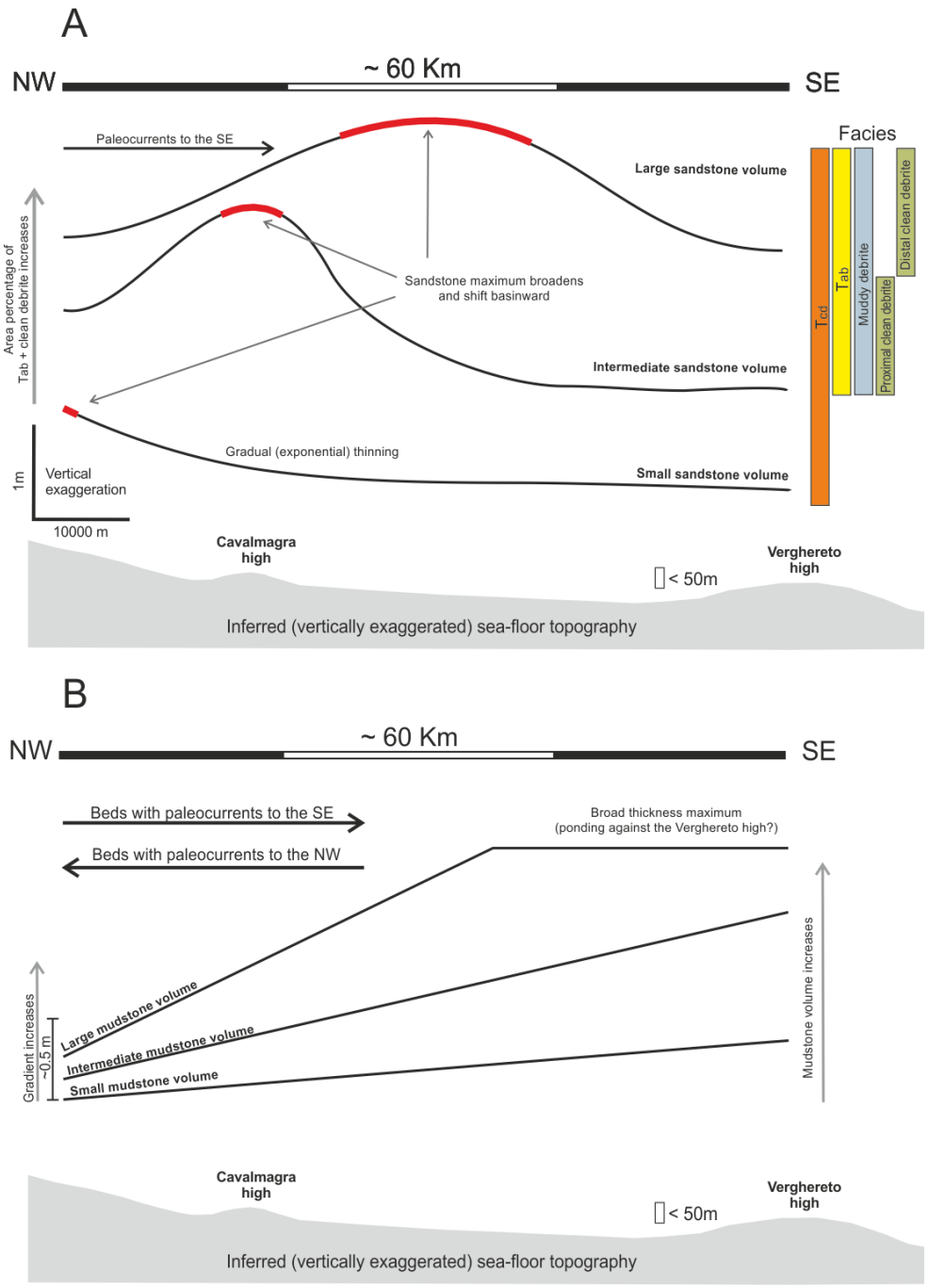

Figure 4.16. *A) Scheme summarizing the variations of bed shape and internal facies architecture for progressively larger sandstone volume beds. B) Scheme summarizing the variations of bed shape for progressively larger mudstone volume beds, and their relationship with the sea-floor topography*

Verghereto High. If that was a major control, one would expect the maximum thickness of the sandstone intervals to be located consistently in the bathymetric low locate just upslope from the high.

Mudstone interval shape appears to be strongly controlled by sea floor topography, as it is similar for beds sourced from opposite sides of the basin (figure 4.16b).

Sediment volumes

The rate at which sandstone thickness decays (the *e-folding)* decreases in small volume beds, as their volume increases. This may be due to larger volume flows carrying a greater fraction of the sand above the bed, resulting in a more tabular deposit. In intermediate and large volume beds, the position and thickness of the observed sandstone maximum is directly correlated to the total sandstone volume carried by the depositing flow. At progressively increasing sediment volumes the maximum thickens, broadens and moves basinward.

Flow concentration and hindered settling

In high density turbidity currents hindered sediment settling becomes important in the near-bed layer (Talling et al., 2012a). Hindered settling starts to occur at sediment volume concentrations of ~10% as grain interactions become important (Bagnold, 1954), and its effects become increasingly (non-linearly) important as volume concentrations increase further (Richardson & Zaki, 1954). High near-bed sediment concentration may reduce near-bed turbulence intensity (Baas & Best, 2002). This may reduce sediment settling velocity, and rates of sediment re-suspension or bed erosion (Talling et al., 2007a). Only a rough estimate (low and high density flow deposits) of the flow sediment concentration can be inferred from outcrop data. However, the distinctive shape of high density deposits described in this study, characterized by a sandstone thickness maximum that thickens, broadens and moves basinward at progressively increasing sediment volumes, is well reproduced in numerical models that include hindered settling (Goater,2011; figure 4.17).

The profiles shown in figure 4.17 clearly indicate the difference that hindered settling can have on the deposit shape at high concentrations. For sediment concentration of 4% ($\phi_0 = 0.04$) the profile is very similar to the exponentially decaying shape expected from a Stokesian settling law. For sediment concentration of 22% ($\phi 0 = 0.22$) a maximum appears in the profiles. Settling initially is highly hindered and so the thickness is relatively lower than expected; as the particles settle out

the hindering decreases and the deposit height increases. Once enough particles settle out the hindering is sufficiently decreased for the settling to behave in a Stokesian manner and thus the

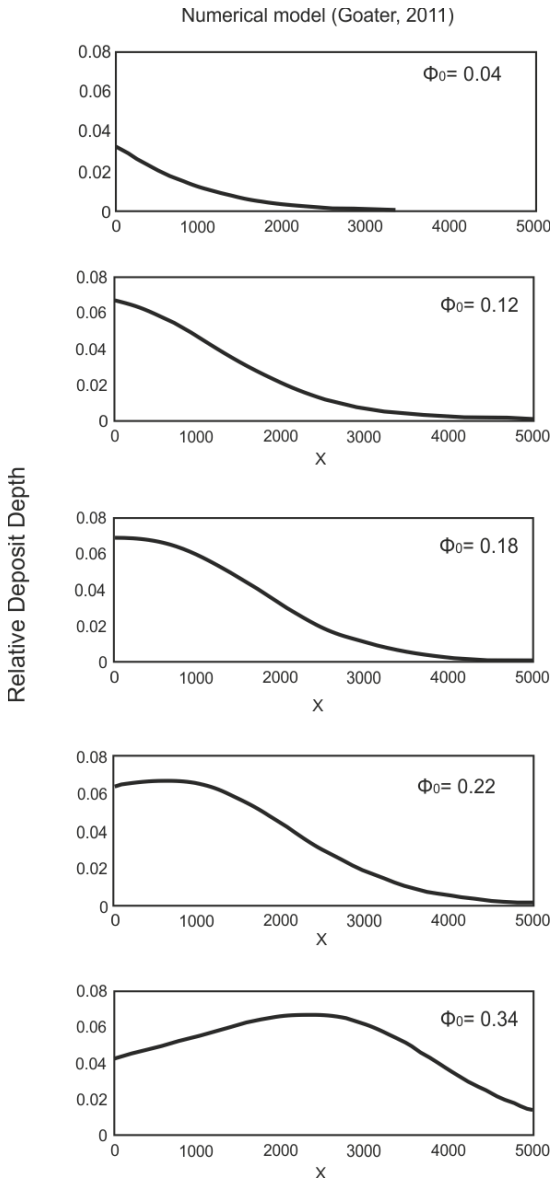

Figure 4.17. *Turbidite deposit shapes obtained from depth-averaged numerical modeling by Goater (2011) for flows with different initial sediment concentration (φ0). The relative deposit depth φ (1- φ)^5, is shown as a function of the distance from the source, X, for initial particle concentration of 0.04, 0.12, 0.18, 0.22, 0.34. See the text for a discussion on the numerical model adopted. Modified from Goater (2011).*

profile decays away exponentially. At progressively higher initial particle concentrations (34%; ϕ0 = 0.34) the maximum moves down-flow, and the thickness profile becomes more tabular. This may be explained, following Talling et al. (2007b), by the fact that in natural flow the near-bed sediment concentration increases rapidly as bed shear stress increases, for relatively low bed

shear stress and flow velocity (Garcia & Parker, 1991, 1993). However, the near-bed concentration probably tends towards a maximum value (ϕ0 ~0.3) as flow velocity and bed shear stress increase (Garcia & Parker, 1991, 1993). This may lead to a relatively uniform near-bed sediment concentration which, in turn, tends to produce relatively uniform rates of suspended sediment transport in a downflow direction, and a spatially rather uniform deposit thickness.

Similar results are also obtained in flume experiments by Middleton and Neale (1989; figure 4.18). Assuming a similar duration of each flow event, flows depositing different sandstone volumes would necessarily have a higher sediment concentration. This may explain the direct relationship between sandstone volumes, the relative proportion of sand deposited by high density flows and the characteristic bed shape observed

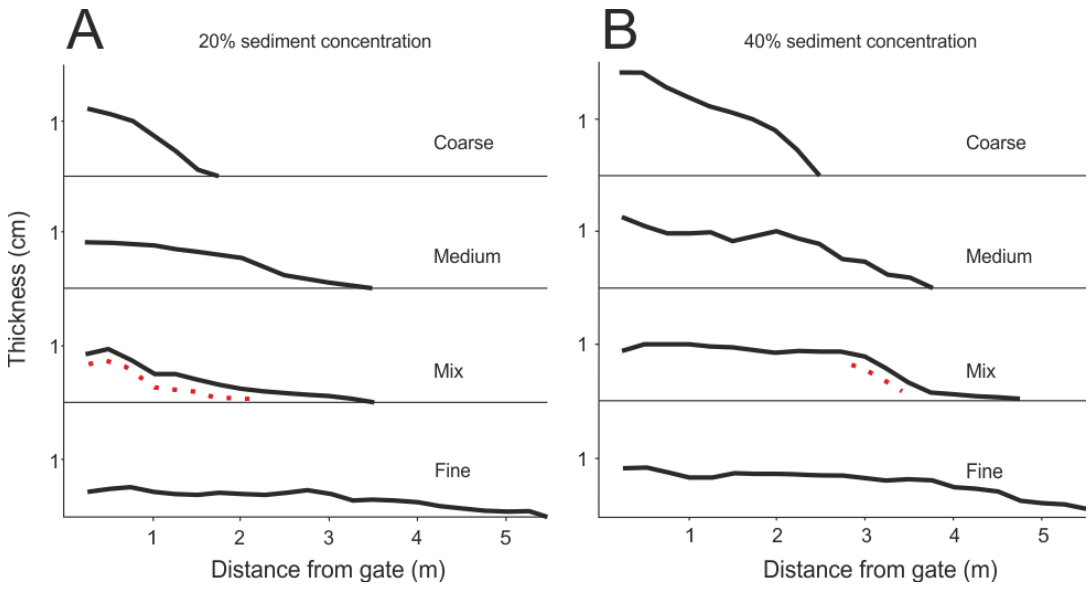

Figure 4.18. *Measured profiles for beds of glass beads from experiments of Middleton and Neale (1989). Coarse (0.258 mm), medium (0.156 mm), fine (0.085 mm) and mixed particles were used in different runs. The dashed red line indicates the observed boundary between upper (finer) and lower (coarser) parts of the bed. A) Runs with an initial sediment concentration of 20% (φ0=0.2). B) Runs with an initial sediment concentration of 40% (φ0=0.4). Modified from Middleton and Neale (1989).*

Proportion of fine particles

The proportion of fine particles in the flow, together with the flow volume, relates to the concept of flow efficiency (Mutti, 1992). Flow efficiency can be defined as the ability of the flow to carry sand in a basinward direction (Mutti, 1992). In this interpretation, high efficiency flows are relatively large-volume flows that carry substantial amounts of fines, whereas poorly

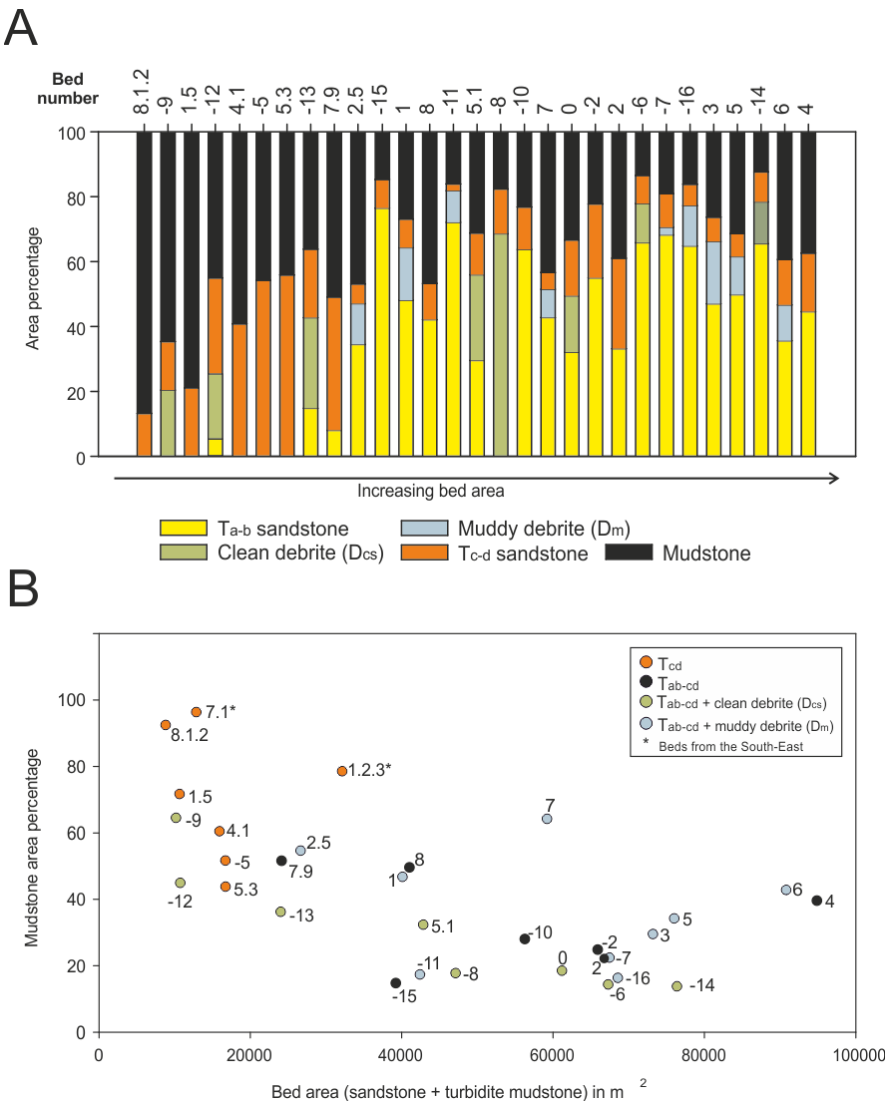

Figure 4.19. *A) Relative area proportion of the different lithofacies in each bed. Only beds with provenance from the North East are included. B) Cross-sectional area percentage of mudstone (Te) plotted against the total bed area for beds with different facies tract. Note that beds comprising clean debrite (Dcs) intervals have a slightly lower mudstone percentage than other beds with similar area.*

efficient flows are relatively small-volume flows loaded with mainly coarse-grained sediment. This concept is supported by laboratory experiments of Middleton and Neale (1989, figure 4.18), Gladstone et al. (1998) and Al Ja'Aidi et al. (2004). The large majority of beds described in this chapter extend for long (>120 km) distances, and contain a substantial amount of fine particles. Mudstone represent between 70 and 100 percent of the volume of thin beds (Talling et al., 2007a; figure 4.19b). Fine-grained thin turbidites can extend for long distances in other non-channelized basin-plain and lobe sequences, such as the Hecho Group of the Spanish Pyrenees (Remacha and Fernandez 2003; Tinterri et al. 2003) and the Pleistocene Otadai Formation on the Boso Peninsula, Japan (Hirayama and Nakajima 1977).

As noted in chapter 3, beds containing a proximal clean debrite interval (Dcs) that pinch-out abruptly are sandier than beds containing turbidite sandstone only. Although the sand/mud ratio of beds containing clean debrite in the Ridracoli element is similar, although slightly lower, to beds with comparable volume (figure 4.19), clean debrite beds deposit a very thin mud cap in other thrust sheets (Amy and Talling, 2006; chapter 3). On the contrary beds not comprising Dcs intervals deposit thick mudstone caps in thrust sheets more external (Isola and Pianetto) and more distal (Pietralunga). This confirms the importance of the relative proportion of fines in the flow to determine the shape and run-out distance of submarine density flow sandstone beds, at least in the special case of beds containing clean debrites.

4.6. CONCLUSIONS

This study presents a quantitative analysis of the shape and internal architecture of 32 individual turbidite beds, deposited in a non-channelized basin plain. This shape was obtained from the correlation of each individual flow deposit between up to 19 stratigraphic sections along a 60 km transect oriented parallel to the main paleocurrent direction. The external shape of sandstone and mudstone intervals is presented for beds with different volume and different down flow facies architecture (facies tracts). The turbidite sandstone interval of small volume beds comprising only Tcd (ripple laminated sandstone and laminated siltstone) intervals thins downflow in an approximately exponential fashion, typical of dilute flows. The rate of thinning is controlled by bed volume. Intermediate and large volume beds are characterized by a proximal thickening of

the sandstone interval followed by a gradual thinning. At increasing sandstone volumes the sandstone maximum thickness increases, broadens and moves basinward.

This shape is well reproduced by numerical modeling of flows with different concentration performed by Goater (2011), indicating that hindered settling act as a major control on the external shape of sediment density flow deposits. Beds containing only turbidite sandstone (facies tract 1) thin more gradually than beds containing muddy (facies tract 2a) or clean (facies tract 3a, 3b and 3c) debrite intervals. The downflow thinning of beds containing clean debrite is abrupt, in agreement with the deposition from a concentrated debris flow that freezes at its margins. Individual beds can be subdivided into a basal “core” deposited by a high density flow phase and an overlying thinner “drape” formed by low-density turbidite sandstone. A grain-size break (that most likely records sediment bypass) sometimes occurs at the boundary between low-density and high-density turbidite components. The mudstone interval shape of all beds show an approximately linear thickening basinward, irrespective of the opposite provenance of some flows. This shape is controlled by the basin floor topography, with mud ponding against subtle intrabasinal highs.

CHAPTER 5:
THICKNESS DISTRIBUTION, CLUSTERING AND TIME FREQUENCY ANALYSIS OF TURBIDITES AND DEBRITES IN THE MARNOSO ARENACEA INNER STAGE

5.1. INTRODUCTION AND AIMS

The Cabelli section is located in the mid-proximal part of the Marnoso Arenacea Formation, in the Bidente river valley (figure 5.1). It is located on the Isola structural element (figure 1a), and consists of a ~1 km thick succession of deposits of the Inner (older) part of the Marnoso Arenacea Formation. This chapter analyses a continuously exposed 526 m thick interval, extending from 343 meters below, to 183 meters above, the Contessa marker bed. The exceptionally continuous exposure in this section (figure 5.2a) makes it ideally suited for understanding the long term frequency recurrence of flow events and the character of deposits in this basin plain.

The first aim of this chapter, undertaken in collaboration with Alessandra Negri (Universita' Politecnica delle Marche) is to date this "type" section using nannofossils biostratigraphy. Only a rough biostratigraphic framework is available in literature for the Marnoso Arenacea Formation (Martelli et al., 1994; Cibin et al., 2004).This new biostratigraphic age control then serves as a basis for analysing the frequency of flow events, and how this changed over time. In this stratigraphic section, event beds are separated by intervals of hemipelagic marl deposited by slow settling of mainly calcareous sediment from the water column. Assuming a constant background sedimentation rate and no significant erosion by successive flows these hemipelagic intervals can be used as a proxy for the time separating individual nearly instantaneous sediment density flow events.

The spatial and temporal distribution and the clustering of turbidites and debrites have important implications both scientifically and for hydrocarbon reservoir modeling. The distribution of hybrid beds comprising mud-rich sandstone intervals (muddy debrites) in distal fringes of submarine fans has been interpreted to be indicative of periods of non-equilibrium of the slope (Haughton, 2009; Tinterri & Muzzi Magahles, 2011). Sandy turbidite deposits (and possibly sandy debrites; chapter 3) represent significant reservoirs and muddy debrite beds represent permeability baffles. The second aim of this contribution is therefore to determine

whether turbidite or debrite intervals cluster temporally or show cyclicity in their vertical distribution within the Cabelli section. Do debrite beds occur in predictable clusters or are they randomly distributed throughout the section? The frequency and the long-term clustering of turbidites and debrites may also provide insight into the triggering mechanisms for these large (often > 1km^3 of sediment) flow events.

The frequency distribution of turbidite bed thicknesses contain information about the flow hydrodynamics, the processes by which flows are initiated and the migration of the source (Rothman and Grotzinger, 1996; Malinverno, 1997; Carlson & Grotzinger, 2001). Two main statistical distributions have been proposed to describe turbidite bed thickness data: a lognormal distribution model (Drummond & Wilkinson, 1996; Murray et al., 1996; Sylvester, 2007) and a (segmented) power law model (Hiscott et al., 1992; Rothman et al., 1994; Bettie & Dade, 1996; Rothman & Grotzinger, 1995; Carlson & Grotzinger, 2001; Bersezio &Felletti, 2008). Beds in the Marnoso Arenacea Formation have been described previously by Talling (2001) and Sylvester (2007) in terms of a lognormal mixture model, showing that intervals with specific basal grain size populations (or Bouma divisions) have lognormal distributions. The third aim of this chapter is to determine the thickness distribution of turbidites and debrites in the Cabelli section, and understand how this thickness distribution compare to that measured for beds previously correlated laterally between many sections. Is the same thickness-frequency distribution observed? If so, what produces this robust distribution?

5.2. MATERIALS AND METHODS

5.2.1. Sedimentary logging

A five hundred and twenty-six meters thick stratigraphic section was logged at a scale 1:10. This stratigraphic interval spans from 343 meters below to 183 meters above the Contessa marker bed. Each measured bed was described in terms of sedimentary structures, character of base and top boundaries and vertical grain size profile. The grain size was estimated using a grain size comparator and hand lens. This method is biased towards the coarser tail of the entire grain size population (Talling et al, 2007a). Where outsized mudstone and sandstone clasts were present, their size (length of the longest axis) was also measured. Palaeocurrent directions were estimated measuring the direction of flutes and grooves on the base of thick beds. A graphic log (figure 5.3) was then produced to summarize this data. In

order to undertake further analysis, data were summarized using a simplified facies scheme, derived from the one used in chapter 3 (table 5.1). Five lithofacies were distinguished: (i)

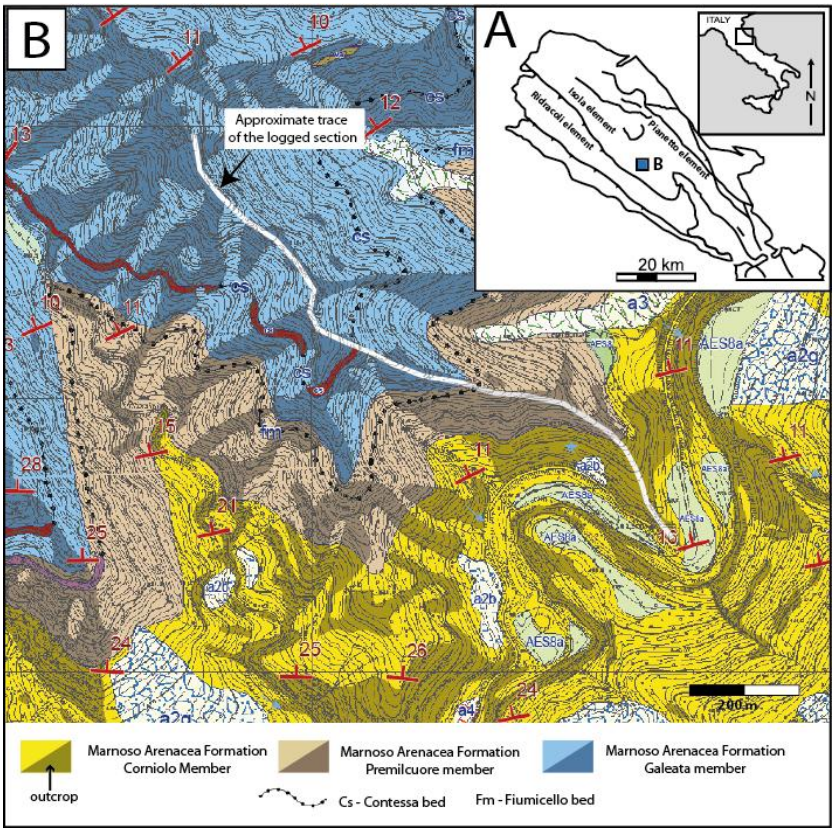

Figure 5.1. *Location and geological map of the Cabelli section. A) Simplified map showing the outcrops of the northern (Romagna) portion of the Marnoso Arenacea Formation. The main tectonic elements are indicated. B) Geological map of the Cabelli area, modified from Martelli et al. (1994). The position of the main marker beds (Fiumicello and Contessa) and the approximate logging line of the section are indicated.*

turbidite sandstone, corresponding to subfacies Cs1, Cs2, Cs3, Cs4, C65 and Cs6, (ii) clean debrite sandstone, corresponding to subfacies Cs7, (iii) muddy debrite sandstone, corresponding to subfacies Ms1 and Ms2, (iv) turbidite mudstone, corresponding to subfacies M1, (v) hemipelagic marl, corresponding to subfacies M2. The data obtained were then compiled in a database file suitable for statistical computation (appendix 5.1). The resolution adopted for recording each interval thickness in the spreadsheet is 1 cm.

5.2.2 Hemipelagite or hemiturbidite?

In this study we interpret the deposits of massive light grey-bluish, calcareous mudstone, sometimes containing visible foraminifer tests (subfacies M2, figure 5.4a) as hemipelagic marls, the product of slow settling of individual hemipelagic particles from the

overlying water column. If not eroded by a subsequent event, these intervals stratigraphically stand above darker turbidite mudstones (subfacies M1). An alternative hypothesis for the

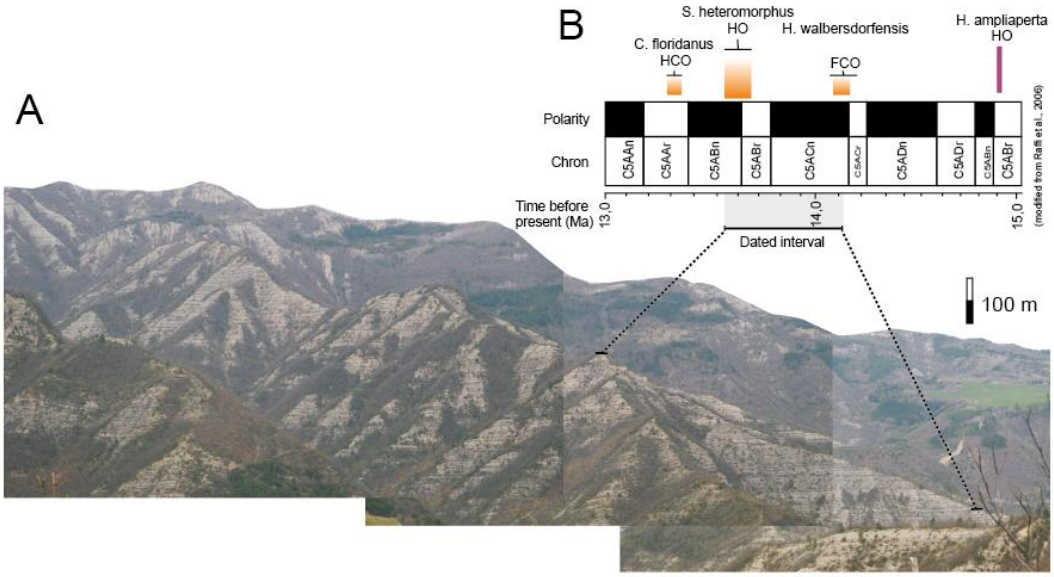

Figure 5.2. *A) Outcrop photograph of the Cabelli section . B) Summary of the absolute age, stage boundaries, magnetic reversals and position of biohorizons in the dated interval. Modified from Raffi et al. (2006).*

origin of M2 intervals in the Marnoso Arenacea Formation was given by Mutti et al. (2002) and Muzzi Magalhaes and Tinterri (2011). Restating the conclusion of Remacha et al. (2005) for the Hecho Group in the Spanish Pyrenees, these authors interpret M2 intervals as hemiturbidites (*sensu* Stow and Wetze, 1990), deposited by the dilute tails of turbidity currents able to erode the carbonate mudstone deposited onto topographic highs. Each hemiturbidite interval in this model is therefore genetically related to the turbidite deposit underneath. If this is the case, each turbidite bed (sandstone plus turbidite mudstone) should be directly overlaid by a correspondingly thick hemiturbidite layer. This is not the case in the Marnoso Arenacea Formation. Figure 5.4b unequivocally shows that there is no correlation between the thickness of turbidite beds and the overlying M2 interval, whilst there is a correlation between thicker and coarser sandstones and thicker overlying turbidite (M1) mud. Bed correlations in chapter 3 and in Amy and Talling (2006) also indicate a laterally consistent thickness for M2 intervals, again supporting the interpretation that they are formed by slow settling of fine hemipelagic material. These correlations show that the darker M1 intervals have variable thickness as would be expected for turbidity current deposits. It is also shown using SEM images (Talling et al., 2007a) that M2 intervals contain dispersed foraminifera and are more calcareous, as would be expected for hemipelagite, whilst M1 interval contain dispersed organic matter and lack dispersed foraminifera.

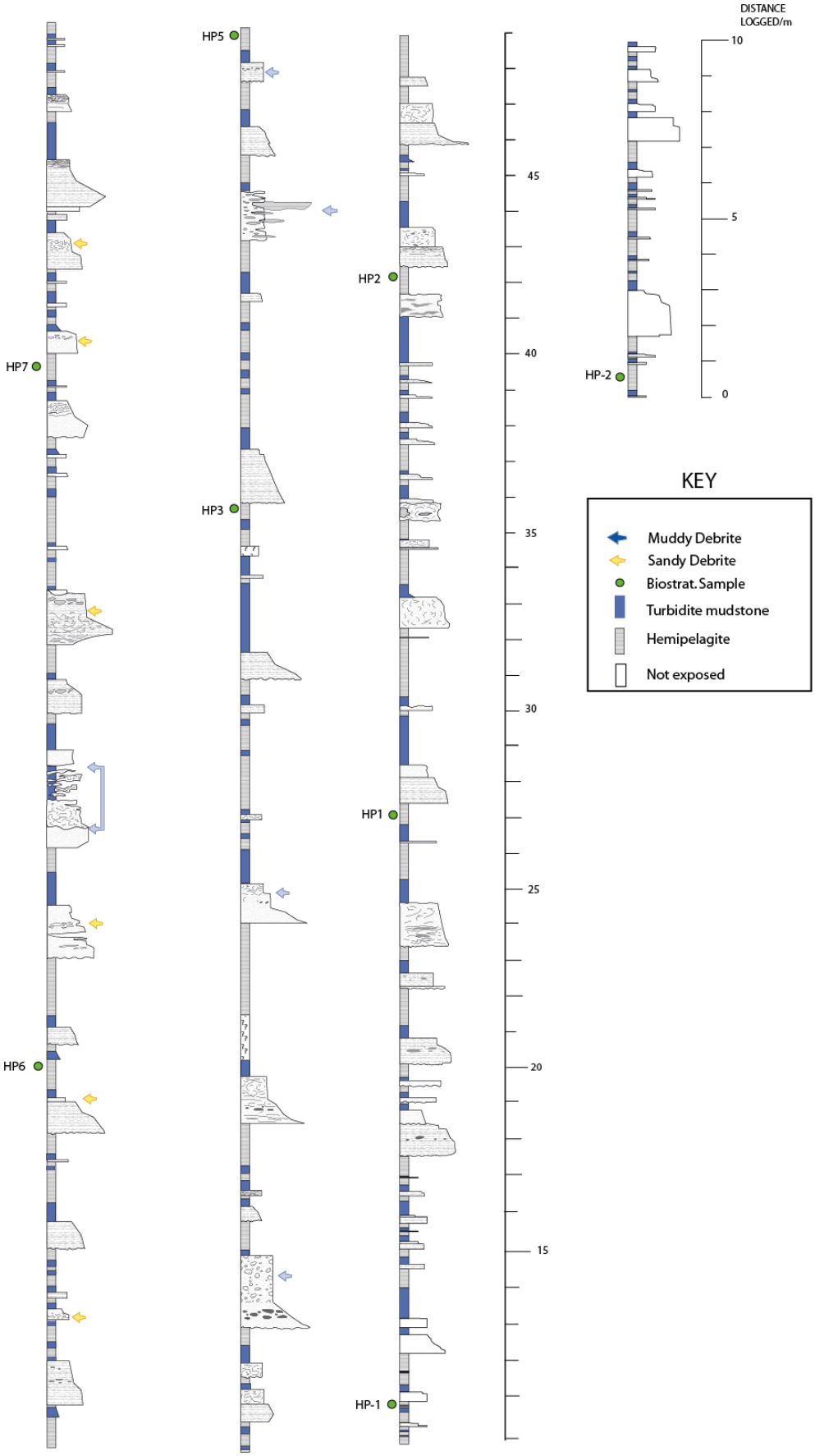

Figure 5.3. *(Continued)*

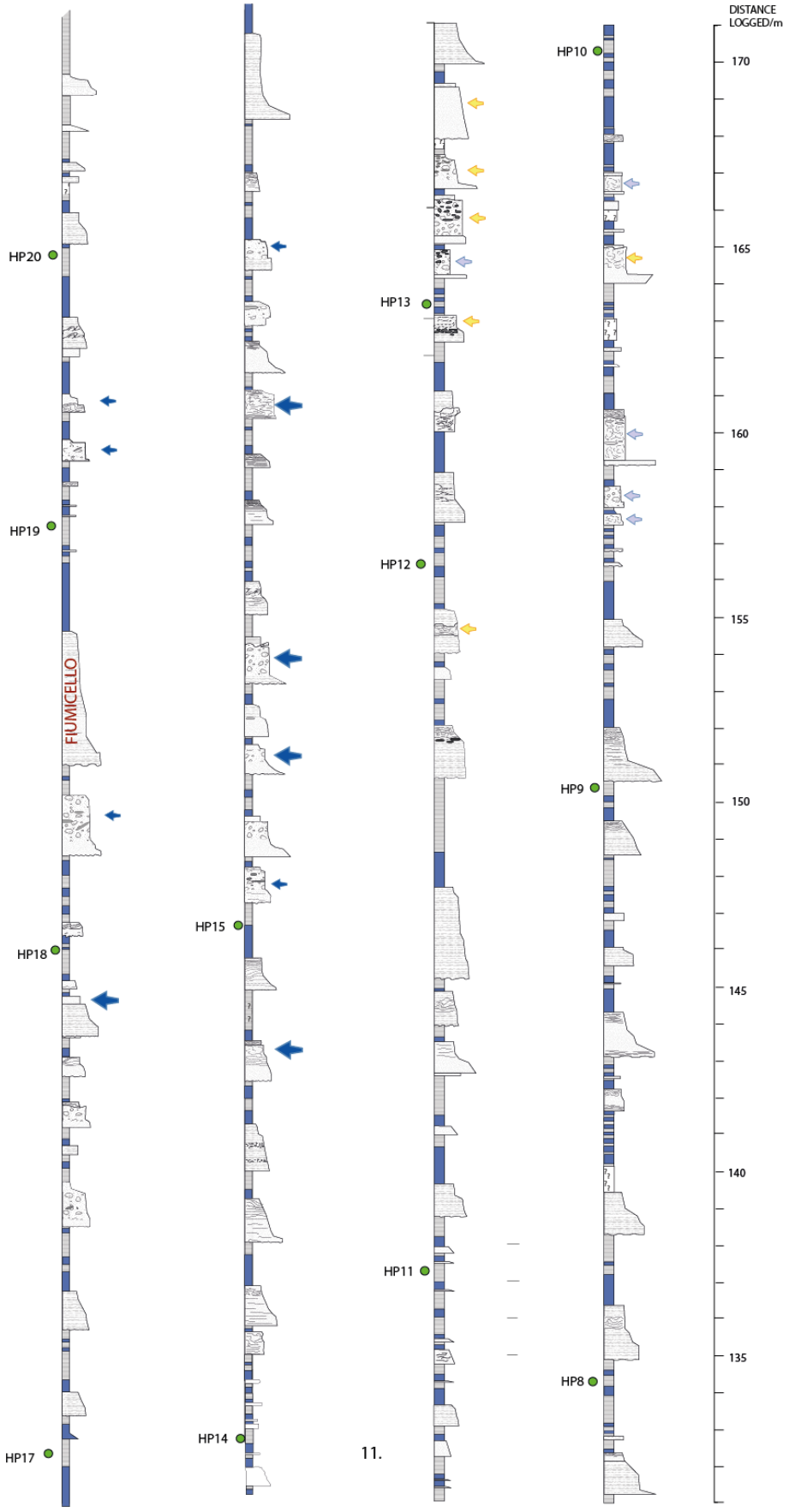

Figure 5.3. *(Continued)*

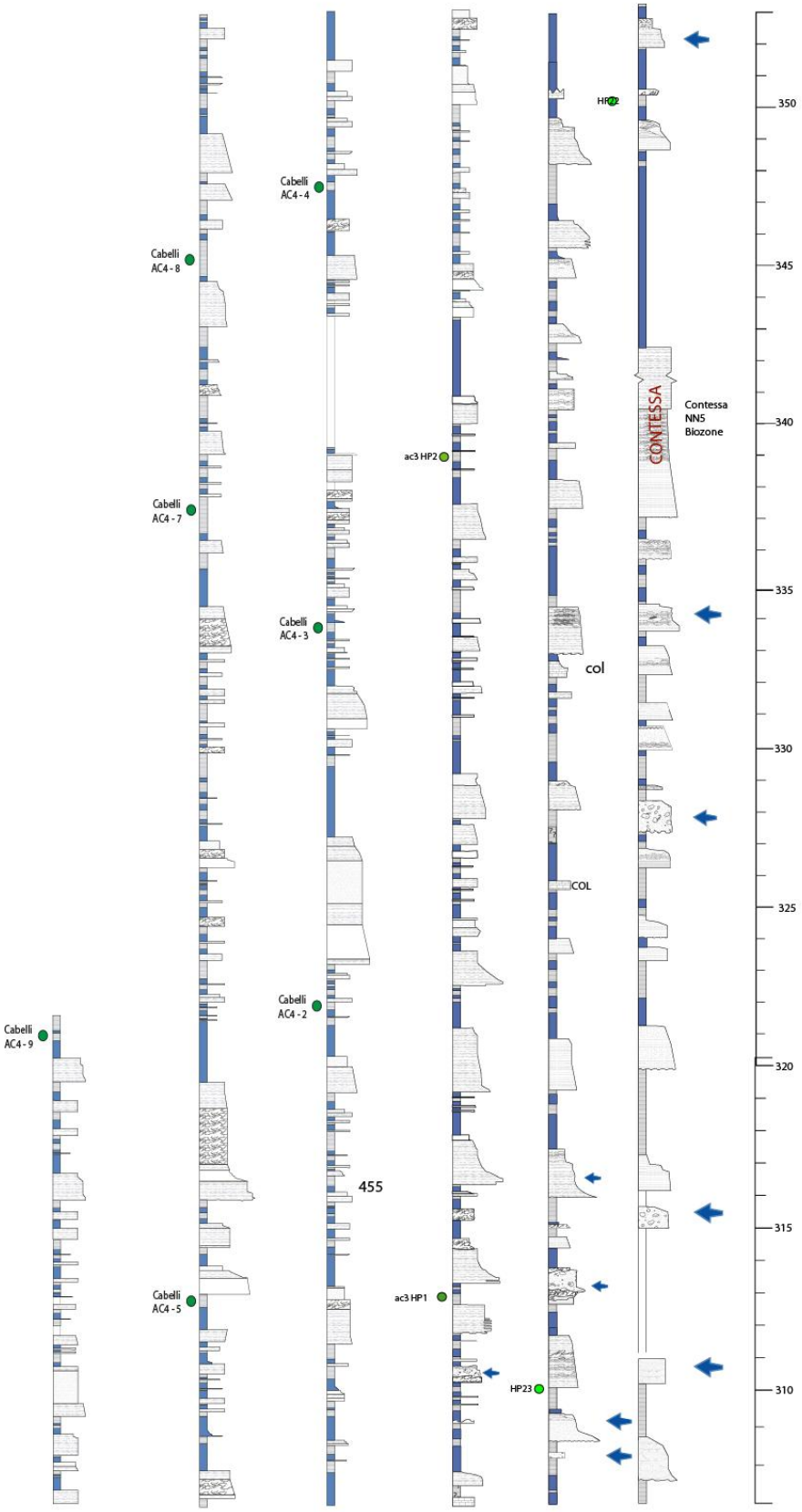

Figure 5.3. *Summary log of the measured section.*

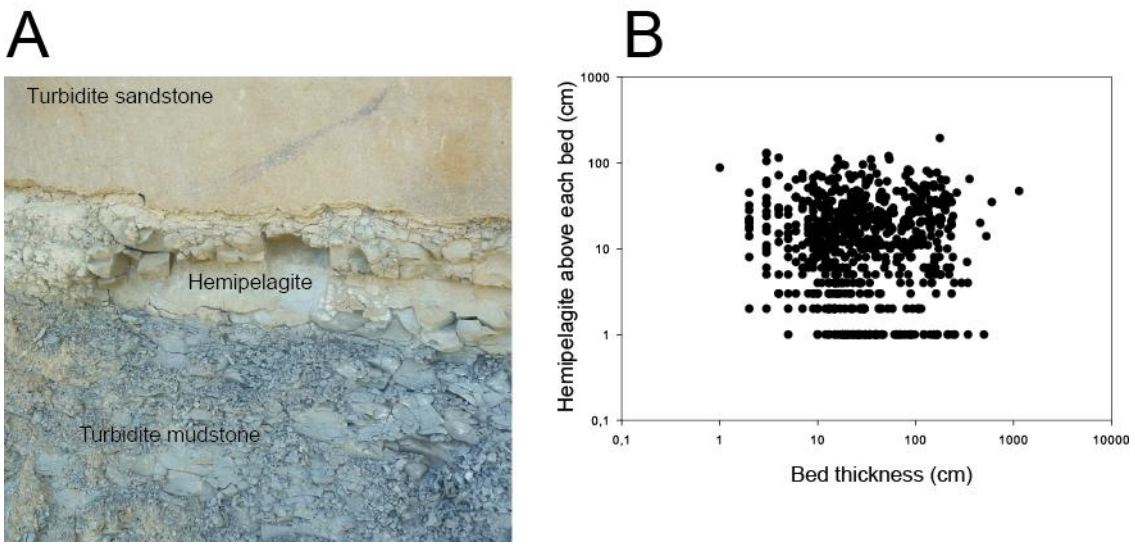

Figure 5.4. *A) Photograph illustrating the difference between turbidite mudstone and hemipelagic marl. Note the difference in color and texture. B) Correlation between the thickness of each event bed and the hemipelagic marl directly above.*

5.2.3. Biostratigraphy

Thirty six samples suitable for biostratigraphic purposes were collected in hemipelagic marl intervals (subfacies M2). Samples analysis was performed by Alessandra Negri at the University of Ancona (Italy). Sample preparation followed standard techniques. A smear slide was mounted with Norland Optical Adhesive. No centrifugation was applied to concentrate the biogenic fraction in order to retain the original composition of the nannofossil assemblage. Estimates of calcareous nannofossil totals and species abundance were carried out using a polarizing light microscope at a magnification of 1250 times. For each smear-slide, at least 300 fields of view were observed in random traverses. Calcareous nannofossil abundance were semi quantitatively evaluated as follows: Total abundance: A=abundant: 10-50 specimens per field of view (FOV); C=common: 1–10 specimens per FOV; F=few: 1 specimen per 1–10 FOV; R=rare: 1 specimen per 11–50 FOV; B=barren).

5.2.4 Thickness frequency distributions

The thickness frequency distribution of (i) the total thickness of each event bed including sandstone and turbidite mudstone intervals (ii) sandstone intervals (Cs1-6), (iii) turbidite mudstone intervals (M1), (iv) sandy debrite intervals (Cs7), (v) muddy debrite intervals (MS1 and 2), (vi) hemipelagic marl intervals (M2) between every bed (vii) cumulative

hemipelagic marl thicknesses between thick (> 40 cm) beds (viii) hemipelagic marl intervals between beds containing muddy or sandy debrite intervals, was analyzed using graphical and numerical methods. Graphical methods include frequency histogram, log-linear exceedence frequency plot, log-log exceedence frequency plot, log-probability plot, cumulative distribution plot and quantile-quantile plot. The Kolmogorov-Smirnov test is used to estimate the goodness-of-fit of the distributions inferred from graphic methods (Sylvester, 2007).

5.2.5 Hurst statistic

The Hurst Statistic (Hurst, 1951) or Rescaled Range Analysis, is a statistical method that provides a way to determine the degree of clustering of low and high values in a sequence (e.g. values of bed thickness or grain size in a stratigraphic section). The method applied in this chapter was proposed for the first time in deep-marine sedimentology by Chen & Hiscott (1999), and successively adopted by Felletti and Bersezio (2010). This analysis was shown to be somewhat helpful in distinguishing depositional environments.

Hurst (1951) derived the following relationship for *K* as an estimator for the Hurst exponent *h:*

$$K=\frac{Log10\ (R(S)}{Log10(N(2)}$$

Where *R* is the maximum range in cumulative departures from the mean (figure 5) over *N* observations and *S* is the standard deviation. To calculate *K* for a series of *N* observations, each measurement is replaced by its logarithm, to base 10. Mean and standard deviation of the data are calculated on these log-transformed values, and *R* is measured directly from a plot of cumulative departures from the mean over the *N* sequential observations. Values for *N*, *R* and *S* are then substituted directly into the previous equation.

Hurst (1951) showed the tendency for a natural sequence of data with a large *N* value (*N* > 100) to yield values of *K* > 0.5. By contrast, for purely random processes he predicted values of *K* close to 0.5. Hurst (1951) demonstrated that, for large N and approximately normally distributed values, high K values are caused by serial dependence that express the natural tendency for natural events to occur in irregular groups in which high and low values predominate. This tendency, known as the Hurst phenomenon (Wallis & Matalas, 1971), allows the quantification of long-term clustering of values.

The value of K for a purely random (Gaussian independent) sequence of values is 0. 5 for an infinite number of measurements (N), but it has been demonstrated that for finite N this value

can be larger (Chen & Hiscott, 1999 and references therein). In order to determine an appropriate expected value of Hurst *K* for randomized turbidite succession, a Monte Carlo

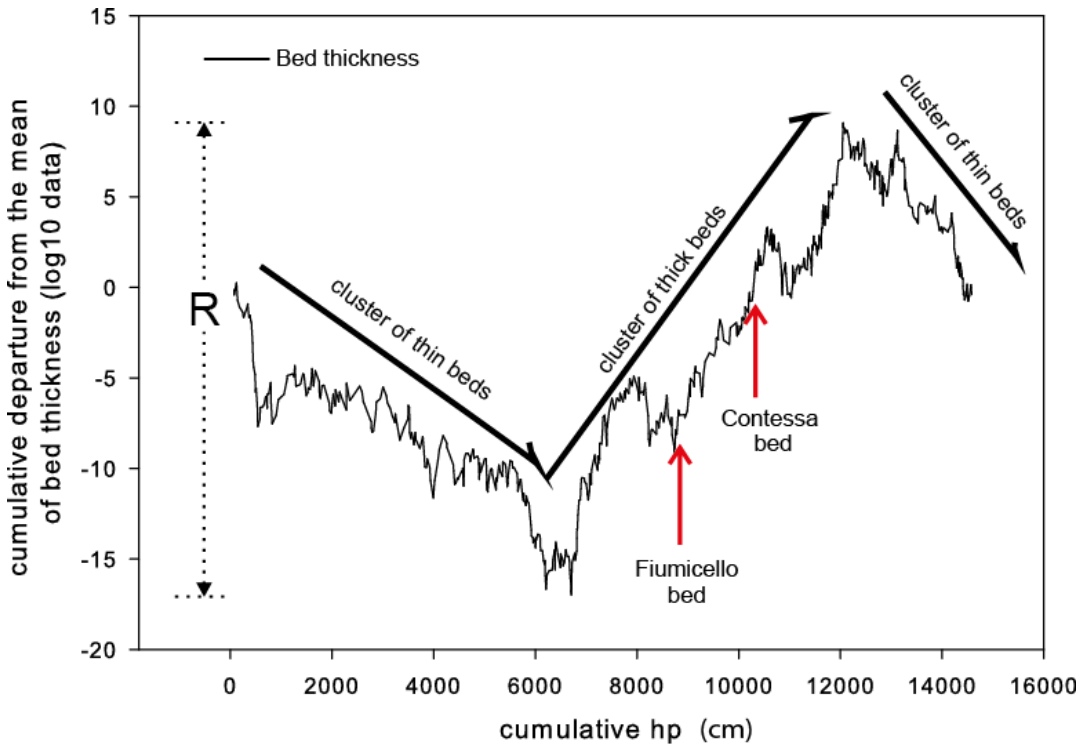

Figure 5.5. *Cumulative departure from the mean plot of single beds (sandstone and turbidite mudstone) thickness. The cumulative departure of log10 transformed thickness values from the mean of all thickness measurements is plotted against the cumulative hemipelagite thickness (proxy for time between events).This curve highlights the presence of irregular vertical clustering of values lower and higher than the mean. Cluster of successive beds thicker or thinner than the mean of all measurements will result as a discernible portion of the curve in this plot. For example a cluster of beds generally thinner than the mean is visible between 0 and 6000 cm. of cumulative hemipelagite. R is the maximum range of values used to calculate the Hurst statistic.*

simulation technique was used. From the original data, 300 randomly shuffled sequences are simulated. The expected value is then compared with the *K* values from the original field section to assess the likelihood that it belongs to the same population. A Fortran-77 program, HURST.FOR (Chen & Hiscott 1999), was used to calculate the Hurst statistics and the Monte Carlo simulation. Known distribution parameters permit the use of hypothesis tests for values of *K* calculated from the original turbidite successions. If K_0 is the Hurst *K* value of a measured turbidite section, and the proportion of sequences with $K>K_0$ in the 300 randomly shuffled sequences is smaller than a selected significance level α, then the hypothesis that the measured vertical sequence is randomly distributed is rejected at that significance.

A prerequisite for the Hurst test is that the values are approximately normally or lognormally distributed (Chen & Hiscott, 1999).The Hurst statistical test was performed on whole bed measurements, sandstone intervals and debrite intervals. Cumulative departure from the mean plots were produced also for non lognormally distributed intervals of hemipelagic marl, because this graph provides useful information on long term clustering, although a rigorous statistical test of this clustering is not possible. Beds with provenance from the south (Contessa and Colombine beds) were not considered in this analysis. A total of 696 beds, 530 sandstone intervals and 82 debrite intervals were tested for the Hurst statistic. Muddy and sandy debrites where grouped together for two reasons: firstly the Hurst statistic is considered reliable only for a minimum number of measurements close to 100. The second reason is that sandy and muddy debrites may be part of a continuum from poorly cohesive to highly cohesive debris flow deposits, and therefore belong to the same population.

5.3. RESULTS

5.3.1 Logged data

Six hundred and ninety-six event beds were measured in the entire section. Beds are numbered from the base of the section. The thickness of each turbidite sandstone, sandy debrite, muddy debrite, turbidite mudstone and the total thickness of each bed are shown in the appendix 5.1. The thickness of hemipelagite under each bed, and the cumulative thickness of the section are recorded in the same table. The thickness of each interval plotted against the cumulative hemipelagite thickness is shown in figure 6. The total thickness of the section is 527 m, of which 145.83 m (27.67%) are hemipelagic marl, 170.2 m (32.33%) are turbidite sandstone, 17.83 m (3.38%) are sandy debrite, 19.66 m (3.54%) are muddy debrite and 175.11 (33.22%) are turbidite mudstone.

5.3.2 Biostratigraphy

All the samples studied show abundant and moderately preserved nannoflora. The assemblage mainly consists of *Reticulofenestra* spp., *C. pelagicus*, *S. moriformis* is abundant throughout the whole section, *C. floridanus* is abundant until sample HP 23 and its abundance decreases abruptly after that sample. *S. heteromorphus* is present from the base of the section but shows a decrease in abundance toward the top of the section and disappear after sample AC 2. *H. ampliaperta* is observed in a single level (sample HP 8) and is probably allochtonous and reworked. *H. walbersdorfensis* is not occurring at the base of the section, its first common

occurrence (FCO) is detected in sample HP3, after this sample its presence is initially discontinuous but becomes continuous after sample HP 18 until the top of the section. *C. premacintyrey* show its first common occurrence (FCO) after sample AC4(1. Finally Discoaster are very rare and have been detected in only three samples (D. variabilis occurrence). The FCO of H. *walbersdorfensis* falls close to the Contessa bed. Therefore on this base we can distinguish the MNN 5a and MNN5b zones of the biostratigraphic scheme proposed by Fornaciari et al. (1996). The last occurrence (LO) of *S. heteromorphus* allows discrimination of the following zone MNN 6, whose base approximates the Langhian Serravallian boundary. In term of absolute age, according to Raffi et al. (2006) the Last occurrence of *S. heteromorphus* dates at 13.5 to 13.6 Ma. The *H. walbersdorfensis* FCO (a local event peculiar of the Mediterranean Sea), according to Abdul Aziz (2008) occurs at 14.1 Ma, although this event may be diacronous over the Mediterranean region. A table synthesizing the results of the biostratigraphical analysis is shown in appendix 5.2. This study is in good agreement with previous biostratigraphic dating on the Marnoso Arenacea Formation (Van Wamel and Zwart, 1990; Martelli et al., 1994; Cibin et al., 2003).

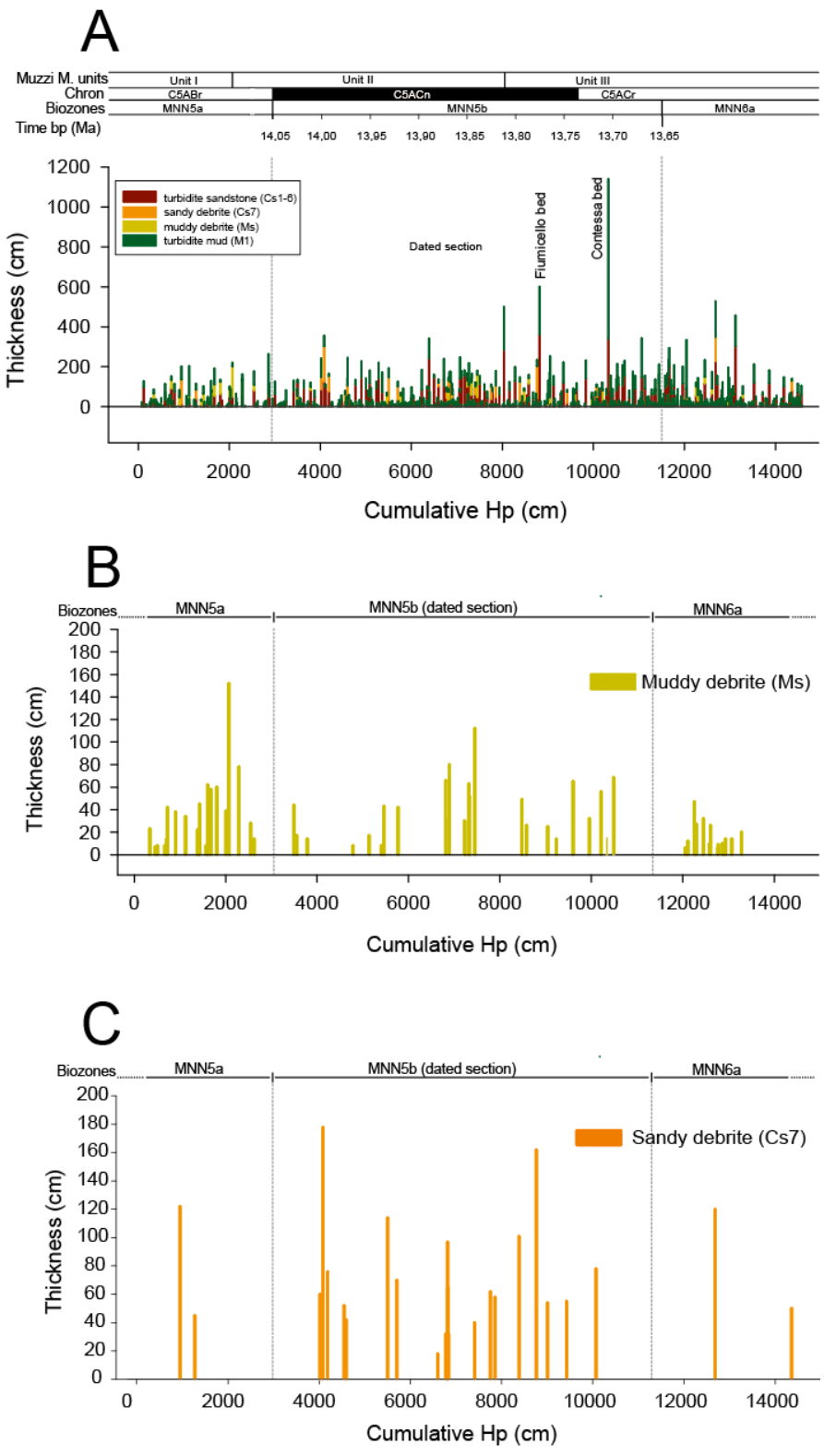

Figure 5.6. *Plot of cumulative hemipelagite thickness as a time axis against turbidite bed thickness. For the dated interval the respective time before present is reported. Biozones, magnetic reversals (chrons) are reported. The position of the main units by Muzzi Magahles and Tinterri (2011) are reported for comparison. A) Plot of cumulative hemipelagite thickness as a time axis against turbidite bed thickness, divided into turbidite sandstone, clean debrite, muddy debrite and turbidite mudstone intervals. B) Plot of cumulative hemipelagite thickness as a time axis against muddy debrite interval thickness. C) Plot of cumulative hemipelagite thickness as a time axis against clean debrite interval thickness.*

5.3.3 Dated section

The total thickness of the section between sample HP3 (FCO of H*. walbersdorfensis)* and sample AC2 (LO of S. heteromorphus) is 357.66 m. The time separating these two events is approximately 600,000 years. The total sedimentation rate is therefore 59. 66 cm/ka. The number of event beds in this interval is 440, giving an average frequency of 733 events per million years, or 1 event on average every 1363 years. Large events that deposit sandstone thicker than 40 cm. occur with a frequency of 1 event on average every 5,343 years. These values are in good agreement with the recurrence intervals proposed by Mutti (1984) for the Marnoso Arenacea Formation of 1000 to 1200 years for thin bedded turbidites and five times more for thick, basin wide beds. Events comprising sandy or muddy debrites occur on average every 10716 years. The cumulative hemipelagite thickness is 91.52 m, giving a background (hemipelagite) sedimentation rate of 15.25 cm/ka, or 1 cm of hemipelagite every 65.37 years assuming a constant hemipelagite sedimentation rate. Taking into account the sediment compaction this rate is also comparable to documented rates of hemipelagite deposition in other locations (Muller and Suess, 1979; Thornton, 1984; Guerra et al., 2008).

5.3.4. Paleocurrents

Paleocurrent measurements, obtained from the direction of flutes and grooves at the base of 80 thick sandstone beds, show a general north-east to south west trend. The modal direction is towards 130°, with a variability of about 90° around this modal value (figure 7d). Beds containing only turbidite sandstone and beds comprising sandy debrite intervals have a consistent direction toward the south-east (figure 7a and 7b). Beds containing muddy debrite intervals show a greater variability, with paleocurrent direction spanning from 70° to 150° (figure 5.7c). Thick beds comprising turbidite sandstone only tend to have flutes at the base, indicating flow turbulence. Beds comprising sandy and muddy debrite intervals generally have thick linear grooves at the base (figure 7d). The origin of this feature is yet poorly understood, but it may be related to the rheology of the different type of flows eroding the muddy substrate.

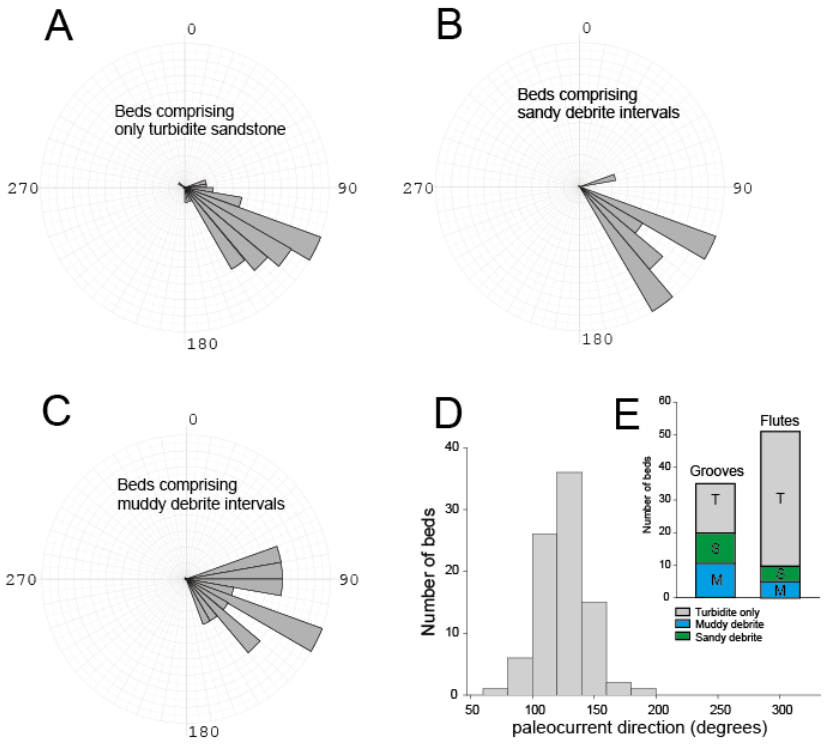

Figure 5.7. *Paleocurrent direction diagrams. A) Rose diagram indicating the paleocurrent directions of beds comprising turbidite sandstone only. B) Rose diagram indicating the paleocurrent directions of beds comprising clean debrite intervals. A) Rose diagram indicating the paleocurrent directions of beds comprising muddy debrite intervals. D) Frequency histogram of paleocurrent directions. E) Distribution of flutes and grooves at the base of beds comprising clean debrite, muddy debrite and turbidite sandstone only.*

5.3.5. Bed thickness distributions

Thickness data are presented on frequency histograms, logarithmic probability plots, log-linear plots and logarithmic cumulative plots. Beds with a provenance from the south (Contessa and Colombines) were excluded from this analysis. Data fitting on an approximately straight line on these plots would follow the corresponding distribution (figure 5.8h). The Kolmogorov-Smirnov test is used to assess the goodness-of-fit to that theoretical distribution. The test statistic is the maximum discrepancy (difference in thickness values) between a cumulative plot of the data and the chosen distribution. This test was performed on lognormal distributions for thickness of whole beds, sandstone, turbidite mudstone, sandy debrite and muddy debrite intervals and on exponential distributions for hemipelagite interval thicknesses between beds. The significance levels of the Kolmogorov-Smirnov test performed are

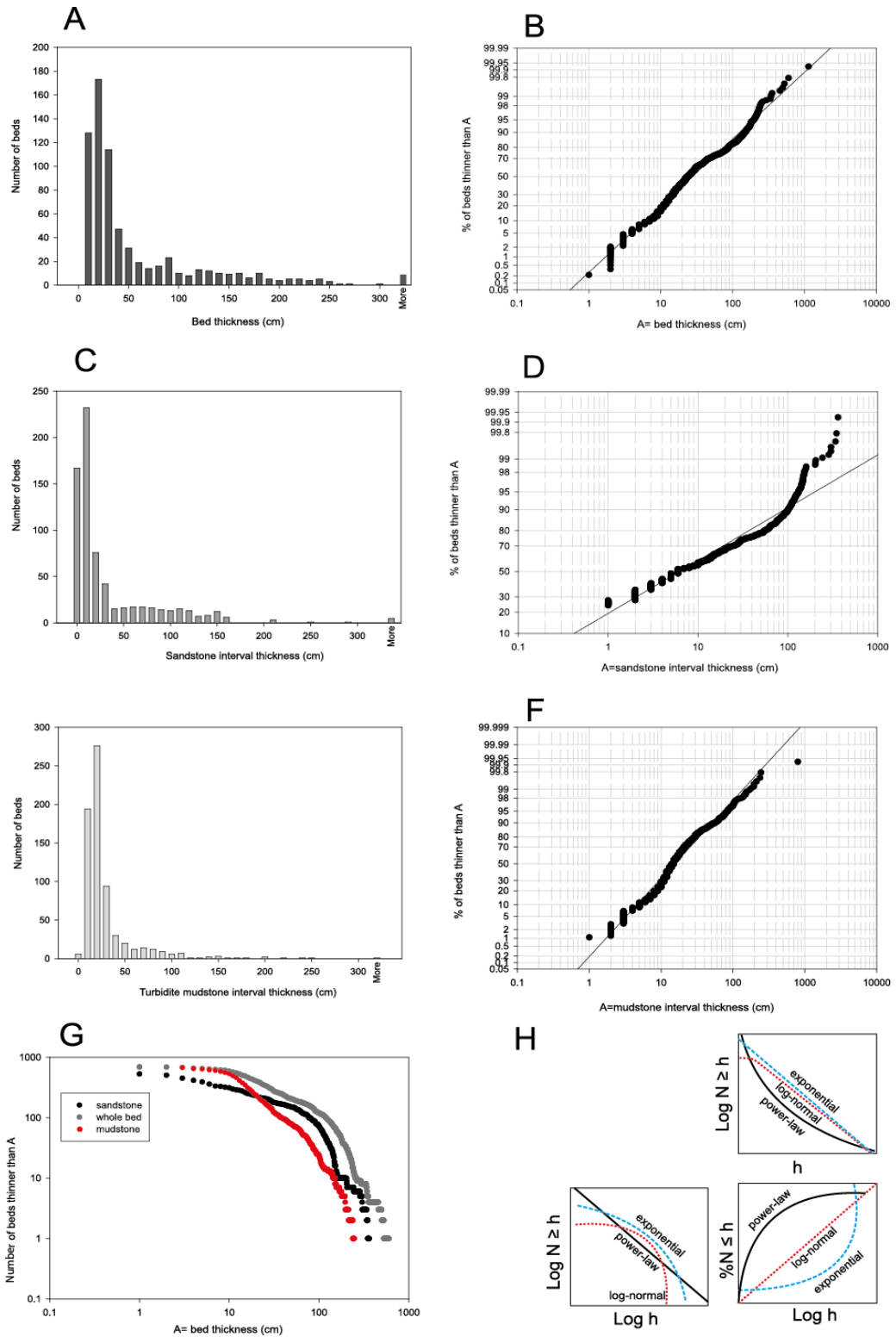

Figure 5.8. *Frequency histograms plots and logarithmic probability plots of A,B) whole beds, C,D) sandstone and E,F) mudstone intervals. Straight line trends on the log-probability plots indicate approximate log-normal frequency distributions. G) Cumulative frequency of thickness on logarithmic axis for whole bed, sandstone and mudstone intervals. A linear trend on this plot indicates an - approximately power-law distribution. H) Illustrative representation of the cumulative frequency of lognormal, exponential, and power-law distributions on log(linear axes, log(log axes and log(probability axes. N≥h is the number of beds greater or equal to a given thickness h. Modified after Sinclair and Cowie (2003).*

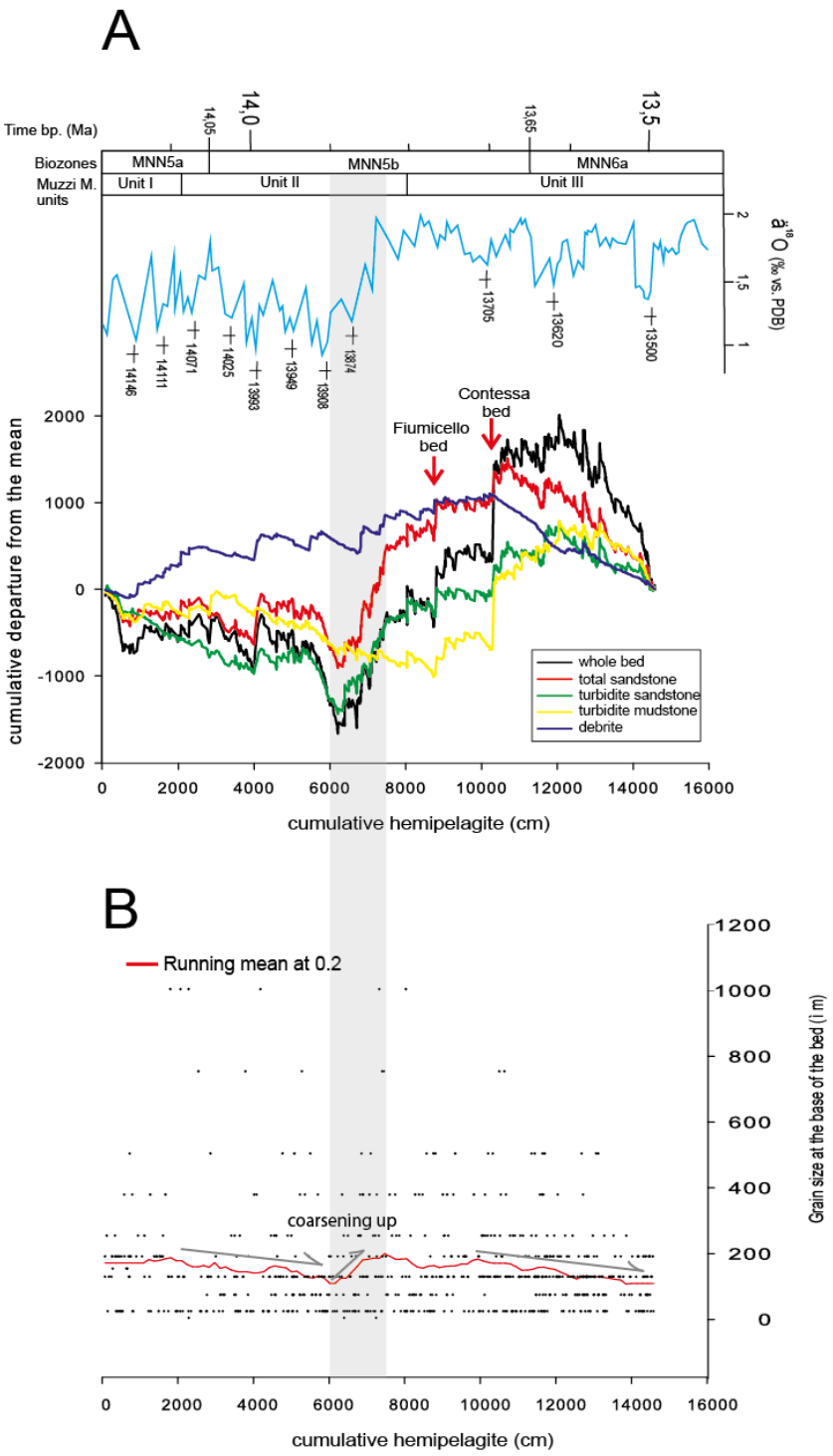

Figure 5.9. *Clustering of turbidite beds.A) Cumulative departure from the mean plot of whole beds, sandstone, debrite and turbidite mudstone intervals plotted against the cumulative hemipelagite thickness as a time axis. For the dated interval the respective time before present is reported. Biozones, magnetic reversals (chrons) are reported. The position of the main units by Muzzi Magahles and Tinterri (2011) are reported for comparison.This curve highlights the presence of irregular vertical clustering of values lower and higher than the mean. For comparison, stable oxygen and carbon isotope data from Ocean Drilling Program (ODP) Site 1146 in Caribbean (Holbourn et al., 2007) are shown. Note the pronounced step at 13.82 Ma representing the Mi3b, Middle Miocene global climate transition. B) Grain size at the base of each event bed plotted against the cumulative hemipelagite thickness as a time axis. The red line indicates a running average smoothing of the data.*

presented in table 1. It should be noted that that almost any test will result in rejection of the null hypothesis if the number of observations is very large (Conover, 1999, p. 454) because natural data very rarely follow an idealized distribution exactly.

5.3.6 Hurst statistic

Table 5.2 shows the result of the Hurst test. The whole bed measurements and the sandstone intervals passed the Hurst test at a ≤1% and ≤5% level respectively. This means that the number of sequences with $K \leq K_0$ in the 300 randomly shuffled sequences is smaller than 1% and 5% (K_0 is the Hurst value of a measured turbidite section and K corresponds to the Hurst value of a randomly shuffled sequence). The results indicate that the vertical clustering of these values is statistically significant. The value of the Hurst exponent K is 0. 67 for whole bed measurements and 0.65 for the sandstone intervals are in good agreement with the values attributed by Chen & Hiscott (1999) to basin plain deposits, including the analysis of the Marnoso Arenacea Formation deposits. The significance of this clustering will be discussed in a subsequent section. The cumulative departures of various types of thickness measurements from their mean value are summarized in figure 5.9a.

The cumulative departure from the mean value of hemipelagite thickness (figure 5.10) indicates the presence of long term clustering. However this clustering cannot be safely statistically tested. The Hurst statistic assumes that the variables are normally distributed. The thickness values of whole beds, sandstone and debrite intervals are approximately lognormally distributed, and therefore have been tested after a Log_{10} transformation. Values of hemipelagite between each bed and between thick beds are exponentially distributed. These values cannot be not safely normalized, and therefore the Hurst test was not performed. The thickness of hemipelagite intervals between beds containing debrite intervals are approximately lognormally distributed. These intervals passed the Hurst test at a significance level ≤ 27.3%. This means that 81 over 300 randomly shuffled sequences of hemipelagite intervals between debrites show results higher than the original sequence, and therefore the Hurst exponent obtained is statistically very poorly significant.

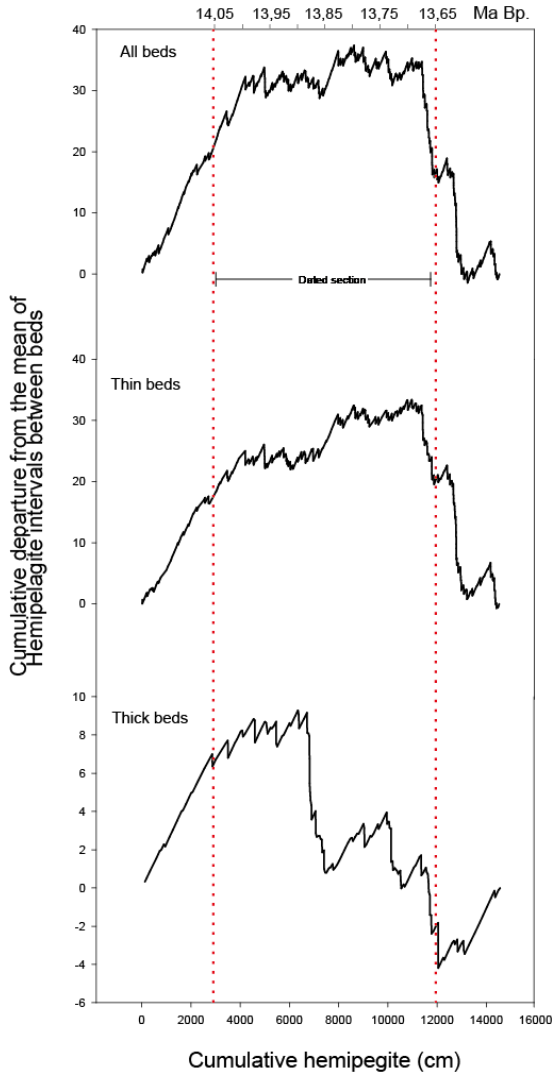

Figure 5.10. *Cumulative departure from the mean plot of hemipelagite intervals between all beds, thin (<40 cm sandstone) and thick (>40 cm sandstone) beds. This curve highlights the presence of irregular vertical clustering of values lower and higher than the mean. The area between the dashed lines represents the dated part of the section.*

5.4. DISCUSSION

5.4. PART 1: THICKNESS DISTRIBUTION AND CLUSTERING OF GRAVITY FLOW DEPOSITS

5.4.1. What is the shape of the frequency distributions of deposit thicknesses?

The frequency histogram of whole event beds (figure 5.8a) shows a distribution markedly skewed towards lower values. The plot is apparently bimodal, with modal values at 20 cm and 90 cm respectively. These values are higher than the ones described by Talling (2001) for other sections in the Marnoso Arenacea Formation of 10 and 40 cm; the difference

can be explained by the fact that the Cabelli section is considered a depocenter (Bidente depocentre; Ricci Lucchi and Valmori, 1980), and both sandstone and mudstone modal values are here considerably thicker than in the section studied by Talling, in the Santerno and Savio valleys. On a first approximation, the cumulative frequency distribution can be reasonably well described by a lognormal distribution. The data plot on an overall straight line on a probability plot with logarithmic y-axis (figure 5.8b). For comparison, a logarithmic cumulative frequency plot is presented (figure 5.8g). This plot shows how the data do not follow a power law distribution, as they do not plot on a straight line on this type of graph. The log-probability plot however shows a number of deviations from a straight line. These variations can be explained subdividing the beds according to the basal Bouma division (Figure 5.11a): beds characterized by a basal Tab (massive and parallel laminated sandstone), Tcd and Te divisions plots on separated straight lines on the log probability plot, and therefore describe 3 lognormal distributions. This result is in agreement with Talling (2001) that explain the bed thickness distribution as the summation of distinct lognormal populations, divided accordingly to the basal Bouma division and grain size classes.

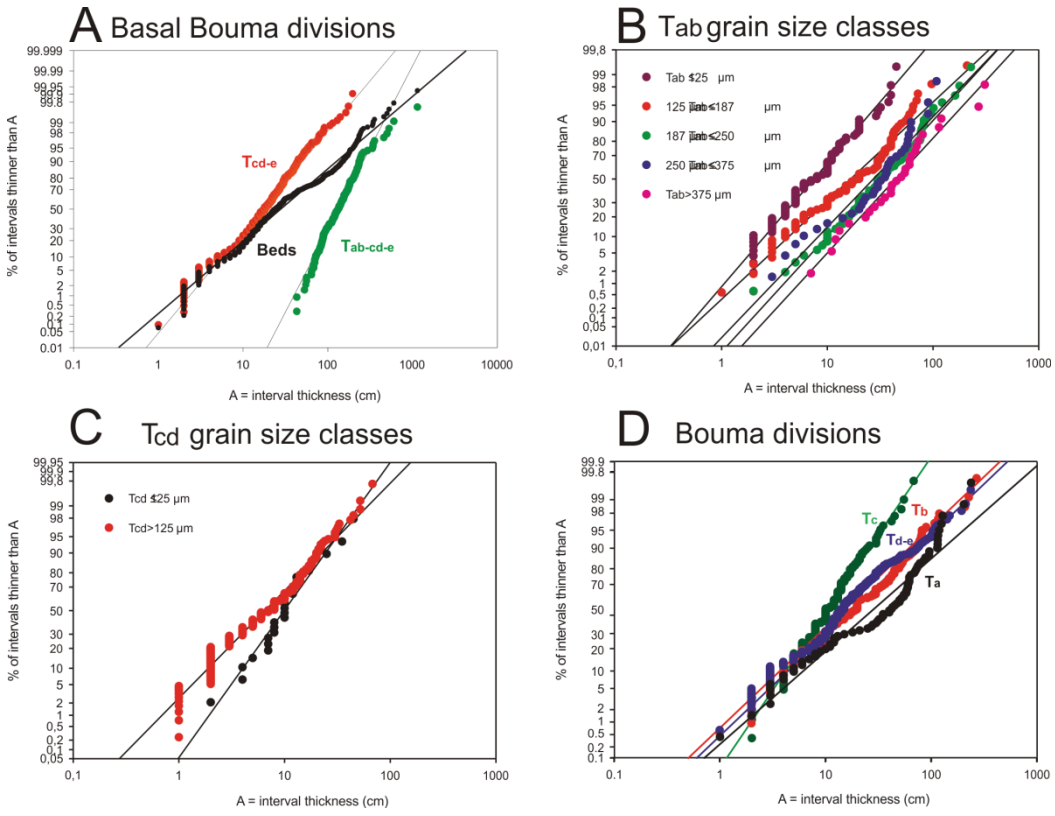

Figure 5.11. *Log-probability plots for beds with different basal Bouma divisions and grain size classes. Straight line trends on the log-probability plots indicate approximate log-normal frequency distributions. A) Plot for all beds, beds with basal T_{ab} division and beds with basal T_{cd} division. B) Plot for beds with basal T_{ab} division divided into grain size classes. C) Plot for beds with basal T_{cd} division divided into grain size classes. D) Plot for different Bouma divisions.*

Talling (2001) describes this summation of lognormal distributions as equivalent to a segmented power law trend (his figure 7). In the Cabelli section this trend is not recognizable, because data plots on a log-log plot as a curve, that do not correspond to linear segments (figure 5.8g).

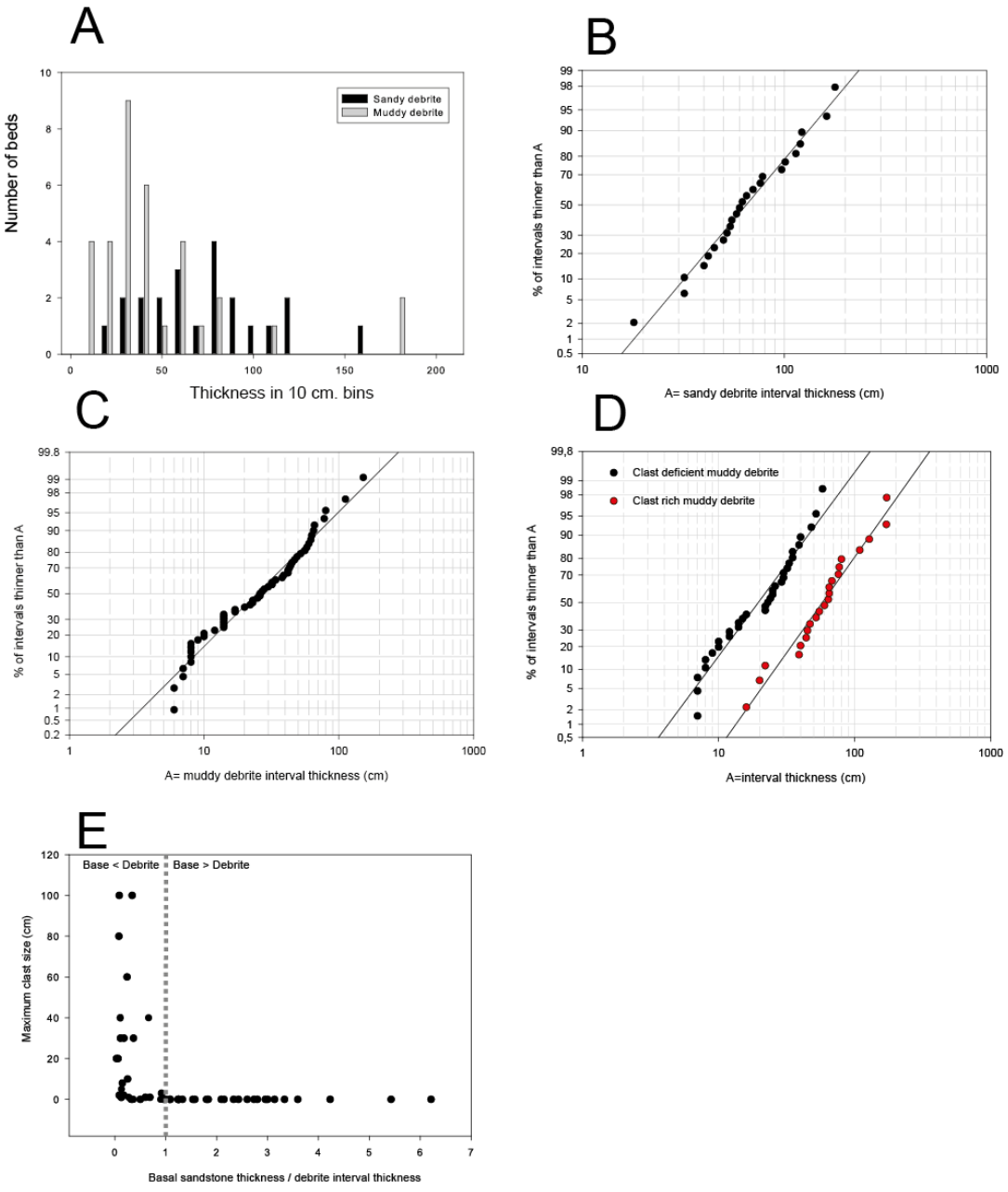

Figure 5.12. *Frequency histogram and log-probability plots for clean and muddy debrites. Straight line trends on the log-probability plots indicate approximate log-normal frequency distributions. A) Frequency histogram for clean and muddy debrites B) Log probability plot for clean debrites. C) Log probability plot for muddy debrites. D) Log probability plot for muddy debrites divided into clast rich and clast deficient populations. E) Diagram showing the relationship between maximum clast size and Debrite(Turbidite sandstone ratio in beds containing muddy debrite intervals.*

Sandstone intervals

The frequency histogram of sandstone intervals (figure 5.8c) is skewed towards thin beds, and shows a clear bimodality, with modal values at 10 cm and 60 cm respectively. The cumulative frequency distribution doesn't plot on a single straight line on the log-probability plot (figure 5.8d), and plots on a curve on a log-log plot (figure 5.8g). Therefore data can't be described by a single lognormal or power law distribution. Thickness of Tab and Tcd sandstone divisions however plot on a straight line on a log-probability plot if divided into grain size classes (figure 5.11b, c). Tb and Tc intervals alone are also lognormally distributed (figure 5.11d).The overall sandstone intervals distribution therefore can be described by the summation of lognormally distributed intervals, divided according to Bouma divisions and grain size classes, as found by Talling (2001).

A small number of unusually thick sandstone intervals (>200 cm) deviates significantly from this distribution (Figure 5.11a), even considering grain size classes (figure 5.11b,c). It may be hypothesized that extremely thick (>200 cm) beds are the result of flow reflection, and therefore form a different thickness population. Although Tinterri and Muzzi Magalhaes (2011) report a small number of "contained – reflected beds" in this location, the 1:10 sedimentary logging undertaken in this study doesn't support any evidence of flow reflection at Cabelli, such as irregular vertical grain size trends or large variations in paleoflow directions (see sedimentary log in figure 3 and paleocurrent directions in figure 7). Despite the absence of sedimentological evidence this hypothesis can't be excluded.

Turbidite mudstone intervals

The distribution of turbidite mudstone intervals is highly skewed to smaller values (figure 5.8e). The data plots close to an overall straight line on a log-probability plot (figure 5.8f), and can be described by a lognormal thickness distribution. It can be noted how the log probability plot of mudstone intervals follow closely the trend of the whole bed measurements, despite the differences in the sandstone intervals distribution (figure 5.8 and 5.13). This may suggest that the overall bed thickness distribution is mainly controlled by the mudstone interval that constitutes half of the total thickness of the section (excluding the hemipelagite).

Muddy debrite intervals

The distribution of muddy debrite (Ms1 and Ms2) intervals is unimodal (figure 5.12a). The data plots close to a straight line on a log-probability plot (figure 5.12c), and therefore can be described by a lognormal thickness distribution (as also found by Talling et al., 2001). Clast rich (Ms1, with mudstone clasts >1cm) and clast deficient (Ms2) populations also plot on 2 different straight lines on a log-probability plot (figure 5.12d). The overall muddy debrite population can therefore be described by the summation of two distinct lognormal distributions for Ms1 and Ms2 debrites. This result highlights the presence in the Marnoso Arenacea Formation of two distinct types of muddy debrite: a clast deficient group, resulting from flow transformation of a turbidity current and a clast rich group, deposited by a debris flow (Talling et al., 2012c). Figure 5.12e suggests that beds containing muddy debrite can be divided in 2 populations also according to the presence of mudstone clasts and the thickness of the basal clean sandstone interval: clast rich debrites generally have a massive or laminated basal division thinner than the debrite interval, while clast deficient debrites have a basal clean sandstone thicker than the debrite interval. It can be noticed that the 2 groups are overlapping for relatively thin (<20 cm) debrite intervals and thin clean sandstone bases. This overlapping can be explained by the fact that clast rich (Ms1) debrites usually contain less clasts (if all) near the point of pinch-out (i.e. bed 2.5 in the Isola element; figure 5.13d). Thin muddy debrite intervals lacking clasts underlie by thin clean sandstone intervals therefore may belong to both Ms1 and Ms2 population. The origin, depositional mechanism and spatial distribution of these two types of muddy debrites are fully discussed by Talling et al. (2012a).

Clean debrite intervals

The characteristics of clean (mud-poor) debrite deposits are described in chapter 3. One of the main criteria for distinguishing such clean debrites from massive sandstones deposited by high-density turbidity currents is the extremely rapid lateral pinch-out of debrite beds. Bed geometry however is unknown when considering a one dimensional section; the recognition of clean sand debrite therefore relies on the characteristic of the deposit (swirly, patchy texture) and the recognition of a clear grain size break with the overlying cross-laminated interval. The distribution of sandy debrite (Cs7) intervals in the Cabelli section is unimodal and has a higher modal value than the muddy debrites (figure 5.14a). The data plots close to a straight line on a log -probability plot (figure 5.12b), and can be described by a

lognormal thickness distribution. The modal value of 80 cm however is very close to the mean value of the distribution, and therefore the distribution is close to a simpler normal (Gaussian) shape, with a lower variability (standard deviation) compared to muddy debrites.

5.4.2 Comparison of thickness distributions at Cabelli with those in laterally correlated beds

If the vertical thickness distribution of turbidite and debrite beds is considered equivalent to a random sampling of the same bed in different locations (Talling et al., 2007a), the vertical distribution of beds in a single location would correspond to the thickness distribution of a small number of beds sampled in different position along the basin, assuming that the sediment volume carried by flows entering the study area didn't change significantly through time. This hypothesis can be tested comparing the results from the Cabelli section to the thickness values of 30 beds in various locations across the outcrop area, obtained from Amy & Talling (2006) and the results of chapter 3. Figure 5.13 shows the result of this comparison for whole beds, muddy debrite and sandy debrite intervals. Turbidite bed thickness distribution is approximately lognormal in both the Cabelli section and the correlated beds (figure 5.13a). The modal value is lower in the Cabelli section than in the correlated beds. This is more likely due to a lower percentage of thin beds in the correlated interval, or to an under sampling of thin beds due to bad exposure in some locations.

Sandy and muddy debrite intervals follow a lognormal distribution in both the Cabelli section and the correlated interval (figure 5.13b, c). The distributions overlap almost perfectly, and the gradient of the resulting line is the same. The modal thickness values for both muddy (20 to 30 cm) and sandy (80 cm) debrites are the same in the two databases. This similarity do not result from beds that all contain similar volume of debrite. Work by Talling et al. (2007a) shows that muddy debrites deposits can have different volumes in the study area. This characteristic thickness distribution may be explained by the observation that debrite beds with larger volume tend to move their maximum thickness further out in the basin, and not to produce thicker deposit (see chapter 4). The log-probability plots also indicate that both sandy and muddy debrites thickness distributions lack the thin values expected from the theoretical lognormal distribution. This can be explained by the characteristic shape of debrites (figure 5.13e). Debrite intervals have an abrupt pinch-out geometry if compared to turbidite beds. The origin of this geometry is most likely due to the freezing of debris flows at their margin, as

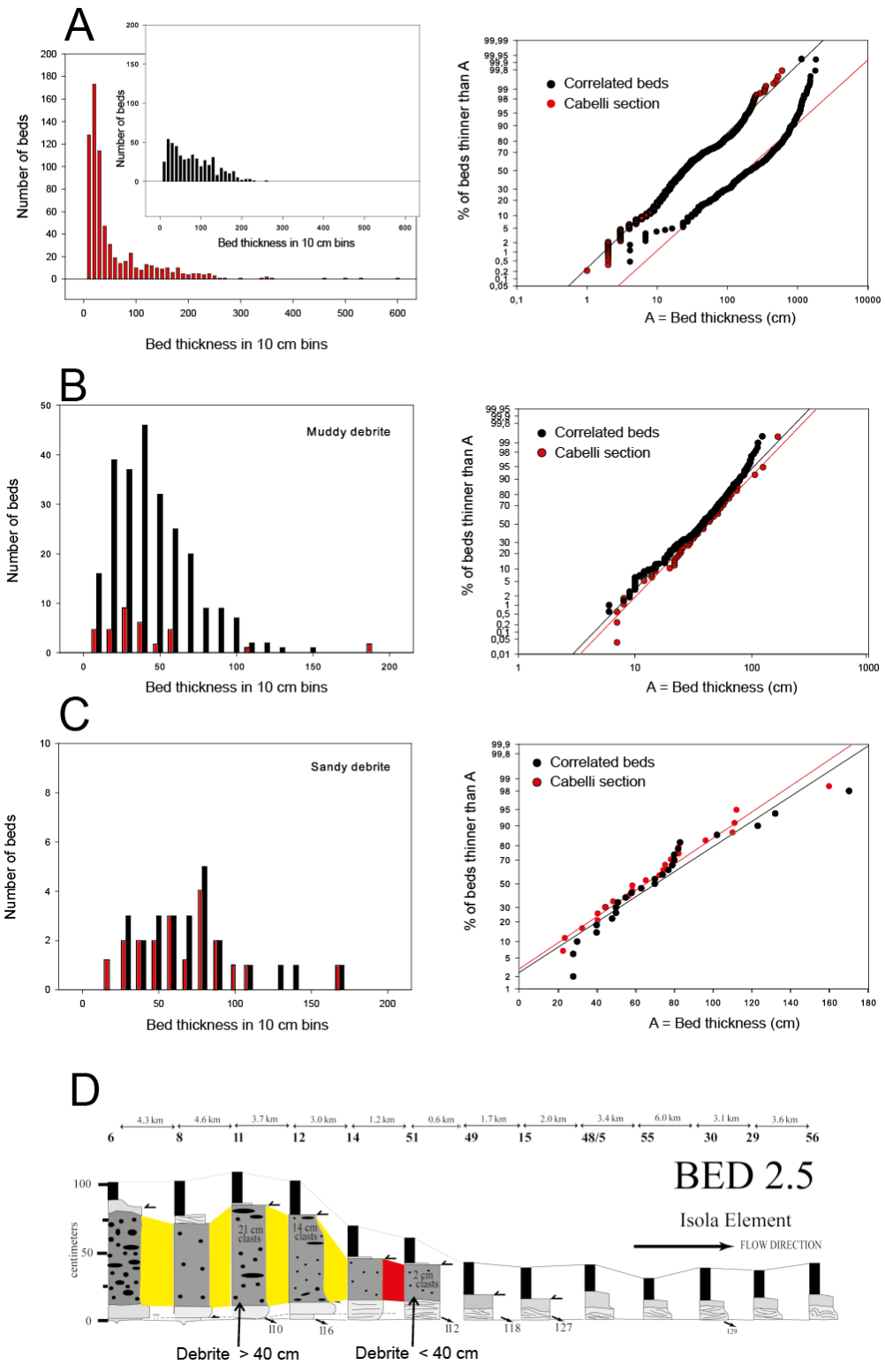

Figure 5.13. *Comparison between the thickness distribution of whole beds, clean and muddy debrites in a vertical section (Cabelli) and in randomly sampled beds in different positions along the basin (beds correlated in chapter 3 and by Amy and Talling., 2006). A) Frequency histogram and log-probability plot of whole beds. Straight line trends on the log-probability plots indicate approximate log-normal frequency distributions. B) Frequency histogram and log-probability plot of muddy debrite intervals. C) Frequency histogram and log-probability plot of clean debrite intervals. D) Correlation panel of bed 2.5 in the Isola Element, highlighting the pinch-out geometry of debrite beds.*

explained in chapter 3. A random sampling of one of these beds would result in a lack of low thickness values, as the probability of sampling the pinch-out are considerably low.

5.4.3. Comparison to deposit thickness distributions in other locations, and Talling (2001)

Talling (2001) described the bed thickness distribution of 13 sections in the Marnoso arenacea formation, in the Santerno and Savio valleys (map in figure 1b). Among these sections, the Coniale section (the most proximal section available for beds with provenance from the North-West) contains 560 beds, and can be compared directly to the Cabelli section which contains 696 beds. The two sections describe roughly the same stratigraphic interval, and are separated by approximately 30 km in downflow direction.

The overall bed thickness distribution appears to have a similar shape in the two stratigraphic sections, with absolute values shifted towards thick beds at Cabelli (figure 5.14a). This is due to the downcurrent thickening of the mudstone intervals, as the sandstone intervals distribution appears to be similar in the 2 sections even in term of absolute thickness values. This result is somewhat surprising, given the 30 km distance between the two sections, but can be explained by the overall tabular shape of sandstone intervals that characterizes the basin plain deposits of the Marnoso Arenacea Formation.

An important difference between the Coniale and the Cabelli section is that the Tcd-e (thin bedded) population at Cabelli has a smaller standard deviation (expressed by a “flatter” regression line on the log-probability plot). On the other hand the Tab-cd-e population (thick bedded) has a greater standard deviation (figure 5.14b). Sylvester (2007) found a similar relationship comparing data from the Tarcău Sandstones to the one studied by Talling (2001) in the Marnoso Arenacea Formation. This difference is tentatively explained by Sylvester (2007) by the fact that thin beds in the Tarcău Sandstones represent levees, while in the Marnoso Arenacea Formation the thin bedded population represents basin plain turbidites. The results of this study suggest that this difference in standard deviation of thickness is not due to changes in depositional settings (i.e. levee versus basin plain), but results from the difference between proximal (Coniale) and mid-distal (Cabelli) sections. The lower variability at Cabelli can be explained by the observation that the mudstone cap of each bed tends to thicken downcurrent. This results in a lower percentage of very thin (<10 cm) beds at Cabelli, that reduces the overall variability (standard deviation) of Tcd-e beds.

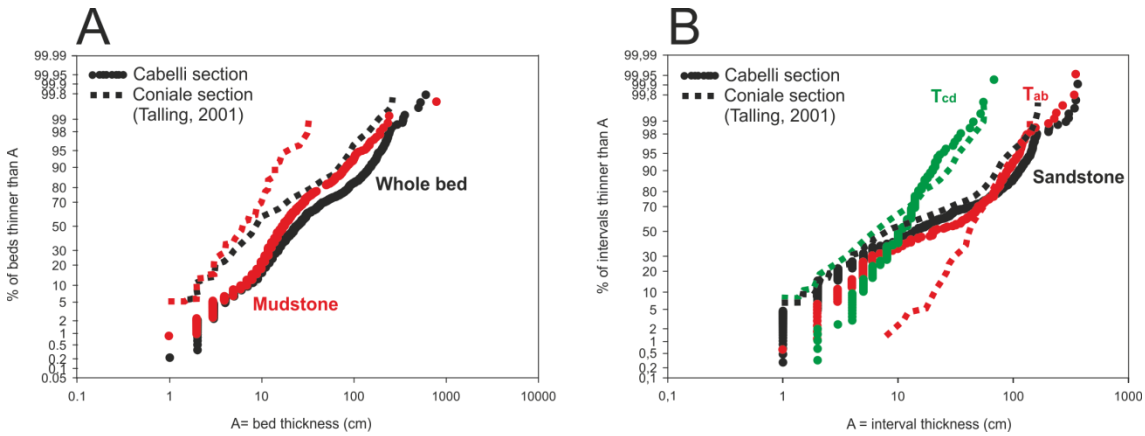

Figure 5.14. *Comparison between data from the proximal Coniale section (Talling, 2001) and the Cabelli section. A) Log probability plot of whole beds, sandstone and mudstone intervals in the two sections. Straight line trends on the log-probability plots indicate approximate log-normal frequency distributions. B) Log-probability plots for beds with different basal Bouma divisions in the Coniale and Cabelli sections.*

The higher variability in thickness of beds with a Tab basal division (figure 5.14b) can be explained considering the characteristic shape of large beds described in chapter 4 and by Amy and Talling (2006). At the most proximal Coniale section both large volume and intermediate volume beds contain thick Tab basal divisions; this, coupled with generally thin mudstone caps, leads to a limited variability of the bed thickness. Further downcurrent, in the mid-distal part of the basin where the Cabelli section is located, large volume beds reach their maximum thickness, while intermediate volume beds tend to thin. Such intermediate volume beds (and beds containing a proximal clean debrite interval) are represented at this location by thinner Tab-cd-e or possibly Tcd-e beds, resulting from the complete pinch-out of the basal Tab divisions. The result is a significantly higher variability in the bed thickness population.

This relationship, with Tab-cd-e bed thickness being more dispersed than Tab bed thickness, is also used by Sylvester (2007) to explain why the lognormal mixture model of Talling (2001) can appear in a log-log plot as a segmented power law, while in the Tarcău Sandstones the same plot results in a smoothly curved line, hardly interpretable as the sum of straight line (power law) segments. A similar result (figure 5.8g) is found for the Cabelli section.

5.4.4 What controls the frequency distribution of deposit thicknesses?

The local thickness of turbidite beds depends on a number of factors, including the shape of the bed and the distance to the source, with bed shape depending upon factors such

as initial sediment volume, grain-size(s), flow duration and flow concentration (Middleton & Neale, 1989; Rothman & Grotzinger, 1996; Malinverno, 1997; Carlson & Grotzinger, 2001; Talling, 2001, Sylvester, 2007). The local bed thickness can also be strongly affected by the basin geometry, possibly controlling processes such as flow confinement and ponding (Malinverno, 1997; Felletti and Bersezio, 2010). The results of this study confirm the initial findings of Talling (2001) and Sylvester (2007): deposits of low-density (Tcd-e) and high density (Tab-cd-e) flows in the Marnoso Arenacea Formation describe different lognormal populations, the convolution of which results in the observed bed thickness distribution. The sandstone division of each of the two populations is the combination of lognormally distributed intervals characterized by specific grain size classes and sedimentary structures (including clean and muddy debrite intervals). The relative proportions of Tab and Tcd intervals vary between proximal (Coniale) and mid-distal (Cabelli) sections: nevertheless the overall bed thickness distribution is remarkably similar.

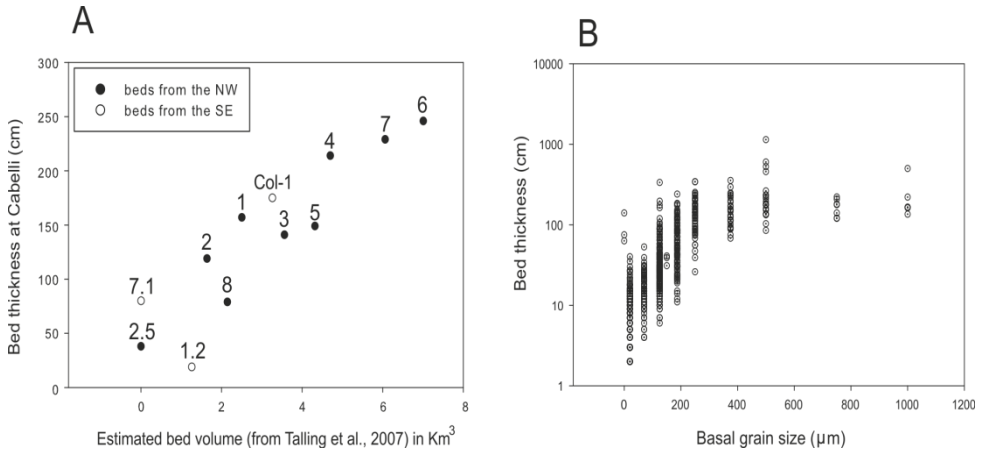

Figure 5.15. *A) Comparison between the bed volumes estimated by Talling et al. (2007) and the thickness of the same beds at Cabelli. B) Relationships between bed thickness and basal grain size for each measured bed.*

The lognormal distribution of sandstone and mudstone intervals at Cabelli is similar to the one obtained with random sampling of a small number of beds in different locations. The characteristic bed thickness distribution in the Marnoso Arenacea formation can be described by a mixture of lognormal populations both in a temporal (bed thickness distribution in a given location) and a spatial (random sampling of few beds in different positions of the basin) direction.

The characteristic shape of each bed is primarily controlled by the sediment volume of the flow, as described in chapter 4. The volume of flow initiating events such as slope failures are

generally found to be power-law distributed, although Chaytor et al. (2009) found that the volume of slope failures in the North American Atlantic margin are most likely lognormally distributed. Talling et al. (2007a) estimated the volume of flow events forming a 30 m thick interval of the Marnoso Arenacea Formation to be lognormally distributed. The distribution of the volume of flow-initiating events however is unlikely to be directly related to the bed thickness distribution in a given location. This is because a number of processes (including but not limited to the grain size present, channelized or unchannelized flow paths, failure of small volume flow deposit to reach the sampling site) can act to modify the initial conditions (Talling et al., 2001; Sylvester, 2007). This can be tested comparing the bed volumes estimated by Talling et al. (2007a) and the thickness of the same beds at the Cabelli section (Fig 5.15a). The plot shows a good correspondence between the volume of large beds with paleocurrent directions from the North-East and their thickness at the Cabelli section; this however may be a characteristic specific of depocentral locations such as Cabelli, where large volume beds reach their maximum thickness. Bed correlations show that in more proximal locations intermediate and large volume beds may have similar local thicknesses (see correlation panel in chapter 3).

Thin beds (usually characterized by the absence of a basal massive sandstone interval) can correspond to two volumetrically distinct bed types: (i) beds that are thin over the entire outcrop area and (ii) thin intervals resulting from the pinch-out of larger beds, containing sandy (Cs7) or muddy (Ms) sandstone intervals (Facies tract 2 and 3 in chapter 3). Thin beds are also not always continuous over the entire outcrop area; a direct correspondence between bed thickness in a given location and bed volume therefore is not always possible.

The local thickness of each bed at Cabelli is found to be positively correlated with the basal grain size (figure 5.15b), with a characteristic inflection point at about 200 μm. Talling (2001; and references therein) interpreted this relationship as the results of a transition in the settling behavior, from viscous to inertial settling as grains become larger, although this is yet untested by modeling.

At Cabelli, only a small (less than 10 over 696) number of beds may be affected by flow reflection. The distance from the source is unlikely to have affected the bed thickness distribution, as most flows entered the study area from the same location in the North-East of the study area (Ricci Lucchi & Valmori, 1980). Minor sources entered the basin plain from the South and South-West (Contessa and Colombines), as confirmed by the analysis of the lithic component of sandstone beds (Gandolfi et al., 1983).

The bed thickness distribution observed results from the relative proportion of flow deposits with characteristic bed shapes: in a given location the range of grain size available for deposition (together with other flow parameters such as sediment concentration, turbulence intensity and flow duration) determines the deposition of lognormally distributed intervals that combine in the resulting thickness distribution. Talling (2001) proposed that the lognormal thickness distribution of each interval results from the multiplication of several randomly distributed parameters, such as flow duration, turbulence intensity and sediment settling velocity that in turn depends on grain size and sediment concentration within the flow.

5.4.5 How strongly stratigraphically clustered are flow deposit thicknesses ?

Whole event beds

Figure 5.6a shows the thickness of each measured bed plotted against the cumulative hemipelagite intervals (considered as a proxy for time between events). As expected in a basin plain succession (Chen and Hiscott, 1999), beds don't show any clear vertical pattern, such as thinning or thickening upward trends. The Hurst statistic however reveals a statistically significant long term irregular clustering of thick and thin beds (figure 5.5). A cluster can be defined here as a part of the studied succession showing common characteristic in terms of bed (or interval) thickness. If each bed is divided into sandstone and mudstone intervals a pattern in the vertical clustering can be observed (figure 5.9):

- in a first cluster (between 0 and 6000 cm(hp) both sandstone and mudstone intervals are substantially stable around the mean;
- in a second cluster (between 6000 and 7500 cm(hp) the sandstone thickness increases, while the mudstone slightly decreases;
- in a third cluster (between 7500 and 13000 cm(hp) sandstone and mudstone intervals are again stable around the mean, with variations given by anomalous thick beds, such as the Fiumicello and the Contessa bed;
- in a fourth cluster (between 13000 and 14500 cm(hp) both sandstone and mudstone thicknesses are slightly thinner than the mean.

Vertical clustering in basin plain sequences (including the Marnoso Arenacea basin plain) was attributed by Chen & Hiscott (1999) to the lateral shifting of depocentres. In a vertical section,

given a certain sediment supply, periods representing deposition in a depocentre will show a general increase in bed thickness. This process however only explains periods where both sandstone and mudstone interval variations follow the same pattern. The clustering observed between 6000 and 7500 cm(hp is likely to be produced by allocyclic factors such as sea level variations, as explained in a later section.

Muddy debrites

A plot of the thickness of muddy debrite intervals against the cumulative hemipelagite thickness (figure 5.6c) does not show any obvious cyclic variation, both in the frequency and in the thickness of the intervals, although an irregular clustering can be observed. The clustering of clast-rich (Ms1) and clast-deficient (Ms2) muddy debrites cannot be tested using the Hurst statistic, as the two populations contain a number of beds <<100, and the result would not be statistically significant (Chen & Hiscott, 1999). The whole debrite population (clean and muddy) has been tested using this method; the resulting clustering is statistically equivalent to a random vertical succession of the same thickness population, and therefore no significant vertical trend can be established for debrite intervals.

Clean sand debrites

Clean debrite (Cs7, or Dcs in the classification by Talling et al., 2012a) deposits are relatively uncommon in the studied section. They occur in 22 of 696 (3.16%) beds, and have a total thickness of 17.84 m (3.38% of the section). However, they are present in the 13.5% of thick beds, and constitute a significant component (10.48 %) of the total sandstone thickness. A plot of the thickness of clean debrite intervals against the cumulative hemipelagite thickness (figure 5.6c) does not show any obvious cyclic variation, both in the frequency and in the thickness of the intervals. It is noted that clean debrite intervals are almost absent (occurring in only 2 beds) between 0 and 4000 cm of hemipelagite; they are relatively common (occurring in 18 beds) between 4000 and 10000 cm ad again very rare (occurring in 2 beds) above 10000 cm. This clustering appears to be related to a general increase in the number of thick beds (figure 5.13) in the same interval, and therefore not characterize clean debrites only.

4.4. PART 2: FREQUENCY OF FLOWS THROUGH TIME

5.4.6 Hemipelagic marl thickness as a proxy for time

In this study we use the thickness of hemipelagic marl between turbidite beds as a proxy for the intervening time between flow events. This approach is based on three assumptions: (i) that hemipelagic marl is clearly distinguishable from turbidite mud, (ii) that the background sedimentation rate is constant in the whole studied succession, so that the same thickness of hemipelagite corresponds to the same amount of time, (iii) that the amount of erosion of hemipelagic marl by the successive flow events is negligible.

As discussed in the method section, hemipelagic marl is clearly distinguishable from turbidite mudstone based on the texture, color and fossil content of the deposits (figure 5.4a).

The background sedimentation rate calculated here (15.25 cm/ka) is based on 2 dated horizons, and therefore it represents only a mean value for a 0.6 Ma period. Although the uniformity of hemipelagic sedimentation within this 600 ka time period cannot be demonstrated, this may be a reasonable first order assumption (Muller and Suess, 1979; Thornton, 1984; Guerra et al., 2008).

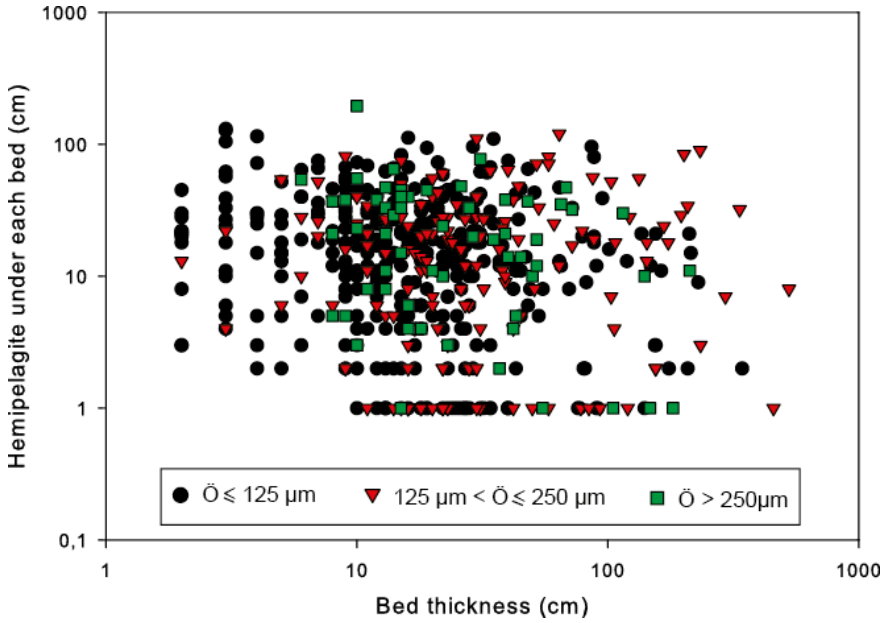

Figure 5.16. *Relationships between bed thickness and the hemipelagite under each bed. Beds are classified according to the basal grain size class.*

Erosion by successive flows would cause an erroneous measurement of the original hemipelagite thickness. Amy and Talling (2006) and Talling et al. (2007a, b) showed how erosion in the Marnoso Arenacea formation was very limited; or at least differential erosion that caused lateral changes in hemipelagite thickness. This is also demonstrated by the lack of bed amalgamation and by the roughly constant thickness of hemipelagic layers between turbidite beds. Erosion is inferred to correspond mainly to the thickness of flutes and grooves at the base of thick beds. To overcome this problem hemipelagite thickness was measured in this study from the basal contact with turbidite mudstone to the base of the overlying bed, including the eventual thickness of flutes and grooves. The graph in figure 5.16 indicates that the thickness of hemipelagite is not correlated with thickness or grain size classes of the overlying bed. Thicker or coarser grained beds do not appear to erode significantly more hemipelagite than thin or fine grained turbidites.

5.4.7 What is the frequency distribution of recurrence times for flow events?

The thickness distribution of hemipelagite intervals is well described by an exponential distribution. The frequency histogram of hemipelagic marl between each event-bed intervals is unimodal (figure 5.17a). The modal value is 1 cm that corresponds to the limit of the resolution adopted. Fourteen event beds are not separated by distinguishable hemipelagic marl intervals, and therefore the value of hemipelagite thickness is set to zero. The distribution plots on an almost perfectly straight line on a log-linear plot for values between 1 and 80 cm. Higher values deviate only slightly from this straight line (figure 5.17b). For comparison, a log-probability plot (lognormal distribution) and a cumulative log-log plot (power law distribution) are shown (Figure 5.17c, d). A quantile-quantile plot, comparing the data to a theoretical exponential distribution confirms that the field data fit this distribution closely (figure 5.17e).

The frequency histogram of hemipelagic marl between thick (>40 cm sandstone) beds is unimodal and skewed to the right (figure 5.18a). Values plots well on a cumulative log-linear plot, and therefore the data are well described by an exponential distribution (figure 5.18b). The 3 highest thickness values (above 230 cm of hemipelagite) differ from this distribution.

Bettie and Dade (1996) documented the same exponential distribution for mudstone intervals in the Izu-Bonin basin in the western Pacific Ocean, and proposed that mudstone intervals could serve as proxy for time between events. These authors however could not differentiate

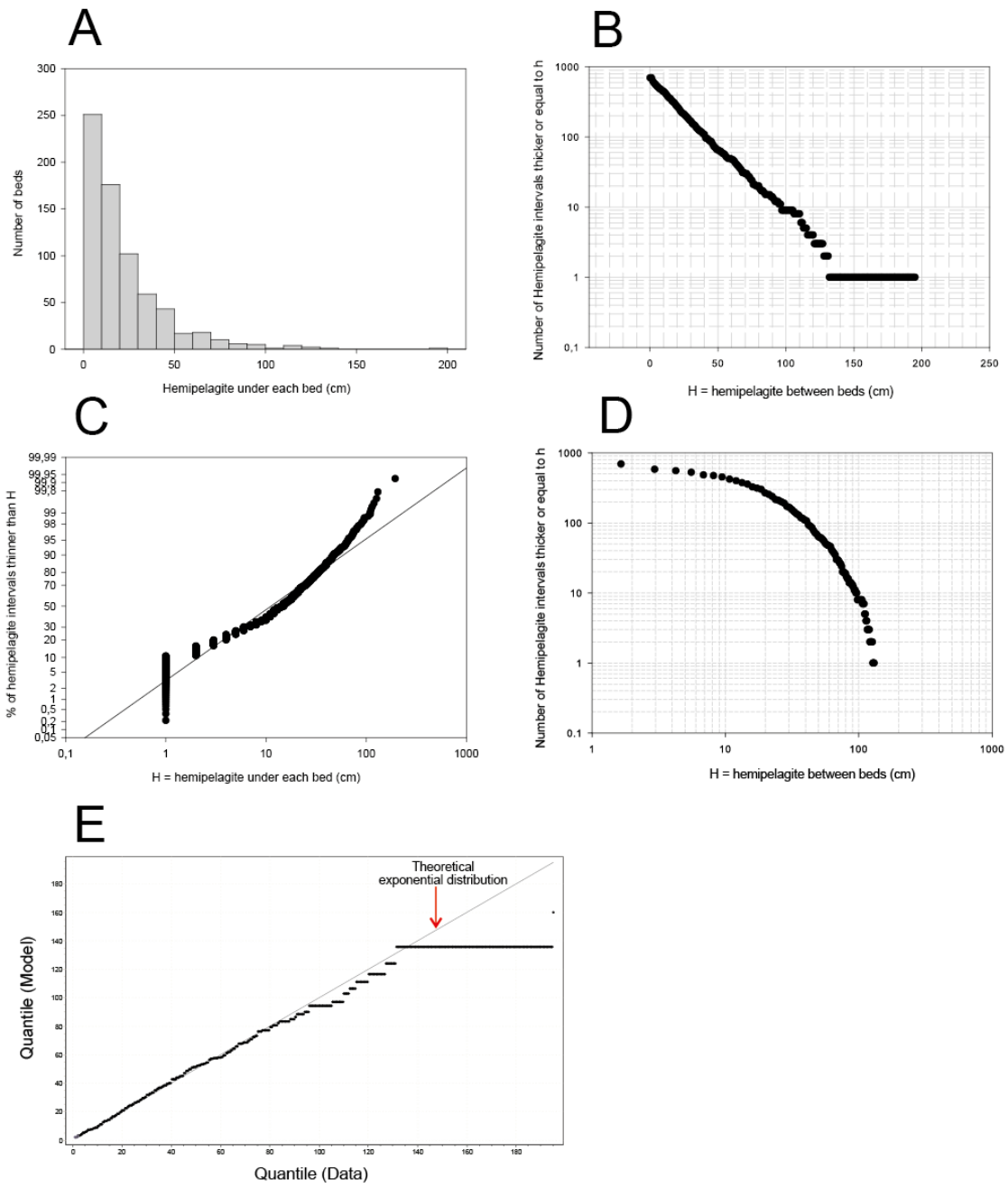

Figure 5.17. *Cumulative distribution of hemipelagite. Data plotting on an approximate straight line on each plot are in good agreement with the corresponding distribution. A) Frequency histogram B) Log-linear plot (Exponential). C) Log-probability (Lognormal). D) Log-log plot (Power-law). E) Quantile-quantile plot comparing a theoretical exponential distribution to the observed values.*

mudstone deposited by sediment density flows from true hemipelagite. In this study we show that turbidite mudstone have a lognormal frequency distribution, related to the deposition from the fine tale of a turbidity current.

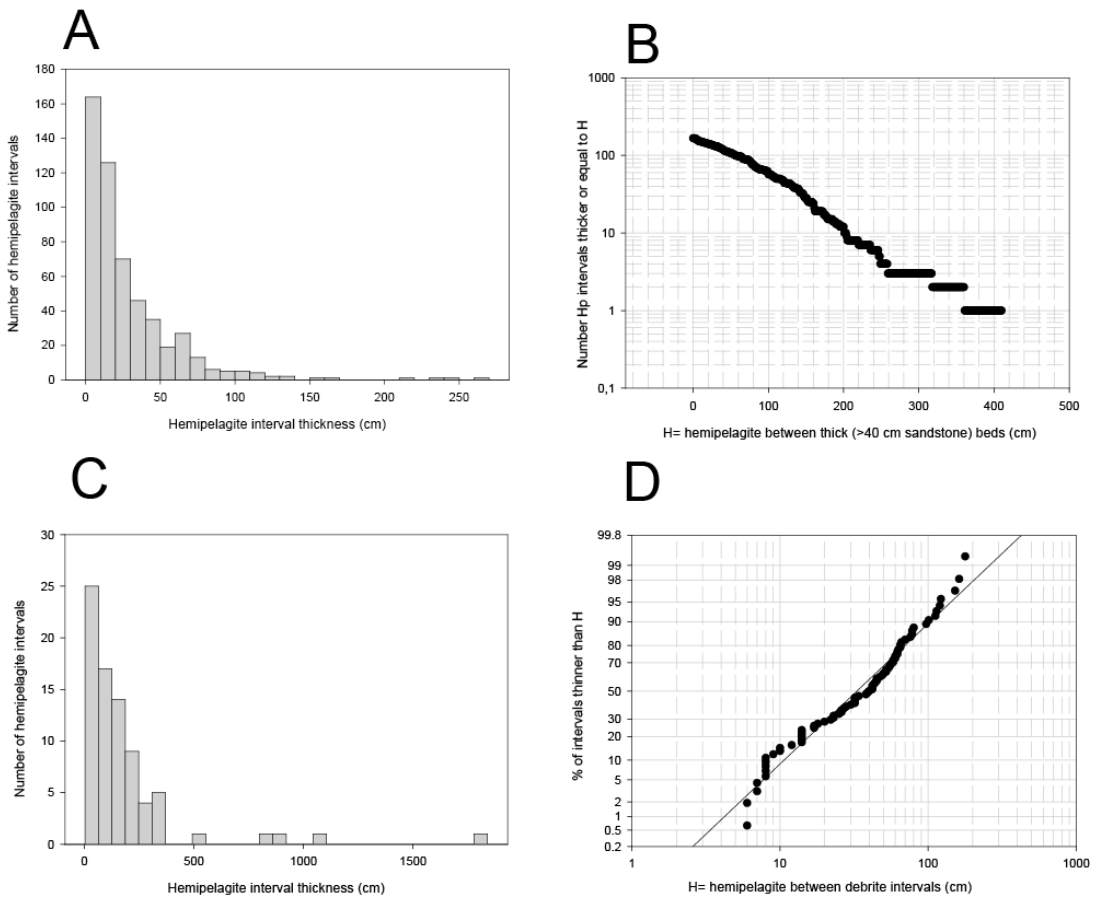

Figure 5.18. *A, B) Frequency histogram and Log-linear plot for the values of hemipelagite between thick (>40 cm sandstone) beds. Data plots on an approximate straignt line on the Log-linear plot, showing a good agreement to an exponential distribution. C, D) Frequency histogram and Log-probability plot for the value of hemipelagite between beds containing clean or muddy debrite intervals. Data plots on an approximate straight line on the Log-probability plot, showing a good agreement to a lognormal distribution.*

The fact that the frequency distribution of whole (turbidite mudstone + hemipelagite) mudstone beds in the Izu-Bonin basin is exponential is somewhat surprising given the results obtained in this study, but it may be related to the fact that turbidites in that basin are particularly sandy, or that the data were obtained from a section close to the source area, so that turbidite mud mainly bypassed that section. Bettie and Dade (1996) also proposed that cumulative mudstone thickness plotting on a straight line against the relative number of beds (their figure 2), can be used as an indicator of constant background sedimentation. However this type of plot only demonstrates that mudstone thickness does not have significant vertical trends. The relationship between thickness of hemipelagic intervals and time strictly depends on the background sedimentation rate that may vary in response to the distance from land, water depth and bathimetric isolation (Colwell and Exxon, 1988).

Poisson processes

Although the constancy of hemipelagic sedimentation cannot be demonstrated, the approximately exponential distribution of time between events in the studied section can still be inferred. A Poisson process is defined as a stochastic process in which events occur continuously and independently one of another, and are identically distributed. In this type of process the time between events is distributed according to an exponential law (Everitt, 2006). Marzocchi and Zaccarelli (2006) studying the time distribution of volcanic eruption, proposed a simple procedure to test if a distribution is exponential, and therefore results from a Poisson process. They showed that in an exponential distribution $\sigma/\mu=1$, where σ is the average value and μ is the standard deviation. The plot in figure 5.19 shows that values of mean and standard deviation are indeed almost equal for every consecutive interval of 50 hemipelagite beds overlapping by 1 bed. Small differences between mean and standard deviation are only recorded between the hemipelagic beds 230-281 and 470-521. These variations are due to the presence of few anomalous large interval of hemipelagite: a large value significantly increases the standard deviation but causes only a small change in the mean of 50 values. These intervals may result from long periods of non-deposition of turbidites, or may contain turbidite intervals below the logging resolution (1 cm). As a result, every possible interval of 50 consecutive hemipelagic beds can be described by an exponential distribution. By definition, the sum of *n* non overlapping exponential distributions is an exponential distribution (Everitt, 2006). Considering time intervals between events, the latter ensure that unless large variation in sedimentation rate occurs over the period of time necessary to deposit << 50 consecutive intervals of hemipelagite, the overall distribution of the recurrence interval of density flows follows an exponential distribution.

The frequency histogram of hemipelagic marl thickness between beds containing sandy or muddy debrite intervals is skewed towards thick intervals, with dispersed values above 500 cm of hemipelagite (figure 5.18c). This distribution plots relatively well on a log-probability plot, and therefore it can be reasonably described by a lognormal distribution (figure 5.18d). However both the fine and the coarse tail of the distribution deviate significantly from this trend. The Kolomogorov-Smirnov test (table 5.1) indicates that the goodness-of-fit between these data and a theoretical lognormal distribution has a lower level of significance compared to the other intervals examined.

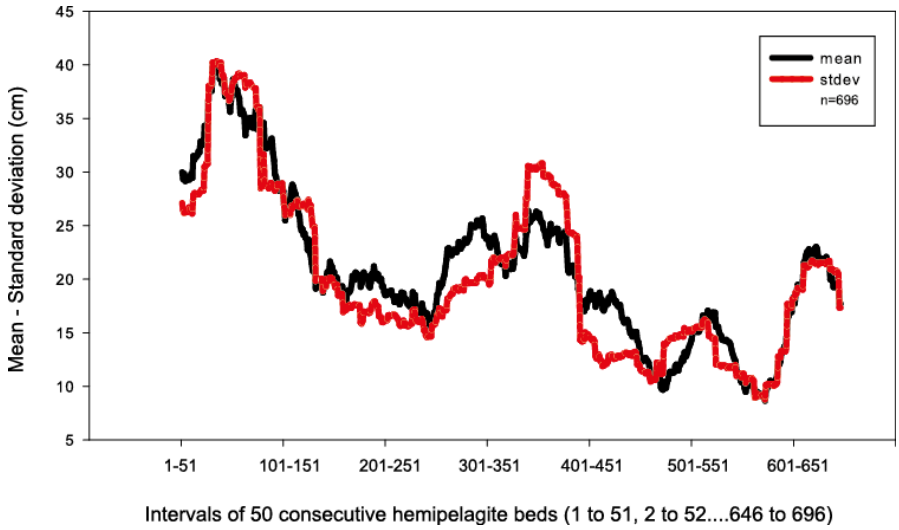

Figure 5.19. *Plot of the values of mean and standard deviation (in cm) for each consecutive 50 intervals of hemipelagite (1 to 50, 2 to 51…..646 to 696). In an exponential distribution the mean value corresponds to the standard deviation.*

5.4.8. Implications of exponential distribution

In this study we have assumed a near constant hemipelagic sedimentation rate over a period of 600 ka. Subsets of 50 consecutive hemipelagite intervals are shown to have thicknesses that are exponentially distributed. Therefore, unless hemipelagic accumulation rates varied marked over the duration of each 50-interval subset (i.e. over periods of ~ 68 ka), the density flows recurrence times have a near exponential distribution. The importance of this finding lies in the characteristics of this statistical distribution. An exponential distribution describes the time between events in a Poisson process, which is a process in which events occur continuously and independently. The independence between events is ensured by the 'lack of memory' property of this distribution (Balakrishnan & Basu, 1996). In terms of recurrence time of flow events, this property ensures that, given that a certain event did not occur during a time period (S) in the past, the chance that an event will occur after an additional time period (T) in the future is the same as the chance that the event would occur after a time period (T) from the beginning of the record, regardless of how long the time period (T or S!) is. The system has no memory, so that each event in the past does not contain any information that can predict the likelihood of events occurring in the future. Using an analogy with volcanic eruption, the probability of an eruption occurring a fixed period (T) in the future, is the same regardless of whether an eruption has (or has not) occurred recently in the past. Another analogy would be with a shop keeper waiting for their first customer. The probability of a customer arriving in the next ten minutes remains the same when the shop first opens at 9 am, and at 10 am after no customers arrive in the first hour.

Although the distribution of time between events can be reasonably well be described by an exponential distribution, related to a Poisson process, the analysis of the vertical clustering of hemipelagite intervals (figure 5.10) reveals that, if the background sedimentation rate is assumed constant, the overall stratigraphic section can be divided into 3 periods characterized by different mean event returning times. A first cluster (from bed 1 to bed 100) with mean returning time of about 2200 years; a second cluster (from bed 101 to bed 400) with mean values of about 1400 years; a third cluster (from bed 401 to bed 696) with values of about 950 years. The time between events in each of these 3 clusters can be described by an exponential distribution. The overall interval therefore results from the sum of 3 non overlapping exponentially distributed intervals with different mean returning times. The 'lack of memory' property of the exponential distribution of returning time between events can provide insights into the tempo and triggers of processes that initiated submarine sediment density flows that entered this ancient basin plain. It is likely that submarine slope failures (landslides) triggered the larger volume flows in this basin, as individual bed volumes can exceed the annual sediment supply from all of the world's rivers (Milliman and Syvitsky, 1992). We also explore whether changes in sea level appear to cause the observed variations in thickness and the average frequency of gravity flow events. This will be discussed further in a later section.

Thickness population	No. of beds	Median (cm)	Distribution	K-S statistic	K-S P-value
Whole beds	696	24	lognormal	0,07142	0,00156
Sandstone intervals	530	14	lognormal	0,07381	0,00594
Turb. Mudstone intervals	696	15	lognormal	0,0854	0,00072
Sandy debrite intervals	24	61	lognormal	0,08047	0,99414
Muddy debrite intervals	55	26.5	lognormal	0,09653	0,649001
Total debrite intervals	79	40	lognormal	0,1022	0,3569
Hemipelagite (incl. 0s)	696	15	exponential	0,06844	0,0028
Hemipelagite (excl. 0s)	679	17	exponential	0,05949	0,02351
Hemipelagite (incl. 0s)	696	15	lognormal	0,10135	0,000011
Hemipelagite between large (>40cm sandstone) intervals	166	18	exponential	0,07399	0,3082

Table 5.1. *Results of the Kolmogorov-Smirnov test for the different thickness populations considered*

Population	Hurst **K**	Hurst **H**	**Significance level**
Whole beds	0,6732	0,6717	< 1%
Sandstone	0,6564	0,6763	< 5%
Mudstone	0,6569	0,6698	< 5%
Hp (Debrite	0,6533	0,6902	< 27,3%

Table 5.2. *Hurst coefficients K and H and significance level for the populations analyzed with the Hurst test. See text for an explanation of the technique adopted*

5.4.9. Clustering of events in time, and temporal changes in mean flow frequency

Clustering of flow events

As shown previously the cumulative departure from the mean plot (figure 5.10a) for hemipelagite thickness between each bed, can be divided into 3 main clusters: a first cluster (from bed 1 to bed 100) of thickness values higher than the mean; a second cluster (from bed 101 to bed 400) of thickness values around the longer-term mean; a third cluster (from bed 401 to bed 696) with thickness values lower than the mean. Assuming a constant background sedimentation rate this would represent a first period of events less frequent than the mean, followed by a period with event with the mean frequency (1 event every 1363 y), and by a third period of events less frequent than the long term mean. The significance of this variation however is uncertain. Calculations suggest that the same variation in hemipelagite thickness can be obtained by differences in sedimentation rate of less than 25% around the mean. Given the lack of information about the background sedimentation rates in the Marnoso Arenacea basin this hypothesis cannot be excluded. If the sedimentation rate was constant however, this clustering shows how the number of beds per unit of time in this section varies according to long (10^5 years) cycles. This long term (> 100 ka) clustering may be due to: (i) phases of fan advance(retreating, possibly due to variations in relative sea level and basin configuration, so that small events can or cannot reach the position of the Cabelli section (about 30 km down flow from the first available outcrop); (ii) long-term variations in the overall sediment supply.

Clustering of event comprising debrite intervals

The Hurst test shows that the vertical clustering of time between event comprising debrite intervals has a high probability of not being statistically significant, and therefore the cumulative departure from the mean plot will not be described here. The time-distributions of beds containing sandy or muddy debrites (in a single location) therefore appear to be close to random. Bed correlations (chapter 3, Amy & Talling, 2006) show how the large majority of the thick (>40 cm sandstone) beds in the 100 m. thick interval between the Fiumicello, the

Contessa and the Colombine 1 marker beds contain muddy debrite intervals in various location, preferentially in the mid-distal part of the basin (Ridracoli, Isola, Pianetto and Rullato structural elements). Clean debrites are most common in the proximal sections of the Ridracoli element (chapter 3), but sometimes they are also present in the mid-distal part of the basin, both in the Ridracoli and in the Isola Elements.

The vertical and spatial distribution suggest that the depositon of clean and muddy debrite intervals in the relatively stable basin plain settings of the Marnoso Arenace Inner stage (Ricci Lucchi & Valmori, 1980; Ricci Lucchi, 1986; Cibin et al., 2004) may be a characteristic of these large unconfined flows, rather than mark periods of disequilibrium of the slope profile (Haughton, 2003) with substantial erosion of the muddy substrate or periods of enhanced erosion due to the onset of mass transport deposits (Muzzi Magalhes & Tinterri, 2010, Tinterri & Muzzi Magalhes, 2011), because such periods would result in a discernible vertical clustering of the deposits.

5.4.10 Implications for processes triggering submarine flows

Two main mechanisms are considered responsible of the initiation of large volume submarine sediment gravity flows: catastrophic sediment failure (possibly seismically triggered) transforming into debris flows and turbidity currents (see the review by Piper & Normark, 2009) and hyperpycnal flows, generated by direct fluvial discharge (Piper & Savoye, 1993; Mulder & Alexander, 2001; Plink Bjorklund & Steel, 2004). Other triggering mechanisms comprise oceanographic processes, such as re-suspension of shelf sediment by waves or tides (Wright et al., 2001). Outcrops of the Marnoso Arenacea Inner Stage only comprise beds deposited in a basin plain, and therefore a direct evidence of the relationships with slope and deltaic deposits is impossible. The most likely triggering mechanisms have to be inferred from the deposits. The frequency, vertical distribution and long-term clustering of turbidite and debrite beds described previously can provide significant insight on the processes responsible of the initiation of sediment density flows, together with the sedimentological characteristics of the deposits.

Evidence that larger flows are landslide triggered

Large volume event beds in the Marnoso Arenacea Formation are found to cover the entire outcrop area of approximately 120x40 km (Mutti, 1984; Ricci Lucchi, 1986; Amy & Talling, 2006). The volume of such beds, estimated by Talling et al. (2007a) is comprised between 0.7 and 7 km^3. These volumes (that don't comprise the sediment deposited outside the outcrop area) represent a mass comparable to the flux of sediments from all the rivers in the world to the oceans (Milliman & Syvitsky, 1992). Oceanographic process would imply a significant erosion of sediments (in the order of 10 km^3 of sediments) before entering the Marnoso Arenacea basin plain (Talling et al., 2007). At present, there is no evidence to indicate such dramatic erosion by turbidity currents generated by river floods or shelf re-suspension. It appears that turbidites within the Marnoso Arenacea Formation were generated by submarine slope failure, with remobilization of detritus from marginal repositories where large volumes of material could accumulate over sufficiently long recharge times (Mutti, 1984; Talling et al., 2007).

Time and size distribution of submarine landslides

The distribution of submarine landslide volume has been suggested to follow a power-law, in the case of debris avalanches off the north coast of Puerto Rico (ten Brink et al., 2006) or a lognormal distribution in the case of debris flows off the U.S. Atlantic coast (Chaytor et al.,2009). The distribution of bed volumes in the Marnoso Arenacea Formation is found to be approximately log normally distributed (Talling et al., 2007).This distribution lacks the large number of small volume beds predicted by a power-law model. However the small volume beds present are especially mud rich (mud represents more than the 75% of the total volume), and it may be hypothesized that sandier small beds didn't reach the outcrop area.

Not much is known about the frequency distribution of submarine landslides, mostly because of the lack of instrumental records of such events. When landslides have been dated in a given location, such as the Amazon Fan (Maslim and Mikkelsen., 1998) or the continental slope off South Eastern Canada (Piper et al., 2003), the limited number of events dated (usually less than 10) do not allow the recognition of any pattern in the returning time.

An exponential distribution of recurrence times has been used by Geist and Parsons (2010) to model the mean recurrence time of submarine landslides in locations where only a few slope failures have been dated. The results of this study confirms that an exponential time

distribution is appropriate for the frequency distribution of submarine slope failure that generated large turbidity currents such as in the Marnoso Arenacea Formation.

From the point of view of hazards from submarine landslides the exponential distribution of returning times imply that the probability that a landslide will occur in the future is independent of whether one has occurred in the past along the margins of the basin.

The technique adopted in this study may be useful, where a turbidite record directly related to landslides or other triggering events is available, to better understand the frequency of gravity flow generating events, and possibly help analyzing the risk of future highly destructive events.

Sea level variations

It is possible to compare the time and thickness distribution of gravity flow events obtained in this study to well known oxygen isotope data (Holbourn et al., 2007) for the late Miocene. Measurements of δ18O in benthic foraminifera are a proxy for ice volume, due to a preferential enrichment in sea water of heavier oxygen isotope (O^{18}) during glacial periods (Miller et al., 2005).

Variations in the $\delta^{18}O$ therefore provide information about climate conditions and global sea-level (Clark and Fritz, 1997). This comparison is shown in figure 5.9. At about 13.8 Ma a rapid increase in the $\delta^{18}O$ is evident. This event, known as Mi3b isotope shift (Miller, 1991) indicates an important cooling step (Abels et al., 2005)., and it has been correlated to the growth of ice sheets and a global sea level drop of about 40 to 50 m. (John et al., 2004; Westerhold et al., 2005). This major event (taking into account the uncertainties related to the biostratigraphic dating) appear to correlate well with the presence of a cluster of thicker, sandier, coarser grained beds in the studied section, as illustrated by figure 5.9.

Rapid sea level changes have been inferred to be the cause of large submarine landslides (Weaver and Kuijpers, 1983). A sea-level drop may have increased the frequency of large submarine landslides on the Marnoso Arenacea basin margins during this period causing a reduced hydrostatic pressure and possibly the presence of destabilized gas hydrate deposits on the basin margin (Haq, 1998; Maslin et al., 1998; Rothwell et al., 1998; Kennett et al., 2003). It can be noticed however how the total number of beds per unit of time in the Cabelli section does not change significantly during this period (figure 10). It appears that during the sea level drop flows became larger and coarser grained, but the overall frequency remained similar.

Alternatively the deposition of this thicker, coarser cluster can be related to a different sediment source in the growing Apennine chain (Apennine 2 input; Gandolfi et al., 1983).

A sea level drop could have caused the onset of smaller submarine fans with dispersal direction perpendicular to the main foredeep, producing an increase in thicker, sandier beds in the studied section. This scenario is considered here less likely for three reasons: (i) a small percentage of the sediment input related to Apenninic sources has been inferred by Gandolfi et al. (1983), based on provenance analysis of arenites, but no physical evidence of fans normal to the main foredeep has been documented in the Marnoso Arenacea Inner Stage. Also, beds with Apenninic 2 provenance are only reported in stratigraphic sections located South of the Cabelli section; (ii) the total number of beds per unit of time remain broadly consistent in this time period (figure 5.10). It is unlikely that the increased event frequency generated by an extra source was compensated by a diminution of the number of events from the main (North –North Western) source; (iii) the general paleocurrent direction does not vary significantly in this interval.

Earthquake frequency

Earthquakes are known to be one of the main triggers for large slope failures (Piper and Normark, 2009). Loading caused by strong seismic accelerations causes a buildup of pore pressures in sediments that at least partially supports the weight of the grains, decreasing the frictional resistance (Hampton et al., 1996). Some notable examples of submarine landslides induced by ground shaking include the Newfoundland Grand Banks earthquake in 1929 (Piper et al., 1999) and the 1964 earthquake in Port Valdez, Alaska (Coulter and Migliaccio, 1966).

Goldfinger et al. (2003) proposed that the turbidite record in a given location could be used as an indicator of paleoseismicity. This implies that a turbidite deposit can be directly correlated to a seismic event. As a consequence it may be hypothesized that the frequency of turbidite events would follow the time-distribution of large earthquakes.

No direct relationship exists between the magnitude of the earthquake and the volume of the slope failure, that depends largely on the availability of thick, widespread unconsolidated sediment prone to failure, even in case of slope failures directly triggered by seismic shock (Piper and Normark, 2009). For this reason a direct relationship between the magnitude-frequency distribution of large earthquakes, known to be power-law distributed (Gutenberg-Richter law; Gutenberg and Richter, 1954) and the volume distribution of submarine landslides (ten Brink et al., 2006) or turbidite deposits (Talling et al., 2007) cannot be established.

Although single turbidite deposits can sometimes be related to seismic events (Goldfinger et al., 2003), not all the main seismic shocks in a given region would produce sediment gravity flow deposits. This is confirmed by the magnitude 9.1 earthquake of Sumatra in the 2004, which produced very little evidence of resedimented deposits in the deep sea (Sumner, personal communication). Document time distribution of earthquakes (both globally and in a given location or margin) is a major scientific challenge, as it could give information about the predictability of the returning times of such large, destructive events. The distribution of returning time of large (usually above a certain magnitude, for example 7) earthquakes is a highly debated topic. The time between a main shock and the subsequent aftershocks is known to follow a power-law distribution, with rate of aftershocks decreasing rapidly with time. This relationship is known as Omori's law (Omori, 1894). However, it is only valid for short (in the order of a few days) periods after a main seismic shock. The time distribution of earthquakes over historical periods (ten to a hundred years) was originally thought to be related to a Poisson-type process (with time between events distributed according to an exponential law). In recent years, however, many authors proposed that even for large earthquakes the recurrence times are not independent (Back et al., 2002; Corral, 2006). The time distribution of large earthquakes in a given region is likely to have a memory (Livinia et al., 2005), or at least some degrees of clustering. These time-models however cannot be compared directly with the returning time distribution of turbidites in the Marnoso Arenacea Formation, because this study investigates a time period of about 1 million years, with a minimum resolution of about 65 years, corresponding to 1 cm of hemipelagite. Historical earthquakes databases records only a few hundred years, with a much higher resolution of many earthquakes per year.

Paleoseismic studies potentially spans over longer time periods (10^3 to 10^4 years) but suffer from severe problems of incompleteness of the catalogue (only certain earthquakes are reported), and therefore can't be directly compared with this study, that reports the estimated frequency of each turbidite large enough to reach the studied section.

5.5. CONCLUSIONS

The 530 meters thick Cabelli Section is located in the mid-distal part of the Marnoso Arenacea Basin, and comprises 696 event beds. In the relatively simple basin plain settings of the Marnoso Arenacea Formation the vertical thickness distribution of turbidite and debrite beds can be considered equivalent to random sampling of a smaller number of beds in different locations. The external bed shape and pinch-out geometry is found to be a major control on

the vertical thickness distribution of the deposits. Because beds with similar volume can have different facies architecture and geometry (chapter 4), we conclude that the distribution of the volume of flow-initiating events is unlikely to be directly related to the bed thickness distribution in a given location. Also, the rapid pinch-out geometry of clean sand debrites and clast-rich muddy debrite explains their thickness distribution in a single location, and why intervals <20 cm are rare.

Low-density (Tcd-e) and high density (Tab-cd-e) turbidites, clean and muddy debrite describe different lognormal populations, the convolution of which results in the observed bed thickness distribution. The sandstone division of each of the two populations is the combination of log-normally distributed intervals characterized by specific grain size classes and sedimentary structures (including clean and muddy debrite intervals).

The Hurst test reveals a long-term clustering in the 600 meters stratigraphic interval that was studied. This clustering can be attributed to lateral migration of the depocenters. However, a stratigraphic interval characterized by increased bed thickness and grain size can be positively correlated to a globally recognized isotopic cooling step, which possibly caused a marked sea level drop. This indicates that that a variation of the global sea-level favored the onset of larger volume flows in the Marnoso Arenacea basin.

Amy and Talling (2006), and Talling et al. (2007a; 2007b; 20012c) and the results shown in chapter 3 demonstrated that two types of muddy debrite deposits can be recognized in the Marnoso Arenacea Formation: clast-rich muddy debrite that show a rapid pinch-out geometry and clast-poor muddy debrite with a more gradual tapering shape. We showed that, in a single vertical section, it is possible to distinguish the two types of muddy debrite based on the ratio between the turbidite and debrite components and the size of the mudstone clasts. This finding may prove useful in subsurface studies, where the external shape and pinch-out geometry of muddy debrite intervals is not available.

The Hurst test and the analysis of the time distribution of beds containing muddy debrite intervals showed that such intervals occur randomly in the whole 600 m stratigraphic section. Their deposition is most likely a characteristic of large, mud-rich unconfined flows, rather than mark periods of disequilibrium of the slope profile (Haughton, 2003) with substantial erosion of the muddy substrate, or periods of enhanced erosion due to the onset of mass transport deposits (Muzzi Magalhes & Tinterri, 2010, Tinterri & Muzzi Magalhes, 2011), because such periods would result in a discernible vertical clustering of the deposits. Clustering of clean debrite intervals is related to a general increase in the number of thick beds, and does not show any obvious vertical pattern.

Nannofossils biostratigraphy indicates that a 360 meters thick interval of the Cabelli section was deposited between 13.5 Ma and 14.1 Ma before present. Beds in this section were deposited on average every 1.400 years. Thick beds occur every 5.300 years, and beds comprising debrite intervals every 10.700 years.

Event beds are constantly separated by interval of hemipelagite, deposited through slow settling from the water column. Turbidite mudstone can be distinguished from background hemipelagite mudstone based on the color, texture and fossil content. Flows caused little or no substrate erosion. For this reason the hemipelagic sediment deposited between turbidite beds is used as an indicator of the time that separates flow events, assuming a constant background sedimentation rate. The distribution of time between events is exponential, therefore related to a Poisson Process. A fundamental characteristic of the Poisson Process is the lack-of-memory property. This ensures that flow events are independent one from the other. The system has no memory, so that each event in the past does not contain any information that can predict the likelihood of events occurring in the future. The 'lack of memory' property of the exponential distribution of returning time between events can provide insights into the tempo and triggers of processes that initiated submarine sediment density flows that entered this ancient basin plain. It is likely that submarine slope failures (landslides) triggered the larger volume flows in this basin, as individual bed volumes can exceed the annual sediment supply from all of the world's rivers. The technique adopted in this study may be useful, where a turbidite record directly related to landslides or other triggering events is available, to better understand the frequency of gravity flow generating events, and possibly help analyzing the risk of future highly destructive events.

CHAPTER 6:
DISTAL PINCH-OUT OF SANDSTONE LOBES: KAROO BASIN, SOUTH AFRICA

6.1 INTRODUCTION AND AIMS

Previous data obtained in the Marnoso-Arenacea Formation demonstrate how sandstone beds showing characteristics of en-masse deposition pinch-out relatively more abruptly than beds deposited in a layer-by-layer fashion by turbidity currents. However this rapid pinch-out has never been directly observed, because of the structural settings of the Marnoso Arenacea basin that doesn't allow beds to be walked-out for more than some hundred meters.

One of the best outcrop examples to directly observe the distal pinch-out of sandstone beds is the Upper Permian Skoorsteenberg Formation, exposed in the Tanqua depocenter, South-West Karoo Basin, South Africa. The Skoorsteenberg Formation represents a sand-rich submarine fan systems (Bouma and Wickens 1991; Wickens and Bouma 2000; Johnson et al. 2001; Wild et al. 2005; Hodgson et al. 2006) that form the lower part of a progradational basin-fill succession. Here, the exceptionally good exposure of the distal pinch-out of sandstone lobes allows a detailed study of the architecture and facies characteristics of the sandstone layers approaching their distal termination.

Bouma and Rozman (2000) and Van der Werff and Johnson (2003) discussed the pinch-out geometry of Fan 3, 4 and 5, and their relation to the whole fan architecture. This study will use a detailed analysis of the pinch out geometry, obtained through detailed correlation of closely spaced (10's of meters) stratigraphic sections coupled with a facies and textural characterization of the deposits, to re-interpret the depositional mechanisms of the flows that deposited massive sandstone beds that pinch-out abruptly at the frontal termination of Fan 4.

The main questions to be addressed in this study are: what is the geometry of the distal termination of Fan 4? Is the rapid pinch-out of massive sandstone beds due to pre-existing topography or to purely depositional processes? Are the sandstone layers that pinch-out abruptly deposited by turbidity currents or liquefied debris flows?

6.2 GEOLOGICAL SETTINGS

The Tanqua Karoo deep-water fan complex is situated in the South-Western part of the Karoo Basin in South Africa (figure 6.1). It forms the basal part of the more than 1-km thick Permian-Triassic foreland basin succession defined as the Karoo Supergroup (figure 2; van der Werff and Johnson, 2003). The Karoo Supergroup represent the sedimentary filling of one of the Late Paleozoic to Mesozoic foreland basins of the southern margin of Gondwana, developed in response to convergent-margin tectonics (De Wit and Ransome, 1992), and includes the Dwika Group (glacigenic deposits), the Ecca Group (siliciclastic marine) and the Beaufort Group (fluvial deposits). The Lower Ecca Group comprises the Prince Albert Formation (cherty shale beds), the Whitehill Formation (black, carbonaceous mudstones with pelagic organisms) and the Collingham Formation (fine-grained turbidites and intercalated ashes). The Upper Ecca Group comprises an approximately 1400 m succession of siliciclastic deposits (figure 2), and includes the Tierberg Formation (dark basinal mudstone), the Skoorsteenberg Formation (fine-grained, sand-rich, submarine- fan systems), the Kookfontein Formation (slope and shelf-edge deltaic sediments) and the Waterford Formation (Bouma and Wickens 1991; Wickens 1994), which mark the overall progradation of the sedimentary system to the north and east (Wild et al. 2005; Hodgson et al. 2006).

The Skoorsteenberg Formation is Late Permian in age (~255 Ma, Fildani et al., 2007) and comprises over 400 m of sediments. It consists of four sandstone-rich bodies interpreted as basin-floor fans (Fans 1 to 4; Wickens & Bouma, 2000) and a top unit representing base-of-the-slope settings (Unit 5; Wild et al., 2005; Hodgson et al., 2006). The grain size range of these submarine fans deposit is narrow (mudstone to fine grained sandstone), and the bulk of the sediment volume in individual submarine fan elements only comprise very fine and fine sandstone (Hodgson et al., 2006). A pattern of fan growth (initiation and basinward movement of the fan fringe), aggradation and fan retreat (landward movement of the fan fringe) has been documented for each basin floor fan; each fan is interpreted to represent the lowstand system tract of a sequence (Hodgson et al., 2006).

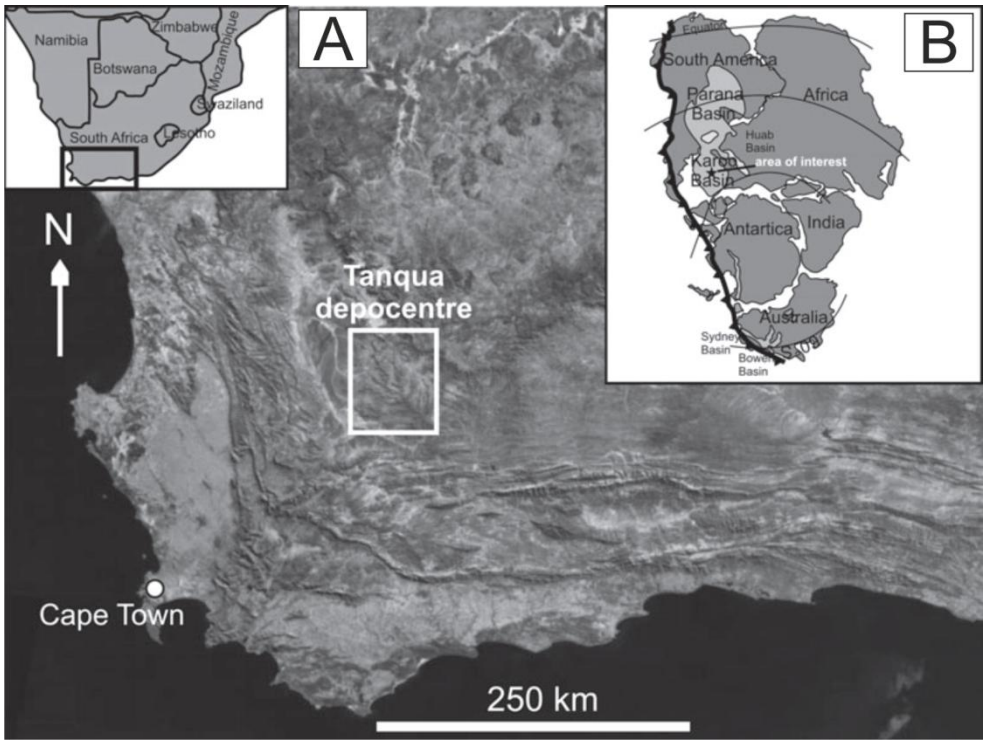

Figure 6.1. *(A) Satellite image of the field area showing the location of the Tanqua depocenter. (B) Generalized and simplified Permian palaeogeographic map of Gondwana (after Faure & Cole, 1999). From Prelàt et al. (2009).*

6.1.2 Fan 4

This study is focused on the distal termination of Fan 4 deposits, in the Kajtjesberg area (figure 6.3a). The overall fan succession has been divided into 12 sand-prone units, with the basal 3 units interpreted as the outcrop expression of the lower division of the fan recognized in core (Hodgson et al.2006). The maximum thickness of the upper division of Fan 4 is 65 meters (figure6.4b; Johnson et al., 2001), and the lower division (not present in the study area) has a maximum thickness of more than 20 meters (Hodgson et al., 2006).

The large-scale paleocurrent patterns, and the distribution of lithofacies, channel-form architecture and fan thickness (figure 6.4) , suggests a major input point for both the upper and lower divisions of Fan 4 at the southwestern basin margin (Hodgson et al., 2006). The general paleocurrent direction is to the East and to the North east (figure6. 4a).

Paleocurrent readings from the lower division of Fan 4 at outcrop and from well logs indicate north to northeast flow directions (Hodgson et al., 2006). In the upper division of the fan, a 90°

switch to a dominant South-East paleocurrent direction has been observed (Johnson et al., 2001). Hodgson et al. (2006) interpret this change in paleocurrent readings in the northern outcrops to be the result of the presence of seabed topography to the north of the outcrop belt, Alternatively, a situation where sediment was transported from the same source area northwards along the shelf and fed down the western margin during deposition of the upper division, without a major change in the input point.

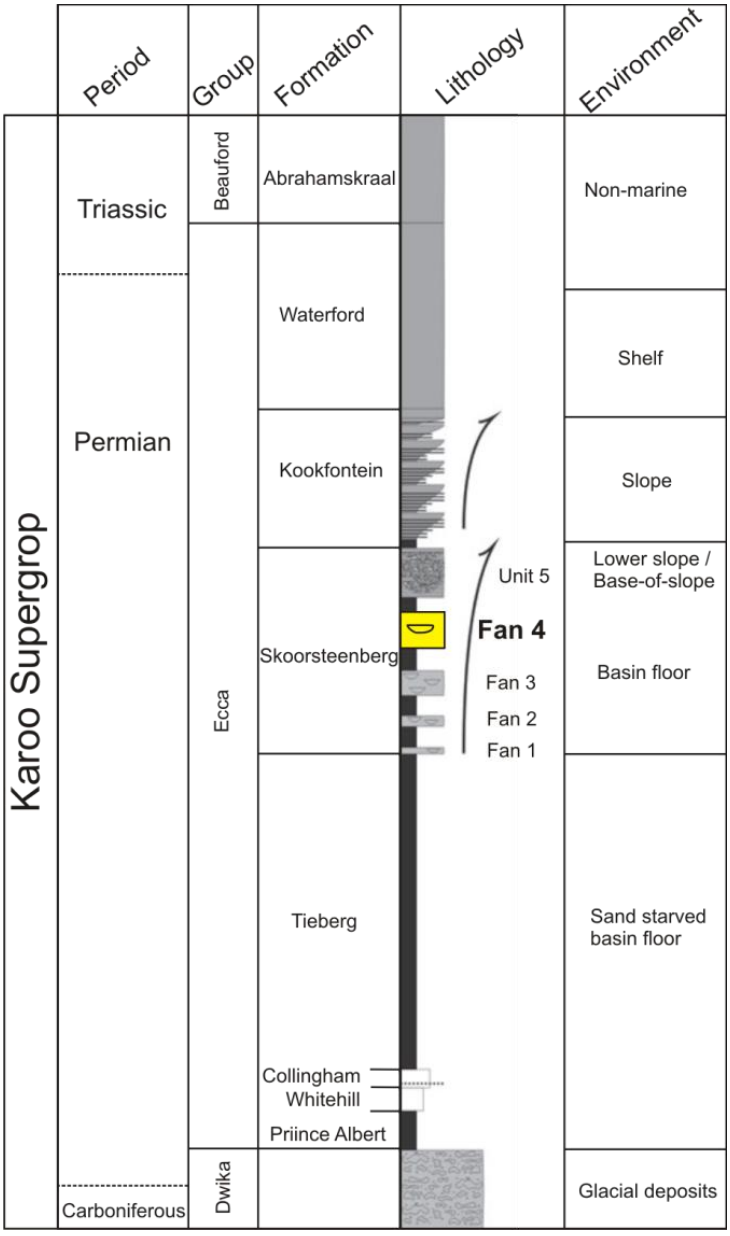

Figure 6.2. *Simplified representative stratigraphic column of the Karoo Supergrop. Thicknesses for formations were obtained from Visser(1993), Faure & Cole (1999), Grecula et al. (2003), Hodgson et al. (2006) and Sixsmith et al. (2004).The position of Fan 4 is indicated. Modified from Prelàt et al. (2009).*

6.2 MATERIALS AND METHODS

6.2.1 Sedimentary logging

Sections were logged from the stratigraphic base of Fan 4, represented by the first thin bedded sandstone bed above the intrafan 3 mudstone to the base of the intrafan 4 mudstone dividing Fan 4 from Unit 5 (figure 6.3c). Sections were logged at a scale of 1:10, and grain size was estimated in the field using a grain-size comparator. Where possible, palaeocurrent directions were measured using flutes and grooves on the base of thick sandstone beds.

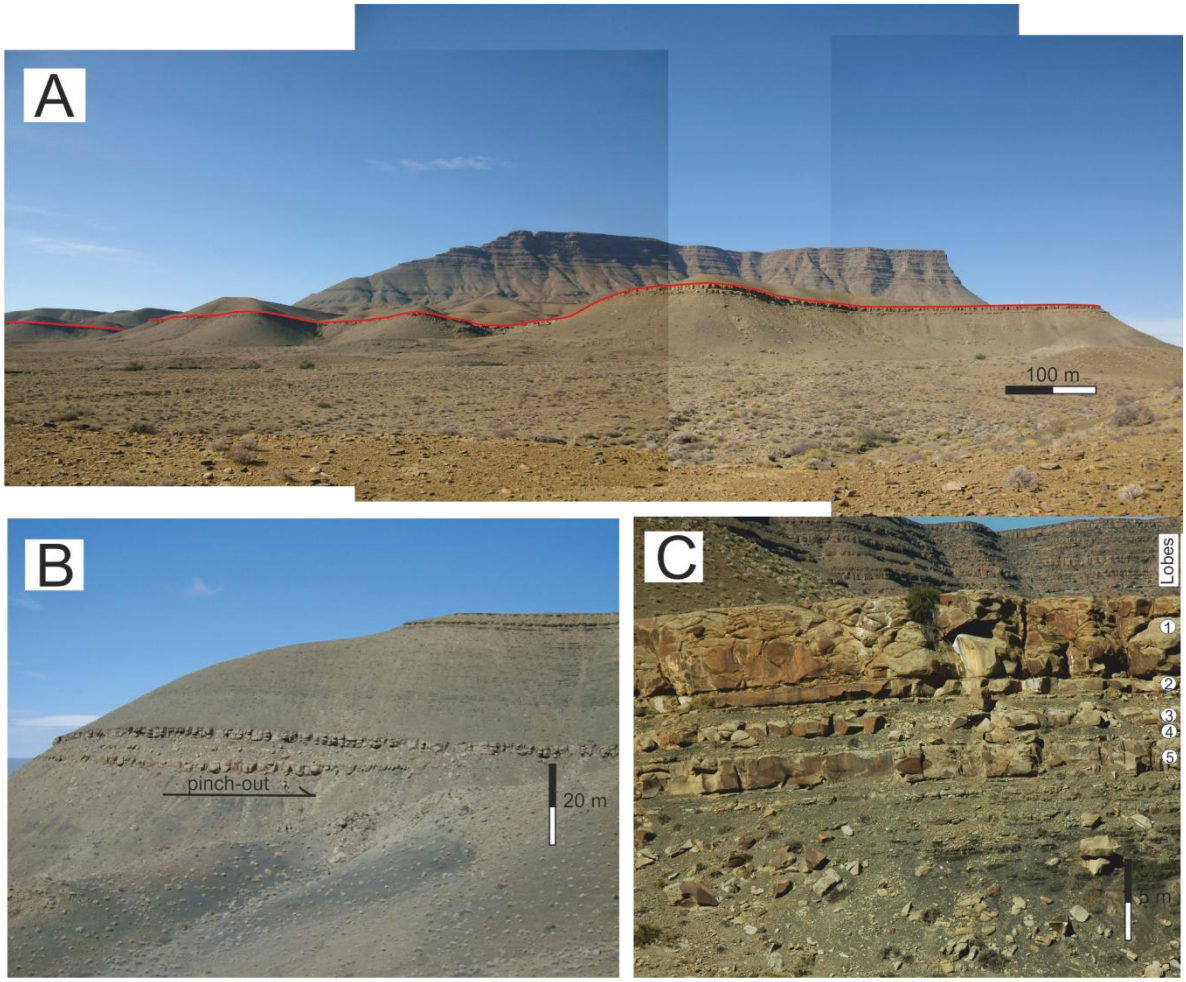

Figure 6.3. *Outcrop photographs of the Katjesberg outcrop. A) Panoramic view of the north face of the Katjesberg outcrop. The red line indicates the top surface of Fan 4. B) Rapid pinch-out of a sandstone lobe. C) Photograph of Fan 4 deposits in section 14. The base and top of the fan are indicated.*

6.2.2 Bed correlations

The main stratigraphic surfaces have been correlated by direct walk-out. Beds have been correlated by empirical pattern matching of vertical bed sequences where a direct correlation was not possible because of a less than perfect exposure. Such indirect correlations are indicated in the panels with a dotted line (figure 6.6 and 6.7).

Two cross sections are presented. The first cross section is oriented oblique to strike, in a East to West direction. It comprises twelve sedimentary logs (14 to 6 meters thick; log 1 to 12) and spans over 1200 meters (figure 6.6). The second cross section (figure 6.7) comprises ten sedimentary logs (11 to 7 meters thick).It is positioned around a gully (figure 6.5), allowing the 3D geometry of lobes pinch-out to be documented over about 250 meters; correlation of section 13 to 18 is oriented in a direction approximately parallel to the paleocurrent (South-Southwest to North-Northeast).

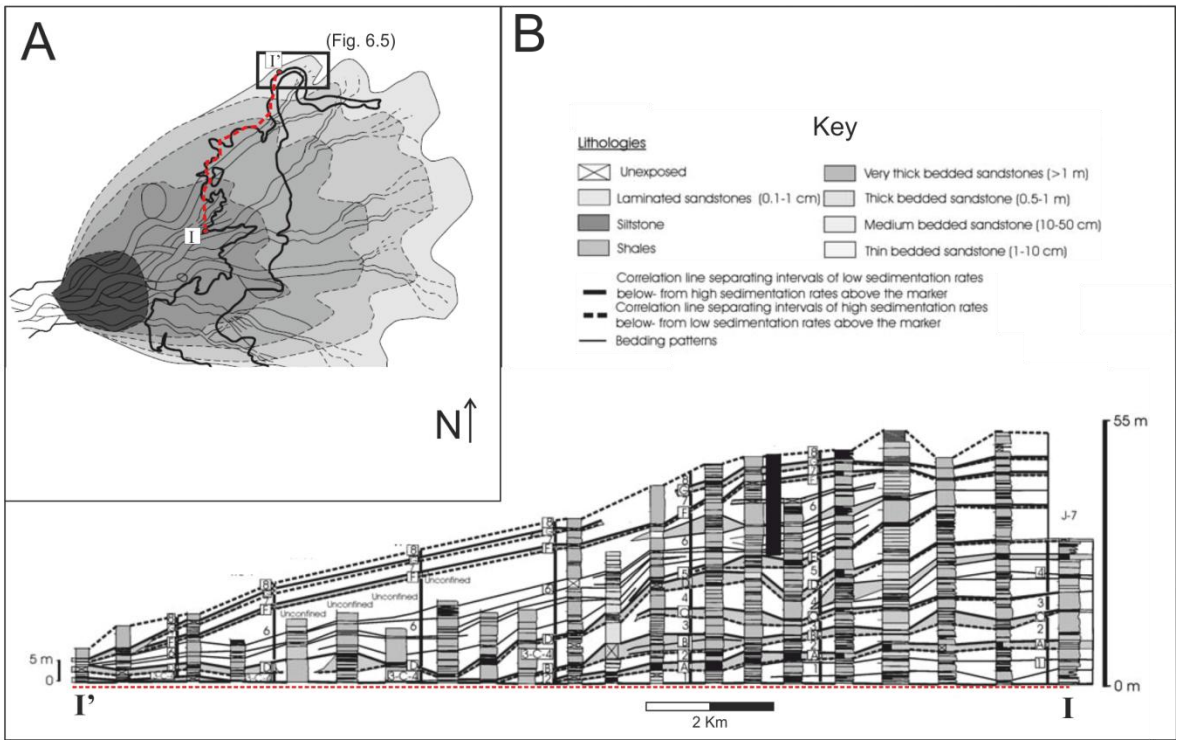

Figure 6.4. *Stratigraphy and paleogeography of fan 4. A) Diagram illustrating the window of observation afforded by the outcrop orientation, compared with the interpreted architecture of fan 4 at the time of deposition. The outcrop area analyzed in this study is indicated. Note the direction of distributaries channels in the outcrop area, indicating a North-East paleocurrent direction. Modified from Johnson et al. (2001). B) Oblique strike-oriented log correlation across the middle–outer fan of fan 4 (length 26.5 km). Modified from Van der Werff and Johnson (2003).*

6.2.3 Textural analysis

Samples were taken to provide information about the textural characteristics of the deposits. A total of 6 samples were collected from bed 5 in three different sections (figure 6.7) in order to highlight the vertical and lateral variation in the grain size profile and sorting. For each sample the grain size was quantified using images from a scanning electron microscope (SEM) in backscatter mode (figure 6.8). Three images with 150 times magnification were taken for each thin section. The longest axis of 100 grains coarser than 20 um were measured each photo using image analysis software. Grain size data derived in this way from two dimensional slices through grains differ from the longest axis of grains (Johnson, 1994) but this technique provides a consistent method for documenting relative changes in grain size vertically through a bed (Talling et al., 2004).

The original mud-matrix content was not quantified, because of the low quality of SEM images obtained, due to the high degree of sample alteration. SEM images however clearly show that bed 5 deposits contain a relatively low mud matrix (grains finer than 20 um) percentage, and they can be described as clean sandstone following the classification adopted in chapter 3 for the Marnoso Arenacea Formation deposits.

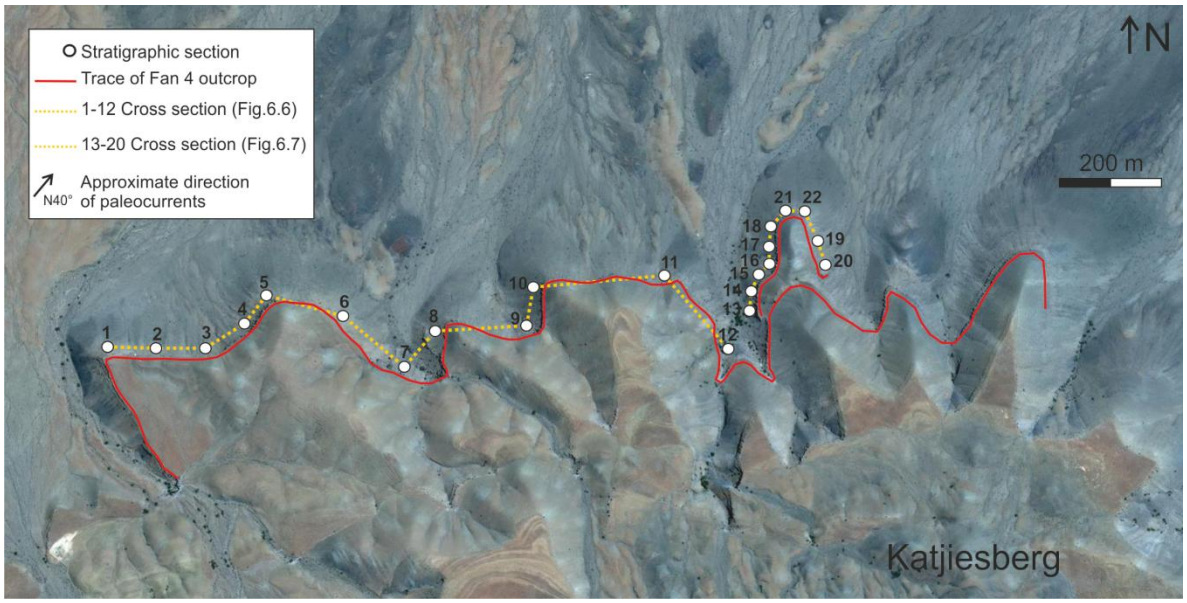

Figure 6.5. *Map view of the northern face of the Katjesberg outcrop, with the position of logged sections. The red line indicates the top surface of Fan 4.Image from Google Earth.*

6.3 RESULTS

6.3.1 Lithofacies and textural analysis

Thick-bedded clean sandstone

Thick (>40 cm) sandstone beds are typically structureless, with the exception of dish and pillar structures, and visually ungraded, with the bed top divisions possibly normally graded from fine to very fine sandstone and faint planar or ripple lamination (figure 6.9a). The vertical grading into planar or cross laminated clean sandstone generally occur without an intervening grain size break, although the recognition of subtle variations may be difficult. A mudstone cap is generally absent. Very thick beds (>1m) commonly show evidence of amalgamation, highlighted by subtle grain-size breaks, intervals of (often convolute) laminae, truncation of dewatering features (pipes and dishes), or thin discontinuous layers of small (< 2 cm diameter) mudstone clasts (figure 6.9b). Such amalgamation is however not always easily recognizable in the field using hand lens and a grain size comparator, possibly because of the narrow range of grain sizes present. Bed bases are sharp, erosive or loaded, with common tool marks. Flutes and linear groove marks occur at the base of very thick (>1m) beds, while thick (40 – 100 cm) sandstone intervals show a flat base, with evidence of trace fossils (figure 6.9e). The origin and depositional mechanism(s) of this lithofacies will be discussed in a later section.

Thin bedded clean sandstone and coarse siltstone

Thin (1 - 40 cm) mud-poor sandstone and coarse siltstone intervals are generally normally graded, fine-parallel or ripple laminated, although structureless divisions are common at the base of some beds (figure 6.9d).

Thin beds generally grade from very fine sandstone at the base to medium-fine silt at the top. They form in cases thickening upward packages constituted by three to ten event-beds. Such packages are laterally continuous for 10’s to 100’s of meters in the outcrop area. The lateral correlation of such packages eventually leads either to the complete pinch-out of each bed or to the amalgamation of the sandstone intervals.

Heterolitic sandstones and siltstones

Thin (<1cm) very fine sandstone to coarse siltstone beds are commonly interbedded with medium to fine siltstone to form heterolithic packages (figure 6.9d). Individual beds are usually rippled or planar laminated although massive intervals are sometimes present. Vertical grading is difficult to recognize, due to the very limited thickness of individual beds.

Hybrid beds

Hybrid beds, bipartite with a basal clean sandstone division and an upper mud-rich sandstone division, have been recognized previously in the Tanqua Karoo basin by Johnson et al. (2001), Luthi (2006), Hodgson et al. (2006) and Hodgson (2009). Hodgson (2009) described 3 different hybrid bed types, named lithofacies D1 (hybrid beds with upper carbonaceous division), D2 (hybrid beds with upper mudstone clast-rich division) and D3 (hybrid beds with upper rounded clast division). In the study area hybrid beds are only found at the base of section 1 and 2, in the western part of the outcrop area. Beds are characterized by a basal massive ungraded clean sandstone division, overlie by a poorly sorted mud rich sandstone division, with dispersed small (<2cm) mudstone clast (figure 6.9c). Following Hodgson (2009) these beds belong to the D2 lithofacies, and can be interpreted to comprise a turbidite with an overlying linked debrite.

Mudstone

A single interval of pure mudstone is present at the base of the Fan 4 exposure. The base of this mudstone interval is not exposed in outcrop, and the top corresponds to the first sandstone bed recognizable in outcrop. Previous studies (Johnson et al., 2001) indicate the thickness of this interval that separates Fan 3 from Fan 4 deposits, to be variable, thinning from South to North. This fine interval (claystone to fine siltstone) appears to be generally massive and structureless, although a good exposure is rare (figure 6.3c).

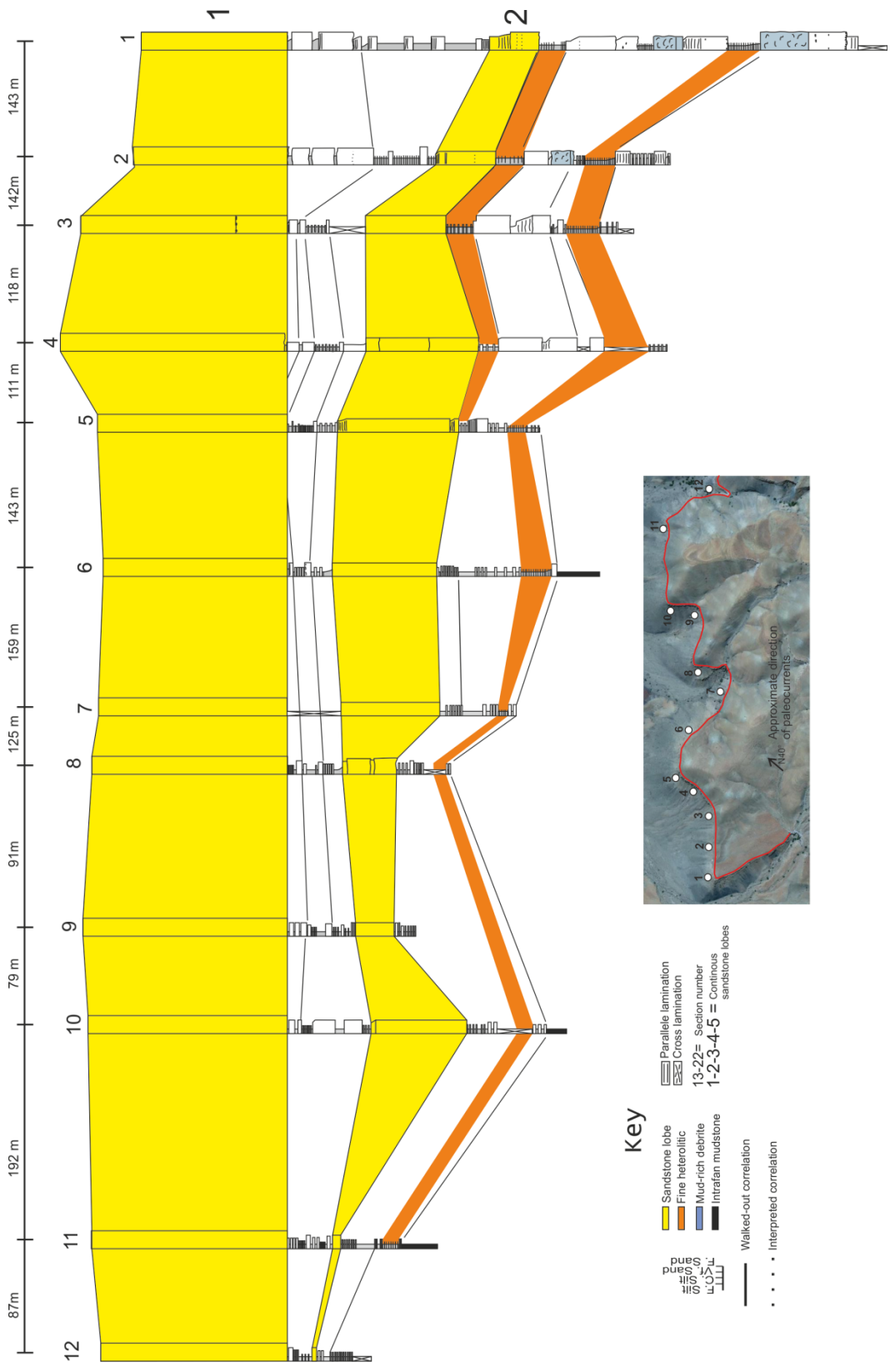

Figure 6.6. *Across stike cross section. The position of the logged stratigraphic sections is indicated*

6.3.2 Bed correlations

Strike-oriented cross section

The architecture of a strike-oriented cross section near the distal pinch-out of Fan 4 at Katjesberg is presented in figure 6.6. Twelve correlated sections are spaced on average 100 meters.

Although only few paleocurrent indicators are available, because of the lack of flute marks at the base of sandstone beds and the lack of good exposure of ripple crests, the paleocurrent directions are in good agreement with the results obtained by Johnson et al. (2001) and Van der Werff and Johnson (2003) considering the general geometry of the fan and the direction of the "pinch-out" channels recognized towards the North-East (Johnson et al., 2001; figure 6.4a). The cross section therefore is oriented slightly oblique-to-strike. The overall Fan succession in this cross section show a rapid thinning from East to West, with the exception of the upper amalgamated sandstone interval (informally termed lobe 1) that maintains a more constant thickness.

Sandstone lobes

A direct walk-out of the major stratigraphic surfaces (base and top of large sandstone units, such as lobe 1 and lobe 5) reveals a widespread amalgamation of single event beds into thicker sandstone units. The lateral continuity of individual beds, representing single flow events, is here limited to few tens of meters; with few exceptions it is impossible to correlate a single bed between more than 2 sections.

Two main lobes, formed by multiple beds, are continuous over the outcrop area. The first lobe (lobe 1) is formed by 4 or more event-beds, and has a thickness comprised between 4 and 5.5 meters. It constitutes the top sandstone interval of the fan, and it is directly overlie by the mudstone constituting the intrafan between Fan 4 and Unit 5 (Hodgson et al., 2006).

Three thick (>40 cm) sandstone beds are present directly underneath Lobe 1 in the thicker stratigraphic sections (section 1, 2 and 10). These beds partially amalgamate into lobe 1 between section 2 and 3, as confirmed by the increased thickness (550 cm) of the lobe in these sections.

The second lobe continuous over the outcrop area (lobe 2) shows a larger thickness variability, between 250 cm and 20 cm. The lobe is formed by the lateral amalgamation of 1 to 4 (or more) beds.

Other amalgamated sandstone beds are recognized only in the first 5 sections, and show a rapid facies change to thin bedded (1 to 40 cm) massive and laminated sandstones, interbedded with coarse siltstone beds. This lateral facies change corresponds to an overall thinning of the fan succession and a general decrease of the number of beds towards the West. The lateral continuity of individual beds, representing single flow events, is here limited to few tens of meters.

Heterolithic packages

Heterolithic packages of thin and very thin beds are generally more continuous, showing limited thickness variability for 100's of meters, between 3 or more sections. One heterolithic package, directly above the base of the fan, is continuous over the outcrop area, showing only very limited thickness changes. The correlation of individual thin beds is however difficult, possibly due to the less than perfect exposure conditions in places.

Hybrid beds

Hybrid beds are only present at the base of the fan in section 1 and 2. Lateral correlation of those beds reveals either an abrupt pinch-out of the muddy sandstone interval or a facies change to massive or parallel laminated clean sandstone intervals.

Dip-oriented cross section

An exceptional continuous exposure allowed the correlation of individual beds on a three dimensional outcrop around a gully (figure 6.7). The cross section is oriented parallel-to dip between section 13 and 18, allowing the detailed description of the rapid pinch-out of sandstone lobes. Single beds are correlated by direct walk-out between closely spaced (40 meters on average) stratigraphic sections.

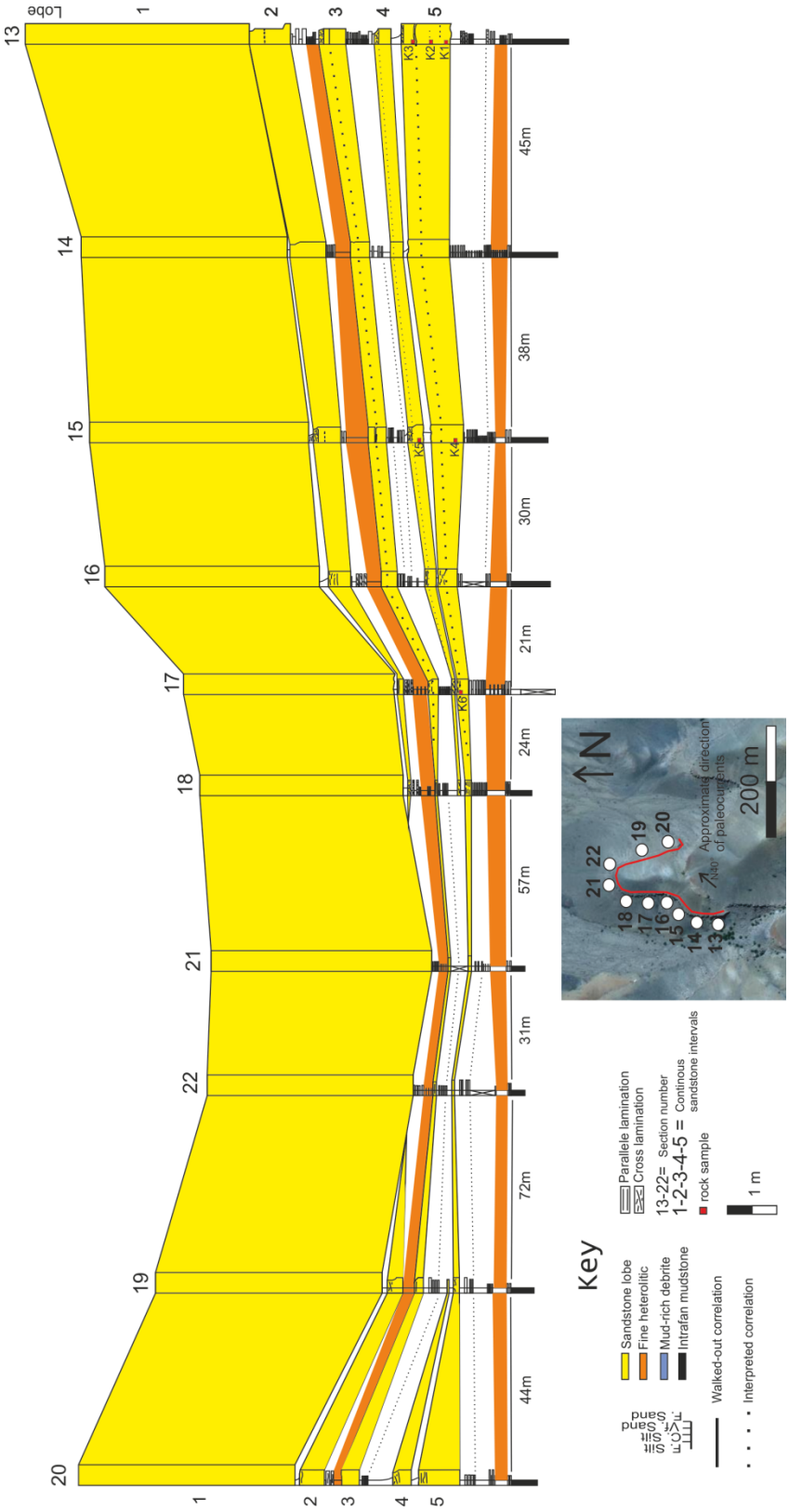

Figure 6.7. *Parallel to Dip cross section. The position of the logged stratigraphic sections is indicated.*

Sandstone lobes

Five thick (>40 cm) sandstone units have been recognized. The top amalgamated unit (lobe 1) maintains an overall constant thickness of about 450 cm and has a locally erosive base.

Lobe 2 is here formed by a single event bed, with a massive ungraded base and a normally graded, ripple laminated top interval. The base of the bed is flat, with evidence of trace fossils (figure 6.9e). The bed is partially amalgamated into lobe 1 in section 13, and is completely eroded by the same lobe between section 21 and 22. The basal massive interval shows a rapid pinch-out from 1 m in section 13 to a few cm in section 17 and between section 20 and 19.

Lobe 3 is formed by 2 individual event beds, as indicated by the amalgamation surface evident in section 13 and 15. Both beds pinch-out rapidly between section 13 and 18 and between section 20 and 19, leaving only a thin (<5 cm) coarse siltstone, cross laminated interval.

Lobe 4 is an individual event bed, with a basal massive ungraded interval and a top ripple laminated interval. The massive base pinch-out abruptly between section 13 and 17, and between section 20 and 19. The top ripple laminated interval has a more constant thickness, although in section 21 and 21 it's not possible to distinguish it from the surrounding fine heterolithics.

Lobe 5 is apparently composed by 2 amalgamated beds. This amalgamation is evident in section 13, indicated by a surface truncating an interval of parallel laminated sandstone (figure 6.8). This amalgamation surface is not directly observed in the other sections, possibly because of the homogeneus vertical grain size profile and the lack of laminated interval indicating the amalgamation surface. The base of the bed is flat, with evidence of trace fossils.

The massive interval pinches-out abruptly between section 13 and 17, and between section 20 and 19. A top cross laminated interval is observed in all the sections but section 14 and 15, possibly because of less than perfect exposure.

Samples were taken in section 13 and 17. The grain size analysis performed on the SEM images obtained confirm the lack of vertical grading in the basal event bed in section 13, although a larger number of sample would be needed to confirm this finding. The sample collected in section 17, situated in the cross laminated top interval of the event bed, indicates a rapid lateral fining of the sandstone deposit.

Heterolithic packages

Two continuous heterolithic packages have been correlated in the cross section. The first package is observed directly above lobe 3. It has a thickness of 25 to 30 cm where a perfect exposure allows the upper limit, corresponding to a 5 cm thick cross laminated sandstone bed, to be observed. In section 18, 21 and 22 the pinch-out of lobe 3 sandstone makes the recognition of the lower limit of the heterolithic package difficult. It consists of a variable number of very thin very fine sandstone, medium siltstone and fine siltstone interbedded layers.

The second heterolithic package is 30 to 40 cm thick, and lies directly above 2 thin cross laminated coarse siltstone beds that marks the first deposits of Fan 4 above the intrafan mudstone. It consists of a large number of very thin medium siltstone and fine siltstone interbedded layers. This package maintains an almost constant thickness across the whole outcrop area, observed also in the across-strike cross section (figure 6.7).

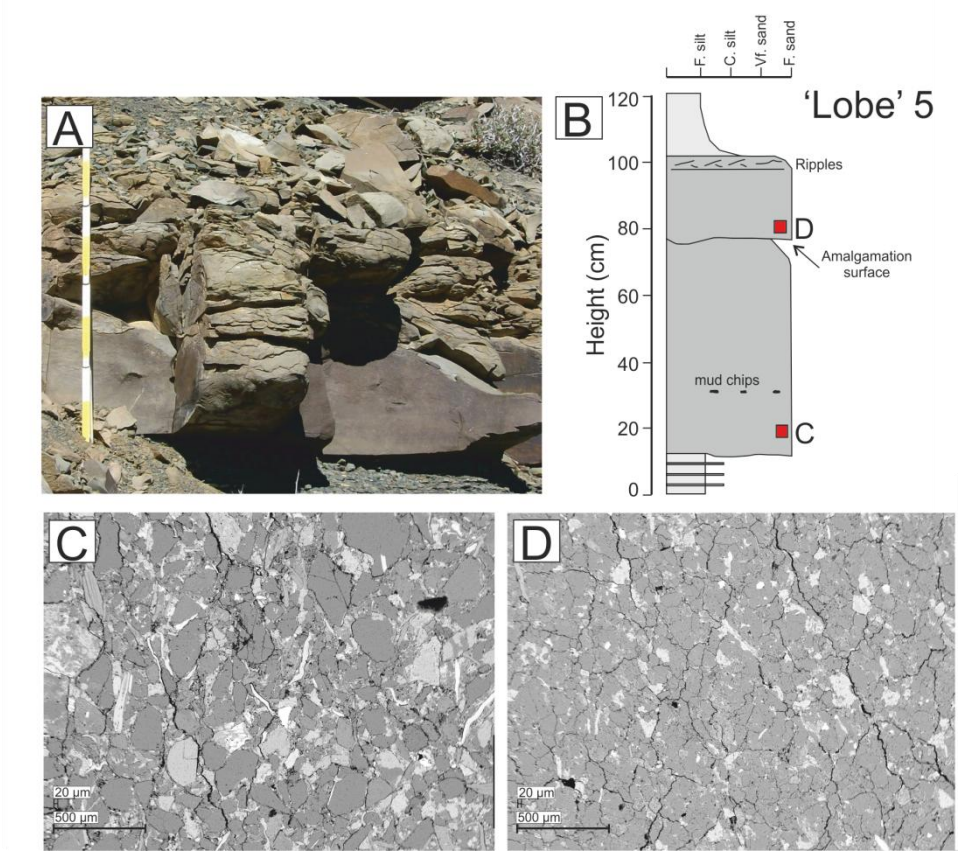

Figure 6.8. *Lobe 5 in section 13. A) Outcrop photograph.B) Graphic log. The position of rock sample taken is indicated. C,D) S.E.M images in backscattered mode of massive sandstone deposits. The magnification is 150x.*

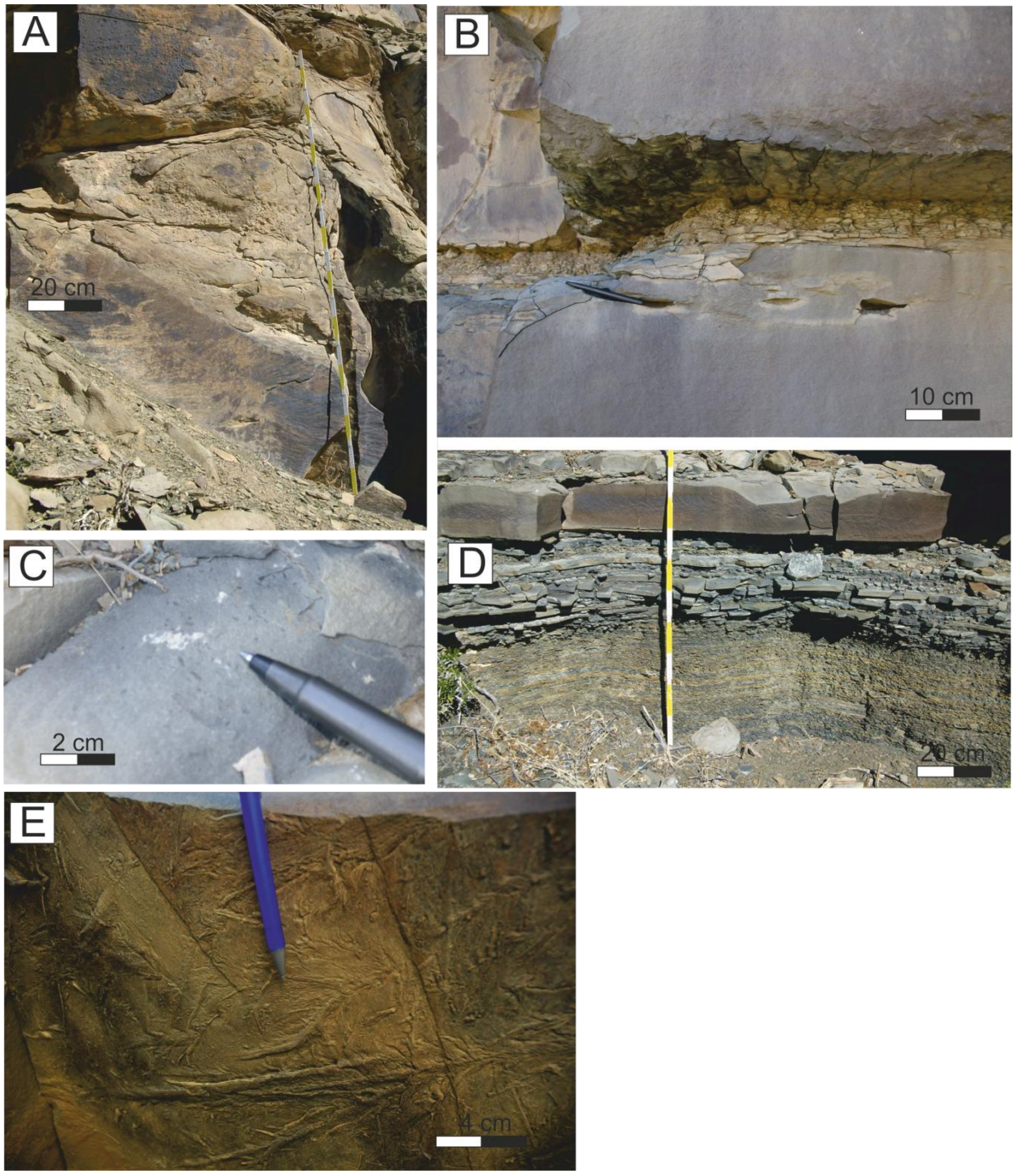

Figure 6.9. *Outcrop photographs of the different lithofacies described. A) Thick amalgamated sandstone lobe (lobe 1). Note the laminated interval suggesting an amalgamation surface. Image from section 2.B) Two massive sandstone lobes separated by a finer siltstone interval. Note the loaded base of the top unit and the aligned mudstone chips in the second lobe, possibly suggesting an amalgamation surface. Image from section 14.C) Detail of small mudstone chips in a hybrid bed. Image from section 1.D) Fine heterolithics overlaid by thin bedded very fine sandstone and coarse siltstone beds. E) Base of lobe 2 in section 14. Note the trace fossils and the absence of flutes or grooves.*

6.4 DISCUSSION

6.4.1 Origin of the abrupt pinch out of clean sandstone lobes

Where individual beds can be recognized (lobe 2 and 4) or safely followed into amalgamated lobes (lobe 3 and 5), a bipartite structure is evident. The basal, massive and ungraded sandstone interval, characterized by a flat base with no evidence of flutes and grooves, pinch-out extremely rapidly down dip. The textural analysis of lobe 5 also indicates that the rapid pinch out is related to an equally rapid fining of the deposit. On the other hand the top, normally graded ripple laminated interval maintain an almost tabular geometry (lobe 2 and 4), although thickening is observed in lobe 5 where the massive base completely pinch-out.

Liquefied debris flows deposits in the Marnoso Arenacea Formation

As described in chapter 3 for the deposits of the Marnoso Arenacea Formation, the rapid pinch-out of sandstone layers may be an indication of en-masse deposition by a liquefied debris flow. The characteristics of the deposits of liquefied debris flows (subfacies Cs7, chapter 3) observed in the Marnoso Arenacea Formation are:

- An irregular vertical grading. This feature implies that the deposition occurred without effective segregation of larger and smaller particles.
- A swirly, patchy texture, with dispersed mudstone clasts. The particular swirly, patchy texture differs from dish and pillar structures identified in turbidite sandstones (Lowe and Lo Piccolo, 1974) and is inferred to be produced by convection during static settling of a high concentration partly-liquefied suspension (Kuenen, 1965; his fig. 1 and 2; Talling et al., 2012b).
- A sharp grain-size break with the overlying cross laminated sandstone interval. This is most likely a distinct interface between the basal, relatively high concentrated flow phase and the overlying more dilute phase (as described for bipartite flow in Mutti et al, 2003).
- A mud matrix content similar to the one observed in sandstone layers deposited in a layer-by-layer fashion by turbidity currents. This relatively low mud content differentiates mud-rich debrites from clean sandstone debrites.

- A rapid pinch-out geometry if compared with turbidite deposits (figure 6.10, 6.11). Clean debrite beds in the Marnoso Arenacea formation completely pinch-out over few km, although the pinch-out has never been directly observed and could be more rapid. After the pinch out only a thin, cross laminated sandstone layer is observed (figure 6.7). On the contrary, beds deposited by turbidite have a gradually tapering shape. This abrupt pinch out suggests that the clean sand layers were deposited by dense debris flow, as similarly abrupt pinch out characterizes debris flow deposits on land and in laboratory experiments (Johnson, 1970; Major and Iverson, 1999).

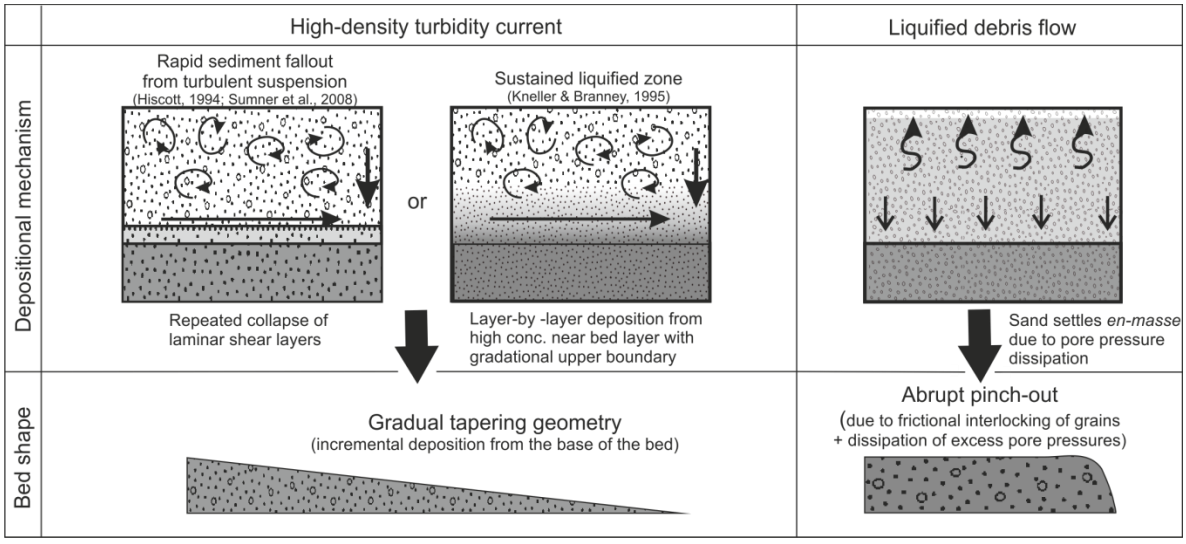

Figure 6.10. *Generalised summary of different process models for deposition of massive sandstone and resulting characteristic deposit shape.*

Previous interpretation of massive sandstone beds in the Skoorsteenberg Formation

Previous studies (Johnson et al., 2001; Hodgson, 2009) suggested that thick massive sandstone beds in the Skoorsteenberg formation were deposited by (high density) turbidity currents, based on the presence of basal tool marks indicating flow turbulence and a common normal grading with laminated bed tops. These features are observed in this study in thick, amalgamated beds, such as the deposits of lobe 1 (figure 6.9a), although the vertical grading is only observed in the top laminated interval. Mudstone clasts are only found in correspondence of amalgamation surfaces and in hybrid beds at the base of the fan (figure 9b).

Possible liquefied debris flow origin of lobes that pinch-out abruptly

Close to the pinch-out zone (i.e. section 13 to 18), beds described in this study are massive and ungraded, without any evidence of dish and pillar structures or patchy areas of different grain size. The analysis of the textural characteristics of the deposits (figure 6.8) reveals a relatively poor sorting, suggesting rapid deposition. Supposing a deposition from a liquefied debris flow, the lack of patchy texture may be due to the narrow grain size range of the deposits of the Skoorsteenberg Formation, ranging from silt to fine sandstone.

The base of each sandstone bed near the pinch out is flat, with common evidence of trace fossils (figure 6.9e). No flutes or grooves are observed, suggesting the lack of vigorous flow turbulence.

A clear grain size break has not been observed in the field. This step in the vertical grain size profile however may be difficult to detect in the field using a grain size comparator and hand lens, because the grain size distribution of the Skoorsteenberg formation lacks large (>500 μm) grains that helped identify grain size variations in the Marnoso Arenacea deposits. For this purpose, a more detailed textural analysis would be needed. The observed lateral continuity of the top cross laminated interval of each bed, that maintains a constant thickness even after the pinch out of the basal massive sandstone layer, however suggest that beds were deposited by a bipartite flow, with a high concentrated flow phase that pinch out abruptly and an overlying more dilute phase.

In the Marnoso Arenacea formation, the lateral facies change from subfacies Cs5 (normally graded massive sandstone) to subfacies Cs7 (swirly patchy sandstone that pinch-out abruptly) in some beds (facies tract 3, i.e. bed 0) suggest a flow transformation from a high density turbidity current to a liquefied debris flow.

In a similar fashion, a high-density turbidity current may have deposited the bulk of the lobe-forming massive sandstones observed. The distal, extremely rapid pinch-out of sandstone beds may be due to a flow transformation to a liquefied debris flow phase. Without any available cohesive mud a flow transformation from a high density turbidity current to a liquefied debris flow would have caused an extremely rapid deposition of the sand carried by the flow, because of the dissipation of the excess pore pressure not decelerated by the presence fine, cohesive particles in the flow (figure 6.10). The pinch-out of sandstone layers observed here, from 1 meter to zero in about 100 meters, is compatible with this interpretation .

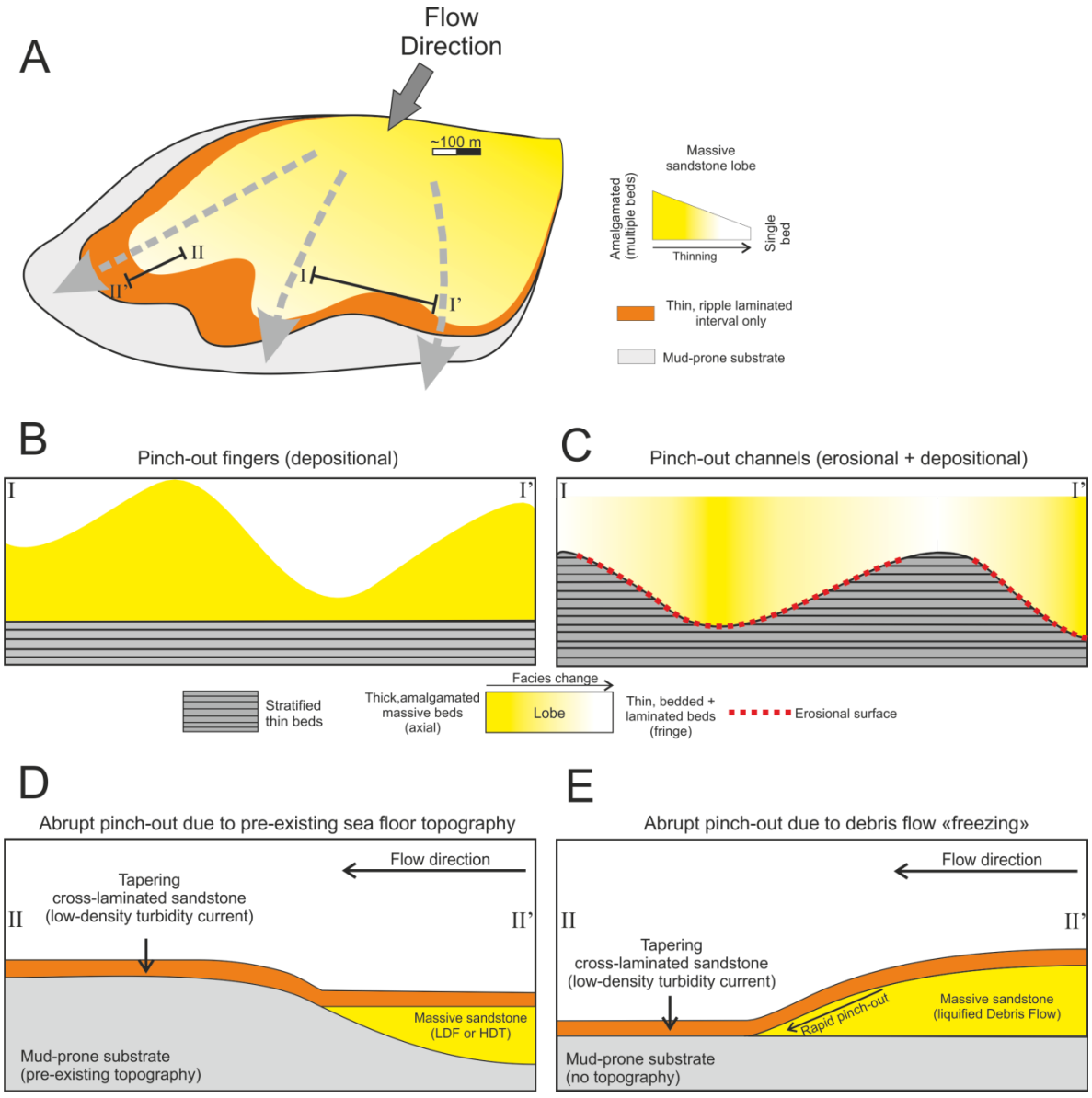

Figure 6.11. *Schematic view of possible mechanisms for the formation of finger-like protrusions. A) map view; B) and C) across strike section; C) and D) parallel to dip section.*

6.4.2 Controls on the finger-like geometry of lobes pinch-out

Correlation of sandstone lobes in a parallel to slightly oblique to strike cross section (figure 6.7) indicates that the lateral continuity of individual event beds is limited to few hundred meters or less. Bed amalgamation is common, and a single sandstone lobe can vary from a relatively thick unit formed by multiple events to a single thin event bed. In some cases (i.e. lobe 2 between section 10 and 11) rapid thickness and facies variations within a single bed are observed, but a

general observation is that in a one km wide cross section each sandstone lobe is formed by the lateral amalgamation of multiple event beds. Single event beds appear to form relatively narrow lenses. The overall lobe geometry is finger-like (Rozman and Bouma, 2000; Van der Weff and Johnson, 2003; Prelàt, 2009; Groenenberg et al., 2010). The finger-like geometry of the lobe has been described by Van der Werff and Johnson (2003) as "pinch-out channel". The lateral changes in thickness of lobe 2 deposits however cannot be explained by basal erosion, because the underlying beds are not truncated and don't show significant changes in thickness (figure 6.11 b and c); however lobe 1, whose pinch-out geometry was not constrained in this study, shows a certain degree of basal erosion.

The pinch-out geometry indicates that the map view shape of lobes is not as smooth and dominated by radial changes as previously envisaged, but can be much more irregular across-strike (figure 6.11), as identified in lobes in Fan 3 (Prelàt et al., 2009), Fan 2 (Rozman, 2000) and previous studies of Fan 4 (Bouma & Rozman, 2000).

Prelàt et al. (2009) proposed 2 alternative mechanisms which could explain this finger like geometry: (i) the control on the finger-like pattern identified may be due to pre-existing sea floor topography (figure 6.11d); (ii) the most distal flows were elongate and deposited finger like bed shapes. The rapid pinch-out of 4 sandstone lobes (figure 6.6) in approximately the same position observed in this study at the base of fan 4 may indicate a certain degree of sea floor topography, although there is no evidence of tectonic or diapiric mechanisms that could generate this radial finger-like geometry (Prelàt et al., 2009). The second mechanism implies an important flow process control: elongated flows were able to set up a topographic pattern depositing elongated fingers with relatively abrupt margins. Prelàt et al., (2009) indicate the deposition of mud rich, cohesive linked debrites, commonly found at the base of each fan sequence (Hodgson, 2009) as a possible mechanism able to deposit such elongate finger-like beds. As indicated by Hodgson (2009) hybrid beds in the Skoorsteenberg Formation can be extremely laterally variable: a hybrid bed can pass from dominantly debrite to turbidite, as a proportion of the total bed, without changes in thickness over 10's of meters, indicating a complicated distribution and possibly transformation of flow rheologies. Whether such hybrid flow events could deposit finger like, elongated deposits is yet to be documented in the Tanqua fan complex.

Numerical models by Groenenberg et al. (2010), based on outcrop observation of Fan 3 lobe deposits, suggest that elongate fingers may be formed by levee-like elongate highs.

The results of this study suggest a different explanation: clean (mud-poor) massive sandstone layers can have an abrupt pinch-out geometry both in dip (figure 6.6) and across strike (lobe 2 in figure 6.7) direction. This abrupt pinch-out, with liquefied debris flows freezing at their margin, may have contributed to set up a complex topographic template, able to control the lateral distribution of successive flow deposits (figure 6.11)

6.4.3 Authigenic origin of some heterolithic packages

The origin of fine heterolithic packages separating sandstone intervals (lobe elements) can be related to authigenic or allogenic processes (figure 6.10). Thin bedded, fine grained packages separating lobe elements (intralobes; Prelàt et al., 2009) can be interpreted as representing periods of fan wide reduced sand supply, controlled mainly by allogenic processes (Van der Werff and Johnson, 2003; Hodgson et al., 2006). In an authigenic origin scenario these fine-grained units would represent the lateral fringes of other sandstone lobes. A detailed analysis of the genesis of intralobe deposits is beyond the porpoise of this chapter. Authigenic versus allogenic controls on fine grained units has been discussed previously by Johnson et al. (2001), Van der Werff and Johnson (2003), Hodgson (2006), Prelàt et al. (2009) based on a much more extensive database. A simple point made on this study is that the same flow event depositing thick, massive sandstones can deposit a very thin, finer siltstone layer, and that the transition between the two may be extremely abrupt (10s of meters) due to the lobe pinch-out. For example, after the pinch-out of the basal massive sandstone interval, lobe 3 in section 18, 21 and 22 is represented only by thin (<1 cm), very fine grained interval. This interval is virtually indistinguishable from the surrounding heterolithics.

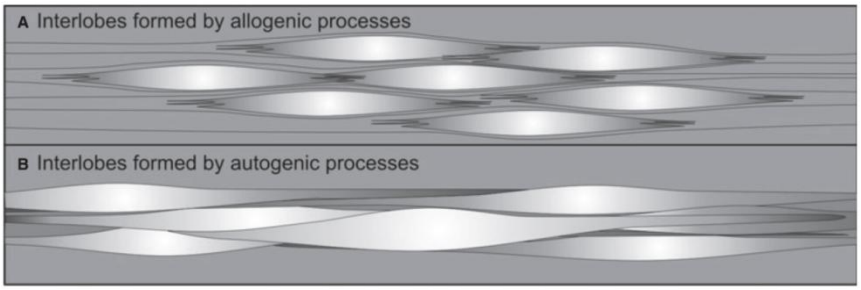

Figure 10. *Cartoon showing the difference between fine-grained units formed by allogenic and auhtigenic processes. A) If formed by allogenic processes, the fine-grained units represent decreases in sediment supply to the whole deep-water system. B) If formed by autogenic processes, the fine-grained units represent the distal fringes of lobes that thicken toward their axes. From Prelàt et al. (2009).*

6.5 CONCLUSIONS

Detailed bed correlations reveal that the distal pinch-out of sandstone lobes in Fan 4 of the Skoorsteenberg Formation (Karoo basin, South Africa) is most likely due to the frictional freezing of liquefied debris flows, rather than to interaction of high density turbidity currents with pre-existing sea floor topography. Close to their pinch-out individual beds are bipartite. A basal massive and ungraded clean (mud-poor) sandstone division that pinches out abruptly is overlaid by a much more extensive thin rippled laminated interval. This bipartite structure is similar to the one observed in liquefied debris flows deposits in the Marnoso Arenacea Formation, although sandstone lobes in Fan 4 lack the swirly, patchy texture interpreted as the product of catastrophic liquefaction. It is acknowledged however that more detailed analysis of the textural characteristic of the deposits, and a more exhaustive study of the relationships between the pinch-out facies observed and the overall lobe facies and architecture, is needed to further test this hypothesis. Previous authors (Johnson et al., 2001; Hodgson, 2009) interpreted the bulk of extensive (10's of kilometers) sandstone lobes in Fan 4 as deposited by (high density) turbidity currents, based on the presence of basal tool marks indicating flow turbulence and a common normal grading with laminated bed tops. The distal, extremely rapid pinch-out of sandstone beds may be due to a flow transformation to a liquefied debris flow phase. This transformation may have favored the rapid (en-masse) deposition of the sand carried by the flow, caused by the dissipation of the excess pore pressure not decelerated by the presence fine, cohesive particles. The abrupt pinch-out geometry of sandstone lobes may have contributed to set up a complex topographic template, able to control the lateral distribution of successive flow deposits, and therefore the finger like geometry of the distal pinch out of submarine fans that is also observed in other locations, such as the Mississippi Fan.

CHAPTER 7:

SUMMARY AND FUTURE WORK

7.1 SUMMARY

This PhD project mainly involved description and analysis of submarine sediment density flow deposits in the Marnoso Arenacea Formation in the Italian Apennines and, to a lesser extent, in the Karoo Basin (South Africa). This work was strongly based of fieldwork, and the author completed more than 150 days in the field during the PhD project.

This thesis highlights how deposits of submarine density flow can be complex, even in the relatively simple depositional settings of the Marnoso Arenacea Formation. A single event can comprise different flow types, and transformations can occur between these flow types. We showed how extensive (10's of kilometers) clean (mud-poor) sandstone layers that pinch-out abruptly can be deposited by liquefied debris flow, most likely formed through flow transformation from a (high density) turbidity current as the flow decelerates on low gradients. Moreover, high density and low density turbidite, clean and muddy debrite intervals can be deposited by a single flow event (i.e. bed 5 in the above Contessa interval). This lateral facies organization of submarine flow deposits was not fully captured by previous well-known depositional models such as the ones form Lowe (1982), Mutti (1992; 1999), Kneller and Branney (1995) and Shanmugam (1995).

The abrupt pinch-out of sandstone lobes at the distal termination of Fan 4 in the Karoo Basin (South Africa) also suggest that such lobes, at least at their distal termination, may have been deposited by liquefied debris flows, rather than (high density) turbidity currents.

The external shape of the deposits is not only controlled by the initial sediment volume of the flow and by interactions with the sea-floor topography. Parameters such as grain size distribution, flow concentration (that determines if deposition is hindered) and mud-matrix content are found to be fundamental. Low density turbidites have a gradual tapering shape, while high density turbidites tend to maintain their thickness for long distances (figure 7.1). In large volume beds a thick "core" (deposited by high-density flow) is commonly separated by a sharp grain size break from the overlying more extensive "drape" (deposited by a low-density flow part). Turbidite mudstone (or

densite mudstone, Talling et al., 20012a) tend to pond in topographic lows, and its capable of draining back (opposite to the main direction of the flow).

The vertical thickness distribution of flow deposit in the 600 meters thick Cabelli section results the combination of log-normally distributed intervals of low-density (Tcd-e) and high density (Tab-cd-e) turbidites, clean and muddy debrites. This thickness distribution is directly related to the relative proportion beds with a characteristic external shape and pinch-out geometry.

The stacking pattern of event-beds indicates a long-term clustering, revealed by the Hurst test. Debrite intervals occur randomly in the 600 m studied section, and bed correlation suggest that almost every large volume flow deposited clean or muddy debrite (or both) intervals in different positions of the basin. This indicates that deposition of debrite intervals may be a characteristic of these large flows, rather that mark periods of disequilibrium of the slope profile or enhanced upslope erosion.

Bed amalgamation is rare in the Marnoso Arenacea Inner (older) Stage deposits, and flows caused little or no substrate erosion. For this reason the hemipelagic sediment deposited between turbidite beds is used as an indicator of the time that separates flow events. Events occur on average every 1400 years. The distribution of time between events is exponential, therefore related to a Poisson Process. A fundamental characteristic of the Poisson Process is the lack-of-memory property. This ensures that flow events (most likely triggered by submarine slope failures) are independent one from the other. The system has no memory, so that each event in the past does not contain any information that can predict the likelihood of events occurring in the future.

A stratigraphic interval characterized by increased bed thickness and grain size is positively correlated to globally recognized isotopic cooling step, which possibly caused a marked sea level drop. This indicates that that a variation of the global sea-level favored the onset of larger volume flows in the Marnoso Arenacea (Proto-Adriatic; Mutti and Di Base, 2002) basin.

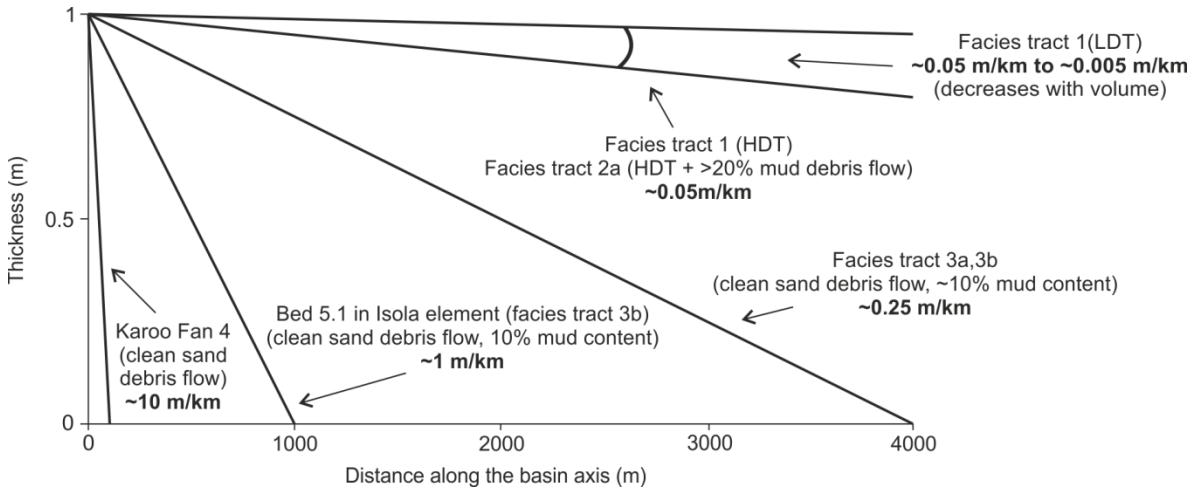

Figure 7.1. Pinch-out rates of the different facies tracts analyzed in this thesis

7.2. RESPONSES TO INITIAL QUESTIONS POSED IN THIS THESIS

1) What is the internal facies architecture of individual submarine density flow deposits obtained from bed-by-bed correlations? Can we use this information to test depositional models?

Despite the relatively simple depositional setting of the Marnoso Arenacea Formation, where voluminous, mud-rich submarine density flows deposited their sediment load on a wide, low gradient basin plain with relatively simple topography and little substrate erosion, a single event can comprise different flow types, and transformations can occur between these flow types. Three main deposit geometries occur in down flow transects through beds. Individual beds can contain more than one of these facies tracts in adjacent thrust sheets.

Facies tracts 1 and 2 contain graded or ungraded massive or laminated clean (mud-poor) sandstone intervals that taper gradually down flow, and were most likely deposited incrementally beneath low and high density turbidity currents. Mud-rich massive sandstone deposited by mud-rich, cohesive debris flow occurs in facies tract 2. Facies tract 3 contains clean sandstone with a distinctive swirly fabric formed by patches of coarser and better sorted grains. This type of clean sandstone pinches out abruptly, and this pinch out geometry suggests it was most likely deposited by liquefied debris flow, as both

subaqueous and subaerial debris flows tend to produce deposits with well-defined steep edges, while dilute turbidity currents produce a different deposit shape that gradually tapers.

2) Are liquefied debris flows able to deposit clean sandstone across large areas of the sea floor? How do such flows originate?

Clean sandstone intervals with a distinctive swirly fabric formed by patches of coarser and better sorted grains (lithofacies Cs7) are interpreted to be the result of pervasive liquefaction. This fabric is not the result of in-situ liquefaction of massive sandstone previously deposited by high density turbidity current, but is most likely due to deposition en-masse by a liquefied debris flow. The patchy texture most likely results from slow convection and elutriation of fine material during the liquefaction process, together with blebs of sand formed by settling down vertical conduits. The upper part of the overlying ripple-cross laminated sandstone (deposited by the same flow-event) is flat lying, suggesting that pore pressure dissipation from the debris flow was completed during deposition of the rippled interval, which was probably deposited shortly after the massive sandstone. The abrupt lateral pinch out of swirly or patchy Cs7 sandstone intervals supports the conclusion that they were deposited by liquefied debris flow.

Liquefied debris flows most likely originated through flow transformation from a turbidity current, as indicated by the up flow transition of Cs7 sandstone into normally graded laminated sandstone, most likely deposited in a layer-by layer fashion. Lateral transitions between liquefied debris flow (Cs7) and laminated (Cs3) or massive (Cs5) turbidite sandstone occur without major changes in the overall sandstone thickness, suggesting that laminated sandstone was deposited by a relatively high concentration turbidity current. Some Cs7 intervals however extend continuously to the most proximal available outcrops, and could have been deposited by debris flows that originated outside the outcrop area.

In a debris flow the cohesive mud content provides yield strength sufficient to support sand, and helps to keep pore fluid pressures elevated as permeability is reduced. Elevated pore pressure aids mobility. Textural analysis indicate that Cs7 deposit contain mud matrix percentage similar to other turbidite sandstone, comprised between 4 and 8%. At elevated

sediment concentrations however this proportion of fine material may be sufficient to provide yield strength, and also greatly increase the time taken for excess pore pressure to dissipate, enhancing the run-out distance of liquefied debris flow to the observed 15 to 30 km over a low gradient basin plain.

3) What is the characteristic external shape of turbidites and debrites? What are the controls on this shape?

The turbidite sandstone interval thickness of fine grained, small volume beds declines rapidly in a 60 km down flow transect over a distance of 20-30 km in an approximately exponential fashion, and small volume beds entering the Marnoso Arenacea foredeep basin from opposite direction are characterized by this similar geometry. This shape is well approximated by an exponentially decreasing function, characteristic of deposition from spatially depletive flows dominated by suspended load deposition. The exponential decay of small volume beds containing clean debrite interval is more rapid, indicating a higher depositional rate.

Intermediate and large volume beds can be divided into a basal "core" (deposited by high-density flow) commonly separated by a sharp grain size break from the overlying more extensive "drape" (deposited by a low-density flow part). In these beds a proximal thickening to a sandstone thickness maximum appears. At progressively increasing sediment volumes the maximum thickens, broadens and moves basinward. The basal division, deposited by high density flow types, controls the position and the downflow extent of the sandstone thickness maximum observed.

The characteristic shape is not controlled by sea-floor topography. This shape is well reproduced by numerical modeling of flows with different concentration performed by Goater (2011), indicating that hindered settling acted as a major control.

High proportion (often > 50%) of fine mudstone particles in the flows enhanced flow efficiency, and allowed beds to be deposited for more than 120 km. Beds containing clean debrite intervals in proximal and intermediate location (facies tract 3a) pinch-out abruptly after 20-30 km. Compared to beds with similar volume, deposits of tract 3a have a higher sand/mud ratio, confirming the importance of the proportion of fine particles in the flow to determine the shape and run-out distance. Beds with facies tract 1, comprising only turbidite sandstone, maintain a constant thickness for more than 20 km, followed by a

gradual thinning in correspondence to the downflow transition from high density to low density deposits.

Turbidite mudstone (or densite mudstone, Talling et al., 20012a) shape, despite local variations due to the less-than-perfect exposure in some stratigraphic section, is well described by a linear function, thickening towards the lowest point of the basin. Mudstone tend to pond in topographic lows, and its capable of draining back (opposite to the main direction of the flow), and therefore his shape is strongly controlled by sea floor gradient and local topography.

4) **What is the bed thickness frequency distribution of turbidites and debrites, and why does it occur? How strongly stratigraphically clustered are flow deposits in the Marnoso Arenacea Formation?**

In the relatively simple basin plain settings of the Marnoso Arenacea Formation the vertical thickness distribution of turbidite and debrite beds can be considered equivalent to random sampling of a smaller number of beds in different locations. The external bed shape and pinch-out geometry is found to be a major control on the vertical thickness distribution of the deposits. Because beds with similar volume can have different facies architecture and geometry (chapter 4), we conclude that the distribution of the volume of flow-initiating events is unlikely to be directly related to the bed thickness distribution in a given location. Also, the rapid pinch-out geometry of clean sand debrites and clast-rich muddy debrite explains their thickness distribution in a single location, and why intervals <20 cm are rare.

Low-density (Tcd-e) and high density (Tab-cd-e) turbidites, clean and muddy debrites describe different lognormal populations, the convolution of which results in the observed bed thickness distribution. The sandstone division of each of the two populations is the combination of log-normally distributed intervals characterized by specific grain size classes and sedimentary structures (including clean and muddy debrite intervals).

The Hurst test reveals a long-term clustering in the 600 meters stratigraphic interval studied. This clustering can be attributed to lateral migration of the depocenters. However, a stratigraphic interval characterized by increased bed thickness and grain size can be positively correlated to globally recognized isotopic cooling step, which possibly caused a

marked sea level drop. This indicates that that a variation of the global sea-level favored the onset of larger volume flows in the Marnoso Arenacea basin.

Amy and Talling (2006), and Talling et al. (2007a; 2007b; 20012c) and the results shown in chapter 3 demonstrated that in the Marnoso Arenacea Formation two types of muddy debrite deposits can be recognized : clast-rich muddy debrite that show a rapid pinch-out geometry and clast-poor muddy debrite with a more gradual tapering shape. We showed that, in a single vertical section, it is possible to distinguish the two types of muddy debrite based on the ratio between the turbidite and debrite components and the size of the mudstone clasts. This finding may prove useful in subsurface studies, where the external shape and pinch-out geometry of muddy debrite intervals is not available.

The Hurst test and the analysis of the time distribution of beds containing muddy debrite intervals showed that such intervals occur randomly in the whole 600 m stratigraphic section. Their deposition is most likely a characteristic of large, mud-rich unconfined flows, rather than mark periods of disequilibrium of the slope profile (Haughton, 2003) with substantial erosion of the muddy substrate, or periods of enhanced erosion due to the onset of mass transport deposits (Muzzi Magalhes & Tinterri, 2010, Tinterri & Muzzi Magalhes, 2011), because such periods would result in a discernible vertical clustering of the deposits. Clustering of clean debrite intervals is related to a general increase in the number of thick beds, and doesn't show any obvious vertical pattern.

5) **What is the frequency of turbidity currents and debris flows in the Marnoso Arenacea basin plain? Can this frequency distribution provide information on tempo and triggers of processes that initiate possibly highly destructive flow events?**

Nannofossils biostratigraphy indicates that a 360 meters thick interval of the Cabelli section was deposited between 13.5 Ma and 14.1 Ma before present. Beds in this section were deposited on average every 1400 years. Thick beds occur every 5.300 years, and beds comprising debrite intervals every 10.700 years.

Hemipelagic sediment deposited between turbidite beds is used as an indicator of the time that separates flow events. The distribution of time between events is exponential, therefore related to a Poisson Process. This ensures that flow events are independent one from the other. The system has no memory, so that each event in the past does not contain any information that can predict the likelihood of events occurring in the future. The 'lack

of memory' property of the exponential distribution of returning time between events can provide insights into the tempo and triggers of processes that initiated submarine sediment density flows that entered this ancient basin plain. It is likely that submarine slope failures (landslides) triggered the larger volume flows in this basin, as individual bed volumes can exceed the annual sediment supply from all of the world's rivers. The technique adopted in this study may be useful, where a turbidite record directly related to landslides or other triggering events is available, to better understand the frequency of gravity flow generating events, and possibly help analyzing the risk of future highly destructive events.

6) **What is the origin of the rapid pinch-out of submarine sandstone lobes in the Tanqua Karoo basin?**

The distal termination of sandstone lobes deposited in Fan 4 (Skoorsteenberg Formation, Karoo Basin, South Africa) reveals an extremely abrupt pinch-out geometry. Sandstone thickness varies from one meter to zero in approximately 100 m. Close to their pinch-out clean sandstone beds are characterized by a bipartite structure. The basal, massive and ungraded sandstone interval, with a flat base with no evidence of flutes and grooves, pinch-out extremely rapidly down dip, while the top, normally graded ripple laminated interval maintain an almost tabular geometry.

The rapid pinch-out, poor sorting (if compared to other sandstone intervals) and lack of basal flutes and grooves, suggesting the lack of vigorous flow turbulence, indicates rapid deposition. Supposing a deposition from a liquefied debris flow, the lack of patchy texture, interpreted as the result of flow liquefaction in clean debrite sandstone described in the Marnoso Arenacea Formation, may be due to the narrow grain size range of the deposits of the Skoorsteenberg Formation, ranging from silt to fine sandstone. It can be hypothesized that high-density turbidity current has deposited the bulk of the lobe-forming massive sandstones of Fan 4. The distal, extremely rapid pinch-out of sandstone beds may be due to a flow transformation to a liquefied debris flow phase. The abrupt pinch-out geometry observed, with liquefied debris flows freezing at their margin, may have contributed to set up a complex topographic template, able to control the lateral distribution of successive flow deposits.

7.3. FUTURE WORK

This thesis work highlights the complexity of submarine sediment density flows and their deposits, even considering the simple basin plain settings of the Marnoso Arenacea formation, where beds were expected to conform classical models such as the Bouma sequence (Kneller and McCaffrey, 2003). In the introduction to his highly influential, and for many aspect fundamental paper on deposits of high-density turbidity currents Lowe (1982) indicated that "a reasonably clear picture has emerged in recent years of the gravity-driven processes that deliver and redistribute coarse sediment in the deep sea". This thesis work indicates a different view, and many aspects of sediment density flows behavior presented here remain to be tested through future work based on field, laboratory and numerical modeling.

The results presented here can be compared in future studies to deposits produced by small-scale laboratory experiments and mathematical models, in order to assess the scaling issues and assumptions involved in such modeling.

In particular, future flume experiments may reproduce key aspects of submarine flows highlighted in this work, such as:

- the role of hindered settling in the deposition of high density turbidity currents, and in determining the shape of turbidite deposits; large experiment facilities will be needed in order to take into account a high (>10% by weight) initial flow concentration).
- how dense liquefied flows of clean sand might originate and move for long distances on low gradients.
- how colloidal mud influences flow dynamics.

To reproduce these features flume experiments will need to incorporate a realistic range of sediment sizes (including colloidal mud). They will also need to be faster moving, to prevent scaling issues, and possibly incorporate sustained settling of sediment into a near-bed layer.

Numerical modeling studies will also need to capture the key aspect of natural flows, and the assumptions on which they are based will need to be independently tested.

Only direct monitoring of natural flows (difficult at present because active flow events are notoriously difficult to monitor directly due to their inaccessible location, unpredictable occurrence and their ability to destroy monitoring equipment placed in their path) will provide essential information such as flow velocity and vertical distribution of sediment concentration. In the meantime however, field studies such as the one presented in this thesis, based on extensive mapping of flow deposits, may provide useful constrains.

As indicated by Mutti et al. (2009) "it is evident that extensive and detailed outcrop studies are becoming increasingly rare among young scientists who have a preference to move towards computerized geology. However, it is the strong conviction of the authors that outcrop studies still form the basis upon which significant depositional models with predictive value may be developed".

In particular future outcrop studies will be extremely useful in the definition of the paleogeographic and sequence stratigraphic significance of hybrid beds and liquefied debris flow deposits, as indicated by previous studies of Haughton et al. (2009) and Hodgson (2009).

The time distribution of sediment flow deposits is at present poorly constrained, because of the difficulty to date individual flow events. The technique proposed in this thesis, that uses hemipelagic deposits as an indicator of time separating events, can provide insights into the tempo and triggers of processes that initiated submarine sediment density flows, especially deep basin plain locations where flow erosion is minimal.

REFERENCES

Abels, H.A., Hilgen, F.J., Krijgsman, W., Kruk, R.W., Raffi , I., Turco, E., and Zachariasse, W.J. (2005) Long-period orbital control on middle Miocene global cooling: Integrated stratigraphy and astronomical tuning of the Blue Clay Formation on Malta: *Paleoceanography*, **20**, 1–17.

Aksu, A.E. and Hiscott, R.N. (1989) Slides and debris flows on the high-latitude continental slope of Baffin-Bay. *Geology*, **17,** 885-888.

Allen, J.R.L. (1982) Chapter 10. Structures and sequences related to gravity-current surges. In *Sedimentary Structures. Their Character and Physical Basis*. Elsevier, Amsterdam, 395-431.

Allen, P. (2007) Earth science: Sediment en route to oblivion. *Nature*, **450,** 490-491.

Amy, L.A., Peakall, J. and Talling, P.J. (2005) Density and viscosity-stratified gravity currents: insights from laboratory experiments and implications for submarine flow deposits. *Sed. Geol*., 179, 5–29.

Amy, L.A. and Talling, P.J. (2006) Anatomy of turbidites and co-genetic debrites intervals based on long distance (120 · 30 km) bed correlation, Marnoso Arenacea Formation, Northern Apennines, Italy. *Sedimentology*, 53, 161–212.

Amy, L., Talling, P.J., Edmonds, V.O., Sumner, E.J. and **Leseuer, A.** (2006) An experimental investigation of sand-mud suspension settling behaviour: implications for bimodal mud contents of submarine flow deposits. *Sedimentology*, **53**, 1411-1434.

Argnani, A.J. & Ricci Lucchi, F. (2001) - Tertiary silicoclastic turbidite systems of tha Northern Apennines. In: Vai, G.B. & Martini, I.P. (Eds.), *Anatomy of an orogen: the Apennines and adjacent Mediterranean basins* Kluwer Academic Publishers*,* 327-350.

Arnott, R.W.C. and Hand, B.M. (1989) Bedforms, primary structures and grain fabric in the presence of suspended sediment rain. *J. Sed. Petrol*., 59, 1062–1069.

Aziz, H. A., A. Di Stefano, et al. (2008). "Integrated stratigraphy and (40)Ar/(39)Ar chronology of early Middle Miocene sediments from DSDP Leg 42A, Site 372 (Western Mediterranean)." *Palaeogeography Palaeoclimatology Palaeoecology* **257**(1-2), 123-138.

Baas, J.H. (1994) A flume study on the development and equilibrium morphology of current ripples in fine sand. *Sedimentology*, **41**, 185–209.

Baas, J.H., Best, J.L., Peakall, J. and Wang, M. (2009) A phase diagram for turbulent, transitional, and laminar clay suspension flows. *Journal of Sedimentary Research*, **79,** 162-183.

Baas, J.H., and **Best, J.L.** (2002), Turbulence modulation in clay-rich sediment-laden flows and some implications for sediment deposition*. J. Sedim. Res.,* **72**, 336-340.

Baas, J.H., Best, J.L., and **Peakall, J.** (2011) Depositional processes, bedform development and hybrod flows in rapidly decelerated cohesive (mud-sand) sediment flows. *Sedimentology*, in press.

Bak, P., Christensen, K., Danon, L., Scanlon, T. (2002) Unified scaling law for earthquakes. *Phys. Rev. Lett.* **88**.

Bagnold, R.A. (1954) Experiments on a gravity-free dispersion of large solid spheres in a Newtonian fluid under shear. *Procs. Royal Soc. London*, **A 225**, 49-63.

Balakrishnan, N. and Basu, A. P. (1996) *The Exponential Distribution: Theory, Methods, and Applications*. New York: Gordon and Breach.

Bannerjee, I. (1977) Experimental study on the effect of deceleration on the vertical sequence of sedimentary structures in silty sediments. *Jour. Sedim. Petrol*., **47**, 771-783.

Best, J. and **Bridge J.** (1992) The morphology and dynamics of low amplitude bedwaves upon upper stage plane beds and the preservation of planar laminae. *Sedimentology*, **39**, 737-752.

Beattie, P. D. and W. B. Dade (1996). "Is scaling in turbidite deposition consistent with forcing by earthquakes?" *Journal of Sedimentary Research* **66**(5): 909-915.

Bersezio, R., F. Felletti, et al. (2009). Trends in bed thickness and facies of turbiditic sandstone bodies: unravelling the effects of basin confinement, depositional processes, and modes of sediment supply. *External Controls on Deep-Water Depositional Systems.* B. Kneller, O. J. Martinsen and B. McCaffrey. Tulsa, S E P M - Soc Sedimentary Geology**:** 303-321.

Birman, V.K., Meiburg, E., Kneller, B. (2009) The shape of submarine levees: exponential or power law? *Journal of Fluid Mechanics* **619**, 367–376.

Blanchette, F., Strauss, M., Meiburg, E., Kneller, B., and Glinsky, M.E. (2005) High resolution numerical simulations of re-suspending gravity currents: conditions for self-sustainment: *Journal of Geophysical Research*, **110**

Boccaletti, M.; Elter, P. & Guazzone, G. (1971) Plate Tectonics models for the development of the Western Alps and Northern Apennines*. Nature*, **234**, 108-111.

Bouma, A.H. (1962) Sedimentology of Some Flysch Deposits; A Graphic Approach to Facies Interpretation. PhD thesis, University of Utrecht, Elsevier, Utrecht, the Netherlands,168 pp.

Bouma, A.H. and Wickens H.D.V. (1991) Permian passive margin submarine fan complex, Karoo Basin, South Africa: possible model to Gulf of Mexico. *Gulf Coast Association of Geological Societies, Transactions*, **41**, 30-42.

Bouma, A.H. and. Rozman, D.J. (2000) Characteristics of fine-grained outer fan fringe turbidite systems. In: *Fine-Grained Turbidite Systems.* A.H. Bouma and C.G. Stone

(eds.). SEPM Special Publication **68,** 291-298.
Bouma, A. H., M. B. DeVries, et al. (1997). "Reinterpretation of depositional processes in a classic flysch sequence (Pennsylvanian Jackfork Group), Ouachita Mountains, Arkansas and Oklahoma: Discussion." *Aapg Bulletin-American Association of Petroleum Geologists* **81**(3): 470-472.

Breien, H., De Blasio, F.V., Elverhoi, A., Nystuen, J.P. and Harbitz, C.B. (2010) Transport mechanisms of sand in deep-marine environments-insights based on laboratory experiments. *Journal of Sedimentary Research*, **80,** 975-990.

Carlson, J. and Grotzinger, J.P. (2001) Submarine fan environment inferred from turbidite thickness distributions. *Sedimentology*, **48**, 1331–1351.

Capozzi, R.; Landuzzi, A.; Negri, A. & Vail, G.B. (1991) Stili deformativi ed evoluzione tettonica della successione Neogenica Romagnola. *Studi Geologici Camerti* **1**, 261-278.

Cerrina Feroni, A., Leoni, L., Martelli, L., Martinelli, P., Ottira, G. and Sarti, G. (2001) The Romagna Apennines, Italy: an eroded duplex. *Geol. J*., **36**, 39–54.

Chaytor, J. D., U. S. ten Brink, et al. (2009). "Size distribution of submarine landslides along the US Atlantic margin." *Marine Geology* **264**(1-2): 16-27.

Chen, C. & Hiscott, R.N. 1999. Statistical analysis of facies clustering in submarine-fan turbidite successions. *Journal of Sedimentary Research*, **69**, 505–517.

Cibin, U., A. Di Giulio, et al. (2004). Factors controlling foredeep turbidite deposition: the case of Northern Apennines (Oligocene-Miocene, Italy). *Confined Turbidite Systems*. S. A. Lomas and P. Joseph. Bath, Geological Soc Publishing House. **222:** 115-134.

Clark, I. D. and P. Fritz (1997). *Environmental Isotopes in Hydrogeology*. New York, Lewis Publishers.

Coleman, J. L. (1997). "Reinterpretation of depositional processes in a classic flysch sequence (Pennsylvanian Jackfork Group), Ouachita Mountains, Arkansas and Oklahoma: Discussion." *Aapg Bulletin-American Association of Petroleum Geologists* **81**(3): 466-469.

Colwell, J. B. and N. F. Exon (1988). "quaternary hemipelagic sedimentation in the basins flanking the solomon-islands volcanic arc." *Geo-Marine Letters* **8**(3): 139-147.

Conover, W.J. (1999) *Practical Nonparametric Statistics*, 3rd edn. John Wiley and Sons, New York, 584 pp.

Corral, A. (2006). "Dependence of earthquake recurrence times and independence of magnitudes on seismicity history." *Tectonophysics* **424**(3-4): 177-193.

Costa, J.E. and Williams, G.P. (1984) Debris-flow dynamics (video). *U.S.G.S. Open File Report*, 84-606, 22 mins.

Coulter, H.W. and Migliaccio, R.R (1996) The effects of the Earthquake of March, 27 at Valdez, Alaska. *United States Geological Survey professional paper*, **542**-C, 36 pp.

Coussot, P. (1997) *Mudflow Rheology and Dynamics.* IAHR Monograph, Balkema, Rotterdam, 272n p.

D'agostino, A. E. and D. W. Jordan (1997). "Reinterpretation of depositional processes in a classic flysch sequence (Pennsylvanian Jackfork Group), Ouachita Mountains, Arkansas and Oklahoma: Discussion." *Aapg Bulletin-American Association of Petroleum Geologist*s **81**(3): 473-475.

Dade, W. B. and H. E. Huppert (1994). "predicting the geometry of channelized deep-sea turbidites." *Geology* **22**(7): 645-648.

De Jager, J. (1979) - The relation between tectonics and sedimentation along the "Sillaro line" (northern Appennines, Italy), *Geologica Ultraiectina* **19**, 97pp.

De Wit, M.J. and. Ransome, I.G.D. (1992) Regional inversion tectonics along the southern margin of Gondwana. In: *Inversion Tectonics of the Cape Fold Belt, Karoo and Cretaceous Basins of Southern Africa.* M.J. De Wit and I.G.D. Ransome (eds.). Rotterdam, Balkema**,** 15-21.

DiBase, D. and Mutti, E. (2002) The 'Proto Adriatic Basin'. *In: Revisiting Turbidites of the Marnoso-arenacea Formation and their Basin-Margin Equivalents: Problems with Classic Models. 64th EAGE Conference and Exhibition Excursion Guidebook*, (Eds E. Mutti, F. Ricci Lucchi and M. Roveri), pp. I-1–I-4, Parma University and ENI-AGIP Division, Parma, Italy.

Dorrell, R. M., A. J. Hogg, et al. (2011). "The structure of the deposit produced by sedimentation of polydisperse suspensions." *Journal of Geophysical Research-Earth Surface* **116**

Druitt, T. (1995) Settling behavior of some concentrated dispersions and some volcanological applications. *J. Volcanol. Geoth. Res*., 65, 27–35.

Drummond, C.N. and Wilkinson, B.H. (1996) Stratal thickness frequencies and the prevalence of orderedness in stratigraphic sections. J*. Geol*., **104**, 1-18.

Dykstra, M., B. Kneller, et al. (2012)"Bed-thickness and grain-size trends in a small-scale proglacial channel-levee system; the Carboniferous Jejenes Formation, Western Argentina: implications for turbidity current flow processes." *Sedimentology* **59(2)**: 605-622.

Enos, P. (1969) Anatomy of a flysch. J*. Sed. Petrol*., 39, 680-723.

Everitt. B. S. (2006). "*The Cambridge Dictionary of Statistics. 3rd Edition*." Cambridge University Press.

Faure, K. and D.I. Cole (1999) Geochemical evidence for lacustrine microbial blooms in the vast Permian Main Karoo, Parana, Falkland Islands and Huab basins of southwestern Gondwana. *Palaeogeography, Palaeoclimatology, Palaeoecology*, **152**, (3/4), 189-213.

Felix, M., 2001, A two-dimensional numerical model for a turbidity current, in McCaffrey, W.D., Kneller, B.C., and Peakall, J., eds., Particulate Gravity Currents: *International Association of Sedimentologists, Special Publication* **31**, 71–81.

Felletti, F. and R. Bersezio (2010). "Validation of Hurst statistics: a predictive tool to discriminate turbiditic sub-environments in a confined basin." *Petroleum Geoscience* **16**(4), 401-412.

Fildani, A., N.J. Drinkwater, A. Weislogel, T. Mc Hargue, D.M. Hodgson and S.S. Flint (2007) Age controls on the Tanqua and Laingsburg deep-water systems: new insights on the evolution and sedimentary fill of the Karoo Basin, South Africa. *Journal of Sedimentary Research*, **77**, 901-908.

Folk, R.L. and **Ward, W.C.** (1957) Brazos River bar: a study in the significance of grain size parameters. *J. Sedim. Petrol.*, **27**, 3–26.

Frenz, M., Wynn, R.B., Georgiopoulou, A., Bender, V.B., Hough, G., Masson, D.G., Talling P.J. and **Cronin, B.T.** (2008) Unravelling turbidite basin fill complexity: A case study from the Late Quaternary turbidite fill of the Agadir Basin, offshore Atlantic Morocco. *Int. J. Earth Sci.,* **98**, 721-733.

Galy, V., France-Lanord, C., Beyssac, O., Faure, P., Kudrass, H., and **Palhol, F.** (2007) Efficient organic carbon burial in the Bengal fan sustained by the Himalayan erosional system, *Nature*, **450**, 407-410.

Gandolfi, G., Paganelli, L. and Zuffa,G.G. (1983) Petrology and dispersal directions in the Marnoso Arenacea Formation (Miocene, northern Apennines). *J. Sed. Petrol*., 53, 493–507.

Garcia, M. and Parker, G. (1991) Entrainment of bed sediment into suspension. J*. Hydraul. Eng*., **117**, 414–435.

Garcia, M. and Parker, G. (1993) Experiments on the entrainment of sediment into suspension by a dense bottom current. *J. Geophys. Res*., **98**, 4793–4807.
Garton, M. and McIlry, D. (2006) Large thin slicing: A new method for the study of fabrics in lithified sediments. *Journal of Sedimentary Research*, **76,** 1252-1256

Gasperi, G. (1995) Geologia regionale. Geologia dell'Italia e delle regioni circummediterranee. Pitagora Editrice Bologna, 266- 298

Geist, E. L. and T. Parsons (2010). *Estimating the Empirical Probability of Submarine Landslide Occurrence*. Dordrecht, Springer.

Ghibaudo, G. (1992) *Subaqueous sediment gravity flow deposits: practical criteria for their field description and classification*. Sedimentology 39, 423–454.

Gladstone, Phillips, et al. (1998). "Experiments on bidisperse, constant-volume gravity currents: propagation and sediment deposition." *Sedimentology* **45**, 833-843

Harris, T.C., *et al.*, 2002, Polydisperse particle driven gravity currents. *J. Fluid Mech.*, **472**, 333-371.

Goater, A (2011) Second year review part B. PhD report, University of Bristol.

Goldfinger, C; A.E. Morey, C.H. Nelson, J. Gutierrez-Pastor, J.E. Johnson, E. Karabanov, J. Chaytor, and **A. Ericcson** (2007) Rupture lengths and temporal history of significant earthquakes on the offshore and north coast segments of the Northern San Andreas Fault based on turbidite stratigraphy. *Earth Planet Sci. Lett*, **254**, 9-27.

Grecula, M., S.S. Flint, H.D.V. Wickens and S.D. Johnson (2003) Upward-thickening patterns and lateral continuity of Permian sand-rich turbidite channel fills, Laingsburg Karoo, South Africa. *Sedimentology*, **50**, 831-853.

Groenenberg, R.M., D.M. Hodgson, A. Prélat, S.M. Luthi and S.S. Flint (2010) Flow deposit interaction in submarine lobes: insights from outcrop observations and process-based numerical model realisations. *Journal of Sedimentary Research*, **80**, 252-267.

Guerra R., Righi S., Accumulation rates and sources of sediment in a northern adriatic coastal lagoon based on radioisotopic tracers *(137Cs AND 210Pb)*, in: *Science and management of estuaries and coasts: a tale of two hemispheres*. ECSA 44st International conference. , s.l, s.n, 2008, pp. 35 (atti di: Science and management of estuaries and coasts: a tale of two hemispheres. ECSA 44st International conference., Bahía Blanca, Argentina, September 29 - October 3, 2008) [atti di convegno-abstract].

Gutenberg, B. and Richter, C.F. (1954) *Seismicity of the Earth and Associated Phenomena*, 2nd ed. Princeton, N.J.: Princeton University Press.

Hampton, M.A., Lee, H.J., Locat, J. (1996) Submarine Landslides. *Review of Geophysics* **34**, 33-59.

Haq, B. U. (1999). "Natural gas deposits - Methane in the deep blue sea." *Science* **285**(5427): 543-544.

Haughton, P.D.W., Barker, S.P. and **McCaffrey, W.D**. (2003) 'Linked' debrites in sand rich turbidite systems - origin and significance. *Sedimentology*, **50**, 459-482.

Haughton, P.D.W., Davis, C., McCaffrey, W., and **Barker, S.P.** (2009) Hybrid sediment gravity flow deposits – classification, origin and significance. In; *Hybrid and Transitional Submarine Flows* (Eds. Amy, L.A., McCaffrey, W.B., and Talling, P.J.) *Marine Petrol. Geol*., **26**, 1900-1918.

Hirayama, J. and **Nakajima, T.** (1977) Analytical study of turbidites, Otadai Formation, Boso Peninsula, Japan. *Sedimentology*, **24**, 747-779.

Hiscott, R.N. (1994a) Traction-carpet stratification in turbidites – fact or fiction. *J. Sedim Res.*, **64**, 204-208.

Hiscott, R.N., and **Middleton, G.V**. (1979) Depositional mechanics of the thick-bedded sandstones at the base of a submarine slope, Tourelle Formation (Lower Ordovician), Quebec, Canada. In: Doyle, L.J., and Pilkey, O.H. (eds.), Geology of Continental Slopes. SEPM Spec. Pub. 27, 307-326.
Hiscott, R.N., and **Middleton, G.V**. (1980) Fabric of coarse deep-water sandstones, Tourelle Formation, Quebec, Canada. *J. Sedim. Petrol.,* **50**, 703-722.

Hiscott, R.N., Colella, A., Pezard, P., Lovell, M.A. and Malinverno, A. (1992) Sedimentology of deep-water volcaniclastics, Oligocene Izu-Bonin forearc basin, based on formation microscanner images. In: *Proc. ODP Sci. Results* (Eds B. Taylor and K. Fujioka), **126**, 75-96.

Hodgson, D. M. (2009)."Distribution and origin of hybrid beds in sand-rich submarine fans of the Tanqua depocentre, Karoo Basin, South Africa." *Marine and Petroleum Geology* **26**(10), 1940-1956.

Hodgson, D. M., S. S. Flint, et al. (2006) "Stratigraphic evolution of fine-grained submarine fan systems, Tanqua depocenter, Karoo Basin, South Africa." *Journal of Sedimentary Research* **76**(1-2), 20-40.

Holbourn, A., W. Kuhnt, et al. (2007) "Orbitally-paced climate evolution during the middle Miocene "Monterey" carbon-isotope excursion." *Earth and Planetary Science Letters* **261**(3-4): 534-550.

Hsu S.K., J. Kuo, C.L. Lo, C.H. Tsai, W.B. Doo, C.Y. Ku, and **J.C. Sibuet** (2008) Turbidity Currents, Submarine Landslides and the 2006 Pingtung Earthquake off SW Taiwan. *Terr. Atmos. & Ocean Sci.,* **19**, 767-772.

Hunt, J. E., R. B. Wynn, D. G. Masson, P. J. Talling, and D. A. H. Teagle (2011), Sedimentological and geochemical evidence for multistage failure of volcanic island landslides: A case study from Icod landslide on north Tenerife, Canary Islands, *Geochem. Geophys. Geosyst*., 12.

Hurst, H.E. 1951. Long term storage capacity of reservoir. *American Society of Civil Engineers*, **116**, 770–808.

Ilstad, T., Elverhøi, A., Issler, D. and Marr, J.G. (2004) Subaqueous debris flow behaviour and its dependence on the sand/clay ratio: a laboratory study using particle tracking. *Marine Geology*, **213,** 415-438.

Iverson, R.M., Reid, M.E. and LaHusen, R.G. (1997) Debris-flow mobilization from landslides. *Annual Review of Earth and Planetary Sciences*, **25,** 85-138.

Iverson, R.M. and Vallance, J.W. (2001) New views of granular mass flows. *Geology*, **29,** 115-118.

Iverson, R.M., Logan, M., LaHusen, R.G. and Berti, M. (2010) The perfect debris flow? Aggregated results from 28 large-scale experiments. *Journal of Geophysical Research-Earth Surface*, **115**.

Ja'Aidi, O. S. A., W. D. McCaffrey, et al. (2004). Factors influencing the deposit geometry of experimental turbidity currents: implications for sand-body architecture in confined basins. *Confined Turbidite Systems*. S. A. Lomas and P. Joseph. Bath, Geological Soc Publishing House. **222:** 45-58.

John, C.M., Karner, G.D., and Mutti, M. (2004) δ18O and Marion Plateau backstripping: Combining two approaches to constrain late middle Miocene eustatic amplitude: *Geology*, **32**, 829–832.

Johnson, M.R. (1994) Thin-section grain-size analysis revisited. *Sedimentology*, **41,** 985-999.

Johnson, S. D., S. Flint, et al. (2001) "Anatomy, geometry and sequence stratigraphy of basin floor to slope turbidite systems, Tanqua Karoo, South Africa." *Sedimentology* **48**(5): 987-1023.

Kane, I. A., W. D. McCaffrey, et al. (2010) "Submarine channel levee shape and sediment waves from physical experiments." *Sedimentary Geology* **223**(1-2): 75-85.

Kennet, J.P., Cannariato, K.G., Hendy, I.L., Behl, R.J. (2003) Methane Hydrates in Quaternary Climate Change. The Clathrate Gun Hypothesis, Washington D.C., American Geophysical Union.

Kligfield R. (1979) The Northern Apennines as a collisional orogen. *American Journal of Sciences*, **279**, 676-691.

Kneller, B. C. (1995) Beyond the turbidite paradigm: physical models for deposition of turbidites and their implications for reservoir potential. In (Hartley, A.J., and Prosser, D.J. eds.) *Characterization of Deep Marine Systems*, Geological Society Special Publication, **94**, 31-49.

Kneller, B.C. and Branney, M.J. (1995) Sustained high-density turbidity currents and the deposition of thick massive sands. *Sedimentology*, **42,** 607-616.

Kneller, B.C. and McCaffrey, W.D. (2003) The interpretation of vertical sequences in turbidite beds: The influence of longitudinal flow structure. *Journal of Sedimentary Research*, **73,** 706-713.706-713.

Kuenen, P.H. (1965) Value of experiments in geology. *Geologie en Mijnbouw*, **44**, 22-36.

Kuenen, P.H. (1966) Experimental turbidite lamination in a circular flume. *Journal of Geology,* 74, 523-545.

Kuenen, P.H. and **Migliorini, C.I.** (1950) Turbidity currents as a cause of graded bedding. *J.Geol.*, **58**, 91-127.

Leclair, S.F. and **Arnott, R.W.C.** (2005) Parallel lamination formed by high-density turbidity currents. *J. Sedim. Res.,* **75**, 1-5.

Livina, V., Tuzov, S., Havlin, S., Bunde, A. (2005) Recurrence intervals between earthquakes strongly depend on history. *Physica*, A **348**, 591–595.

Lowe, D.R. (1976) Subaqueous liquefied and fluidized sediment flows and their deposits. *Sedimentology*, **23,** 285-308.

Lowe, D.R. (1982) Sediment gravity flows .2. depositional models with special reference to the deposits of high-density turbidity currents. *Journal of Sedimentary Petrology*, **52,** 279-298.

Lowe, D.R. (1997) Reinterpretation of depositional processes in a classic flysch sequence (Pennsylvanian Jackfork Group), Ouachita Mountains, Arkansas and Oklahoma: Discussion. *A. A.P.G. Bull*., 81, 460-465.

Lowe, D.R. and **Guy, M.** (2000) Slurry-flow deposits in the Britannia Formation (Lower Cretaceous), North Sea: a new perspective on the turbidity current and debris flow problem. *Sedimentology*, **47**, 31-70.

Lowe, D.R., Guy, M. and **Palfrey, A**. (2003) Facies of slurry-flow deposits, Britannia Formation (Lower Cretaceous), North Sea: implications for flow evolution and deposit geometry. *Sedimentology*, **50**, 45-80.

Lucente, C.C. (2004) Topography and paleogeographic evolution of a middle Miocene foredeep basin plain (Northern Apennines, Italy). *Sed. Geol*., 170, 107–134.

Magalhaes, P. M. and **R. Tinterri** (2010). "Stratigraphy and depositional setting of slurry and contained (reflected) beds in the Marnoso-arenacea Formation (Langhian-Serravallian) Northern Apennines, Italy." *Sedimentology* **57**(7): 1685-1720.

Marr, J.G., Harff, P.A., Shanmugam, G. and Parker, G. (2001) Experiments on subaqueous sandy gravity flows: The role of clay and water content in flow dynamics and depositional structures. *Geological Society of America Bulletin*, **113,** 1377-138.

Major, J.J. (1997) Depositional processes in large-scale debris-flow experiments. *Journal of Geology*, **105,** 345-366.

Malinverno, A. (1997) On the power law size distribution of turbidite beds. *Basin Res*., **9**, 263–274.
Martelli, L., Farabegoli, E., Benini, A., DeDonatis, M., Severi, P., Pizziolo, M., Pignone, R., Cerrina Feroni, A., Ricci Lucchi, F., Kearton, M.C., Angelelli, A. and Forni, S. (1994) La geologica del Foglio 265 – S. Piero in Bagno*. In: La Cartografia Geologica della Regione Emilia-Romagna*, Servizio Cartografico e Geologico, Regione Emilia Romagna, Bologna, SELCA, Florence, 117 pp.

Marzocchi, W. and L. Zaccarelli (2006). "A quantitative model for the time-size distribution of eruptions." *Journal of Geophysical Research-Solid Earth* **111**(B4).

Maslin, M., and Mikkelsen, **N.** (1998) Timing of the late Quaternary Amazon fan complex mass-transportdeposits, in *Geological evolution of ocean basins; results from the Ocean Drilling Program*, edited by Cramp, A., MacLeod, C. J., Lee, S. V., and Jones, E. J. W., *Geol. Soc. Spec. Publ*., **131**, 129–150.

Maslin, M., N. Mikkelsen, et al. (1998). "Sea-level- and gas-hydrate-controlled catastrophic sediment failures of the Amazon Fan." *Geology* **26**(12), 1107-1110.

McAnally, W.H., C. Friedrichs, D. Hamilton, E. Hayter, P. Shrestha, H. Rodriguez, A. Sheremet and **Teeter, A.** (2007) Management of fluid mud in estuaries, bays, and lakes. I: Present state of understanding on character and behaviour. *J. Hydr. Eng,* **133**, 9-22.

Middleton, G.V. (1970) Experimental studies related to the problems of flysch sedimentation. In (Lajoie, J. ed.) *Flysch Sedimentology in North America*, Geol. Soc. Canada, Special Paper, **7**, 253-171.

Middleton G.V. and **Hampton M.A.** (1973) Sediment gravity flows: mechanisms of flow and deposition: In *Turbidites and Deep-Water Sedimentation.* S.E.P.M. Pacific Section, Short course lecture notes, p. 1-38.

Middleton, G. V. and W. J. Neal (1989). "Experiments on the thickness of beds deposited by turbidity currents." *Journal of Sedimentary Petrology* **59**(2): 297-307.

Miller, K.G., Wright, J.D., Fairbanks, R.G., (1991). Unlocking the ice house: Oligocene–Miocene oxygen isotopes, eustacy and marginal erosion. *J. Geophys. Res*. **96**, 6829–6848.

Miller, K. G., M. A. Kominz, et al. (2005). "The phanerozoic record of global sea-level change." *Science* **310**(5752): 1293-1298.

Mohrig, D., Elverhoi, A. and Parker, G. (1999) Experiments on the relative mobility of muddy subaqueous and subaerial debris flows, and their capacity to remobilize antecedent deposits. *Marine Geology*, **154,** 117-129.
Mulder, T., and **Alexander, A.** (2001) The physical character of subaqueous sedimentary density flows and their deposits. *Sedimentology,* **48**, 269-299.

Mulder, T., Migeon, S., Savoye, B. and Faugeres, J. (2001) inversely graded turbidite sequences in the deep Mediterranean: a record of deposits from flood-generated turbidity currents? *Geo-Marine Letters*, **21,** 86-93.86-93.

Mulder, T., Syvitski, J.P.M., Migneon, S., Faugeres, J.C., and **Savoye, B.** (2003) Marine hyperpycnal flows: initiation, behaviour, and related deposits. A review. *Mar. Petrol. Geol.*, **20**, 861-882.

Müller, P. J. and E. Suess (1979) Productivity, sedimentation rate, and sedimentary organic matter in the oceans-I. Organic carbon preservation. *Deep-Sea Res*., *26*, 1347–1362.

Murray, C.J., Lowe, D.R., Graham, S.A., Martinez, P.A., Zeng, J., Carroll, A., Cox, R., Hendrix, M., Heubeck, C., Miller, D., Moxon, I.W., Sobel, E., Wendebourg, E. and Williams, T. (1996) Statistical analysis of bed-thickness patterns in a turbidite section from the Great Valley Sequence, Cache Creek California. *J. Sed. Petrol*., **66**, 900-908.

Mutti, E. (1992) Turbidite Sandstones. Istituto di Geologia Universita di Parma & AGIP, 275pp.

Mutti, E., F. R. Lucchi, et al. (1984). "Seismoturbidites - a new group of resedimented deposits." *Marine Geology* **55**(1-2): 103-116.

Mutti, E., Ricci Lucchi, F. and Roveri, M. (2002) Revisiting Turbidites of the Marnoso-arenacea Formation and their Basin-Margin Equivalents: Problems with Classic Models. *64th EAGE Conference and Exhibition Excursion Guide- book*, ParmaUniversity and ENI-AGIP Division, Parma, Italy.

Mutti, E., Tinterri, R., Benevelli, G., di Biase, D. and Cavanna, G. (2003) Deltaic, mixed and turbidite sedimentation of ancient foreland basins. *Marine and Petroleum Geology*, **20,** 733-755.

Mutti, E., Benoulli, D., Ricci Lucchi, F. and **Tinterri R.** (2009) Turbidite and turbidity currents from Alpine 'flysch' to the exploration of continental margins. *Sedimentology,* **56**, 267-318.

Mutti, E., Bernoulli, D., Lucchi, F.R. and Tinterri, R. (2010) Reply to the Discussion by Ganapathy Shanmugam on "Turbidities and turbidity currents from Alpine flysch to the exploration of continental margins" by Mutti et al. (2009), Sedimentology, 56, 267-318. *Sedimentology*, **57,** 933-934.

Milliman, J.D. and **Syvitski, J.P.M**. (1992) Geomorphic tectonic controls of sediment discharge to the ocean – the importance of small mountain rivers. *J. Geology,* **100**, 525-544.

Nakajima, T. and Kneller, B.C. (2011) Quantitative analysis of the geometry of submarine levees. In *Internal architecture, bedforms and geometry of turbidite channels*" conference abstract, Geological Society, London.

Omori F. (1894) "On the aftershocks of earthquakes". *Journal of the College of Science, Imperial University of Tokyo* **7**, 111–200.

Pieri M., Groppi G. (1981), *Subsurface geological structure of the Po Plain. Progetto Finalizzato Geodinamica/Sottoprogetto 'Modello Strutturale'*, Publ. Italian CNR.

Pickering, K., Stow, D., Watson, M. and Hiscott, R. (1986) *Deep-water facies, processes and models: a review and classification scheme for modern and ancient sediments*. Earth-Sci. Rev., 23, 75–174.

Piper, D.J.W., Cochonat, P. and **Morrison M.L.** (1999) The sequence of events around the epicenter of the 1929 Grand Banks earthquake: initiation of the debris flows and turbidity current inferred from side scan sonar. *Sedimentology,* **46**, 79-97.

Piper, D.J.W. and **Savoye, B.** (1993) Processes of Late Quaternary turbidity-current flow and deposition on the Var deep-sea fan, North-west Mediterranean Sea. *Sedimentology*, **40**, 557-582.

Piper, D.J.W. and **Normark, W.R.** (2009) Processes that initiate turbidity currents and their influence on turbidites: a marine geology perspective. *J. Sedim. Res.,* **79**, 347-362.

Pini, G.A. (1999) - Tectonosomes and Olistostromes in the Argille Sagliose of the Northern Apennines, Italy*. Geological Society of America, Special Publications*, **335**, 69 pp.

Plink-Bjorklund, P. and Steel, R.J. (2004) Initiation of turbidity currents: outcrop evidence for Eocene hyperpycnal flow turbidites. *Sedimentary Geology*, **165,** 29-52.

Prelat, A., Hodgson, D. M. et al. (2009) "Evolution, architecture and hierarchy of distributary deep-water deposits: a high-resolution outcrop investigation from the Permian Karoo Basin, South Africa." *Sedimentology* **56**(7), 2132-U2125.

Remacha, E. & Fernández, L.P. (2003) High-resolution correlation patterns in the turbidite system of the Hecho Group (South-Central Pyrenees, Spain). In: Mutti, E.; Steffens. G.S.; Pirmez, C.; Orlando, M. & Roberts, D. (Eds.), *Turbidites: Models and Problems*. *Marine and*

Petroleum Geology, **20**, 711-726.

Ricci Lucchi, F. (1981) The Miocene Marnoso Arenacea turbidites, Romagna and Umbria Apennines. In: *International Association of Sedimentologists Excursion Guidebook, 2nd European Regional Meeting*, pp. 231–303, Tripoli, Libya.

Ricci Lucchi, F. (1986) The Oligocene to Recent foreland basins of the northern Apennines. In: Foreland Basins (Eds P.A. Allen and P. Homewood), *Int. Assoc. Sedimentol. Spec. Publ., Blackwell Scientific*, 8, 105–139.

Ricci Lucchi, F. and Valmori, E. (1980) Basin-wide turbidites in a Miocene, over- supplied deep-sea plain: a geometrical analysis. *Sedimentology*, 27, 241–270.

Ricci Lucchi, F. & Ori, G.G. (1985) - Field Excursion D: syn-orogenic deposits of a migrating basin system in the NW Adriatic Foreland: examples from Emilia Romagna region, Northern Apennines. In: Allen, P.; Homewood, P. & Williams, G. (Eds.), *International Symposium on Foreland Basins*. Excursion Guidebook, 137-176.

Richardson, J F and **Zaki W N.** (1954) The sedimentation of a suspension of uniform spheres under conditions of viscous flow. *J. Chem. Eng. Science*, ***3*** **(2),** 65–73

Roest W.R. and Srivastava S.P. (1991) Kinematics for the plate boundaries between Eurasia, Iberia and Africa in the North Atlantic from the Late Cretaceous to the present. *Geology*, **191**, 613-616.
Rothman, D.H. and Grotzinger, J.P. (1995) Scaling properties of gravity-driven sediments. *Nonlinear Processes Geophys*., **2**, 178–185.

Rothman, D.H., Grotzinger, J.P. and Flemings, P. (1994) Scaling in turbidite deposition. J*. Sed. Petrol*., A**64**, 59-67.

Rothwell, R. G., J. Thomson, et al. (1998). "Low-sea-level emplacement of a very large Late Pleistocene 'megaturbidite' in the western Mediterranean Sea." *Nature* **392**(6674): 377-380.

Roveri, M., F., R.L., Lucente, C.C., Manzi, V. and Mutti, E. (2002) Stratigraphy, facies and basin fill history of the Marnoso Arenacea Formation*. In: Revisiting Turbidites of the Marnoso-arenacea Formation and their Basin-Margin Equivalents: Problems with Classic Models. 64th EAGE Conference and Exhibition Excursion Guidebook*, (Eds E. Mutti, F. Ricci Lucchi and M. Roveri), pp. III-1–III-26, Parma University and ENI-AGIP Division, Parma, Italy.

Shanmugam, G. (1997) The Bouma Sequence and the turbidite mind set. *Earth-Science Reviews*, **42,** 201-229.

Shanmugam, G. (2000) 50 years of the turbidite paradigm (1950s-1990s): deep-water processes and facies models - a critical perspective. *Marine and Petroleum Geology*, **17,** 285-342.

Shanmugam, G. (2002) Ten turbidite myths. *Earth-Science Reviews*, **58,** 311-341.

Shanmugam, G. and Moiola, R.J. (1995) Reinterpretation of depositional processes in a classic flysch sequence (Pennsylvanian Jackfork Group), Ouachita Mountains, Arkansas and Oklahoma. *Aapg Bulletin-American Association of Petroleum Geologists*, **79,** 672-695.

Shanmugam, G. and R. J. Moiola R.J. (1997). "Reinterpretation of depositional processes in a classic flysch sequence (Pennsylvanian Jackfork Group), Ouachita Mountains, Arkansas and Oklahoma: Reply." *Aapg Bulletin-American Association of Petroleum Geologists* **81**(3): 476-491.

Simons, D.B., Richardson, E.V. and **Nordin, C.F.** (1965) Sedimentary structures formed by flow in alluvial channels. In: Primary Sedimentary Structures and their Hydrodynamic Interpretation (Ed. G.V. Middleton), *SEPM Spec. Pub*., **12**, 34-53.

Sinclair, H.D. and Cowie, P.A. (2003) Basin-Floor Topography and the Scaling of Turbidites. J*. Geol.*, **111**, 277–299.

Sixsmith, P.J., S.S. Flint, H.D.V. Wickens and S.D. Johnson (2004) Anatomy and stratigraphic development of a Basin floor turbidite system in the Laingsburg Formation, Main Karoo Basin, South Africa*. Journal of Sedimentary Research*, **74**(2), 239-254.

Skene, K.I., Piper, D.J.W., and Hill, P.S. (2002),Quantitative analysis of variations in depositional sequence thickness from submarine channel levees: *Sedimentology*, **49**, 1411–1430.

Slatt, R.M., Weimer, P. and **Stone, C.G.** (1997) reinterpretation of depositional processes in a classic flysch sequence (Pennsylvanian Jackfork Group), Ouachite Mountains, Arkansas and Oklahoma [discussions and reply]. *AAPG Bull*., **81**, 139–145.

Stow, D.A.V. and Johansson, M. (2000) Deep-water massive sands: nature, origin and hydrocarbon implications. *Marine and Petroleum Geology*, **17,** 145-174.

Stow, D.A.V. and Wetzel, A., 1990. Hemiturbidite:a new type of deep-water sediment. In: Cochan, J.R., Stow, D.A.V. (Eds.), *Proceedings of the ODP scientific results*, **116**, pp. 25–34.

Sumner, E.J., Amy, L.A. and Talling, P.J. (2008) Deposit structure and processes of sand deposition from decelerating sediment suspensions. *Journal of Sedimentary Research*, **78,** 529-547.529-547.
Sumner, E.J., Talling, P.J. and Amy, L.A. (2009) Deposits of flows transitional between turbidity current and debris flow. *Geology*, **37,** 991-994.

Sumner, E.J., Talling, P.J., Amy, L.A., Wynn, R.B., Stevenson, C.J. and **Frenz, M.** (2012) Facies architecture of individual basin-plain turbidites: comparison to existing models and implications for flow processes. *Sedimentology*, *in press.*

SYLVESTER, Z. (2007) Turbidite bed thickness distributions: methods and pitfalls of analysis and modelling: *Sedimentology***, 54**, 847–870.

Sylvester, Z. and Lowe, D.R. (2004) Textural trends in turbidites and slurry beds from the Oligocene flysch of the East Carpathians, Romania. *Sedimentology*, **51,** 945-972.945-972.

Talling, P.J. (2001) On the frequency distribution of turbidite thickness. *Sedimentology*, **48**, 1297–1331.

Talling, P. J., Amy, L. A., Wynn, R. B., Peakall, J. and **Robinson, M.** (2004) Beds comprising debrite sandwiched within co-genetic turbidite: origin and widespread occurrence in distal depositional environments. *Sedimentology*, **51**, 163-194.

Talling, P.J., Amy, L.A., Wynn, R.B., Blackbourn, G., and Gibson, O. (2007a) Turbidity current evolution deduced from extensive thin turbidites: Marnoso Arenacea Formation (Miocene), Italian Apennines. *Journal of Sedimentary Research*, 77, 172-196.

Talling, P.J., Amy, L.A. and **Wynn, R.B.** (2007b) New insights into the evolution of large nvolume turbidity currents; comparison of turbidite shape and previous modelling results. *Sedimentology,* **54**, 737-769*.*

Talling, P.J., Wynn, R.B., Masson, D.G., Frenz, M., Cronin, B.T., Schiebel, R., Akhmetzhanov, A.M., Dallmeier-Tiessen, S., Benetti, S., Weaver, P.P.E., Georgiopoulou, A., Zuhlsdorff, C. and Amy, L.A. (2007c) Onset of submarine debris flow deposition far from original giant landslide. *Nature*, **450,** 541-544.

Talling, P.J., Wynn, R.B., Schmmidt, D.N., Rixon, R., Sumner, E. and Amy, L. (2010) How did thin submarine debris flows carry boulder-sized intraclasts for remarkable distances across low gradients to the far reaches of the mississippi fan? *Journal of Sedimentary Research*, **80,** 829-851.

Talling, P.J., Sumner, E.J., Malgesini, G., and Masson, D.G., (2012a) Submarine Turbidity Currents and Their Deposits. Sedimentology, *in press*.

Talling, P.J., Malgesini, G. and **Felletti, F.** (2012b) Can liquefied (debris) flows deposit clean sandstone over large areas of sea floor? Field evidence from the Marnoso-arenacea Formation, Italian Apennines. *Sedimentology, in press.*

Talling, P.J., Malgesini, G., Sumner, E.J. , Amy L.A. , Felletti, F. , Blackbourn, G., Nutt, C., Wilcox, C., Harding, I.C. and **Akbari, S.** (2012b) Planform geometry, stacking pattern, and extrabasinal origin of low-strength and higher-strength cohesive debris flow deposits in the Marnoso arenacea Formation. Geosphere, *in press*.

ten Brink, U.S., Giest, E.L., Andrews, B.D. (2006) Size distribution of submarine landslides and its implication to tsunami hazard in Puerto Rico. *Geophys. Res. Lett*. **33**.

Thornton, S.E., (1984) Basin model for hemipelagic sedimentation in a tectonically active continental margin: Santa Barbara Basin, California continental borderland. In Stow, D.A.V., and Piper, D.J.W. (Eds.), *Fine grained Sediments: Deep-water Processes and Fades*. Geol. Soc. Spec. Publ. London, **15**, 377-394.

Tinterri, R. and P. M. Magalhaes (2011). "Synsedimentary structural control on foredeep turbidites: An example from Miocene Marnoso-arenacea Formation, Northern Apennines, Italy." *Marine and Petroleum Geology* **28**(3): 629-657.

Tinterri, R., Drago, M., Consonni, A., Davoli, G. and Mutti, E. (2003) Modelling subaqueous bipartite sediment gravity flows on the basis of outcrop constraints: first results. *Marine and Petroleum Geology*, **20,** 911-933.

Vai, G.B. (2001) – Strutture and stratigraphy: an overview. In: Vai G.B. & Martini I.P. (Eds.) *Anatomy of an orogen: the Apennines and adjacent mediterranean basins*, 15-32.

van der Werff, W. and Johnson, S.D. (2003) "Deep-sea fan pinch-out geometries and their relationship to fan architecture, Tanqua Karoo basin (South Africa)." *International Journal of Earth Sciences* **92**(5,: 728-742.

Van Wamel, W.A. and Zwart, P.E. (1990) The structural geology and basin development of the Romagna-Umbrian zone (Upper Savio- and Upper Bidente Valleys, N.Italy). *Geol. Mijnbouw*, 69, 53–68.

Visser, J.N.J. (1993) Sea-level changes in a back-arc foreland transition - the late Carboniferous - Permian Karoo Basin of South Africa. *Sedimentary Geology*, **83**, 115-131.

Wallis, J.R. & Matalas, N.C. 1970. Small sample properties of *H* and *K* estimator of the Hurst coefficient *h*. *Water Resources Research*, **6**, 1583–1594.

Weaver, P. P. E. & Kuijpers, A. (1983) Climatic control of turbidite deposition on the Madeira Abyssal plain. *Nature* **306**, 360–363.

Weimer, P. and **Pettingill, H.S.** (2007) A global overview of fields and discoveries in deep water deposits. In: *Atlas of Deepwater Outcrops* (Eds. Nielsen, T., Shew, R.D., Steffens, G.S. and Studlick, J.R.J.) AAPG Studies in Geology 56, Shell Exploration and Production and American Association of Petroleum Geologists, 12-16.

Westerhold, T., Bickert, T., and Röhl, U. (2005) Middle to late Miocene oxygen isotope stratigraphy of ODP Site 1085 (SE Atlantic): New constrains on Miocene climate variability and sea-level fluctuations: *Palaeogeography, Palaeoclimatology, Palaeoecology*, **217**, 205-222.

Wickens, H.D.V. and Bouma A.H. (2000).The Tanqua Fan Complex, Karoo Basin, South Africa - Outcrop analogue for fine-grained, deepwater deposits In: Fin*e-grained turbidite systems.* A.H. Bouma and C.G. Stone (eds.). AAPG, Memoir 72 and SEPM, Special Publication **68,** 153-165.

Wild, R. J., D. M. Hodgson, et al. (2005) Architecture and stratigraphic evolution of multiple, vertically-stacked slope channel complexes, Tanqua depocentre, Karoo Basin, South Africa. *Submarine Slope Systems: Processes and Products*. D. M. Hodgson and S. S. Flint. Bath, Geological Soc Publishing House. **244,** 89-111.

Wright, L.D., Friedrichs, C.T., Kim, S.C., and **Scully, M.E.** (2001) The effects of ambient currents and waves on gravity-driven sediment transport on continental shelves. *Mar. Geol.*, **175**, 25-45.

Wynn, R.B. and **Masson, D.G.** (2003) Canary Islands landslides and tsunami generation. In *Proc. 1st Int. Symposium on Submarine Mass Movements and their Consequences* (Eds. Mienert J. and Locat, J.) Kluwer, Dordrecht, 325-332.

Wynn, R.B., Talling, P.J. Masson, D.G. Stevenson, C.J. Cronin B.T. and **Le Bas, T.P.** (2010) Investigating the timing, processes and deposits of one of the World's largest submarine gravity flows: the 'Bed 5 event' off northwest Africa. In: *Submarine mass movements and their consequences (*Eds. Mosher D.C., Shipp R.C., Moscardelli, L., Chaytor J.D., Baxter, C.D.P., Lee, H.J., and Urgeles R.) Elsevier. **28**, 463-474.

Wynn, R.B., Talling, P.J., Masson, D.G., Le Bas, T.P., Cronin, B.T., Stevenson, C.J. (2012). The influence of subtle gradient changes on deep-water gravity flows: a case study from the Moroccan Turbidite system. *SEPM Special Publication.*

Zattin, M., Picotti, V. and Zuffa, G.G. (2002) Fission-track reconstruction of the front of the Northern Apennine thrust wedge and overlying Ligurian Unit. *Am. J. Sci*., **302**, 346– 379.

Zeng, Z., and Lowe, D.R., 1997, Numerical simulation of turbidity current flow and sedimentation: II Results and geological applications: *Sedimentology*, **44**, 85–104.

APPENDICES

Appendix 1 - Ridracoli and Pietralunga elements

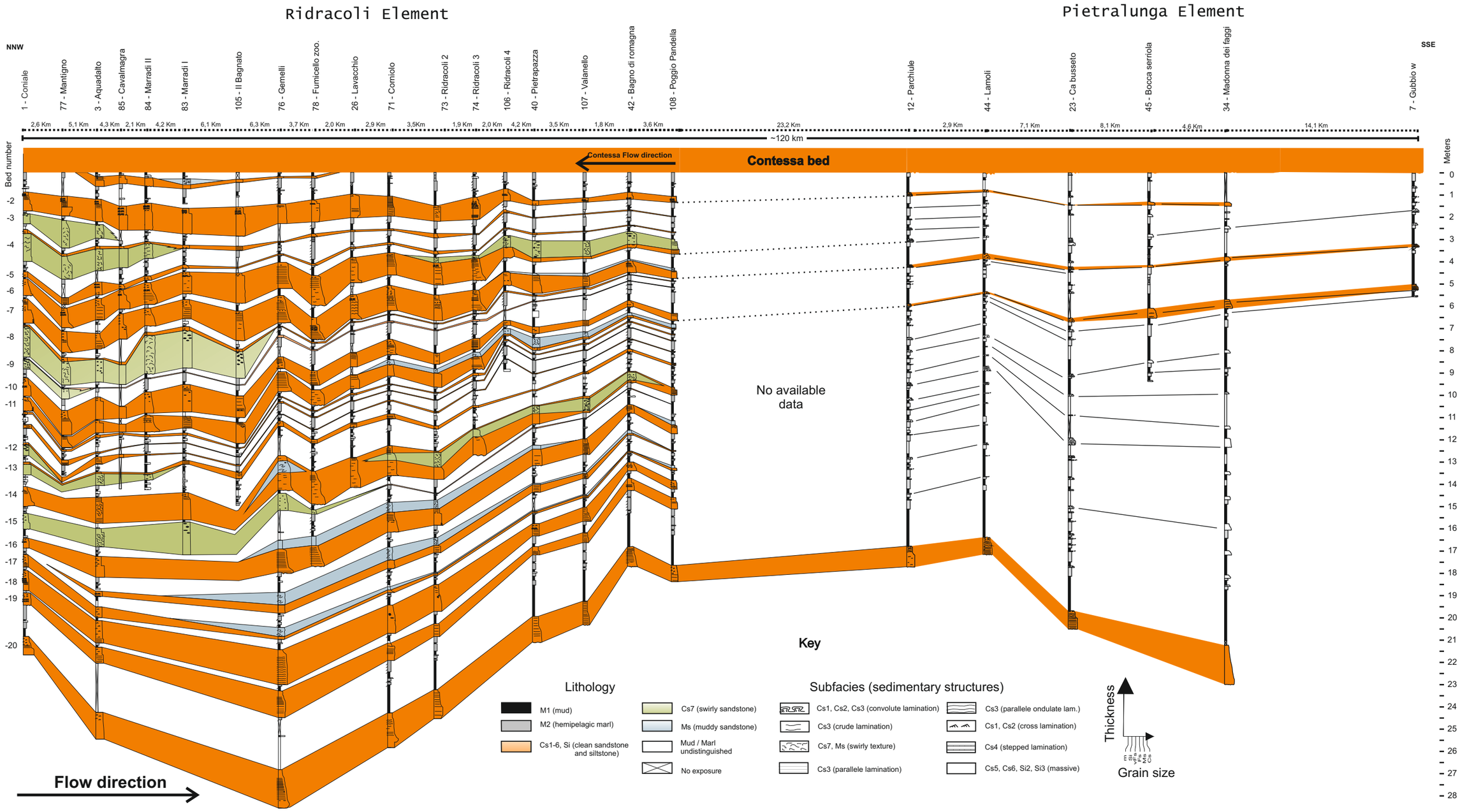

Appendix 1. Cross-section along the Ridracoli element showing the correlation of the first 20 thick (>40 cm) beds below the Contessa marker bed. Key is provided. Only few beds can be directly correlated between the Ridracoli and Pietralunga elements.

Appendix 2 - Isola Element

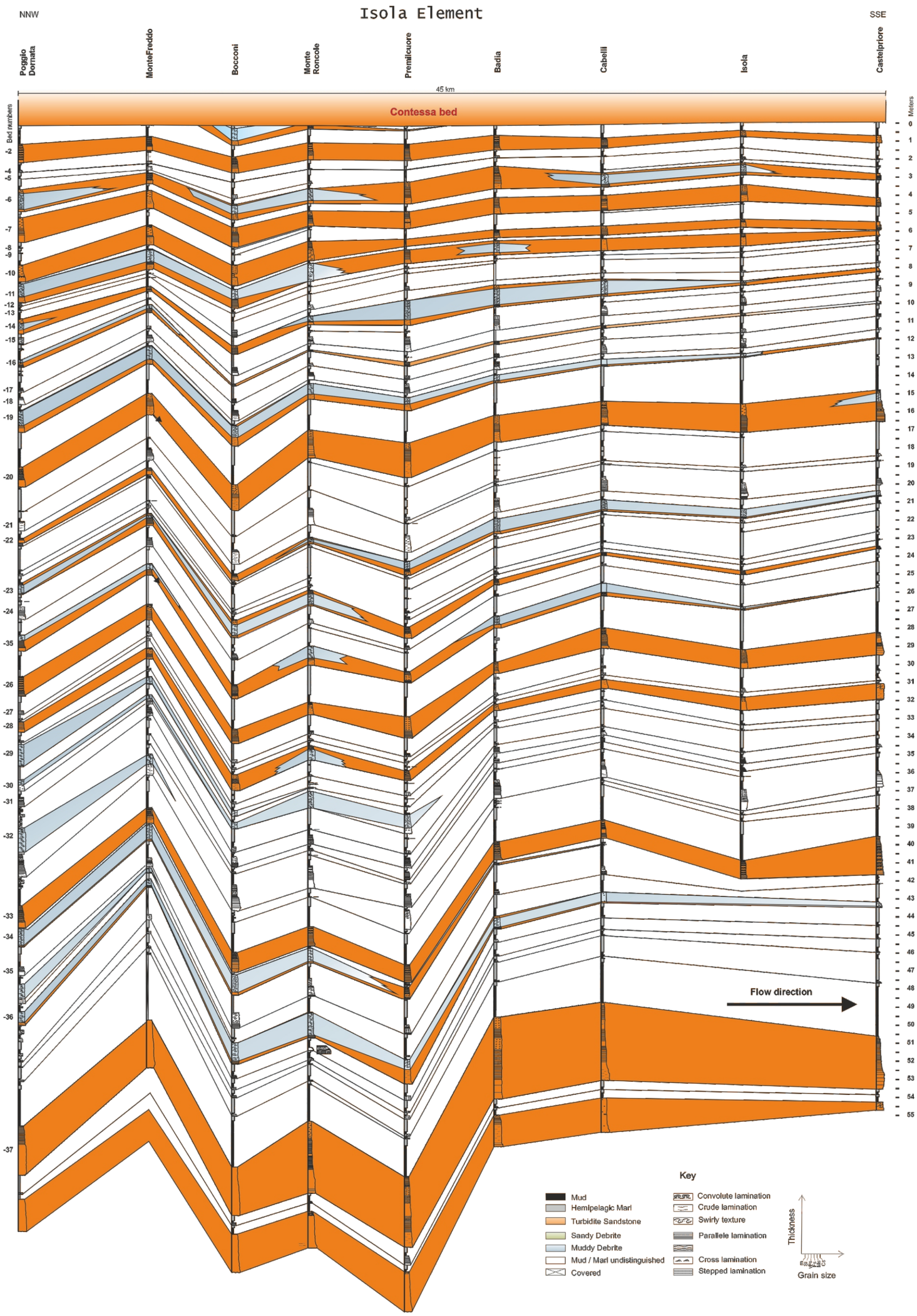

Appendix 2. Cross-section along the Isola element showing the correlation of the first 37 thick (>40 cm) beds between the the Contessa and the Fiumicello (bed -37) marker bed. Key is provided.

Appendix 3 - Transverse cross section

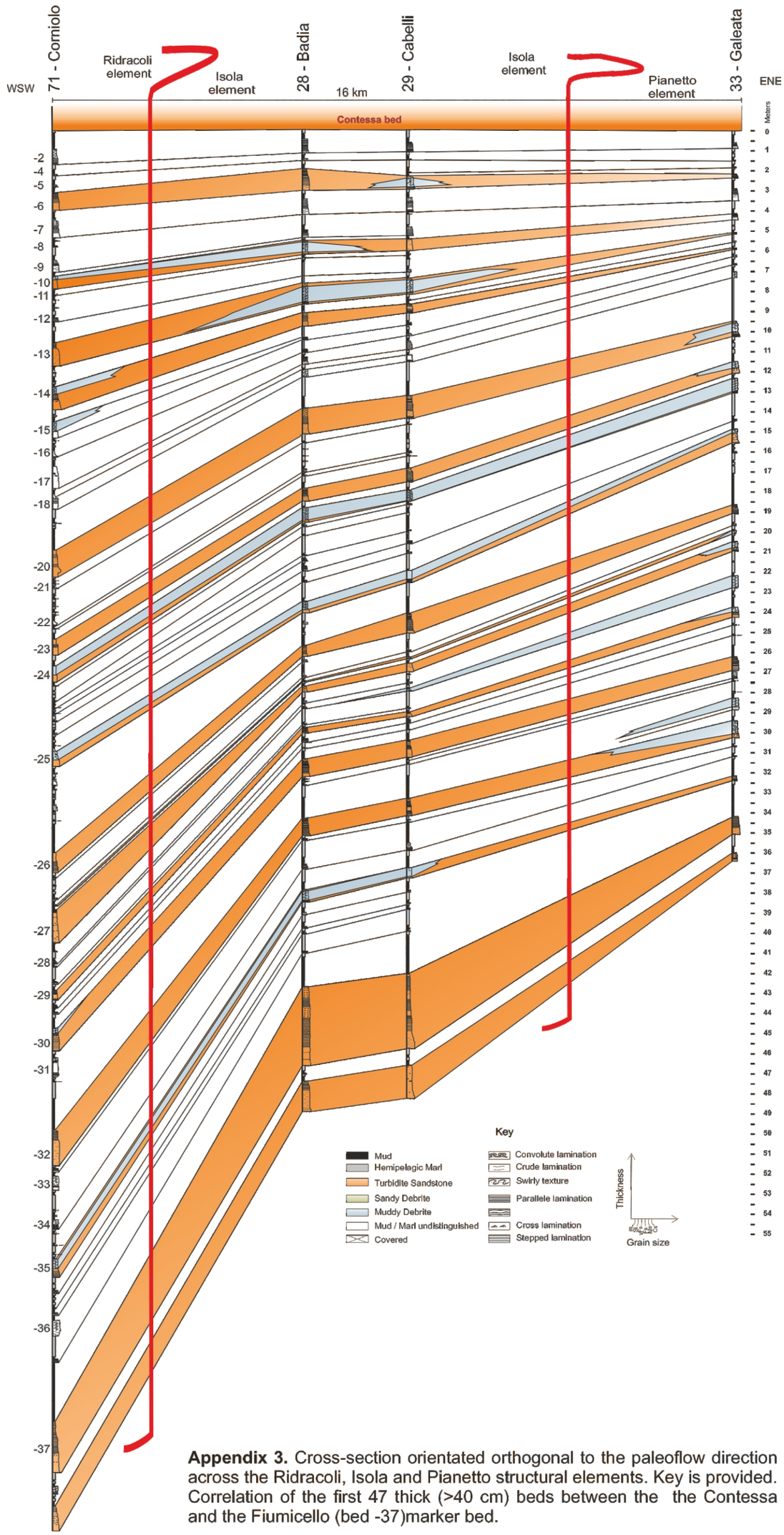

Appendix 3. Cross-section orientated orthogonal to the paleoflow direction across the Ridracoli, Isola and Pianetto structural elements. Key is provided. Correlation of the first 47 thick (>40 cm) beds between the the Contessa and the Fiumicello (bed -37)marker bed.

Appendix 4 - Fan 4 oblique-to-strike correlation panel

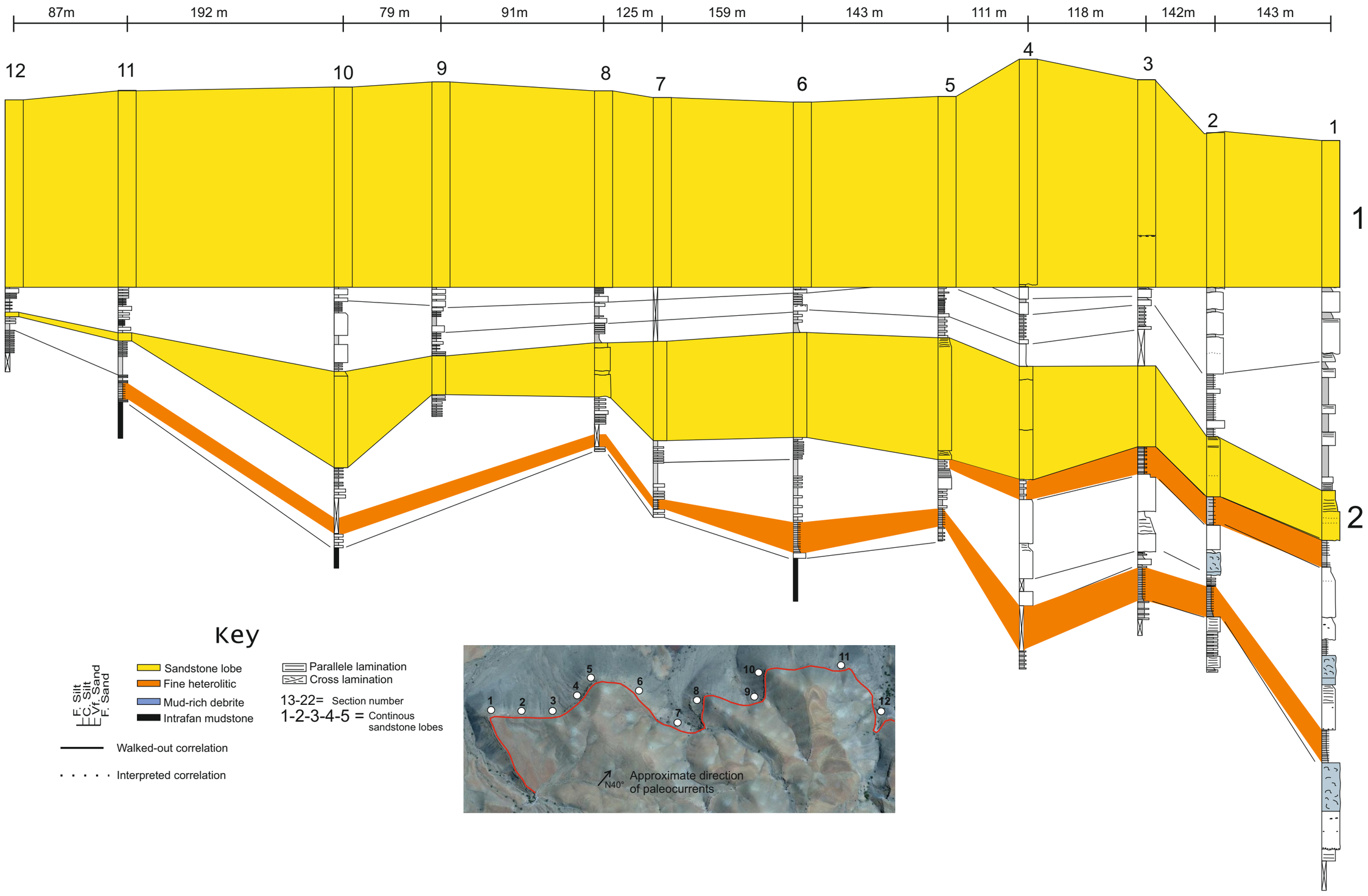

Key

F. Silt
C. Silt
Vf. Sand
F. Sand

- Sandstone lobe
- Fine heterolitic
- Mud-rich debrite
- Intrafan mudstone

- Parallele lamination
- Cross lamination

13-22= Section number

1-2-3-4-5 = Continous sandstone lobes

Walked-out correlation

Interpreted correlation

Appendix 5 - Fan 4 oblique-to-dip correlation panel

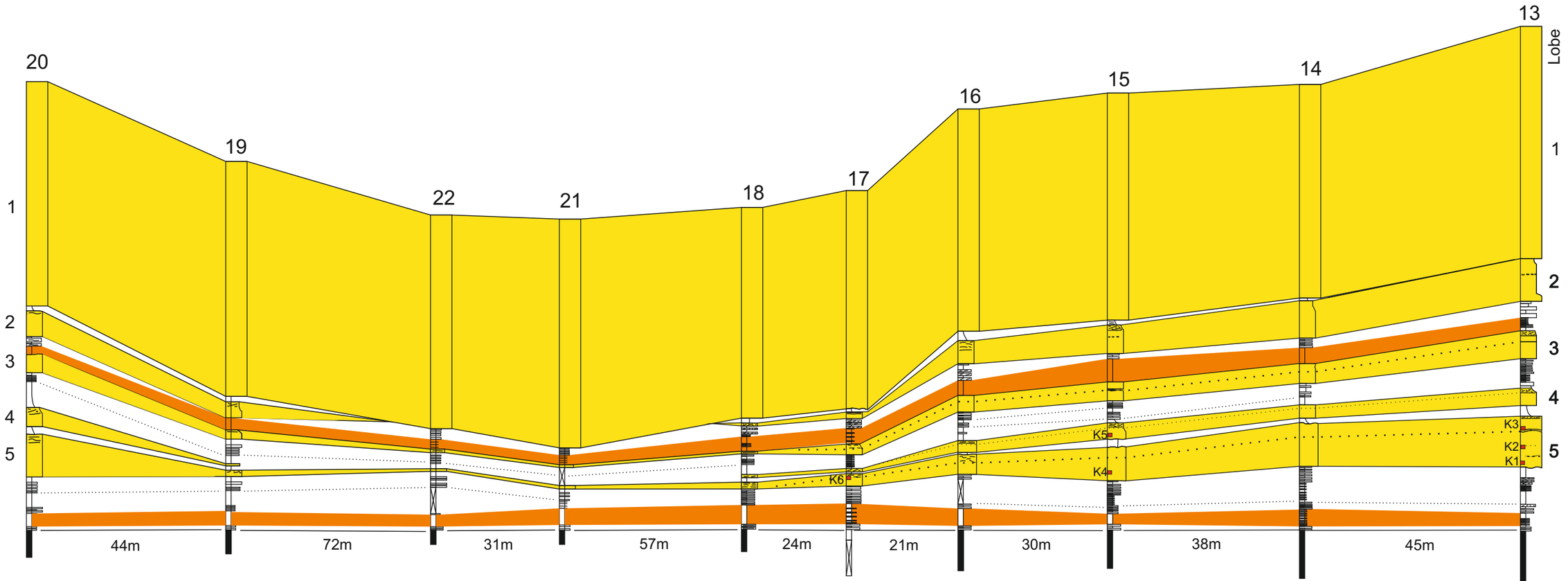

Key

F. Silt
C. Silt
Vf. Sand
F. Sand

- Sandstone lobe
- Fine heterolitic
- Mud-rich debrite
- Intrafan mudstone

- Walked-out correlation
- Interpreted correlation

- Parallele lamination
- Cross lamination

13-22= Section number

1-2-3-4-5 = Continous sandstone intervals

- rock sample

1 m

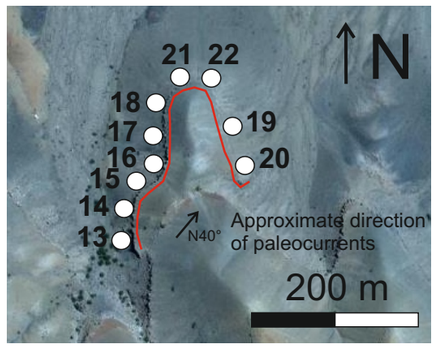

Appendix 6 - Summary